The Dissertation Committee for Jamie Sloan Levine Certifies that this is the approved version of the following dissertation:

In Situ Melt Generation in Anatectic Migmatites and the Role of Strain in Preferentially Inducing Melting

Committee:

Sharon Mosher, Supervisor

William D. Carlson

Mark Cloos

Nathan Daczko

Christine Siddoway

In Situ Melt Generation in Anatectic Migmatites and the Role of Strain in Preferentially Inducing Melting

by

Jamie Sloan Levine, B.A.; M.S.Geo.Sci

Dissertation

Presented to the Faculty of the Graduate School of

The University of Texas at Austin

in Partial Fulfillment

of the Requirements

for the Degree of

Doctor of Philosophy

The University of Texas at Austin

August 2011

Acknowledgements

Over the five years that I spent working on my dissertation, there were many people who provided emotional, intellectual and physical support, and I would like to take the time to thank them.

I would like to begin with my adviser, Dr. Sharon Mosher, who always supported me 100%. Despite the fact that I chose to tackle some questions that were unpopular and challenging, she believed in my ability to prove skeptics wrong and she continually encouraged me to pursue the research questions I wanted to answer. Even though she was quite busy as chair and then dean, she took the time to meet with me, discuss ideas, look at thin sections, help me prepare for job interviews, watch many talks, and perhaps most importantly to read drafts of my dissertation in a very short timeframe. I feel lucky to have an adviser that was so supportive, patient and encouraging. Sharon is a fantastic adviser and I am so happy that I returned to the University of Texas for my PhD, because there is no one I would rather have had as an adviser.

I would like to thank all of my committee members: Dr. Bill Carlson, Dr. Mark Cloos, Dr. Nathan Daczko and Dr. Christine Siddoway. Bill Carlson frequently took time to discuss the intricacies of garnet zoning, metamorphic textures and mineral assemblages with me. He also helped me to network at national meetings by introducing me to colleagues and he took time to write reference letters on my behalf. Although he has been skeptical of some of my ideas, he continued to encourage me to prove him wrong and I appreciate his skepticism because it has better prepared me for inevitable skepticism in the wider geologic community. I also enjoyed TAing for Bill in igneous and metamorphic petrology and his classes were some of the toughest, but also some of the most valuable courses I have ever taken.

Dr. Mark Cloos has been invaluable in his willingness to discuss research and for being such an enthusiastic committee member. Mark has given me advice on how to better my talks, and is one of the people who most enjoys talking about research. He is very good at getting me excited about what I'm working on and also asking probing

questions, that I hadn't necessarily considered. Additionally, he took time to write letters of reference for jobs this winter and he read my dissertation chapters in record time. I have also appreciated the opportunity to TA for Mark in both structural geology and field methods for non-majors. Mark also gave me the opportunity to go to California this past winter, which was a spectacular experience to see a lot of new and different rocks and I am so appreciative of the experience.

Dr. Nathan Daczko was invaluable during his visit to Austin for my defense this past May. As the only geochemist on my committee he spent hours upon hours talking about the geochemistry of the Albany-Fraser rocks (see Chapter 4) with me and helping me improve that chapter greatly. He has a true passion for metamorphic petrology and I really enjoyed looking at thin sections and discussing metamorphic reactions with him. He was very thorough with his comments and very insightful, and I look forward to continuing to collaborate with him in the future.

Dr. Christine Siddoway has been a great resource both in the field, and in thinking about big-picture questions brought up by this research. She has also been very helpful with editing and writing style and has provided great information on networking and academic jobs at small liberal arts colleges. I have really enjoyed spending time in the field with her and co-chairing a GSA session together.

Mark Helper, you have always gone above and beyond what anyone else could do. I still marvel at how many people you help on a daily basis and how sought after you are. I have appreciated all of your feedback on my research, reading copies of my comps proposal, attending my talks and asking thought-provoking questions. I have also immensely enjoyed being a TA for field camp six times and also TAing field methods for you. I have learned so much about being in the field and organizing a group of students; that information is invaluable and I have enjoyed every minute of it. I also appreciate the opportunity to supervise two undergraduate honors students with you and for all of your letters of recommendation.

The Mosher research group (Miriam Barquero-Molina, John Singleton, Paul Betka, Matt Carter and others) has also been a great source of support, humor, scientific

discussion and just generally a great group of friends. Miriam, I enjoyed sharing an office with you for three years, a month of my life in Australia and three summers of field camp. I hope we continue to share our love for running, cookies, Colin Firth and bad comedies. John, I have been so lucky to have started my PhD at the same time as you and to have had an excellent sounding board for research questions, running questions, political discussions and I hope that we continue to keep in touch throughout our long academic careers. Paul, thank you for keeping me sane during the last year of my dissertation; you were the one in the office with me most often, and I appreciate your support and your good humor.

There are many people in the department whose praises frequently go unsung. Greg Thompson, thank you so much for making hundreds of thin sections for me. Roger Gary, thank you for always having a positive attitude and making any random request seem easy and immediately achievable. Michelle Damvar, thank you for dealing with weird purchase orders and always making sure everything happened efficiently.

Philip Guerrero is truly the best graduate coordinator anyone could imagine. He always makes sure that grad students see as little red tape as possible, and is beyond patient. He is always looking out for everyone and is one of the most compassionate and selfless people I know.

I have had the great opportunity to make some great friends over the many years I have been at the University of Texas and I thank all of you for your support over the years. In particular, I would like to thank Lindsay Olinde for being a positive force in my life for the past two and a half years. You have continued to talk me down from my panic attacks and stress moments (days, months) and I feel so lucky to have met you!

Above all, I would like to thank my parents for their never-ending support, their constant encouragement and for being the best parents in the world. My sister Rachel has also been there for me and reminded me of all of the things I have to offer, thanks Bozy!

In Situ Melt Generation in Anatectic Migmatites and the Role of Strain in Preferentially Inducing Melting

Publication No._____

Jamie Sloan Levine, Ph.D.

The University of Texas at Austin, 2011

Supervisor: Sharon Mosher

Deformation and partial melting have long been recognized to occur together, but differentiating which actually occurred first has remained enigmatic. Prevailing theories suggest that partial melting typically occurs first, and deformation is localized into melt-rich areas because they are rheologically weak. However, evidence from three different areas, suggests the role of strain has been underestimated in localizing partial melting.

The Wet Mountains of central Colorado provide evidence for synchronous partial melting and deformation, with each process enhancing the other. Throughout the Wet Mountains, deformation is concentrated in areas where melt producing reactions occurred, and melt appears to be localized along deformation-related features. Melt microstructures present within the Wet Mountains correlate well with crustal-scale plutons and magmatic bodies and provide a proxy for crustal-scale melt flow.

Granitic gneisses from the Llano Uplift, central Texas, provide evidence for partial melting occurring within small-scale shear zones and surrounding country rocks, synchronously. In the field, shear zones appear to contain former melt, whereas the country rock does not provide macroscopic evidence for partial melting. However, detailed microstructural investigation of shear zones and country rocks indicates the same

density of melt microstructures, in both rock types. Melt microstructures are important for understanding the full melting history of a rock and without detailed structural and petrographic analysis, erroneous conclusions may be reached.

Granulite-facies migmatites of the Albany-Fraser Orogen, southwestern Australia, have undergone partial melting, synchronous with three phases of bidirectional extension. Four major groups of leucosomes, including: foliation-parallel, cross-cutting, boudin neck and jumbled channelway leucosomes and late pegmatites were analyzed via whole-rock geochemistry, and there is evidence for fluid-saturated and -undersaturated biotite- and amphibole-dehydration melting.

Migmatites from these three locations contain pseudomorphs of melt along subgrain and grain boundaries, areas of high dislocation density, in quartz and plagioclase. For these rocks that involve multicomponent systems, the primary cause for preferential melting in high strain locations is enhanced diffusion rates along the subgrain boundary because of pipe diffusion or water associated with dislocations.

Table of Contents

List of Tables

List of Figures

Chapter 1: Introduction

In migmatitic terranes, leucosomes, which are roughly granitic in composition and emplaced as melt or melt and crystals, ordinarily occupy structural sites parallel to foliation, axial planar to folds, and within shear zones or interboudin necks, all high strain locations. This association is usually attributed to melt segregation into structures that can act as dilatant conduits for transport of melt laterally or to higher crustal levels (Brown, 1994; Sawyer, 1994). The structures may be pre-existing with melt injected or migrating into them, or may form synchronously in the case of stress-induced gradients driving melt migration into shear zones (Brown et al., 1995; Vanderhaeghe, 2001). However, the spatial association of former melt within structural sites has led to the suggestion that melts may have been preferentially generated within these structures because a high dislocation density would lead to increased stored strain energy that serves to lower the activation energy needed for melting reactions to occur (Hand and Dirks, 1992). In this case deformation would precede or be synchronous with anatexis, and strain localization would induce melt generation. In my dissertation research I set out to investigate the role of strain-facilitated melting. Investigation of the formation of melt in high strain locations advances our understanding of how and where melt is generated, and has larger implications for the rheology and physical behavior of the mid-lower crust and the temperatures and timing of deformation within orogenic belts.

I investigated this problem over length scales of several orders of magnitude, from the kilometer down to the micron scale, through field work, studying shear zones and high-strain rocks such as mylonites, and through detailed analysis of melt microstructures, metamorphic reactions, whole rock geochemistry and mineral chemistry. I conducted this research in three field areas with contrasting metamorphic conditions, in an effort to evaluate differences between the melting mechanisms in rocks that have undergone fluid-present granite melting versus dehydration melting, in the degree of partial melting, and in the scale of the high-strain zones. The outcomes of the work are

here presented in four chapters, each written as a manuscript to be submitted to a peer-reviewed journal.

The second chapter examines similarities between the extent of partial melting within both granitic gneisses and small-scale shear zones in the Lost Creek Gneiss of the Llano Uplift, central Texas. On the outcrop scale, there is visible evidence of former melt located only within the shear zones, but a comparison of melt microstructures, chemical compositions, and modal abundances of leucosome-rich and leucosome-poor shear zones and country rocks suggests that melting has occurred uniformly across the entire area. Microstructural evidence indicates that melting occurred late in the tectonic history, based on the lack of deformation of melt pseudomorphs and the presence of former melt within shear zones formed during latest deformation; this latest partial melting was likely synchronously with widespread syn-post tectonic granite plutonism in the Llano region. This study indicates that full characterization of the partial melting process requires both detailed field and microstructural observation, not solely of the migmatite constituents expected to have hosted melt.

The third chapter examines the relationship between partial melting and deformation in the Wet Mountains of central Colorado, emphasizing a spatial and temporal association and potential feedback loop between the two processes. In the Wet Mountains, a correlation exists between the degree of strain and the amount of *in situ* partial melting. Rocks in the northern Wet Mountains are the lowest strain as evidenced by lack of recrystallization and grain elongation, and widely spaced foliations in gneisses record minor evidence of partial melting, whereas rocks in the south have experienced higher-temperature conditions, contain features indicative of abundant melt throughout the system, and are intensely deformed, with local mylonitization. Melting and deformation were synchronous in the Wet Mountains; deformation is concentrated in areas where melt-producing reactions occurred, and melt pseudomorphs appear to be localized along deformation-related features. The distribution of small-scale features, particularly the melt microstructures observed on the thin section scale, correlate well

with the larger tectonic models, which suggest minor plutonism in the north and anatexis with plutonism and pervasive crustal flow in the south.

The fourth chapter examines differences in whole rock geochemistry of five structurally distinct groups of leucosomes and pegmatites, which provide evidence for fluid-saturated and -undersaturated partial melting reactions. Granulite-facies migmatites of the Albany-Fraser Belt of southwestern Australia have undergone three phases of bidirectional extension and associated with each phase of extension are abundant leucosomes. Additionally, leucosomes are associated with each type of structure, including: foliations, shear zones, and boudins, and several large, meter wide, melt channels and late pegmatites. Major and trace element geochemistry indicates early-formed leucosomes have low SiO_2 and K_2O and high CaO contents, are consistent with in situ formation from fluid-saturated or -unsaturated amphibole-dehydration melting and may contain plagioclase accumulations. Later leucosomes have higher SiO_2 and K_2O and lower CaO compositions, reflecting fluid-absent biotite-dehydration melting and some degree of K-feldspar accumulation. Pegmatites cross-cut all other structures and earlier and later-crystallized pegmatites can be distinguished, based primarily on Ba content.

The fifth chapter presents evidence for strain-induced melting on the micron scale, using observations made from each of the three areas described in the previous chapters. I present evidence of partial melting in quartz and plagioclase along subgrain boundaries, areas of high dislocation density. This relationship indicates eutectic melting in multiple-component systems preferentially occurs in more strained areas of a crystal lattice, and although the mechanisms are different, this is consistent with observations from simpler one-dimensional systems studied in metallurgy and material science. I provide a model of how melting occurs along subgrain boundaries and propose preferential melting occurs along subgrain boundaries, as a result of enhanced diffusion rates because of pipe diffusion and water present along dislocations.

Throughout this dissertation I use many specialized terms that are applicable to migmatites and partial melting. The terminology associated with migmatites can be a bit cumbersome and confusing because various authors have used the terms in different

ways. I will follow the most common usage (after Mehnert, 1968; Johannes, 1983; Sawyer, 2008) and to minimize genetic terms. An explanation of key terms is:

- Leucosome is the felsic, light-colored portion of the migmatite, inferred to represent products of crystallized melt. It is derived from segregated partial melt and its composition is unlikely to represent anatectic melt; fractional crystallization or accumulation may have occurred.
- Melanosome is the darker, mafic portion of the migmatite equated with residual material left over after partial melting. This term can be used interchangeably with residuum.
- Neosome includes the leucosome and melanosome and refers to new material that was produced by migmatization.
- Paleosome is material that was unaffected by migmatization, commonly inferred to have an infertile composition.

  The protolith is most commonly no longer in evidence in migmatitic terrains because it has undergone migmatization and is now the neosome.
- Country rock is commonly used synonymously with both paleosome and protolith, which can create unnecessary confusion. In this dissertation, it is used to signify rocks that host leucosome and do not contain visual evidence for partial melting; they do not contain macroscopically visible leucosome material.
- Diatexites are migmatites composed primarily of neosome material, with no discrete segregations of leucosome and melanosome. Previous structural features have typically been destroyed and may have been replaced by syn-anatectic flow features. They are interpreted to represent higher melt fractions than metatexites (Sawyer, 2008).
- Metatexites are heterogeneous migmatites (at the outcrop scale), with neosome segregated into leucosome and melanosome. They are interpreted to represent melt fractions of less than 20% (Sawyer, 2008).

Perhaps the most important terms used throughout this dissertation are melt pseudomorphs and former melt. These terms are used interchangeably and are used to

describe material that is inferred to have crystallized from partial melts. The material now present in the rock does not necessarily represent the primary anatectic melt due to the ability of melt to migrate, mix and evolve in composition during the high-temperature and dynamic conditions that are sustained. They commonly represent only a snapshot of the original melt composition and extent. These terms are used throughout the dissertation, particularly in reference to the melt microstructures. When they are used to describe microstructural remnants of melt, they almost always represent a composition that has been altered by crystallization and possibly melt extraction.

Chapter 2: In situ partial melting within small-scale shear zones and adjacent country rock in the Lost Creek Gneiss, Llano Uplift, central Texas

2.1 ABSTRACT

The Lost Creek Gneiss, located in the Llano Uplift, central Texas has undergone partial melting within the country rock and small-scale shear zones synchronously with syn-post-tectonic granitic magmatism. Rocks of the Llano Uplift have undergone five phases of deformation, each defined by meter to tens of meter scale folding and an associated axial planar foliation. Sinistral small-scale shear zones, up to several m in length and 1-3 cm in width are located within the Lost Creek Gneiss of the western Uplift, where a sixth extensional phase of deformation, associated with emplacement of syn-post-tectonic granites, has been identified. Macroscopically, some of these shear zones appear to contain abundant leucosome material, as evidenced by a coarse grain size, a granular, sugary texture, a lack of well-developed foliation and a decrease in modal abundance of mafic phases. The country rock does not macroscopically appear to contain former melt, and is instead characterized by a well-developed foliation defined by elongate quartzofeldspathic material alternating with layers of biotite and amphibole.

Comparison of leucosome-rich and leucosome-poor shear zones and country rocks from two locations within the Lost Creek Gneiss show that despite marked differences in morphology identified in the field, samples from both country rocks and shear zones have the same density of melt microstructures, chemical composition and modal mineralogy. This conclusion is supported by detailed thin section analysis of types and densities of melt microstructures, modal mineralogy, and chemical analyses on plagioclase and K-feldspar. In fact, greater differences are found between the two field locations where samples were collected, than between country rock and shear zone samples. These similarities between shear zones and country rocks indicate melting occurred synchronously across the area during latest deformation, and the lack of visible deformation in melt pseudomorphs suggests this pervasive partial melting outlasted deformation.

2.2 INTRODUCTION

Anatectic migmatites are commonly found in the cores of orogenic belts, areas that have experienced both deformation and metamorphism. Many migmatites are deformed and leucosomes are found parallel to foliation (Mehnert, 1968; Brown, 1973; Sawyer, 1994; Brown and Rushmer, 1997), within shear zones (Brown, 1994; Hollister and Crawford, 1986; Allibone and Norris, 1992; Sawyer, 1994; Brown and Rushmer, 1997; Brown and Solar, 1998), axial planes of folds (Hand and Dirks, 1992; Collins and Sawyer, 1996; Brown and Rushmer, 1997) and necks of boudins (Mehnert, 1968; Allibone and Norris, 1992; Sawyer, 1994; Brown and Rushmer, 1997). This relationship has led to the interpretation that melting precedes deformation, and deformation is localized into the molten areas because they are rheologically weak (Hollister and Crawford, 1986; Brown, 1994; Brown and Solar, 1998).

Partial melting will begin at triple junctions and along grain boundaries where reactant minerals are present (Mehnert et al., 1973). Melt forms in the country rock along these grain boundaries and triple junctions and as more melt is generated, even in the absence of deformation, an interconnected melt network may form as a result of porous flow if wetting angles are appropriate, with melt fractions as low as 5% (Jurewicz and Watson, 1984, 1985; Wolf and Wyllie, 1991; Laporte et al., 1997). In an actively deforming system, melt will begin to segregate into pre-existing structures within the rock or into structures forming synchronously with partial melting (Sawyer, 1994; Brown et al., 1995; Brown and Rushmer, 1997). Melt will first segregate into smaller-scale structures, such as foliation-parallel grain boundaries and may then move into small-scale shear zones, and then larger-scale structures, eventually leading up to crustal-scale shear zones and larger granitic bodies, possibly even plutons (Solar et al., 1998).

Melt segregation has been attributed to a variety of driving forces including: surface energy (Jurewicz and Watson, 1985), volume changes due to melting reactions (Wickham, 1987; Beckerman and Viskanta, 1988; Davidson et al., 1994; Brown et al., 1995), buoyancy related to gravity (McKenzie, 1984; Wolf and Wyllie, 1991), and pressure gradients caused by applied differential stress (Robin, 1979; Stevenson, 1989;

Cooper, 1990; Sawyer, 1994; Collins and Sawyer, 1996; Marchildon and Brown, 2001; Mancktelow, 2002). Although all of these driving forces may cause segregation of melt to some degree, differential stress, which in turn leads to pressure gradients in the system, will likely have the greatest effect on widespread melt movement (Brown et al., 1995; Vanderhaeghe, 2001).

In the specific case of leucosome material within shear zones, it is generally thought that melt migrated into the shear zones because they are dilatant, low-pressure locations (Sawyer, 1994; Brown, 1994). Thus this interpretation implies that melt was generated elsewhere in the rock and migrated into the shear zone, where it crystallized. This interpretation is supported by the likely mechanism for melt segregation and the typical field observation that pseudomorphed melt is found within shear zones. In the surrounding country rocks, pseudomorphed melt is usually less abundant, although it may be located within foliation-parallel stromatic leucosomes (Brown et al., 1995; Brown and Rushmer, 1997; Brown and Solar, 1998).

In deformed migmatitic terrains many authors suggest the interpretation that a rock has experienced partial melting, is best made in the field, because migmatites are more easily identified in the field (Sawyer, 1999, 2001). In the field the leucosome, representative of the crystallized products of melting, and the melanosome, the mafic portion inferred to represent restitic material, are commonly segregated. New developments in interpretations of melting from microstructural analysis and petrographic relationships have provided additional constraints on identification of anatectic migmatites (Harte et al., 1991; Sawyer, 1999; Rosenberg and Riller, 2000; Waters, 2001; Holness and Isherwood, 2003; Barbey, 2007; Holness, 2008; Holness and Sawyer, 2008; Sawyer, 2008; Sawyer, 2010). Microstructural analysis provides a more complete picture of how melting occurred on the grain scale, and field observations constrain how segregation and transport have operated on an outcrop to kilometer scale. Analysis from the thin section to kilometer scale, allows a more thorough understanding of the melt formation, segregation and migration.

Field observations and microstructural data, however, may appear to provide conflicting information. In this chapter, I provide detailed evidence from field observations, melt pseudomorph microstructures, petrographic relationships and chemical data for partial melting occurring synchronously within both granitic gneiss country rock and small-scale shear zones of the Lost Creek Gneiss, located in the Llano Uplift, central Texas. In the field, small-scale shear zones, up to several meters in length, and approximately 1-3 cm in width, macroscopically appear to contain leucosome material, whereas the surrounding country rock does not. These shear zones formed during latest deformation (D_6) in an area that experienced protracted deformation and metamorphism attributed to continent-continent collision during the Grenville orogeny (Mosher, 1998; Hunt, 2000; Levine and Mosher, 2010). Results of this study suggest that field observations, without microstructural analysis, can be misleading and that shear zones are not only sites of melt segregation but can also be sites of melt generation.

2.3 GEOLOGICAL SETTING

The Llano Uplift of central Texas is part of the Grenville province of North America and is comprised of multiply deformed metasedimentary, metaplutonic and metavolcanic rocks intruded by syn-post tectonic granites (Figure 2.1). Deformation and metamorphism have been attributed to both arc-continent and continent-continent collision (Roback, 1996; Mosher, 1998; Mosher et al., 2008). Earliest high pressure metamorphism related to continent-continent collision occurred at eclogite-facies conditions as evidenced by relict eclogite pods, recording P-T conditions of 775° C and 2.4-1.6 GPa in the western uplift and 610-690° C and 1.4 GPa in the eastern uplift (Carlson et al., 2007). High-temperature dynamothermal metamorphism was concurrent with five phases of deformation at amphibolite-facies conditions or greater, with P-T conditions of 700° C and 0.7 GPa (Mosher, 1998; Carlson et al., 2007). Each phase of deformation (D_1-D_5) is defined by folding (F_1-F_5) and formation of an associated axial planar foliation (S_1-S_5) (Mosher, 1998, and references therein; Hunt, 2000; Levine and Mosher, 2010). Latest metamorphism was locally static and synchronous with intrusion

of syn-post tectonic granites, and P-T conditions have been interpreted to range from 525-625° C at 0.3 GPa (Carlson, 1998; Reed, 1999). The presence of granitic material within small-scale shear zones formed during D_6 deformation, suggests locally temperatures and pressures were sufficient for granite wet melting to occur (Hunt, 2000; this study). Based on opposite orientations of folds and foliations, structural stacking, and associated directions of tectonic transport, the Llano Uplift has been divided into an eastern and western portion, although the structures can be correlated across the Uplift (Mosher, 1998; Hunt, 2000; Mosher et al., 2008; Levine and Mosher, 2010).

The eastern uplift is comprised of three lithotectonic domains: 1) the Coal Creek Domain, containing serpentinites, gabbros, diorites and tonalites, interpreted as an island arc, with U-Pb crystallization ages of 1326-1275 Ma (Roback, 1996), 2) the Packsaddle Domain, made up of schists, metasediments, and quartzofeldspathic rocks, interpreted as metamorphosed basinal sediments and volcanic rocks of the continental margin, with protolith U-Pb ages of 1274-1238 Ma (Garrison, 1981; Walker, 1992; Mosher, 1993; Reese et al., 2000), and 3) the Valley Spring Domain, comprised dominantly of granitic gneisses, schists and amphibolites, a continental margin arc, with protolith U-Pb ages of 1288-1232 Ma, and one basement U-Pb age of 1366 +/-3 Ma (McGehee, 1979; Walker, 1992; Reese et al., 2000). These three lithotectonic domains are bounded by shear zones and tectonic transport is to the northeast; the Valley Spring Domain is the deepest structural domain (Reese et al., 2000). Within the eastern uplift, partial melting has been documented only at the deepest crustal levels, within the Valley Spring Domain (Hoh, 2000; Mosher et al., 2004).

The western uplift contains the Packsaddle and Valley Spring Domains, but there is no evidence of the Coal Creek Domain (Hunt, 2000). In the west, the Packsaddle Domain is dominated by schists, gneisses and metasedimentary rocks and the Valley Spring Domain is comprised mainly of granitic gneisses with minor schists and metasedimentary rocks. Between the Packsaddle Schist and the Valley Spring Domain, in the western uplift, is the Lost Creek Gneiss, a deformed porphyritic granitic pluton. All of these domains have experienced five phases of deformation that correlate with the

deformation recorded in the eastern uplift, but the structural stacking and interpreted direction of tectonic transport are opposite (Hunt, 2000; Mosher et al., 2008; Levine and Mosher, 2010). Within the western uplift all of the lithotectonic domains have undergone partial melting associated with early high-temperature deformation (Hunt, 2000; Levine and Mosher, 2010). Throughout the western uplift, late small-scale shear zones, which correlate with a D_6 period of extension likely associated with emplacement of late granites (Hunt, 2000), commonly appear to contain leucosome-material. The late leucosome-rich shear zones and surrounding country rock of the Lost Creek Gneiss, and the development of partial melt during latest deformation, are the focus of this study.

2.4 FIELD RELATIONSHIPS

Shear zones and country rock of the Lost Creek Gneiss were studied at two locations, 650 m apart, along the Llano River about 6 miles west-southwest of Castell, TX (Figure 2.1). The country rock is a granitic gneiss with a pervasive foliation, which is the dominant foliation (composite S_1-S_2) seen in the Llano Uplift (Figure 2.2A, B). Mapping by Hunt (2000) at a scale of 1:3,000-5,000 demonstrated that this foliation is folded by F_3, F_4 and F_5 folds, and subsequently cut by the shear zones. Foliation is defined by alternating bands of quartzofeldspathic material, including some K-feldspar augen, and bands of biotite +/- hornblende. Shear zones, although small and laterally discontinuous, can be identified by the sinistral foliation deflection across the zone and the appearance of leucosome material (Figure 2.2A). Many of the shear zones have variable amounts of former melt along the length of the shear zone, and as a result within any given shear zone there is commonly a leucosome-rich portion and a leucosome-poor section. Leucosome-rich shear zones are differentiated from leucosome-poor shear zones in the field, based on the macroscopic appearance of former melt. Areas that macroscopically appear to contain crystallized melt are more granular-looking, have a less well-developed foliation, are coarser-grained, richer in K-feldspar and have randomly oriented biotites (Figure 2.2A, B). These observations are consistent with criteria used to identify former melt in the field, which includes granular and sugary

textures (Sawyer, 1999, 2001). Leucosome-poor or -absent shear zones (Figure 2.2E) resemble the country rock but are distinguished by the left-lateral foliation deflection and more closely-spaced foliation. It is not possible to quantify the amount of former melt that is present in leucosome-rich or -poor shear zones, because much of the former melt likely nucleated and crystallized onto pre-existing mineral grains. As a result, the classification of shear zones as leucosome-rich or -poor, is qualitative.

Both localities along the Llano River contain small-scale shear zones, ranging from 0.5-3 m in length and 1-3 cm wide. Samples were collected at both locations by using a paleomagnetic drill, because the outcrops have water-polished surfaces and sampling with a hammer and chisel were unsuccessful. At each shear zone sampled, at least one sample was taken within the shear zone and one sample was taken within the surrounding country rock, approximately 1-3 cm away from the shear zone. The country rock sample was chosen so that it contained the same foliation as in the adjacent sample from the shear zone (Figure 2.2C-F). The core from the paleomagnetic drill is 2.5cm across and 3-6 cm in length. In all, eight different shear zones and adjacent country rock were sampled. Samples from the westernmost locality are all located within 100 m of each other (Figure 2.2C, D), whereas samples from the eastern location are all within 250 m of each other (Figure 2.2E, F).

2.5 Petrographic Analysis

All of the cores taken from within the shear zones and the surrounding country rock were prepared for thin section analysis. Twenty-three thin sections were made, with nine samples from the country rock and fourteen from the shear zones, with nine from leucosome-poor portions of shear zones and five from leucosome-rich portions. Thirteen samples are from the western locality and ten samples are from the eastern location. Each thin section was oriented as close to perpendicular to the foliation as possible. Thin sections were made to examine whether the macroscopic field observations are consistent with the microscopic details. Specifically, microstructural evidence for partial melting was analyzed to provide constraints on where the melt was originally generated, and

whether apparently leucosome-rich shear zones (as identified in the field) have different densities of melt microstructures than the surrounding country rocks and the leucosome-poor shear zones. Relationships between melt microstructures and deformation also provide constraints on the timing of partial melting relative to the polyphase deformational history of the Llano Uplift.

2.5.1 Mineral Assemblages and Associated Deformation

The country rock and leucosome-poor shear zone samples of the Lost Creek Gneiss exhibit a well-developed foliation (Figure 2.3A, B). Leucosome-rich shear zone samples do not have a well-developed foliation, and instead have a coarse, granular appearance with sparse biotite and amphibole (Figure 2.3C). In samples with a well-developed foliation, the foliation is defined by aligned biotite or amphibole alternating with moderately elongate quartzofeldspathic material.

Quartz in all samples has well-developed subgrains and many grains display chessboard extinction (Figure 2.4A), which forms because both basal and prism a-slip systems are active and is indicative of high-temperature deformation (Kruhl, 1996). Grain size of quartz varies from approximately 0.5-4 mm in diameter. Plagioclase grains are typically smaller than quartz grains, with sizes ranging from 0.2-2.5 mm in diameter. Plagioclase grains in contact with K-feldspar have rims not in optical continuity with the rest of the grain (Figure 2.4). Myrmekite is commonly found at the edges of grains (Figure 2.4B, F). Many plagioclase grains do not display internal deformation; however some have continuous undulatory extinction or development of subgrains (Figure 2.4D). K-feldspar has two common morphologies, a coarse-grained augen, up to 10 mm in diameter, typically containing plagioclase grains with well-developed myrmekite and finer grains, 0.5-2 mm in diameter. Both morphologies have well-developed microcline twinning and are perthitic (Figure 2.4B-D); K-feldspar shows continuous undulatory extinction in a few samples.

All three of these minerals can also be found as thin films along grain boundaries, as thin as 20-100 μm thick (Figure 2.4A, C-E). However, this morphology is attributed to partial melting and will be discussed in more detail in the following section.

2.5.2 Melt Microstructures

Textures related to partial melting can be difficult to identify in thin section, particularly within granitic samples when the protolith and the neosome (newly formed portion of the rock as a result of migmitization) are compositionally similar. Diagnostic features which have been attributed to the presence of partial melt and have been identified in these thin sections include: 1) cuspate or serrate grain boundaries with low dihedral angles (Harte et al., 1991; Rosenberg and Riller, 2000; Holness, 2008; Holness and Sawyer, 2008); 2) pseudomorphs of melt along grain boundaries of unlike phases (Harte et al., 1991; Sawyer, 2001) (i.e. K-feldspar between two plagioclase grains); and 3) the string-of-beads texture, where small blebs of former melt are found along grain boundaries (Holness and Isherwood, 2003) (Figure 2.4). I have also identified the presence of melt pseudomorphs along subgrain boundaries (Figure 2.4D) in quartz or plagioclase in these rocks. This texture has not been previously described, but strongly resembles melt pseudomorphs on grain boundaries. Consequently, these are the four main textures that were analyzed in each thin section.

Melt pseudomorphs and former melt are terms that are used to describe material inferred to have once been melt, but now is made up of one or more minerals. Regional metamorphic terranes are unlikely to preserve glass, but textural similarities between glass produced in experimental partial melting studies and these pseudomorphs of melt, suggest the thin films of material found along grain boundaries represent former melt. The compositions of melt pseudomorphs are unlikely to represent the melt composition at the time of crystallization. Melt pseudomorphs are typically comprised of the least abundant phases in the sample (Harte et al., 1991; Rosenberg and Riller, 2000; Holness and Sawyer, 2008), or the least abundant phase within a small area of the thin section. In a rock of granitic composition, assuming eutectic fluid-present melting is occurring, the

melt produced will have quartz, plagioclase and K-feldspar components. As this melt crystallizes, it is thermodynamically favorable for each component of the melt to crystallize and nucleate onto preexisting grains of the same composition (Harte et al., 1991; Rosenberg and Riller, 2000; Holness and Sawyer, 2008). For example, if a small pool of melt is located between quartz and plagioclase grains, the quartz component of the melt will nucleate on the quartz grains and the plagioclase component of the melt will nucleate onto the plagioclase grains. In this case, the K-feldspar component of the melt would be left to crystallize in place with sufficient undercooling, and the melt pseudomorph would be comprised entirely of K-feldspar (Holness, 2008; Holness and Sawyer, 2008).

Two other textures were identified and analyzed in these samples, but their origin is ambiguous. They are vermicular inclusion patterns (Figure 2.4B, F), dominantly, but not entirely myrmekite, and intergranular albite (Figure 2.4), which is a rim of albite on a more Ca-rich plagioclase grain, only found when plagioclase is in contact with K-feldspar. Both of these textures have been proposed to have formed as a result of partial melting (Rogers, 1961; Hibbard, 1979), but they also form in locations where there is no possibility of an anatectic origin (Phillips, 1974, 1980; Simpson and Wintsch, 1989). Myrmekite has been attributed to crystallization from a melt (Hibbard, 1979), exsolution mechanisms (after Schwantke, 1909), various sub-solidus replacement reactions between K-feldspar and plagioclase (after Becke, 1908) and as deformation assisted replacement leading to nucleation of myrmekite in more highly strained areas (Phillips, 1974, 1980; Vernon et al., 1983; Simpson and Wintsch, 1989). Similarly, formation of intergranular albite has been attributed to sub-solidus unmixing of the sodic component of K-feldspar (Tuttle, 1952; Ramberg, 1982; Carstens, 1967), replacement of K-feldspar by albite, occurring via a liquid, during late-stage crystallization (Peng, 1970) and finally synchronous formation of albite and K-feldspar in the presence of a fluid (Rogers, 1961).

2.5.2.1 Melt Microstructure Point Count Analysis

Thin sections were analyzed using a modified point counting technique, where six types of textures related to partial melting were documented and counted. The textures counted were: 1) cuspate/serrate grain boundaries, 2) pseudomorphs of melt along grain boundaries, 3) string-of-bead-texture, 4) melt pseudomorphs along subgrain boundaries, 5) vermicular inclusion patterns and 6) intergranular albite. In contrast to typical point counting where a selected number of random points are counted, the total number of melt microstructures per thin section is low, relative to the number of grains, requiring measurement of the total number of each melt microstructure in the thin section to provide a more complete dataset for microstructure statistics. Thin sections were not all the same size; they ranged from 52.5 - 85.6 mm^2, and the numbers of melt microstructure were divided by the thin section area to normalize the data for comparison. Data are given as number of microstructure per mm^2, herein referred to as melt microstructure density.

For each sample, the four main types of melt microstructure (serrate/cuspate grain boundaries, melt pseudomorphs on grain boundaries and subgrain boundaries, and string of beads texture) were summed and divided by thin section area. As each type of melt microstructure had varying abundance in any given thin section, I summed all the microstructures and divided by the thin section area to obtain a more robust estimate of former partial melt in the sample. The melt microstructure density in all samples is displayed as a histogram. In Figure 2.5A, samples from country rock are shown in light gray, leucosome-poor shear zone samples are shown white, and leucosome-rich shear zone samples are shown in black. A shear zone sample has the highest density of melt microstructures, but the second highest density comes from a country rock sample. Similarly, the country rock samples have the two lowest abundances of melt microstructures, but the third least abundant is a shear zone sample. It appears that the shear zone and country rock samples have roughly the same density of melt microstructures and that there are larger differences within each group than there are between the groups.

When the shear zone samples are evaluated as leucosome-rich and leucosome-poor samples, a slight pattern emerges (Figure 2.5A). Generally leucosome-rich shear zone samples have a slightly higher density of melt microstructures than both the leucosome-poor shear zones and the country rocks. The average density in melt microstructures per mm^2, for leucosome-rich shear zones is 2.25, whereas country rocks have 2.17 and leucosome-poor shear zones have 1.98 (Table 2.1). When all types of samples are averaged, the mean is 2.12 melt microstructures per mm^2. The samples from the eastern and western localities were also plotted (Figure 2.5B), and although there were no significant differences, the western location had a slightly higher mean value of 2.21 than the eastern location with a value of 2.00 melt microstructures per mm^2. Despite these small differences, there do not appear to be major differences in abundance of melt microstructures in any of these samples.

Microstructures not definitively tied to partial melting were also counted and the results plotted to evaluate patterns and abundances between country rocks and shear zones (Figure 2.6). The vermicular inclusions show a greater abundance in shear zones of both types than in the country rocks (Figure 2.6A). The country rocks average 2.28 vermicular inclusions per mm^2, whereas leucosome-rich shear zones have 3.54 and leucosome-poor shear zones have 3.48 vermicular inclusions per mm^2 (Table 2.1). Although there is an apparent pattern related to density of vermicular inclusions, the ambiguity of vermicular inclusions tied to partial melting and a lack of any pattern for other types of melt microstructures, suggest these differences may not be related to partial melting. The intergranular albite appears to have less of a pattern than the vermicular inclusions (Figure 2.6B). The country rock samples and the leucosome-poor shear zones have similar abundances, with averages of 14.22 and 14.45 microstructures per mm^2, respectively, whereas the leucosome-rich shear zones have greater numbers of intergranular albite, averaging 15.62 microstructures per mm^2 (Table 2.1).

2.5.2.2 Melt Microstructures and Deformation

Constraints on timing of crystallization can be related to the presence or absence of deformed melt microstructures. It can be difficult to determine whether melt microstructures are deformed because they are quite small, typically on the order of 50 μm in thickness. An additional difficulty is the fact that many pseudomorphs of melt are now present as microcline, and it can be difficult to differentiate undulatory extinction from twinning on such small blebs of material. Many of the melt microstructures are undeformed, but there are some examples with undulatory extinction. Deformed melt pseudomorphs are less abundant than undeformed melt pseudomorphs, and even when these pseudomorphs display undulatory extinction it is only incipiently developed. None of the former melt is pervasively deformed. Electron backscatter diffraction (EBSD) could help determine whether the melt pseudomorphs are deformed, by looking at crystallographic orientation across each melt pseudomorph.

Some previous studies on melt pseudomorphs have found an association between the spatial orientation of the pseudomorphs and either foliations or lineations within the rock (Sawyer, 2001; Marchildon and Brown, 2002, 2003; Hasalova, 2008). Despite the presence of a fairly well-developed foliation in the Lost Creek Gneiss, no evidence suggests a spatial orientation relationship between melt pseudomorphs and foliation. Pseudomorphs of melt are commonly found along grain boundaries, but because of earlier recrystallization during D_1-D_5 deformation and modification of the grain boundaries during the melting process, the grain boundaries tend to be irregular and not all parallel or perpendicular to the main foliation orientation in these rocks.

2.5.2.3 Melt Pseudomorph Compositions

Within samples from the Lost Creek Gneiss, compositions of melt pseudomorphs were totaled during the melt microstructure point counting process. The string of beads melt microstructure was the only one of the four main types of melt microstructures where it was not possible to determine the composition of melt pseudomorphs. For the other three main types of microstructures, in addition to counting the number of each type

of microstructure, the composition of both the melt pseudomorphs and minerals adjacent to pseudmorphs were recorded.

The serrate/cuspate grain boundaries are by far the most abundant type of microstructure, generally comprising 60% of the total of the four primary melt microstructures. Serrate/cuspate grain boundaries occurred between all phases in the samples; one of the phases was K-feldspar in 80% of the counted microstructures, plagioclase in 77% of samples, and quartz in only 40% of samples (Table 2.2). These percentages do not total 100% because in every serrate/cuspate melt microstructure there are at least 2 phases involved. Melt pseudomorphs on grain boundaries are the next most abundant microstructure (roughly 25%). In this case 77% of the former melt is comprised of K-feldspar, 3% is plagioclase and 2.5% is quartz (Table 2.2). The unaccounted for 17.5% is unknown; many of the melt pseudomorphs are too small to accurately determine composition without obvious twinning. All of the unknown 17.5% are either quartz or feldspar. Melt pseudomorphs on subgrain boundaries make up 13.4% of the melt microstructures and the pseudomorph compositions are 69% K-feldspar, 9% plagioclase and 1.5% quartz (Table 2.2). The remaining 20.5% is unknown, again with all of the pseudomorphs comprised of either quartz or a feldspar, but too small to definitively determine. The string of beads texture, by definition, consists of small blebs of melt along grain boundaries, and when seen in these rocks, it was nearly impossible to determine which minerals formed the "beads." However, in these samples, this texture only made up 1.4% of the four main melt microstructures.

2.5.3 Modal Mineralogy

Modal mineralogy was estimated via point counting, to determine whether macroscopic and microscopic observations are consistent and whether there are chemical differences between country rock and shear zone samples. Each thin section was point counted, with a minimum of 200 points counted. In hand sample and thin section there did not appear to be any major differences in mineralogy between the three types of

samples: leucosome-rich shear zones, leucosome-poor shear zones, and country rocks, but the point counting was done to provide a quantitative estimate for each sample.

All samples have the assemblage plagioclase + quartz + microcline + biotite + amphibole. Although some variation exists in the samples, when all samples are averaged the mean abundances are: 33.9% plagioclase, 31.5% quartz, 27.3% microcline, 4.1% biotite, 2% amphibole and 1.1% accessory phases, including: epidote, Fe-oxides, titanite, apatite and chlorite (Table 2.3). Despite the presence of biotite and amphibole, partial melting occurred as a result of fluid-present granite eutectic melting. Biotite and amphibole have idioblastic habits and do not have corroded or skeletal morphologies, suggesting they did not dehydrate as part of a partial melting reaction (Sawyer, 1999, Waters, 2001; Barbey, 2007). Instead, the likely reaction is:

$$\text{Quartz} + \text{Plagioclase} + \text{K-feldspar} + H_2O = \text{Melt}.$$

Samples were evaluated by type, with averages calculated for samples from leucosome-rich shear zones, leucosome-poor shear zones and country rocks as well as by location, with the eastern and western localities separated. All mineral mode data and range in composition is shown in Table 2.3.

Shear zone samples have slightly higher (8%) abundances of accessory phases, including Fe-oxides, epidote, chlorite, titanite and epidote, but the most abundant phases are within 5% of the average values. When shear zones are divided into leucosome-rich and leucosome-poor zones there are some slight deviations from average. The leucosome-poor shear zones have plagioclase, quartz and microcline values that are within 5% of average, but biotite and amphibole are enriched by 7% and 17% respectively. Leucosome-rich shear zones contain average amounts of plagioclase and quartz, but are enriched in microcline, with 12% greater than average. Microcline present within leucosome-rich shear zones is typically the finer-grained morphology, 0.5-2 mm in diameter; coarse-grained augen are not abundant. Biotite and amphibole have lower abundances in leucosome-rich shear zones; biotite is 29% less abundant and amphibole 23% less abundant than average. However, accessory phases have a 22% increase from average.

Country rock samples also have values that are very close to the average for all Lost Creek Gneiss samples. The major phases: quartz, plagioclase and microcline, are all consistent with average values, whereas biotite is more abundant in the country rock with an increase of 9% from average. Accessory phases are less abundant in the country rock, with a decrease of 12%.

When samples are evaluated by locality, much greater deviations from average modal abundances are observed, with all phases differing from average by more than 5%. All rock types from the westernmost location contain less plagioclase, biotite, amphibole, and accessory phases and have more quartz and microcline than average. These western samples contrast with all rock types from the eastern locality and each individual group, separated out by rock type: leucosome-rich shear zones, leucosome-poor shear zones, country rocks; these all have plagioclase as the most abundant phase, however in all westernmost rocks, evaluated as a group, quartz is the most abundant phase.

2.6 MINERAL CHEMISTRY

Microprobe mineral analyses were conducted on a JEOL JXA-8200 at the University of Texas at Austin. The operating conditions were 15 kV accelerating voltage, a 10 nA beam current, a spot size of 5 μm and counting times were 20 s for peaks and 10 s for backgrounds.

Chemical data are consistent throughout the field area, although the eastern and western field sites appear to have very slight differences in composition of plagioclase and K-feldspar. Minerals from samples within the shear zones are compositionally identical to samples from the surrounding country rock. The western location, sample numbers LCG-5 to LCG-17, contains plagioclase cores that are slightly more albitic, and K-feldspar that is more orthoclase-rich than at the eastern location (Table 2.4). In this location, plagioclase compositions range from An_9 to An_{14} in the core and have nearly pure albite rims with compositions of An_{0-2}, wherever plagioclase is in contact with K-feldspar. Cores of plagioclase grains with albitic rims, and plagioclase grains not in contact with K-feldspar, have the same anorthite contents, with a composition of An_{9-14}.

K-feldspar also has fairly uniform compositions, with typical compositions of $Orth_{91-97}$ (Table 2.4). The K-feldspar is perthitic and albite lamellae are abundant within the microcline.

At the eastern location, sample numbers LCG-18 to LCG-27, have compositions similar to those in the western location, but the plagioclase is slightly more anorthitic and the K-feldspar has slightly lower orthoclase contents (Table 2.4). The plagioclase composition in the core of the grains typically ranges from An_{13} to An_{17}, again with albitic rims ranging in composition from An_{0-2}, and the K-feldspar has compositions that range from $Orth_{90-95}$. Perthitic K-feldspar in this location also contains abundant albite lamellae.

2.7 DISCUSSION

Microstructural, chemical and mineralogical data from granitic gneisses within the Lost Creek Gneiss of the Llano Uplift, central Texas, indicate partial melting occurred synchronously within shear zones and surrounding country rock syn- to post-D_6. Although microscopic evidence of former partial melt is consistent across the area, macroscopic observations show evidence of former partial melt only in some shear zones. These zones contain quartzofeldspathic material with equigranular grains, a sugary texture, a coarse grain size, low modal amounts of biotite and amphibole, and a lack of obvious foliation. Country rock and leucosome-poor shear zone samples have a pervasive foliation and a finer grain size than leucosome-rich shear zones and lack a granular and sugary texture.

These types of field observations have led previous workers to two possible interpretations. The first, most widely held interpretation is that melting occurred in the country rock, and differential stress acting on these rocks caused melt to flow out of the country rock, perhaps along foliation planes, into larger structures, such as the small-scale shear zones where some of the melt crystallized (Sawyer, 1994; Brown, 1994). The second interpretation is that melting occurred preferentially within the shear zones, because shear zones act as conduits, and fluids preferentially migrated into the system

through the shear zones resulting in partial melting (Mogk, 1992; Slagstad et al., 2005, Hasalova et al., 2008). Either of these processes may have taken place and affected the partial melting and/or subsequent transport of material, but neither interpretation explains the same types and amount of melt microstructures within the country rock and leucosome-poor shear zones as in the leucosome-rich shear zones.

Based on the data collected, I propose that melting occurred within country rocks and shear zones synchronously during syn- to post-tectonic granitic magmatism. Melt microstructures within country rocks and both leucosome-rich and leucosome-poor shear zones have some variability in density of microstructures, but there are larger differences within each group than between the groups (Table 2.1). The four main types of melt microstructures all provide evidence for melt pseudomorphs present within the system, but in granitic rocks it is difficult to differentiate former melt that migrated through the system and former melt that formed in situ. In granitic wet melting, the reactant minerals are compositionally the same as the product liquid. Upon crystallization these phases are both solid and consequently they are compositionally similar.

Nonetheless, the types and orientations of melt microstructures seen in the Lost Creek Gneiss provide strong evidence for melting in situ. First, the presence of melt pseudomorphs along subgrain and grain boundaries, and the absence of large pores or extended networks of former melt, suggests that melt was not travelling to any great extent along grain boundaries and that textural equilibrium was not reached between the melt and solid phases (Holness, 2008; Holness and Sawyer, 2008). These thin films of melt pseudomorphs, particularly those present along unlike grain boundaries (likely reactant grains), may indicate both formation and crystallization in situ (Holness and Sawyer, 2008). Secondly, there is no preferred orientation to the melt microstructures; they are not found either parallel or perpendicular to the main foliation in the rock, implying that they did not travel to their current location as a result of deformation or differential stress gradients in the rock (e.g. Sawyer, 2001). In migmatites where melting occurred synchronously with shearing, structures containing former melt were found perpendicular to elongation direction (Rosenberg and Riller, 2000; Sawyer, 2000;

Marchildon and Brown, 2003), and in rocks undergoing contraction, leucosome material is typically found parallel to foliation (Brown and Rushmer, 1997; Sawyer, 2001; Vernon and Paterson, 2001). The absence of both of these preferred orientations for structures containing melt pseudomorphs, suggests the partial melting process occurred in the absence of deformation, and thus melt pseudomorphs likely represent original locations of partial melting.

The presence of similar densities, morphologies, and chemistries of melt microstructures within country rocks and leucosome-rich and leucosome-poor shear zones indicates that melting occurred uniformly across the area, and specifically that melt was generated within all locations. Differences in chemistry and modal mineralogies between the eastern and western field sites, suggests there is some variation in composition of the Lost Creek Gneiss. The compositional differences between locations are larger than any differences between shear zones and country rocks, which suggests the processes occurring within shear zones and country rocks have only a minor effect on mineral chemistry or modal abundances.

The presence of higher modal amounts of microcline within leucosome-rich shear zones is unlikely to be related to the very latest melting, because there is no increase in melt pseudomorphs that are now crystallized as microcline. Instead, the increased abundance in microcline is of the fine-grained morphology, 0.5-2 mm in diameter. This increased abundance of microcline could be related to melting that led to the macroscopically visible former melt, seen only within leucosome-rich shear zones.

Increased density of vermicular inclusions within shear zones compared to country rocks is unlikely to be related to partial melting. Vermicular inclusions, specifically myrmekite, have not been clearly tied to partial melting. The increased density of vermicular inclusions within shear zones of all types could provide evidence for the role of strain in nucleating myrmekite. Also an increase in vermicular inclusion density in the eastern location could be explained by an increased amount of plagioclase there. Plagioclase is typically the host phase for the vermicular inclusions, so the higher modal abundance of plagioclase in the east could explain this increased density.

However, no significant difference in modal abundance of plagioclase exists between country rock and shear zone samples. In fact, country rock samples have an intermediate modal abundance of plagioclase between leucosome-rich and leucosome-poor shear zones (Table 2.3). Consequently, the best explanation appears to be that higher strain within the shear zones led to strain-induced nucleation of myrmekite as suggested by previous authors (Phillips, 1974, 1980; Simpson and Wintsch, 1989).

Differences in melt microstructure density between leucosome-rich and leucosome-poor shear zones is more likely to result from sampling bias than a difference reflecting partial melting processes. Only five samples from leucosome-rich shear zones were point counted, whereas nine samples each from country rocks and leucosome-poor shear zones were point counted to determine melt microstructure density. Leucosome-poor shear zones have a wider range in melt microstructure density than either country rocks or leucosome-rich shear zones. If more samples from leucosome-rich shear zones were collected, there might be a similar range in melt microstructure density as seen in samples from leucosome-poor shear zones. However, if there really is a difference in greater density of melt microstructures within leucosome-rich than leucosome-poor shear zones, it would provide more support for a protracted partial melting event synchronous with shear zone formation and some melt migration into dilatant shear zones.

One puzzling observation is still the presence of macroscopically abundant melt within some shear zones and in no other locations. Detailed observation of the melt microstructures within these leucosome-rich shear zones clearly shows the exact same melt microstructures as those found within country rocks. Specifically within the texturally more coarse-grained, granular locations, there are still very fine pseudomorphs of melt along grain boundaries.

Three possible explanations for the macroscopically visible former melt present within some shear zones and not others, coupled with the similarity in abundance of melt microstructures within country rocks and all shear zones, include: 1) During partial melting across the area, minor amounts of melt migrated into some slightly dilatant shear zones as they were forming, producing the leucosome-rich zones and giving rise to the

minor enrichment in microcline. The microstructures in the leucosome-rich shear zone samples represent the last stages of crystallization of this melt but are similar in character to those observed in the rest of the rock. 2) An earlier episode of partial melting occurred either within some shear zones or within the country rock and migrated into some of the shear zones, causing the coarse granular texture in the leucosome-rich zones. Subsequently another episode of partial melting occurred across the area, and the observed melt microstructures found within all rock types record melting that postdates the formation of the shear zones and earlier localized melting or melt migration. 3) Melting occurred synchronously within shear zones and country rocks during and after latest deformation. Some shear zones were more dilatant than others and acted as accumulation sites for partial melt (leucosome-rich shear zones), whereas others were less dilatant and did not accumulate melt (leucosome-poor shear zones). Temperatures likely hovered near the melting temperature, and crystallization and subsequent remelting of leucosome material within the shear zones, led to formation of the delicate melt microstructures within the shear zones.

The similarity in microstructures throughout, suggests the melting seen across the area postdates formation of the macroscopic former melt within shear zones or that repeated crystallization and remelting occurred, as a result of fluctuations above and below the melting temperature. The third hypothesis seems most consistent with the field and microstructural observations, and requires only one extended melting phase. It also accounts for the possibility that early in the process some melt migrated from the country rock into dilatant shear zones and crystallized there. Regardless of which hypothesis may be correct, the widespread melt microstructures provide timing constraints on the melting, because the shear zones formed during a D_6 period of extension, which has been proposed to be synchronous with intrusion of syn-post tectonic granites (Hunt, 2000).

The Lost Creek Gneiss is multiply deformed and if melting had occurred earlier in the deformation history of these rocks, it would be expected that leucosome material would parallel the main foliation. Partial melting that occurred during D_2 and D_3 deformation throughout the Llano Uplift is characterized by foliation-parallel stromatic

leucosomes (Hoh, 2000; Hunt, 2000; Levine, 2005; Mosher et al., 2004; Levine and Mosher, 2010). The absence of these types of leucosome-rich structures in this location, suggests that melting occurred very late and melt migration of any significance was unlikely to have been caused by deformation. Also, if melting had occurred earlier in the deformational history of the area, it is unlikely that such delicate microstructures would still be preserved. Recrystallization was pervasive during earlier deformation, so thin films of former melt along grain boundaries and subgrain boundaries would not have lasted through such intense deformation. In fact, most of the melt pseudomorphs appear undeformed or display only weak undulatory extinction, suggesting partial melting occurred during very latest deformation and outlasted it.

2.8 CORRELATIONS WITH REGIONAL PLUTONISM

Within the Llano Uplift, abundant granitic plutons formed syn- to post-tectonically (Walker, 1992; Mosher, 1998; Reed, 1999). Several of the plutons are deformed and have a well-developed foliation, but others do not show any fabric (Reed, 1999). The Lost Creek Gneiss is located within the western uplift proximal to several plutons as well as smaller dikes and granitic bodies (Figure 2.1). The timing of the partial melting that occurred within shear zones and country rocks of the Lost Creek Gneiss appears synchronous with the latest syn- to post-tectonic granitic plutonism in the area. This synchronicity in timing of partial melting and plutonism suggests these processes are related.

Small-scale shear zones formed during D_6 extension, which locally contain leucosome material, are present within all three units of the western uplift (Hunt, 2000). Additionally, the Valley Spring Gneiss in the western uplift also shows evidence of late partial melting (Levine and Mosher, 2010). Thus it seems likely that syn-to post-tectonic partial melting was widespread across the western uplift, and a link exists between latest anatexis and migmatization and larger-scale plutonism.

Isotopic and whole rock geochemical studies on syn-post-tectonic granitic plutons within the Llano Uplift suggest that some of the plutonism in the Llano region is related

to anatexis of the surrounding country rocks (Smith et al., 1997, 2010). Additionally, the lack of mafic rocks, regional homogeneity in composition of granitic plutons, and the widespread syn-post-tectonic Llano plutonism suggests some input from partial melting of crustal rocks (Smith et al., 1997, 2010). However, another recent study (Barker and Reed, 2010) has suggested that the post-tectonic Llano granites are derived from Proterozoic mantle and lower crust on the basis of Sr, Nd and Pb isotopic data. Despite these differences in opinion on the source of the Llano granites, post-tectonic melting whether in the form of local anatexis, or widespread plutonism, is likely related to the same heat source. Mosher et al. (2008) proposed the syn-post tectonic juvenile granites were related to slab breakoff and subsequent asthenospheric upwelling. This source of heat for production of syn-post tectonic granites would also provide heat for local anatexis.

2.9 CONCLUSIONS

Melt microstructures present both in the shear zones and in the country rocks of the Lost Creek Gneiss are the same. Both types of samples show serrate/cuspate grain boundaries, string of beads texture, and melt pseudomorphs present along grain boundaries and subgrain boundaries in quartz and rare feldspars. Macroscopically, the two types of samples do look different. In the field, shear zones clearly show areas of coarser grain size with equigranular and sugary textures and have less biotite and amphibole; no specific foliation plane can be traced across the shear zone. However, density, morphology, modal abundance, and chemistry of melt microstructures in leucosome-rich and leucosome-poor shear zones and in country rocks are the same. All of this data indicates both the shear zones and the country rock experienced melting synchronously.

Partial melting must have occurred during latest deformation and outlasted it based on timing of shear zone formation during a D_6 period of extension and shearing and because of a lack of deformation or only minor deformation of the melt

microstructures. Also, the delicate textures of the melt microstructures would not be preserved through multiple phases of penetrative deformation.

Finally, results from this study suggest that field observations alone are insufficient to determine a partial melting history in migmatitic terrains. Melt microstructures are important for understanding the full melting history of a rock and without detailed structural and petrographic analysis, erroneous conclusions may be reached.

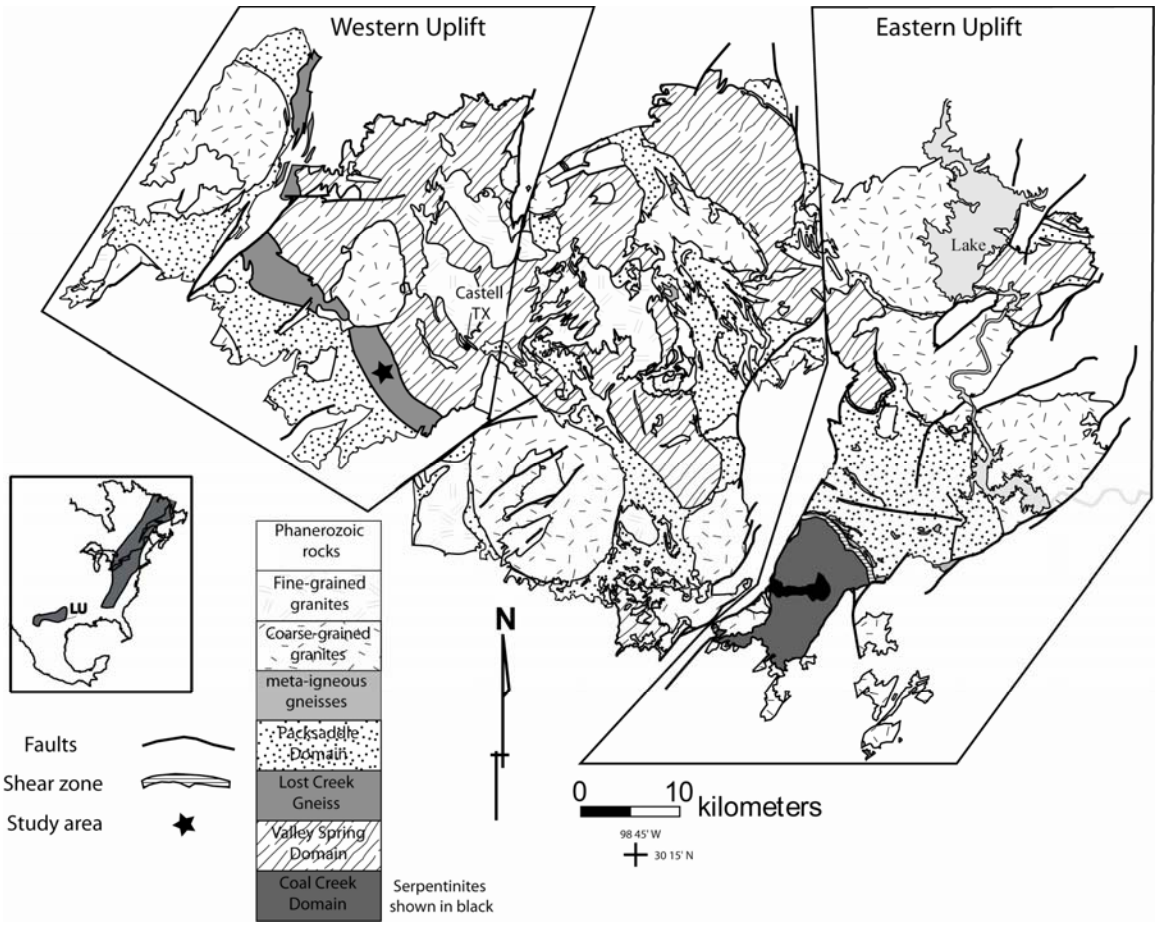

Figure 2.1. Geologic map of the Llano Uplift, central Texas (after Barnes, 1981); inset shows location of Grenville-aged exposures. Boxes represent boundaries of the eastern and western portions of the uplift and are bounded by Paleozoic faults. The star represents the study location within the Lost Creek Gneiss.

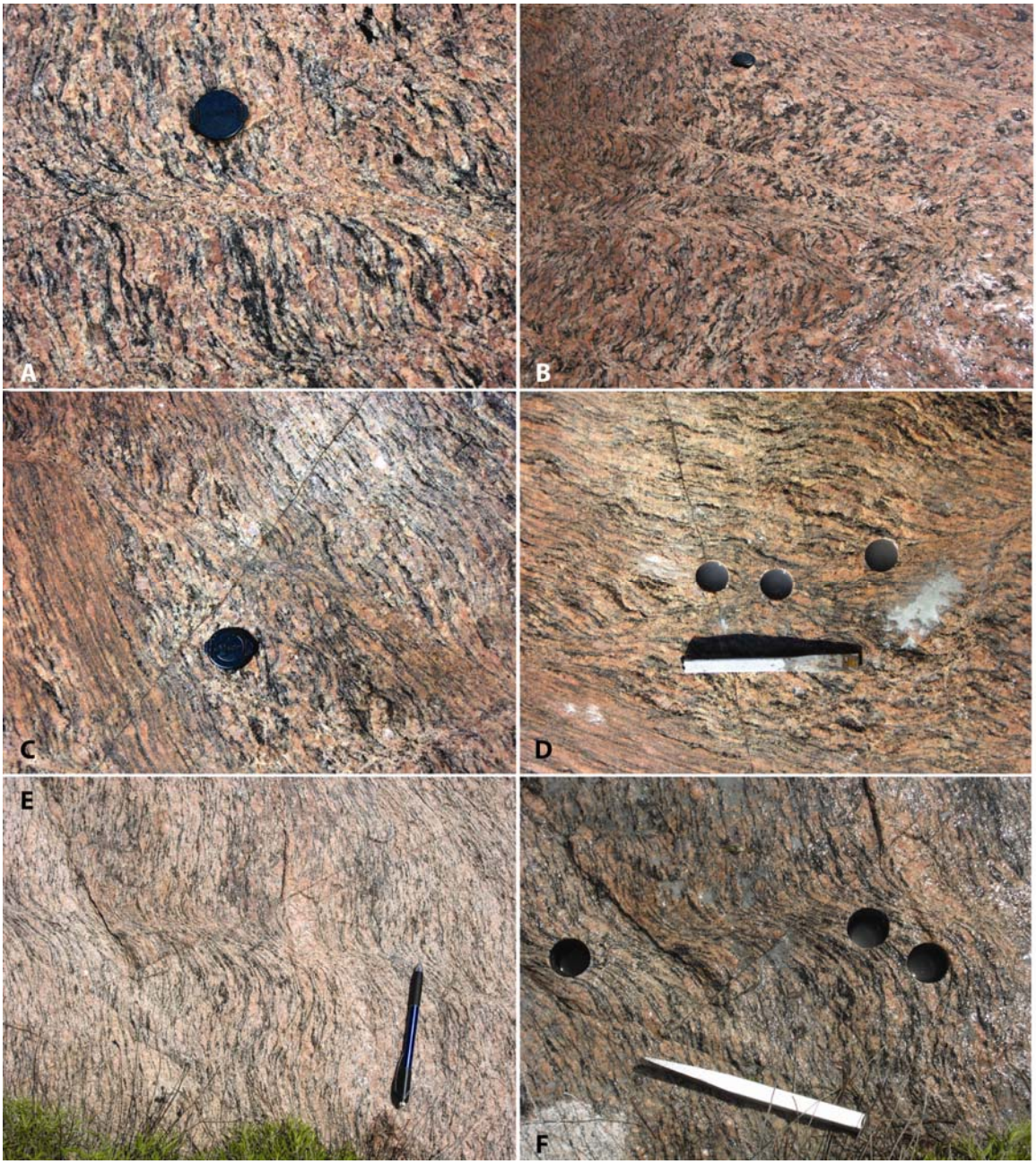

Figure 2.2. (continued on next page). Field photographs of the Lost Creek Gneiss. A. A small-scale shear zone within the Lost Creek Gneiss with sinistral offset. Within the shear zone macroscopically visible former melt is interpreted, as evidenced by granular, sugary, coarse-grained texture and lack of foliation within the shear zone. The composite S_1-S_2 foliation within the country rock is defined by alternating layers of biotite/amphibole and quartzo-feldspathic material. B. Pavement surface with a few small-scale shear zones present with sinistral offset and macroscopically visible former melt within the shear zones.

C. One of the sample locations in the western field area with some macroscopically visible former melt within the shear zone, but variable amounts of former melt along the length of the shear zone. D. Same area as in C, but after paleomagnetic cores had been taken. The two samples on the right side of the photo were taken within the shear zone; the far right is a leucosome-rich portion of the shear zone, the more central sample is a leucosome-poor portion of the shear zone, and the one on the left is a sample within the country rock. The chisel is approximately 15 cm long. E. A sample location from the eastern field area. This is the only photo that is not taken when the surface was wet. There are variable amounts of interpreted macroscopic former melt along the length of the shear zone. F. Same area from E, but after paleomagnetic cores had been taken. The sample on the far right of the photograph is from the country rock and both of the other samples come from leucosome-poor portions of the shear zone. The chisel is approximately 15 cm long.

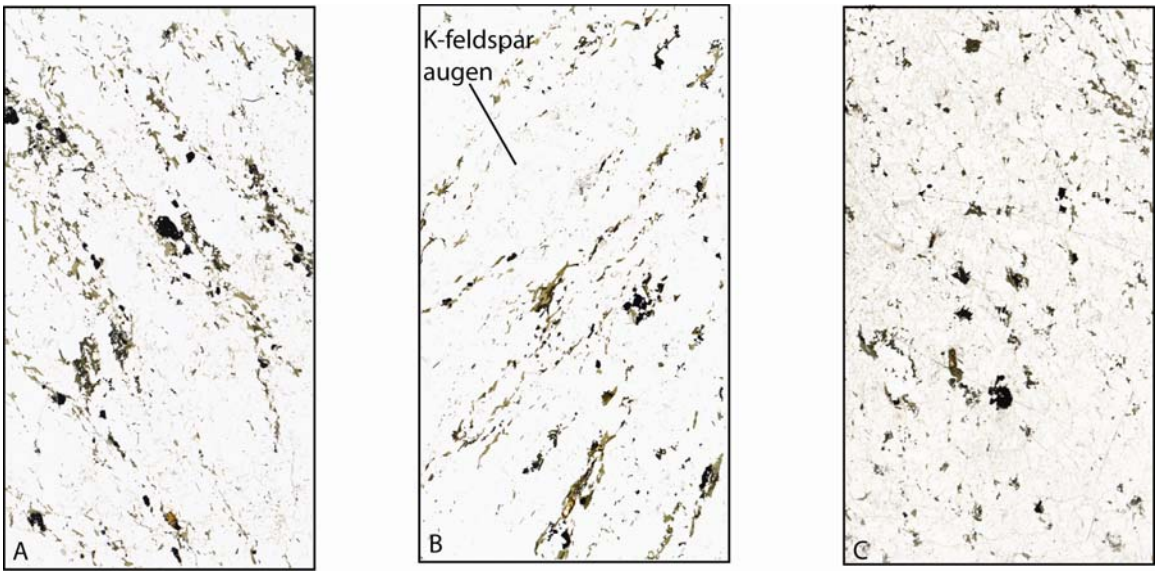

Figure 2.3. Plane-polarized scans of thin sections. A. Sample taken from the country rock. Alternating layers of quartzofeldspathic material and biotite/amphibole rich layers that define the composite S_1-S_2 foliation seen throughout the uplift. B. Sample taken from a leucosome-poor shear zone. Here the composite S_1-S_2 foliation is again visible and a K-feldspar augen is visible towards the top left of the thin section. C. Sample taken from a leucosome-rich shear zone that lacks foliation, and contains randomly oriented biotite and amphibole and a more granular texture. In the top right of the thin section, a sliver of country rock is visible and it has a much more developed preferred orientation of minerals defining a foliation.

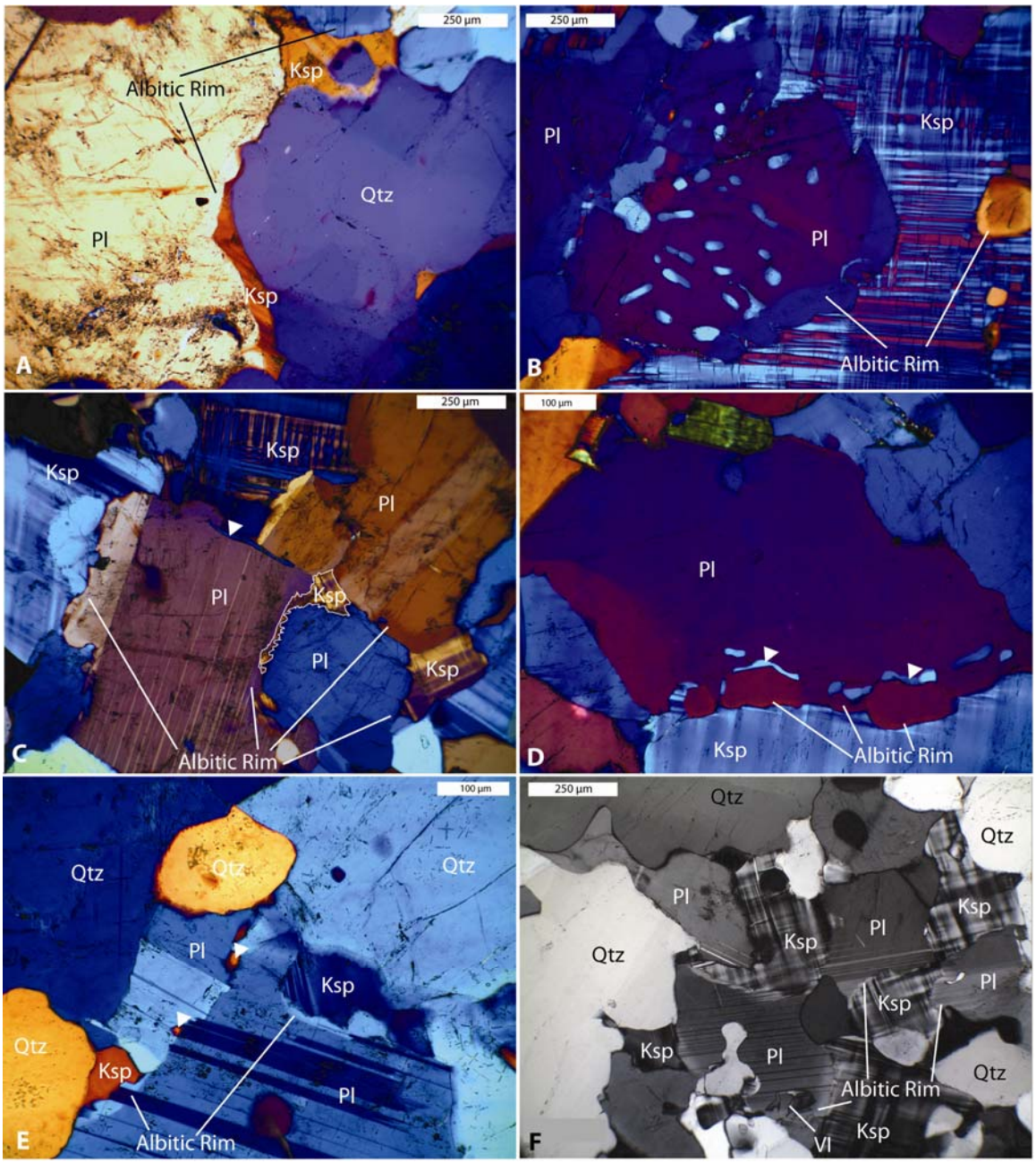

Figure 2.4. (continued on next page). Photomicrographs of melt microstructures from leucosome-rich shear zones (A and B), leucosome-poor shear zones (C and D), and country rocks (E and F). The melt microstructures are similar within all of the different types of samples. All photomicrographs are taken with the gypsum plate inserted, except for F, which is taken in crossed polarized light. Ksp = K-feldspar, Pl = Plagioclase, and Qtz = Quartz. A. An interpreted melt pseudomorph (now K-feldspar – orange in color) along a grain boundary between quartz and plagioclase. The plagioclase grain has albitic rims (paler than the rest of the grain). The former melt along the grain boundary appears

to be optically continuous with former melt present at a quadruple junction at the top center of the photomicrograph. Plagioclase and quartz in contact with the melt pseudomorph have serrate/cuspate grain boundaries and chessboard extinction is visible in quartz. B. A grain of plagioclase that has a vermicular texture, with quartz as the vermicular phase. Intergranular albite is found on plagioclase grains adjacent to K-feldspar and the edges of the plagioclase grain are cuspate. C. Former melt (now K-feldspar) found along grain boundaries and at a triple junction between grains of plagioclase. This former melt is outlined in white and plagioclase grains adjacent to this melt pseudomorph have serrate/cuspate grain boundaries. A bleb of former melt (blue in color, now likely quartz) is marked by a white triangle, along a grain boundary between K-feldspar and plagioclase. Plagioclase adjacent to K-feldspar has albitic rims. D. A melt pseudomorph (now K-feldspar) along subgrain boundaries in plagioclase (marked with white triangles). Intergranular albite is present on the edges of plagioclase (now orange in color) in contact with K-feldspar. E. Melt pseudomorphs (marked by white triangles) along grain boundaries between plagioclase grains. Former melt (now K-feldspar) in slightly larger pools is also found along grain boundaries and at triple junctions between quartz and plagioclase. Intergranular albite is present when plagioclase is in contact with K-feldspar. F. Serrate/cuspate grain boundaries between plagioclase and K-feldspar grains and between quartz and K-feldspar grains (left side of photomicrograph). Intergranular albite is present on plagioclase in contact with K-feldspar. Vermicular inclusion patterns (labeled as VI) are present in plagioclase grain in the center bottom of the photomicrograph.

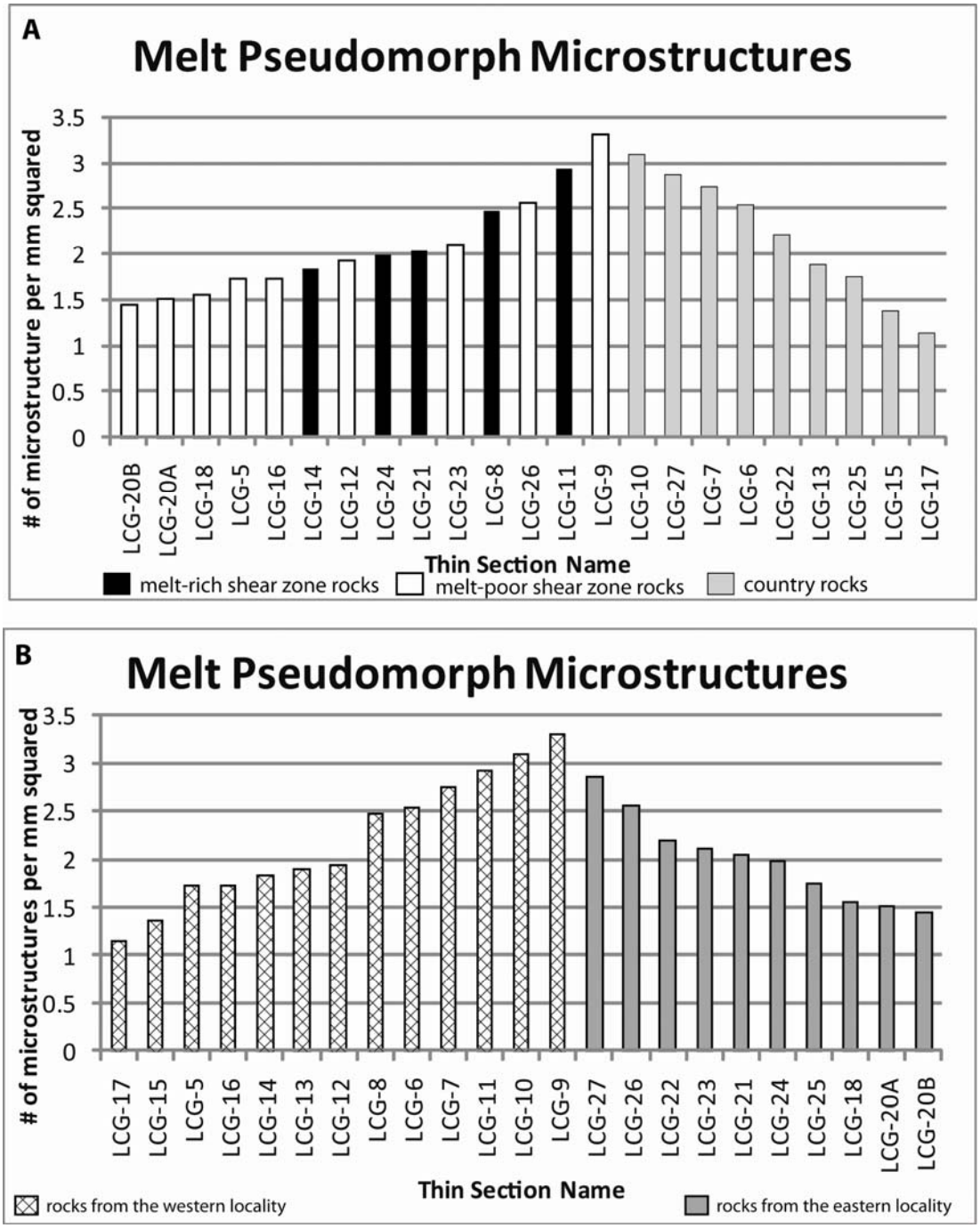

Figure 2.5. A. Histogram of melt microstructure density in number of melt microstructures per mm^2 (including serrate/cuspate grain boundaries, former melt on grain boundaries and subgrain boundaries, and string-of-beads texture). Leucosome-rich shear zones are black, leucosome-poor shear zones are white and country rocks are in light gray. B. Histogram of microstructure density in number of melt microstructures per mm^2, divided between eastern (gray) and western (cross-hatched) localities.

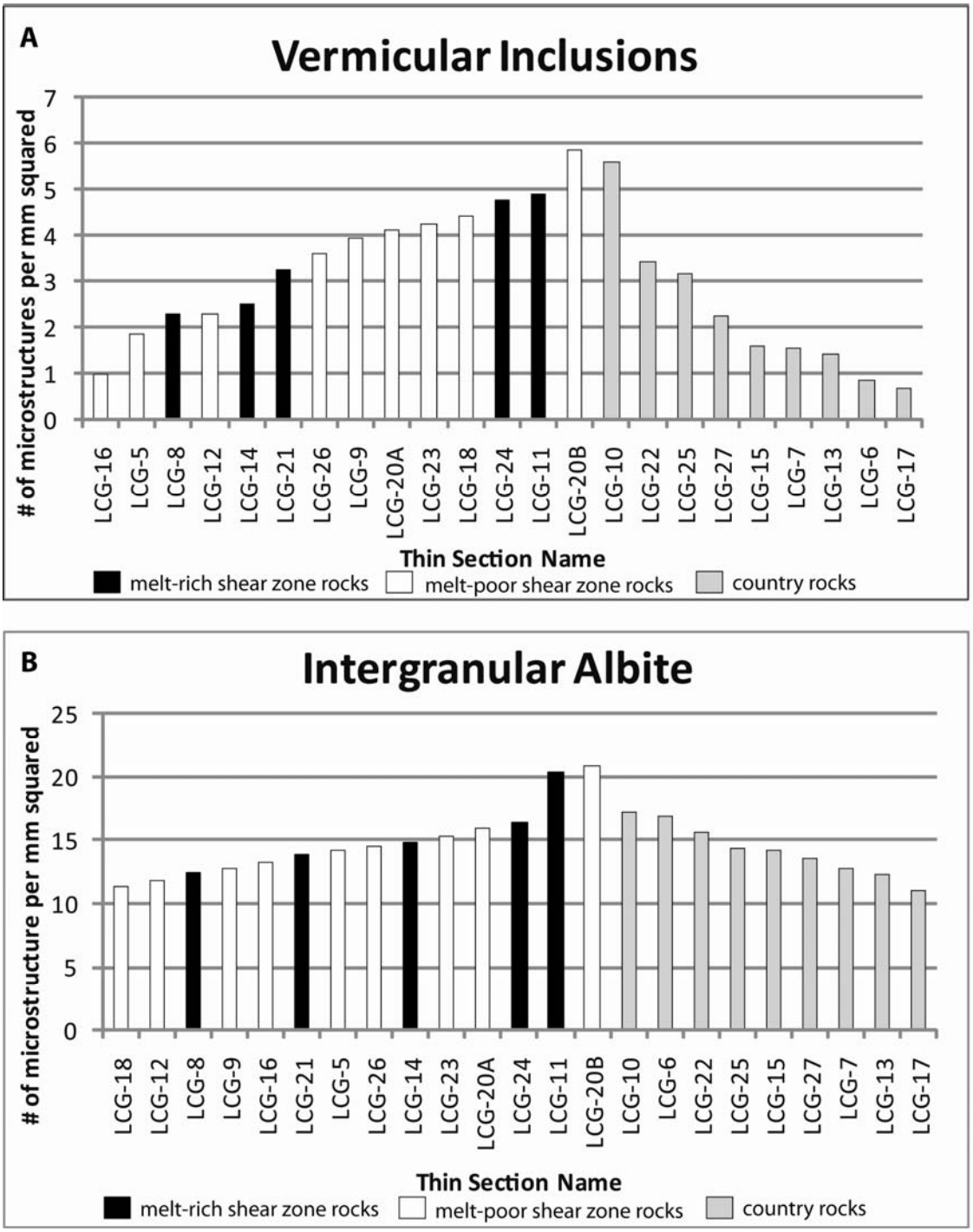

Figure 2.6. A. Histogram of vermicular inclusion density in number of melt microstructures per mm^2 in leucosome-rich shear zones (black), leucosome-poor shear zones (white) and country rocks (light gray). B. Histogram of intergranular albite density in number of melt microstructures per mm^2 in leucosome-rich shear zones (black), leucosome-poor shear zones (white) and country rock (light gray).

Table 2.1: Melt Microstructure Point Counting Average and Range for All Rock Types

		Combined Primary Melt Microstructures*	Vermicular Inclusions	Intergranular Albite
All Samples	Average (per mm squared)	2.1	3.0	14.6
	Range (per mm squared)	1.1-3.3	0.7-5.9	11.1-20.8
Country Rocks	Average (per mm squared)	2.2	2.3	14.2
	Range (per mm squared)	1.1-3.1	0.7-5.6	11.1-17.2
All Shear Zones	Average (per mm squared)	2.1	3.5	14.9
	Range (per mm squared)	1.4-3.3	1.0-5.9	11.3-20.8
Melt Rich Shear Zones	Average (per mm squared)	2.3	3.5	15.6
	Range (per mm squared)	1.8-2.9	2.3-4.9	12.4-20.4
Melt Poor Shear Zones	Average (per mm squared)	1.9	3.5	14.5
	Range (per mm squared)	1.5-3.3	1.0-5.9	11.3-20.8
Eastern Locality	Average (per mm squared)	2.0	3.1	15.2
	Range (per mm squared)	1.5-2.9	2.2-5.9	11.3-20.8
Western Locality	Average (per mm squared)	2.2	2.4	14.2
	Range (per mm squared)	1.1-3.3	0.7-5.6	11.1-20.4

* The 4 primary melt microstructures are serrate/cuspate grain boundaries, melt on grain boundaries, melt on subgrain boundaries and the string-of-beads texture. For this column they are combined.

Table 2.2: Mineralogical Breakdown of Melt Microstructures

	Serrate/Cuspate Grain Boundaries	Relict Melt on Grain Boundaries	Relict Melt on Subgrain Boundaries	String-of-Beads Texture
Percentage of Total Melt Microstructures	59.9	25.4	13.4	1.4
One of phases involved is K-feldspar	80.3			
One of phases involved is Plagioclase	77.4			
One of phases involved is Quartz	40.7			
K-feldspar is relict melt		77.2	69.2	
Plagioclase is relict melt		3.0	9.0	
Quartz is relict melt		2.5	1.5	
Unknown phase is relict melt		17.3	20.4	

		Plagioclase	Microcline	Quartz	Biotite	Amphibole	Other
Average of all data	Average (%)	33.9	27.3	31.5	4.1	2.0	1.3
	Range (%)	22.6-45.9	12.2-36.5	21.5-44.5	1.2-7.9	0-4.9	0-3.3
All Shear Zones	Average (%)	34.1	28.2	30.3	3.9	2.1	1.4
	Range (%)	22.6-45.9	20-36.5	21.5-38.7	1.9-7.1	0-4.9	0-3.3
	Difference from average (%)	0.7	3.6	-3.6	-5.9	2.7	7.8
Melt Poor Shear Zones	Average (%)	34.9	26.9	30.1	4.4	2.4	1.3
	Range (%)	22.6-45.9	20-36.3	21.5-38.7	2.0-7.1	1.0-4.9	0-2.9
	Difference from average (%)	3.0	-1.2	-4.2	6.9	17.1	0.2
Melt Rich Shear Zones	Average (%)	32.7	30.6	30.7	2.9	1.6	1.5
	Range (%)	27.2-42.4	21.0-36.5	25.3-35.6	1.9-5.1	0-3.0	0.9-3.3
	Difference from average (%)	-3.4	12.2	-2.5	-29.2	-23.5	22.0
Country Rocks	Average (%)	33.5	25.7	33.2	4.5	1.9	1.1
	Range (%)	28.0-39.8	12.2-33.1	22.7-44.5	1.2-7.9	0.9-4.7	0-2.0
	Difference from average (%)	-1.1	-5.6	5.6	9.3	-4.2	-12.1
Eastern Locality	Average (%)	37.5	25.1	28.4	4.8	2.4	1.8
	Range (%)	30.6-45.9	20.1-32.2	21.5-35.7	2.0-7.9	0.8-4.9	0.7-3.3
	Difference from average (%)	10.7	-7.9	-9.8	15.9	20.5	41.8
Western Locality	Average (%)	31.1	28.9	33.8	3.6	1.7	0.9
	Range (%)	22.6-38.1	12.2-36.5	22.7-44.5	1.2-5.6	0-2.5	0-2
	Difference from average (%)	-8.2	6.1	7.5	-12.3	-15.6	-31.9

Other includes: epidote, titanite, Fe-oxides, apatite and chlorite.

Table 2.3: Modal mineralogy and ranges in composition for all rock types and locations.

Table 2.4: Chemical Element Data from Lost Creek Gneiss Samples

	Western Location - Sample LCG12								Eastern Location - Sample LCG25							
	Ksp	Plag	Plag	Plag	Plag	Plag	Plag	Ksp	Ksp	Ksp	Plag	Plag	Plag	Plag	Plag	Plag
Na2O	0.68	12.03	11.32	10.28	10.62	9.72	12.01	0.73	0.83	0.81	11.51	9.39	9.49	9.66	9.40	9.26
CaO	0	0.20	0.22	2.72	2.20	2.59	0.21	0	0	0	0.43	3.32	3.22	3.39	3.45	3.49
K2O	15.84	0.11	0.09	0.15	0.19	0.14	0.09	15.94	15.43	15.55	0.11	0.23	0.26	0.27	0.21	0.22
Al2O3	18.30	19.76	19.48	21.62	21.35	21.64	19.43	18.54	18.42	18.42	19.83	22.05	22.34	21.95	22.20	22.30
SiO2	65.10	68.85	68.31	65.14	65.72	65.62	67.95	65.19	65.30	65.15	68.73	64.82	65.35	64.77	64.78	64.16
Total	99.92	100.95	99.44	99.90	100.08	99.71	99.68	100.39	99.98	99.93	100.60	99.81	100.67	100.05	100.03	99.43
Na	0.061	1.011	0.963	0.878	0.905	0.830	1.023	0.065	0.074	0.072	0.970	0.803	0.804	0.826	0.802	0.796
Ca	0	0.009	0.011	0.128	0.104	0.122	0.010	0	0	0	0.02	0.157	0.151	0.160	0.163	0.166
K	0.932	0.006	0.005	0.009	0.011	0.008	0.005	0.935	0.906	0.914	0.006	0.013	0.015	0.015	0.012	0.012
Al	0.996	1.009	1.008	1.123	1.107	1.123	1.006	1.005	0.999	1.010	1.015	1.146	1.151	1.140	1.152	1.164
Si	3.005	2.984	2.997	2.872	2.889	2.888	2.984	2.997	3.006	3.003	2.985	2.858	2.857	2.855	2.852	2.842
Total	4.994	5.020	4.984	5.01	5.015	4.970	5.027	5.001	4.985	4.990	4.995	4.977	4.978	4.996	4.980	4.980
X_{Ab}	0.061	0.985	0.984	0.865	0.888	0.865	0.986	0.065	0.075	0.073	0.974	0.825	0.829	0.825	0.822	0.817
X_{An}	0	0.009	0.011	0.126	0.102	0.127	0.009	0	0	0	0.02	0.161	0.156	0.16	0.167	0.17
X_{Or}	0.939	0.006	0.005	0.008	0.01	0.008	0.005	0.935	0.925	0.927	0.006	0.013	0.015	0.015	0.012	0.013

Representative transect across K-feldspar into plagioclase (and back into K-feldspar for the Western Location).

Chapter 3: Distribution and abundance of syn-deformational melt microstructures, across the Wet Mountains, central Colorado: Small-scale features as a proxy for crustal-scale magmatism

3.1 Abstract

The Wet Mountains of central Colorado provide evidence for synchronous in situ partial melting and deformation of Proterozoic gneisses, with each process enhancing the other. Locations that have undergone partial melting, as evidenced by the presence of melt pseudomorphs and peritectic minerals that are products of partial melting, are more deformed, as indicated by higher degrees of recrystallization, finer grain size and closer spacing of foliation than locations that lack evidence of partial melting. Similarly, areas that are more deformed have preferentially undergone partial melting. The Wet Mountains trend northwest-southeast, and metamorphic grade increases towards the southeast. In the northwest Wet Mountains, migmatitic foliation is moderately well-developed, and partial melting occurred via muscovite-dehydration melting and granite wet melting, with rare melt pseudomorphs remaining on grain boundaries. At Dawson Mountain in the central Wet Mountains, former melt channels are preserved along grain and subgrain boundaries, deformation is more intense and anatexis occurred through biotite-dehydration melting. Farthest to the south there is evidence for the most intense deformation, with very tightly-spaced foliations, abundant recrystallization and local mylonitization occurring in rocks of granitic composition, and partial melting via granite wet melting and biotite-dehydration melting. Metapelitic rocks contain garnets with Mn-rich rims and Mn-poor cores mantled by plagioclase, decussate biotite and quartz, textures indicating back-reaction between melt and garnet. Despite intense deformation in the south, these textures indicate there was abundant melt pooling within these rocks and extensive melt-rock interaction. Throughout the Wet Mountains, deformation is concentrated in areas where melt producing reactions occurred, and melt appears to be localized along deformation-related features, suggesting a positive feedback loop. The degree of partial melting and spatial location of melt microstructures present within the

Wet Mountains correlate well with the location and abundance of crustal-scale plutons and magmatic bodies and provide a proxy for crustal-scale melt flow.

3.2 INTRODUCTION

Deformation acts to decrease grain size through recrystallization, creating more intergranular pathways for enhanced diffusion and increased surface area along which reactions can take place (Kerrich et al., 1977; Brodie and Rutter, 1985; Yund and Tullis, 1991). Deformation can enhance fluid flow, which increases diffusion rates and thus reactions (Etheridge et al., 1984). Metamorphic reactions promote deformation through reaction-enhanced ductility (White and Knipe, 1978; Rubie, 1983) and through reactions that produce fluids, which when present weaken the rock and localize deformation (Fyfe, 1976; Brodie and Rutter, 1985).

In migmatites, melting reactions are generally thought to precede deformation, and subsequently deformation is localized into melt-rich areas that are rheologically weaker (Sawyer, 1994; Brown, 1994; Brown and Rushmer, 1997; Sawyer, 2001). However, deformation can also promote partial melting reactions, with deformation contributing to melting in migmatites through enhanced diffusion rates and a contribution from stored strain energy.

Two melting reactions are common: granitic wet melting reactions and muscovite- and biotite-dehydration melting reactions. Fluid-present granite eutectic melting (Quartz + Plagioclase + K-feldspar + H_2O = Melt) is generally the first melting reaction line to be crossed in migmatitic rocks of an appropriate bulk composition at temperatures of approximately 650° C (Huang and Wyllie, 1975). Although this assemblage is ubiquitous in migmatitic terrains and the reaction is fairly simple, it can be difficult to determine where melting occurred within a given sample, because of the lack of peritectic reaction products.

Dehydration reactions have the advantage of clearly indicating the site of melt generation, because of peritectic products of melting, but they occur at higher temperatures than fluid-present granite melting. The muscovite dehydration reaction

(Quartz + Muscovite = Melt + Sillimanite + K-feldspar) typically occurs at 675-725° C, depending on pressure (Le Breton and Thompson, 1988; Spear, 1995; Spear et al., 1999). Biotite-dehydration melting (Biotite + Quartz + Plagioclase + Sillimanite = Melt + Garnet + K-feldspar) occurs at slightly higher temperatures than muscovite-dehydration melting, generally 760-800º C, increasing at higher pressures and depending on the presence of other minerals involved in the reaction (Le Breton and Thompson, 1988).

Microstructures indicative of former partial melt or textures recording melting reactions have been described recently by many authors (Sawyer, 1999; Sawyer, 2001; Waters, 2001; Barbey, 2007; Holness and Sawyer, 2008; Kriegsman and Álvarez-Valero, 2010). In rocks of a metapelitic composition where peritectic products of melting formed, melt textures are comparatively easy to identify. They include: solid products of melting reactions with euhedral crystal faces against the melt (Sawyer, 1999, 2001), reactant phases with rounded or corroded boundaries surrounded by melt films (Mehnert et al., 1973; Busch et al., 1974), small cuspate-shaped melt pools similar to those formed in experimental studies (Harte et al., 1991; Sawyer, 1999; Rosenberg and Riller, 2000; Holness and Sawyer, 2008) and also intergrowths between quartz and solid products of melting (Waters, 2001; Barbey, 2007). More specifically, garnets surrounded by a halo of coarse-grained quartz that is absent of biotite has been attributed to garnet growth as a result of biotite-dehydration melting (Waters, 2001, Barbey, 2007).

Microstructures are more difficult to identify in rocks of a granitic composition because the crystallized melt is made up of the same components as the reactants (Holness and Sawyer, 2008; Sawyer, 2010). Some textures that can be used to infer the former presence of melt specifically in granitic rocks include cuspate or serrate grain boundaries with low dihedral angles, pseudomorphs of melt along grain boundaries of unlike phases (i.e. K-feldspar between two plagioclase grains), and melt pseudomorphs present at grain boundary triple junctions and multiple grain junctions (Harte et al., 1991; Rosenberg and Riller 2000; Sawyer, 2001; Holness and Sawyer, 2008).

In this chapter, I investigate the potential for deformation promoting partial melting and partial melting localizing deformation in the Wet Mountains of Colorado.

There, former melt is preferentially found in high-strain locations, as evidenced by degree of recrystallization and spacing of foliation, and deformation is localized in areas that have undergone partial melting. For this study, I conducted a microstructural and petrographic analysis that provides better constraints on metamorphic pressure and temperature conditions and that clarifies the relationships between deformation, metamorphism, and partial melting, particularly in the central and southern Wet Mountains. In addition to determining the metamorphic and melt-producing reactions, I characterized differences in structural styles and the associated metamorphism and magmatism between the northern and the central/southern Wet Mountains. I present data and observations along a transect, from northwest to southeast in the Wet Mountains, that indicates partial melting and deformation were synchronous, and each promoted the other concurrent process. Finally, I find that degree of partial melting and the spatial location of the melt microstructures present in these rocks parallel the larger crustal-scale structures and plutonism in the region. I propose that in the Wet Mountains, microstructures may be used as a proxy for larger tectonic processes and that deformation and melting processes enhance each other, possibly leading to a positive feedback loop.

3.3 GEOLOGIC SETTING/PREVIOUS WORK

The Wet Mountains are a northwest-trending mountain range, composed of Proterozoic-aged gneisses, schists, amphibolites and granites, located in the Rocky Mountains of south central Colorado (Figure 3.1). From north-northwest to south-southeast the metamorphic grade increases, from greenschist/amphibolite to granulite facies as a result of exhumation of progressively deeper crust towards the south (Siddoway et al., 2000). Associated with this increasing depth of crustal exposure is a change in structural style from upright open folds and vertical foliation in the north to shallowly-moderately dipping foliation and more widespread and pervasive plutonism in the central and southern part of the range (Jones et al., 2010). The oldest metamorphic rocks are interpreted to have been a volcanic and sedimentary sequence formed in a convergent margin between 1780-1717 Ma (Bickford et al., 1989; Reed et al., 1987).

Rocks in the northern Wet Mountains include garnet, sillimanite and cordierite gneisses or schists, amphibolites, felsic gneisses, and siliceous schists, and are the lowest grade rocks in the area, with temperatures and pressures of ~700 °C and 0.5 GPa (Givot and Siddoway, 1998; Siddoway et al., 2000). Higher-grade rocks including migmatitic gneisses and amphibolites are found throughout the central and southern Wet Mountains and have experienced upper amphibolite- to granulite-facies metamorphism (Lanzirotti and Condie, 1988; Brock and Singewald, 1968).

Three episodes of granitic plutonism are recognized from field relationships and U-Pb geochronology (Bickford et al., 1989; Jones et al., 2010). The oldest plutons are found in the northern Wet Mountains and are Paleoproterozoic in age, ranging from 1705-1615 Ma (Bickford et al., 1989). Additionally some smaller dikes and sheets of granitoid intrusions can be linked with these Paleoproterozoic intrusive bodies (Bickford et al., 1989; Siddoway et al., 2000). All of the Paleoproterozoic magmatism is described as the G_1 magmatic event (Jones et al., 2010). Mesoproterozoic plutons are divided into those older than 1400 Ma, and a smaller group of ~1360 Ma plutons (Bickford et al., 1989; Jones et al., 2010). In addition to larger plutons, smaller dikes and sills, also yield similar Mesoproterozoic ages.

New U-Pb geochronologic data from Jones et al. (2010) have served to better distinguish the two episodes of Mesoproterozoic magmatism. In the northern Wet Mountains, the Mesoproterozoic magmatism appears to be part of a single protracted episode. A syntectonic pegmatite within the Five Points deformation zone gives a U-Pb zircon age of 1430 +5/-3 Ma. The West McCoy Gulch pluton, yields an age of 1474 +/- 7 Ma (Bickford et al., 1989) and is located several kilometers southwest of the Five Points deformation zone. The Oak Creek pluton located 10 km south/southwest of Cañon City, gives a U-Pb zircon age of 1442 +/- 7Ma (Bickford et al., 1989; Cullers et al., 1993). In the southern Wet Mountains, Jones et al. (2010) have distinguished foliated coarse-grained granites within 1-5 m thick sills (G_2) concordant with host gneiss foliation from finer-grained foliated granites within 0.5-5 m thick sills (G_3) that cross-cut both host-rock foliation and the foliation in G_2 granites. The coarse-grained G_2 granite gives a

U-Pb zircon age of 1435 +/- 4 Ma, whereas the fine-grained G_3 granite gives a younger U-Pb zircon age of 1390 +/- 10 Ma (Jones et al., 2010).

Rocks in the Wet Mountains have undergone three phases of deformation, but differences in crustal exposure from north to south have led to preservation of primary bedding and earliest deformation fabrics only in low-strain locations in the northern Wet Mountains (Siddoway et al., 2000). Cordierite poikiloblasts, up to 20 cm in length, within cordierite schists exposed in the Five Points Gulch, near the Arkansas River Canyon of the northern Wet Mountains, preserve evidence of relict bedding which is defined by patterns of quartzofeldspathic and opaque mineral inclusions (Siddoway et al., 2000). In this vicinity D_1 is recorded by a penetrative crenulation cleavage of S_0 bedding, S_1, and associated F_1 folds, which are both synchronous with growth of the cordierite poikiloblasts (Siddoway et al., 2000). Exposures in the central and southern Wet Mountains preserve little evidence of D_1 due to overprinting by higher grade migmatitic fabrics (Siddoway et al., 2000).

The S_2 foliation is the dominant foliation throughout the Wet Mountains and is typically found with an associated mineral lineation, L_2. In the northern Wet Mountains, this foliation strikes east-west to northwest-southeast and dips moderately to steeply, with lineations plunging moderately to the north-northeast, whereas in the central and southern Wet Mountains, foliations strike east-west to northeast-southwest and dip moderately to steeply, with lineations plunging moderately to the northeast, north and northwest (Siddoway et al., 2000; Jones et al., 2010). F_2 folds are tight to isoclinal in style and are more easily recognized in the compositionally varied gneisses of the northern Wet Mountains than in more compositionally uniform, migmatites of the central and southern Wet Mountains (Siddoway et al., 2000).

D_1 is constrained to have occurred synchronously with 1.67 Ga metamorphism based on U-Pb zircon ages from granulites in the central portion of the range, and granodioritic sills containing foliation that is concordant with host-rock foliation (1.67 Ga, Bickford et al., 1989). The subsequent D_2 deformation had been thought to coincide with Paleoproterozoic magmatism, however new U-Pb data from Jones et al. (2010)

shows that D_2 is associated with the Mesoproterozoic G_2 magmatism. The timing of D_2 is determined on the basis of U-Pb ages for metamorphic zircons in amphibolite gneisses that are 1436 +/- 2 Ma for igneous zircons from G_2 granitic sills that give an average age of 1435 +/- 4 Ma.

Throughout the Wet Mountains, high-strain zones exhibit an S_3 foliation that is distinct in orientation from S_2, attributed to a D_3 event (Siddoway et al., 2000). One of the zones, the Five Points deformation zone, is a 2-5 km wide shear zone with N-S striking foliation that truncates a kilometers-scale F_2 fold on its western boundary and bounds domains of contrasting metamorphic grade (Siddoway et al., 2000; Jones et al., 2010). High-strain zones in the central and southern Wet Mountains have west-southwesterly striking foliations with shallower dips than lower-strain fabrics outside of these zones. The boundaries of the high-strain zones are poorly defined and probably are gradational.

3.4 METHODOLOGY

This study relied on previous detailed structural mapping throughout the Wet Mountains and the recognition of an increase in metamorphic grade from northwest to south-southeast (Brock and Singewald, 1968; Lanzirotti, 1988; Siddoway et al., 2000 and references therein; Jones, 2005; Jones et al., 2010) to identify optimal study locations within high-strain domains developed within migmatites. Seven locations were selected for study, with one in the north, three within the central Wet Mountains and three in the southern part of the range (Figure 3.1). Although each location contains migmatitic rocks, the amount of former melt, used as an indication of the degree of partial melting is variable between locations, and the degree of strain is not always uniform across a location. Degree of partial melting was determined qualitatively by the abundance of melt microstructures, degree of preservation of original textures, corrosion of reactant minerals, and inferred back-reaction between melt and peritectic minerals. An actual estimate of the amount of melt produced during anatexis is beyond the scope of this

study. A qualitative degree of strain was determined by analyzing foliation-spacing, degree of recrystallization and recrystallized grain size.

At each of the seven field localities (Figure 3.1), foliations and lineations were measured, as well as fold hinges when available; mineral assemblages, types and textures of migmatites, and relationships between deformation and partial melting were described, and oriented samples were collected. In all, 100 samples were collected over the course of four weeks of field work in August 2008 and July and August 2009. One hundred ninety-seven thin sections were made to identify and describe mineral assemblages, melt microstructures, and relative timing of partial melting and deformation, and nine of these samples were selected for compositional analysis via electron microprobe.

3.5 Five Points Deformation Zone

The Five Points deformation zone extends for 2-5 km along the Arkansas River and is well-exposed in spectacular roadcuts along Highway 50 (Figure 3.1). West of the Five Points deformation zone is the Texas Creek domain, which is dominated by a kilometer-scale F_2 anticline that is truncated by the Five Points deformation zone (Siddoway et al., 2000). Rocks within the Texas Creek domain are compositionally similar to those in the Five Points deformation zone. East of the deformation zone is the Sheep Basin domain, which is comprised mainly of tonalites, quartz diorites and granodiorites of the Crampton Mountain pluton (Bickford et al., 1989).

3.5.1 Field Observations

Rocks found within the deformation, or high-strain, zone are dominated by muscovite-biotite-quartzofeldspathic gneisses (Figure 3.2A). Many rocks contain lineation-parallel "pods" of sillimanite and muscovite, up to 5 cm in length. Garnets are in the centers of some of these pods of muscovite and sillimanite (Figure 3.2A). Other elliptical pods of quartzofeldspathic material that contain magnetite porpyroblasts appear to be related to partial melting but instead form as a result of solid-state metamorphic segregation and are known as flecked gneisses (Trumbull, 1988). Other rocks found in

this area include amphibolites, biotite-rich granitic gneisses and rarer sillimanite-biotite schists.

Structurally, these rocks are characterized by the east-west to northwest-southeast striking, steeply north to northeast dipping S_2 foliation (Figure 3.3A). L_2 lineations are usually defined by aligned "pods" of sillimanite and muscovite, or biotite, and they plunge moderately-steeply to the north-northeast (Figure 3.3A). Abundant granitic and pegmatitic veins are present and most of them are deformed; most veins are isoclinally folded, foliated, concordant with foliation in the host rock, but rarely boudinaged. However, a few pegmatite dikes, generally 20-50 cm wide, cut across the host-rock foliation.

3.5.2 Mineral Assemblages and Associated Deformation

These rocks are composed of quartz, plagioclase, K-feldspar, biotite and muscovite +/- sillimanite, amphibole, porphyroblasts of garnet or magnetite and accessory minerals including, apatite, zircon, epidote and titanite. The muscovite-biotite-quartzofeldspathic gneisses have a weak to moderately well-developed foliation defined by aligned biotites +/- muscovite alternating with layers of elongate quartz and feldspar, parallel to foliation (Figure 3.4A). Foliation spacing ranges from 1-5 mm. Additionally there are small pockets of coarser quartz and feldspar, up to several mm in diameter; these pockets are aligned parallel to foliation. Plagioclase is variably sericitized in these rocks, and subgrains are locally poorly developed. In several samples when plagioclase is in contact with K-feldspar, albitic rims on the plagioclase and myrmekite are locally developed. K-feldspar displays microcline twinning and is typically perthitic. Quartz has well-developed subgrains present, and rarely displays chessboard extinction.

The previously described "pods" are composed of coarse muscovite, fibrolitic sillimanite and quartz. Fibrolitic sillimanite is typically found as inclusions within muscovite, although some samples have mats of fibrolitic sillimanite apparently isolated from muscovite grains. It is possible that muscovite is present in the third dimension and not visible in this two-dimensional slice. Many of the muscovite grains have a

symplectic and/or poikiloblastic texture with quartz; fibrolitic sillimanite extends into the quartz grains from muscovite. In several rocks, garnets are present within these pods, but are typically separated from the muscovite and sillimanite by quartz. Pods are surrounded by the foliation characteristic of the muscovite-biotite-quartzofeldspathic gneisses and appear as islands containing coarser minerals and abundant sillimanite.

A few of the collected rocks contain garnets in the Five Points deformation zone, but in all but one sample, the garnets are highly disaggregated. These disaggregated garnets are separated into round or square, small, 50-200 μm in diameter, crystals, surrounded by quartz and they appear to have once been a single coarser garnet crystal. Garnets are surrounded by quartz that has well-developed subgrains and are usually void of finer-grained quartz and feldspar and foliation parallel biotite and/or muscovite (Figure 3.4B, 4C). However, the disaggregated grains are commonly joined together by coarse single grains of muscovite or biotite or fine-grained chlorite (Figure 3.4B). Rocks from the Texas Creek Domain to the west of the Five Points have similar textures, but garnets are more highly disaggregated and are joined by coarse calcite, chlorite and muscovite. Within the Five Points area one sample containing garnet exhibits a xenoblastic texture, but it is not disaggregated. The garnet is also surrounded by a leucosome composed mostly of deformed quartz, but there is a discontinuous envelope of slightly sericitized plagioclase immediately surrounding the garnet.

3.5.3 Interpreted Melt Microstructures and Metamorphic Reactions

Melt microstructures in rocks at Five Points are either found adjacent to minerals that have broken down in a melt-producing reaction, such as muscovite, as melt pseudomorphs along grain boundaries, or as crystals with serrate/cuspate grain boundaries adjacent to melt pseudomorphs (Figure 3.4D, E). Samples containing abundant muscovite provide evidence for the greatest number of melt microstructures, including former melt adjacent to embayed and corroded muscovite grains and along grain boundaries, typically between quartz and plagioclase. This former melt is typically preserved as K-feldspar.

Throughout this paper, the melt pseudomorphs are described as being composed of the minerals that now occupy the location of the former melt. In granitic eutectic melting, the melt is composed of quartz, plagioclase and K-feldspar components. When the melt begins to crystallize, each component of the melt will nucleate and crystallize onto any pre-existing mineral grains of the same composition (Harte et al., 1991; Rosenberg and Riller, 2000; Holness and Sawyer, 2008). For example, if melt is present between quartz and plagioclase, the plagioclase component of the melt will crystallize onto the pre-existing plagioclase grain, and the quartz will crystallize onto pre-existing quartz grains. The K-feldspar component of the melt will not have any pre-existing grains of K-feldspar on which to nucleate and crystallize, so the K-feldspar will be preserved on the quartz-plagioclase grain boundary as a melt pseudomorph.

Abundant muscovite in these rocks with symplectic or embayed edges and inclusions of quartz and sillimanite, surrounded by plagioclase, quartz, +/- K-feldspar provides evidence for muscovite-dehydration melting (Figure 3.4D). However, the presence of muscovite remaining within these rocks indicates that the reaction did not proceed to completion. The main muscovite-breakdown reaction occurring in these rocks appears to be,

Muscovite + Quartz = Melt + Sillimanite +/- K-feldspar

based on the presence or absence of K-feldspar immediately adjacent to corroded and embayed muscovite grains. Spear et al. (1999) claim that the amount of K-feldspar produced by this reaction is small because a large amount of the potassium will dissolve into the melt. This reaction occurs at temperatures of 675-725° C (Spear, 1995; Spear et al., 1999) depending on pressure, and based on previous pressure estimates in this area of 0.5 GPa (Givot and Siddoway, 1998) temperatures were approximately 675° C.

Former melt found along grain boundaries between quartz and feldspar provides evidence for granitic wet melting

Quartz + Plagioclase + K-feldspar + H_2O = Melt

within these rocks. Fluid-present granite eutectic melting occurs at temperatures lower than muscovite-dehydration melting, so as long as H_2O was available, it makes sense that

granite wet melting also occurred in this area. At a pressure of 0.5 GPa granite fluid-present melting would start to occur at temperatures of approximately 650° C (Huang and Wyllie, 1975; Spear, 1995). The presence of abundant muscovite remaining in these rocks suggests that granite fluid-present melting was the primary melting reaction that occurred in these rocks and/or that some of the muscovite is retrograde. Fluid-present granite melting occurs at lower temperatures than muscovite dehydration melting, and all of the reactants needed for the fluid-present granite melting are present in these rocks. Thus, this reaction may have occurred preferentially and produced more of the melt. Although much of the muscovite in these rocks is corroded and grungy, there is some fresh-looking muscovite, which may be retrograde. Consequently, it is likely that fluid-present granite melting may have produced more melt than muscovite-dehydration melting and that some of the muscovite is retrograde.

3.6 DAWSON MOUNTAIN

Dawson Mountain is adjacent and to the north of the Oak Creek Pluton (Figure 3.1), a compositionally variable pluton, that ranges from diorite to granodiorite to monzogranite (Cullers et al, 1993; Dean et al., 2002). The Oak Creek pluton has a U-Pb zircon age of 1442 +/- 7 Ma (Bickford et al., 1989) and on its margins has a well-developed foliation that is concordant with the foliation in host rocks. Previous workers (Cullers et al., 1993; Dean et al., 2002) have proposed that the Oak Creek pluton was emplaced during high-temperature, 600-800° C, and low-pressure 0.2-0.5 GPa, conditions.

3.6.1 Field Observations

Gneisses at Dawson Mountain are high-strain as evidenced by the closely spaced foliation and are compositionally diverse, ranging from biotite-garnet-cordierite-sillimanite gneisses to biotite-rich granitic gneisses, to granitic gneisses containing quartzofeldspathic leucosomes with magnetite porphyroblasts (Figure 3.2B). These rocks all contain a pervasive dominantly northeast striking and southeast dipping S_2 foliation, and some L_2 lineations are present, typically defined by aligned biotite, plunging

moderately to the southwest (Figure 3.3B). Some of the garnet-cordierite-sillimanite-rich, metapelite layers are isoclinally folded, with hinge lines parallel to the pervasive biotite lineation. All of these rocks have undergone partial melting, with clear evidence for in situ partial melting indicated by garnets that are surrounded by leucosomes of quartz (Figure 3.2B). In addition to evidence for in situ partial melting, there are abundant granitic and pegmatitic veins, some concordant to foliation and others cross-cutting host gneiss foliation, throughout the field area, at least some of which appear to be externally derived.

In the field, biotite-rich granitic gneisses are the most abundant rock type, but in isolated locations, no more than 10 square meters in size, there are garnet-rich metapelites, with abundant evidence for spatially-localized partial melting. Some of these metapelites contain rounded to elliptical leucosomes immediately surrounding the garnets, whereas others contain more continuous veins or veinlets of leucocratic material enveloping multiple garnets, slightly oblique to the main foliation, spaced 2-3 cm apart. A few contain foliation parallel, laterally continuous leucocratic veins. The presence of garnets surrounded by leucosomes is characteristic of biotite-dehydration melting (Barbey, 2007), and because the site of reaction can be pinpointed by the location of garnets, a peritectic product of melting, these metapelites are the focus of most of the microstructural and chemical analysis.

3.6.2 Mineral Assemblages and Associated Deformation

Metapelitic rocks at Dawson Mountain have fairly uniform mineral assemblages and contain quartz, plagioclase, K-feldspar, biotite, garnet, sillimanite and cordierite, plus accessory minerals including, epidote, zircon, and hematite. These rocks are strongly foliated, with a spacing of 1-2 mm, and the S_2 foliation is defined by aligned biotite and sillimanite, alternating with layers of elongate quartzofeldspathic material, dominantly quartz (Figure 3.5A). In rare locations, isoclinally folded S_1 foliation, defined by sillimanite is visible, but an axial planar foliation is rare. The S_2 foliation defined by sillimanite has a somewhat wispy character (Figure 3.5A).

Garnets are up to 2 cm in diameter and have a rounded to moderately embayed shape. Within embayed areas, garnets tend to be disaggregated and strings of disaggregated material generally parallel the foliation (Figure 3.5A). Some of the garnets contain inclusions of sillimanite that are needlelike and in some places look somewhat ragged and grungy. Within several of the garnets containing sillimanite, some sillimanite forms the shape of an isoclinal fold. It is unclear whether the sillimanite has actually been folded or whether the sillimanite is mimicking minerals it has replaced that were once folded, possibly crenulated biotite. In either case, it is clear some deformation preceded the growth of garnets.

Garnets are either surrounded by a lens of leucosome material that is comprised entirely of quartz or in some cases they are rimmed by a very thin, <1mm thick rim of plagioclase (Figure 3.5A, B). The quartz is highly deformed and commonly displays chessboard extinction, which occurs when basal and prism a-slip occur together, indicative of deformation at high temperatures (Kruhl, 1996) (Figure 3.5C). Plagioclase rims around garnets are optically continuous and commonly surround more than one garnet or isolated portions of the same garnet. The leucocratic envelopes surrounding garnet are void of biotite and sillimanite, and other minerals that define the foliation (Figure 3.5A, 5B).

Microprobe analyses on garnets from the metapelites indicate they are almandine garnets. On a transect from rim to rim across the garnet, no major element zoning is observed within the garnets, suggesting they are equilibrated; they have compositions in the range of X_{Fe} = 0.75-0.79, X_{Mg}=0.18-0.19, X_{Mn}= 0.01-0.06 and X_{Ca}=0.01 (Table 3.1). Parallel to foliation, along grain boundaries and a few sub-grain boundaries, locally abundant K-feldspar or cordierite contains sillimanite, rare biotites and some rounded quartz grains (Figure 3.5D-F). The texture between the K-feldspar and sillimanite is the same as that between cordierite and sillimanite, with optically continuous K-feldspar or cordierite, extending along the entire length, 4 cm, of the thin section. These bands are pervasive in most thin sections; they have a wispy character with variable thickness, but generally range from 50-200 μm thick, with rare areas up to 1-2 mm thick. K-feldspar is

typically perthitic and has albitic rims surrounding the K-feldspar (Figure 3.5D). Cordierite is commonly pinitized with yellowish, brownish or greenish, isotropic, somewhat ragged material along the edges, and locally containing fine needles of sericite (Figure 3.5A, E). Throughout some thin sections, large swaths of pinite are present, with almost no original cordierite remaining. Plagioclase rims are also found on some of the pinite or cordierite that contains sillimanite and biotite (Figure 3.5E). The pinite contains the same textural association with both sillimanite and biotite and are compositionally identical to cordierite (Table 3.1). Some of the sillimanite within K-feldspar, cordierite and pinite is idioblastic, with a square to slightly rectangular shape, with no apparent cleavages visible; other sillimanite are needlelike and may have more tapered ends (Figure 3.5D-G). Biotite grains within the K-feldspar/cordierite/pinite do not contain euhedral crystal faces; instead they are jagged or appear somewhat skeletal (Figure 3.5D, E).

3.6.3 Interpreted Melt Microstructures and Metamorphic Reactions

Garnet-rich metapelites at Dawson Mountain contain distinctive melt microstructures in the form of relict "melt channels" (Figure 3.5G) and envelopes of former melt surrounding garnets (Figure 3.5D). Both of these textures were described briefly in the above section, but here, their association with melting is discussed. The interpretation of the microstructures as relict "melt channels" or flow paths, is based on 1) volumetrically small, optically and laterally continuous grains of K-feldspar/pinite/cordierite that extend the length of the thin section, 2) the presence within these laterally continuous grains of prismatic sillimanite, rare skeletal or jagged biotite and rounded quartz grains (Figure 3.5G), and 3) the presence of the K-feldspar/cordierite/pinite only along grain boundaries and subgrain boundaries (Figure 3.5D-F) and locally rimming garnets (Figure 3.5B). It is well established that melt migrates through rocks along grain boundaries, particularly those that are foliation parallel (Mehnert et al., 1973; Sawyer, 2001; Marchildon and Brown, 2003; Sawyer, 2008), and the microstructures described above are interpreted as channels along which

melt migrated. The melt that flowed through these channelways likely connected with larger conduits that moved melt to higher crustal levels. However, no larger conduits are preserved within the samples analyzed in this study.

The small rounded quartz grains found to varying extents within the K-feldspar/cordierite/pinite (Figure 3.5G) are interpreted to be original grains of quartz that were surrounded and affected by melt flowing through the rock. In locations where these small rounded quartz grains are adjacent to prismatic sillimanite, the quartz component of the melt appears to have nucleated onto these preexisting grains (for example see the light green quartz grain in Figure 3.5G). Coarser quartz grains (Figure 3.5D) are also somewhat rounded, also likely due to melting of the quartz grain, but these grains appear to have remained rigid and in place, with former melt present only along their grain boundaries; they have not been entirely incorporated into the melt channels. Biotite grains that are slightly jagged, embayed, or skeletal in appearance and found either within or adjacent to the K-feldspar/cordierite/pinite regions, have a morphology suggesting that they broke down as a result of biotite-dehydration melting. All of the observations relating to biotite and quartz morphology, in addition to the location of K-feldspar/cordierite/pinite along grain boundaries and sub-grain boundaries, leads to the interpretation of these features as relict melt channels.

The other distinctive melt microstructure within the Dawson Mountain metapelites is the thin rim of plagioclase surrounding many of the garnets (Figure 3.5B, D). When the garnets were produced as a peritectic product of melting, the plagioclase component of the melt crystallized as a thin rim surrounding the garnet. The quartz component of the melt crystallized as the coarse quartz grains that commonly display chessboard extinction (Figure 3.5C), indicating deformation after crystallization of melt.

The mineralogy of these metapelites provides evidence for the melt and garnet producing reaction due to the breakdown of biotite:

$$\text{Biotite} + \text{Quartz} + \text{Plagioclase} = \text{Melt} + \text{Garnet}$$

No muscovite is present in these samples suggesting that temperatures have already surpassed the second sillimanite isograd and all muscovite disappeared through

metamorphic reaction. The sillimanite seen in these samples may have been produced during an earlier, lower-temperature reaction, related to muscovite breakdown and crossing of the second sillimanite isograd. Biotite-dehydration melting is likely to occur at temperatures of 760-800º C, depending on pressure (Le Breton and Thompson, 1988). When the melt crystallized, this biotite-dehydration reaction was not entirely reversed, as evidenced by a lack of resorption zoning of Mn within garnets. If garnets had been extensively involved in reaction with melt, they would likely have Mn-rich rims, with low-Mn cores (Nyström and Kriegsman, 2003). A minimal reaction between garnet and melt is likely because of the somewhat embayed character of the garnets, but the volume of melt was probably small enough that zoning did not develop.

3.7 NEWLIN CREEK/LOCKE MOUNTAIN DEFORMATION ZONE

The Newlin Creek deformation zone is immediately to the south of the Oak Creek pluton, and consequently shares a similar spatial proximity to the pluton as Dawson Mountain (Figure 3.1). Siddoway et al. (2000) have previously differentiated rocks found in the Newlin Creek shear zone and those found at Locke Mountain, just to the west of the Newlin Creek area, on the basis of differences in strain and foliation orientations. However, based on similarities in rock type, relative degree of strain, within these rocks, similarity in melt microstructures, and position within the crust they are grouped together for the purposes of this study as the Newlin Creek/Locke Mountain deformation zone.

3.7.1 Field Observations

Rocks in the Newlin Creek/Locke Mountain deformation zone are dominated by migmatitic biotite-granitic gneisses, with rare amphibolites. Granitic gneisses have a range of grain sizes from fairly coarse with K-feldspar augen up to 2-3 cm in diameter (Figure 3.2C) to fine-grained rocks with crystals less than 0.5 cm in diameter. Amphibolites are fairly coarse grained with some amphibole crystals up to 1 cm in diameter; layers of nearly pure amphibole alternate with more plagioclase-rich layers. All samples contain the S_2 foliation, but it varies from poorly developed in one or two

samples to pervasive in most of the samples and extremely well-developed with a protomylonitic fabric. The foliation is typically defined by alternating layers of aligned biotite and quartzofeldspathic material, some of which is interpreted as crystallized partial melt. Foliation in the eastern part of the area, in Newlin Creek proper, trends north-northwest and dips moderately to the northeast, whereas foliation in the Locke Mountain area strikes west-northwest to west-southwest and dips shallowly to steeply to the northwest-north (Figure 3.3C). Pegmatites and granitic veins are both abundant in the Newlin Creek/Locke Mountain deformation zone; some are concordant with the foliation in the host rock, others are late and cross-cut the gneissic foliation (Figure 3.2C).

3.7.2 Mineral Assemblages and Associated Deformation

Rocks of granitic composition are composed of quartz, plagioclase, K-feldspar, biotite, and some samples contain amphibole; accessory minerals include zircon, opaques, titanite and apatite. In thin section, abundant recrystallization, as evidenced by growth of new grains with a very fine grain size, has occurred within migmatitic biotite granitic gneisses (Figure 3.6A). The degree of recrystallization is variable, with many samples containing 5-10% new grains, whereas others have less than 2-3%. Along grain boundaries between feldspars there are abundant new grains of plagioclase and K-feldspar less than 50 μm in diameter, that commonly resemble pockets of chert, characteristic of bulge recrystallization of feldspar, and some of these areas show development of myrmekite (Figure 3.6A, B). Plagioclase grains display continuous undulatory extinction and rare crystals show development of subgrains. K-feldspar is perthitic and displays microcline twinning. Pockets of quartz are comprised of equigranular grains, which generally have straight edges, and a moderate lattice preferred orientation.

Amphibolites are composed of hornblende, plagioclase, quartz, clinopyroxene, biotite, and accessory minerals including apatite, opaques and zircon. Plagioclase is locally sericitized, many grains display undulatory extinction, some rare crystals show subgrain development and new grains have formed as a result of recrystallization. Rare

quartz grains have formed ribbons, and several equant grains display chessboard extinction. Each thin section shows several examples of coarse amphiboles, 0.5-1 cm in diameter, which are wrapped by foliation and appear to be porphyroblasts. Foliation is defined by alternating layers of moderately sized, typically 5 mm in diameter, amphiboles and more plagioclase- or quartz-rich layers with sparse fine-grained amphiboles, approximately 1 mm in diameter.

3.7.3 Interpreted Melt Microstructures and Metamorphic Reactions

Migmatitic biotite granitic gneisses commonly have melt pseudomorphs, commonly K-feldspar, on grain boundaries, typically between quartz and plagioclase (Figure 3.6B). Most of these pseudomorphs are less than 100 μm wide, however in some locations former melt films are more than 200 μm wide and form a moat-like structure, surrounding another grain, usually quartz (Figure 3.6B). Former melt is also found on triple and multiple grain junctions; commonly these melt pseudomorphs are now composed of K-feldspar. Finally, there are locations where former melt is found at cuspate/serrate indentations within a crystal (Figure 3.6B).

Melt microstructures are found only in the migmatitic biotite granitic gneisses; amphibolites do not appear to have undergone partial melting. As a result, these rocks appear to have undergone fluid-present granite melting, via the reaction

$$\text{Quartz} + \text{Plagioclase} + \text{K-feldspar} + H_2O = \text{melt}.$$

The presence of fluid-present granitic melting but a lack of amphibole-dehydration melting constrains temperatures in this area to between 650° C and 750-800° C (Wolf and Wyllie, 1994).

3.8 North Hardscrabble Creek

North Hardscrabble Creek is located in the central-southern Wet Mountains, south of the Newlin Creek/Locke Mountain by about 10 km (Figure 3.1). Highway 96 follows Hardscrabble Creek between the intersection of Highway 96 and 67 and the turnoff to Highway 165. These rocks are not adjacent to major plutons. Roadcuts along Highway 96 were studied.

3.8.1 Field Observations

Rocks range from biotite-rich granitic gneisses to biotite-amphibole-clinopyroxene gneisses. These gneisses have a well-developed S_2 foliation that strikes roughly east-west and dips moderately to the north (Figure 3.3C). The foliation is defined by aligned biotites or amphiboles, alternating with layers of quartzofeldspathic material (Figure 3.2D). Locally, rocks in the Hardscrabble area have strung-out feldspars with tails, but do not display a clear shear sense (Figure 3.2D). Evidence for boudinage is found within leucocratic layers surrounding more mafic material; the felsic material displays a pinch and swell structure, and the mafic material is broken into discrete blocks enveloped within the leucocratic material. Pegmatite dikes are fairly common in this area; they range in thickness from 1-50 cm thick and some are boudinaged.

3.8.2 Mineral Assemblages and Associated Deformation

These rocks are all composed of quartz, plagioclase, biotite, and K-feldspar and contain varying amounts of amphibole and clinopyroxene; accessory minerals include zircon, apatite, opaques, and titanite. All samples have a pervasive foliation defined by aligned biotite and/or amphibole alternating with layers of elongate quartzofeldspathic material (Figure 3.6C). Biotites are locally chloritized and show undulatory extinction along the length of a single grain, suggesting minor folding, but macroscopic folds are not visible.

The quartzofeldspathic layers tend to be fairly coarse grained with some K-feldspar megacrysts up to 1 cm wide and 2 cm in length. Coarse K-feldspar crystals also have square or rounded fine-grained (less than 50 μm in diameter) exsolution blebs of albite across the entire grain. Quartz has two main textures in these rocks; either it is very elongate, forming ribbons (up to 2 mm in length) with abundant subgrains and an aspect ratio of 3-5:1, or it tends to be more equant and has well-developed chessboard extinction. Plagioclase has well-developed subgrains, in some locations it has undulatory extinction across the grain and contains abundant myrmekite. Abundant new grains of feldspar are found between plagioclase and K-feldspar grains, with typical grain sizes of

approximately 20-50 μm. Core and mantle structure around feldspars is present in many of these rocks.

3.8.3 Interpreted Melt Microstructures and Metamorphic Reactions

Melt microstructures in the Hardscrabble Creek area are abundant, with pseudomorphs of melt along grain boundaries and at triple junctions, moat structures and former melt along subgrain boundaries in both quartz and plagioclase (Figure 3.6C). Grain boundaries between quartz and feldspar or between plagioclase and K-feldspar are commonly serrate and cuspate with thin (less than 0.02 mm thick) melt pseudomorphs separating grains. Most of the former melt is now preserved as K-feldspar, although rare examples of plagioclase and quartz melt pseudmorphs are visible. On some plagioclase-plagioclase grain boundaries, thin pools of K-feldspar contain grains of quartz, a moat-like structure. This structure may be a result of crystallization of former melt. The plagioclase component nucleated onto the pre-existing plagioclase grains, the K-feldspar component nucleated against the plagioclase because of a similar crystal structure, and the quartz nucleated separately in the interior of the former melt pocket.

Melt pseudomorphs are also found adjacent to biotite grains that are ragged, or have embayed edges. The presence of former melt associated with biotite grains suggests that there may be small amounts of biotite-dehydration melting in these rocks, in addition to the more abundant fluid-present granite eutectic melting. However, no peritectic minerals are visible in these rocks, suggesting that the contribution from biotite-dehydration melting is quite small and only occurred incipiently. The main melting reaction in these rocks is,

$$\text{Quartz} + \text{Plagioclase} + \text{K-feldspar} + H_2O = \text{melt}$$

as indicated by the lack of peritectic minerals, and the presence of former melt primarily between quartz, plagioclase and K-feldspar crystals, the reactant phases.

3.9 WILLIAMS CREEK ROAD

The Williams Creek Road is in the southern Wet Mountains (Figure 3.1), within the San Isabel National Forest. Access to these rocks is along Forest Service roads and

most of the best exposures are located along Forest Service Road 402, which parallels Williams Creek. These rocks are dominantly granitic gneisses and are adjacent to and include Mesoproterozoic plutonic rocks. Rocks along the Williams Creek Road are highly strained, with local mylonitization.

3.9.1 Field Observations

Rocks along the Williams Creek Road are biotite-hornblende-granitic gneisses that appear to be made up of interlayered G_2 and G_3 granites. G_2 granitic gneisses are more abundant and are identified by their coarse grain size, K-feldspar augen, well-developed foliation, and streaky biotite lineation, which locally weathers into rods (Figure 3.2E). The degree of strain appears variable in these rocks, but some rocks appear to have a protomylonitic fabric. G_3 granitic gneisses are rarer but can be identified by their fine grain size, less abundant mafic phases and locally mylonitic fabric. S_2 foliation within both the G_2 and G_3 rocks strikes northeast-southwest and dips moderately towards the northwest. Lineations plunge shallowly-moderately towards the north-northwest (Figure 3.3D). Shear-sense indicators are generally rare in these rocks, but when visible they suggest a top to the southwest motion. Along the Williams Creek Road, from north to south, the degree of strain appears to increase, as evidenced by mylonites and protomylonites only found in the most southern outcrops.

3.9.2 Mineral Assemblages and Associated Deformation

These rocks are dominantly composed of quartz, K-feldspar, plagioclase, biotite and hornblende; they contain accessory phases including, zircon, apatite, epidote, chlorite, titanite, and opaques including hematite. Rocks along the northern, likely lower strain part of the road, have a moderately-developed foliation, with a spacing of 2-3 mm and the southern rocks with higher degrees of strain have a closely spaced foliation, in some areas spaced at less than 0.5 mm. A dextral shear sense is visible in one sample (Figure 3.6D).

Equant quartz grains have well-developed chessboard extinction; quartz grains elongate parallel to foliation, form ribbons (up to 2 mm in length) with aspect ratios of 6-

10:1, and in rare cases the quartz ribbons also display chessboard extinction (Figure 3.6E, 6F). Plagioclase grains tend to be equant and have either undulatory extinction or moderately-developed subgrains. Plagioclase grains that are adjacent to K-feldspar typically have edges that are serrate and cuspate (Figure 3.6G) and are marked by a change in extinction that likely represents a more albitic rim. The degree of sericitization is variable in plagioclase, and myrmekite is locally developed (Figure 3.6G). K-feldspar is pervasively recrystallized in these rocks and tends to have an equant or slightly elongate shape. In monomineralic domains, the K-feldspar grains appear statically recrystallized with 120° grain intersections (Figure 3.6F). K-feldspar is also found as small (less than 0.2 mm in length) blebs of material within quartz ribbons or along grain boundaries, usually between quartz and plagioclase. Microcline twinning is displayed in all K-feldspar grains, and they have a perthitic texture. Along grain boundaries between plagioclase and K-feldspar, abundant new grains of both minerals have formed as a result of recrystallization (Figure 3.6G). The degree of recrystallization is variable in these rocks, but it typically ranges from 10-20% new grains up to nearly 70% in the mylonitic sample.

3.9.3 Interpreted Melt Microstructures and Metamorphic Reactions

Melt microstructures in these rocks strongly resemble those seen at Hardscrabble Creek, with former melt found along many grain boundaries, triple junctions and serrate/cuspate grain boundaries adjacent to melt pseudomorphs (Figure 3.6E-G). In this area the melt pseudomorphs are generally preserved as K-feldspar, which appears common for most of the Wet Mountains. Recrystallization appears to have preferentially occurred in many of the locations where former melt is located along grain boundaries between plagioclase and K-feldspar. Thin blebs of optically continuous K-feldspar, representing former melt, commonly grade into new grains formed as a result of recrystallization, along the length of a plagioclase grain with serrate/cuspate edges (Figure 3.6G).

Melt pseudomorphs are more easily identified in less-strained rocks, largely because the former melt is found on grain boundaries, and these locations are marked by recrystallization in more highly strained rocks. Thus, it is likely that more highly strained rocks had at least as many melt psuedomorphs as lower strain samples, but the melt pseudomorphs were recrystallized. In some locations, the serrate/cuspate grain boundaries are visible next to areas of pervasive recrystallization (Figure 3.6G). Similarly, on grain boundaries between quartz and plagioclase, some areas of recrystallized K-feldspar were undoubtedly once melt pseudomorphs. Despite overprinting by recrystallization, these melt microstructures are far more abundant than those found in the Five Points Deformation Zone.

Former melt is also found along the edges of the quartz ribbons and in some cases on the boundary between two ribbons (Figure 3.6E, F). Several of the quartz ribbons contain melt pseudomorphs, now K-feldspar, along subgrain boundaries that either parallel or are oblique to the long direction of the quartz grains (Figure 3.6E, F). All the melt microstructures are located along grain or subgrain boundaries between quartzofeldspathic phases, indicating the dominant melting reaction in these rocks is

$$\text{Quartz} + \text{Plagioclase} + \text{K-feldspar} + H_2O = \text{melt}.$$

3.10 Southern Greenhorn Peaks

The Salt Road, also known as Forest Service Road 409, and the Cisneros Trail are within the San Isabel National Forest and are the southernmost exposures investigated in the Wet Mountains (Figure 3.1). Rocks in these locations are not adjacent to any mapped granitic plutons, but there are abundant G_2 and G_3 intrusions present throughout the area.

3.10.1 Field Observations

Rocks in this area are comprised dominantly of migmatitic biotite +/- hornblende granitic gneisses and migmatitic garnet-biotite +/- sillimanite gneisses. Both rock types contain foliation-parallel stromatic migmatites that are locally isoclinally folded. The dominant S_2 foliation in the area strikes west-northwest and dips moderately to steeply to the north-northeast (Figure 3.3D). This foliation is steeper and strikes more westerly than

the foliation found in the Williams Creek area. Granitic gneisses are the most abundant rock type in this area, and their foliation is defined by alternating quartzofeldspathic layers and biotite +/- hornblende-rich layers (Figure 3.2F). They are quite pink in color, indicating the abundance of K-feldspar, but unlike rocks from Williams Creek and the Newlin Creek/Locke Mountain deformation zone, they do not contain abundant K-feldspar augen.

Garnet-rich metapelitic gneisses contain coarse garnets, up to 3 cm in diameter, which are commonly surrounded by leucocratic material, although some garnets are located within the restitic material (Figure 3.2F). However, all of the rocks that contain garnets have abundant foliation-parallel leucocratic layers no more than 2 cm away from any of the garnets.

All of the rocks in this vicinity, regardless of rock type, provide evidence for abundant former melt in the system despite the absence of larger plutons. There are many foliation-parallel pegmatites and granitic dikes, several cross-cutting granitic dikes, and in metapelitic areas, garnets are surrounded by leucosome material. These rocks appear to contain more former melt than other localities, and they are the best examples of stromatic migmatites within the Wet Mountains.

3.10.2 Mineral Assemblages and Associated Deformation

Granitic gneisses are comprised of quartz, K-feldspar, plagioclase, biotite +/- hornblende and accessory phases including apatite, titanite, opaques, epidote, and zircon. S_2 foliation in these rocks is defined by alternating layers of elongate quartzofeldspathic material, in some cases quartz ribbons and biotite grains aligned parallel to foliation. Quartz grains are typically equant with chessboard extinction, or are slightly more elongate (but do not have well-developed ribbons like the rocks from Williams Creek), and have sharp subgrain boundaries. Plagioclase is far less abundant than K-feldspar, contains variable amounts of sericite, and has albitic rims. Plagioclase grains typically display either continuous undulatory extinction or have poorly-developed subgrains. Myrmekite appears to be located along subgrain boundaries within plagioclase grains, but

is also found in grains that do not have subgrains. K-feldspar has well-developed microcline twinning and contains abundant perthitic texture. It is generally equant and coarse-grained, commonly containing inclusions of plagioclase, or is elongate parallel to the foliation. Locally it is found as small blebs on grain boundaries, particularly between plagioclase and quartz.

Metapelitic samples contain quartz, plagioclase, garnet and biotite, +/- sillimanite, cordierite, K-feldspar and accessory phases including apatite, zircon and opaques. K-feldspar and cordierite are not present within the same thin sections, perhaps due to variation in bulk composition across the area. Foliation in these rocks is defined by alternating layers of aligned biotite +/- sillimanite and elongate quartzofeldspathic material, locally containing garnets, with a spacing of 1-2 mm (Figure 3.7A, B). In most garnet-rich samples, the biotite-rich layers appear to wrap around garnets as well as the pocket of leucosome surrounding the garnet (Figure 3.7B). Quartz in these samples either displays chessboard extinction or has well-developed subgrains. Plagioclase and cordierite both display continuous undulatory extinction or rare subgrains.

Garnets are generally poikiloblastic with rounded to square inclusions of quartz, biotite and plagioclase (Figure 3.7B, C). They are generally surrounded by an envelope between 100-800 μm thick of plagioclase and decussate biotite, or vermicular cordierite and biotite, or plagioclase, vermicular cordierite and biotite (Figure 3.7C-H). Some of these envelopes, particularly the plagioclase-rich ones, have undulatory extinction. This envelope immediately surrounding the garnet is either surrounded by the typical foliation in the rock or an envelope of quartz, commonly displaying chessboard extinction.

Microprobe analyses were conducted on five garnet-rich samples from this vicinity, and two of the samples display resorption-zoning of Mn in garnets (Figure 3.7D, G); the others have flat zoning profiles. All of the garnets are Fe-rich, indicating they are almandine garnets, but there is variation in the Mn and Mg content in zoned samples. Rims of zoned garnets have compositions of X_{Fe} = 0.67-0.72, X_{Mg}=0.05-0.08, X_{Mn}= 0.17-0.25 and X_{Ca}=0.03-0.04 (Table 3.2). The cores have compositions of X_{Fe} = 0.73-0.76, X_{Mg}=0.09-0.13, X_{Mn}= 0.09-0.15 and X_{Ca}=0.03-0.04 (Table 3.2). Samples that have

garnets with fairly flat profiles have X_{Fe} = 0.75-0.76, X_{Mg}=0.16-0.17, X_{Mn}= 0.04-0.05 and X_{Ca}=0.02 (Table 3.2).

Biotites in these rocks generally have two different morphologies and compositions. Biotite defining the foliation has a typical appearance with light brown to brown pleochroism and a composition of: X_{Fe} = 0.57-0.58 or 0.42, X_{Mg} = 0.36-0.4 or 0.54, and X_{Ti} = 0.03-0.06 (Table 3.2). These brown biotites have different Fe and Mg contents, depending on the sample, but they all have high Ti contents relative to the green biotites. Green biotites are found surrounding and within garnets and they are commonly corroded, or very narrow and have a pleochroism from pale green to light brownish-yellow. Their composition is X_{Fe} = 0.57-0.58, X_{Mg} = 0.40-0.42 and X_{Ti} = 0.003-0.005 (Table 3.2).

3.9.3 Interpreted Melt Microstructures and Metamorphic Reactions

The rocks of the southernmost Wet Mountains contain melt microstructures in the form of melt pseudomorphs adjacent to corroded and embayed biotite grains and envelopes of plagioclase or cordierite surrounding garnets (Figure 3.7C-H). These envelopes surrounding the garnets are not typically classified as a melt microstructure, but in these rocks, their formation is related to the melting process; they appear to represent a back-reaction between garnet and melt. Additionally, there are very rare films of K-feldspar between quartz and plagioclase, but this type of melt microstructure is quite minimal.

Melt pseudomorphs adjacent to biotite are typically quartz, between biotite and feldspar, or biotite and cordierite; in samples that have an appropriate bulk composition, the blebs may also be comprised of K-feldspar. In sillimanite-rich rocks the blebs of quartz adjacent to biotite commonly contain euhedral, prismatic sillimanite, similar in appearance to the sillimanite at Dawson Mountain. These biotite-quartz +/- sillimanite intergrowths have been interpreted to record reaction between melt and biotite during crystallization (Waters, 2001; Barbey, 2007; Kriegsman and Álvarez-Valero, 2010).

Sample WMG123 has well developed zoning in all of the garnets, with Mn-rich rims and Mn-poor cores (Figure 3.7D). These garnets are surrounded by an envelope of plagioclase with decussate biotite within the envelope (Figure 3.7C, E). Plagioclase is also found rimming quartz inclusions within the garnet (Figure 3.7C, E). Inclusions in garnets containing quartz rimmed by plagioclase tend to be square in shape, likely indicating the phase in contact with the garnet was melt, which is preserved as plagioclase. The quartz component of the melt would have crystallized onto adjacent quartz, and thus the melt pseudomorphs are preserved as plagioclase, the remaining component of the melt. Undulatory extinction within some of the plagioclase enveloping the garnets indicates deformation continued after the growth of the plagioclase. Biotite within the envelopes is green in color, indicating low Ti-content, but biotite defining the foliation is much browner in color, indicating higher Ti-contents. This difference in biotite composition suggests the foliation-parallel biotite grew at a different time than the decussate biotite within the plagioclase envelope. Low-Ti green biotite that is texturally late has been interpreted to represent a melt-consuming reaction (Kriegsman and Álvarez-Valero, 2010).

The presence of Mn-rich rims in garnets has been attributed to back reaction with melt (Nyström and Kriegsman, 2003; Kriegsman and Álvarez-Valero, 2010). At such high-temperatures garnets will typically exhibit flat zoning profiles because they have been homogenized (Spear, 1991), but the presence of Mn-rich rims is attributed to garnet resorption (Nyström and Kriegsman, 2003; Kriegsman and Álvarez-Valero, 2010). The Mn present within the garnet will diffuse towards the center of the garnet as the garnet breaks down, because the other mineral phases surrounding the garnet will take in minimal Mn. Consequently the Mn present in the edge of garnet has diffused inwards, but if a large portion of the garnet volume is not lost, the interior of the garnet will retain the homogenized core composition.

The envelope of plagioclase and biotite is here interpreted to be the product of back-reaction between garnet and melt causing a reversal of the original melting reaction.

The zoned garnets surrounded by an envelope of plagioclase and biotite, with rare quartz grains indicate the reaction was,

Garnet + melt = Biotite + Plagioclase + Quartz.

Although sillimanite and K-feldspar may have been involved in the original melt-producing reaction, sillimanite is no longer present in these rocks, and K-feldspar is only found in the matrix, as an elongate, foliation-defining mineral.

Sample WMG117 shows weak resorption-zoning of Mn in two of the garnets (Figure 3.7G). The third garnet present in sample WMG117 is entirely rimmed by plagioclase, with no cordierite present and it has a flat profile, with no Mn-zoning of any type. Garnets in this sample with weak resorption-zoning of Mn, are texturally similar to garnets from WMG123 and are surrounded by plagioclase and biotite, plus cordierite (Figure 3.7F, H). The areas that show higher Mn are adjacent to biotites, the presence of plagioclase or cordierite does not seem to influence Mn zoning. In this case, there also appears to be back reaction with melt. Most likely two different reactions, reflecting garnet resorption, occurred including:

Garnet + melt = Biotite + Plagioclase + Quartz,

the same reaction as seen in WMG123, as well as:

Garnet + melt = Biotite + Cordierite + Quartz.

Cordierite is generally only present in these rocks surrounding garnets or as single grains with a vermicular texture. These isolated grains of cordierite may be surrounding garnets, not exposed in thin section, but would represent the edge of a three-dimensional envelope of material surrounding the garnet. Evidence for this comes from several thin sections that were remade and consequently had a new surface exposed at least 50 μm below the original sample. In the original thin section cordierite was visible, and in the new one garnet was present in the same location, instead of the cordierite. The proximity of cordierite grains to garnets suggests cordierite growth is somehow associated with garnet breakdown.

The presence of resorption-zoning of Mn within garnets from two different locations, suggests that abundant melt was in the system within the Southern Wet

Mountains. The presence of far more abundant stromatic migmatites in this location also provides evidence for far more abundant melt in this vicinity.

3.11 DISCUSSION

Exposures in the Wet Mountains provide evidence for deformation and metamorphism occurring synchronously and an increase in metamorphic grade and abundance of former melt towards the south-southeast. Data presented here document an increase in strain towards the southeast, as indicated by more closely spaced foliation, increasing degrees of feldspar recrystallization, higher aspect ratios in quartz ribbons, and localities in the south with local mylonitization. However, samples for this study were primarily collected near plutons or abundant granite and pegmatite veins, and samples came from a variety of rock types, so strain cannot be compared uniformly in all rocks. Despite these considerations, within the samples studied, gneisses from the northern Wet Mountains had lower aspect ratios on quartz and plagioclase grains parallel to foliation, wider foliation spacing, and lower degrees of recrystallization than gneisses in the central and southern locations. Former melt is found sparsely in the Five Points Deformation Zone, relict melt channels are present at Dawson Mountain, and in the southernmost Wet Mountains there is evidence for back-reaction with melt, indicating abundant melt was present in the system as crystallization began.

In the Five Points Deformation Zone, foliation is moderately well-developed, and quartz and feldspar are elongate parallel to foliation, but there is little evidence for recrystallization in these rocks. The best evidence for high-temperature deformation in these rocks comes from coarse-grained quartz, generally surrounding garnets, that has well-developed subgrains and in rare cases, chessboard extinction. Chessboard extinction occurs when both basal and prism slip are active in quartz and this typically occurs at temperatures at or higher than 700° C (Kruhl, 1996). Rare examples of chessboard extinction and more typical examples of only well-developed subgrains suggest that deformation likely occurred at temperatures below 700° C.

Evidence for partial melting in this area comes from melt pseudomorphs along grain boundaries as well as the embayed, somewhat corroded muscovite grains, in association with sillimanite and K-feldspar. However, the presence of some muscovite within these rocks indicates that muscovite-dehydration was not complete. Rare melt pseudomorphs in conjunction with a moderately well-developed foliation and a lack of recognizable recrystallization indicate that the Five Points Deformation Zone had moderate degrees of both melting and deformation.

Farther to the south and east at Dawson Mountain, both the degree of melting and intensity of strain are increased. The foliation spacing in these rocks is much more closely-spaced than in the Five Points Deformation Zone. The most striking feature at Dawson Mountain is the preservation of melt channels, comprised of K-feldspar/cordierite/pinite and plagioclase. These melt channels suggest that there was melt flowing through these rocks, primarily along grain boundaries and subgrain boundaries, parallel to foliation. However, in these rocks, unlike the ones in the very southern Wet Mountains, there is no zoning in garnets even when garnets are in contact with these relict melt channels. The lack of zoning in these garnets indicates that garnet was only minimally or not at all involved in reaction prior to the crystallization of melt, and either the volume of melt present in these rocks was far smaller than in the Southern Greenhorn Peaks or melt did not stay in the system for very long and instead large quantities of melt migrated through the system. Some of this melt may be associated with magmatism related to the Oak Creek pluton. Shaw et al. (2005) have proposed the central and southern Wet Mountains are adjacent to a mid-crustal magma layer and the geotherms are consequently steeper in this area as a result of magmatism. The location at Dawson Mountain is proximal to the Oak Creek pluton, and the rocks were hotter than those in the Five Points region. The evidence for former partial melt and abundant granitic and pegmatitic veins suggests melt was travelling through these rocks and may have been transported to higher crustal levels.

The presence of coarse quartz grains with chessboard extinction surrounding garnets at Dawson Mountain, suggests that these coarse quartz grains are melt

pseudomorphs that were subsequently deformed at high-temperatures, above 700° C (Kruhl, 1996). Former melt present along subgrains in quartz provides evidence for melting occurring after deformation, because the subgrains had to form before they could be exploited by melt. Thus, deformation appears to have started before melting and outlasted crystallization of melt.

Rocks of mostly granitic composition are found in the central and southern Wet Mountains in the Newlin Creek/Locke Mountain deformation zone, at Hardscrabble Creek and in the Williams Creek exposures. In the Newlin Creek/Locke Mountain deformation zone the presence of quartz grains that are equigranular, straight sided, and have a moderate lattice preferred orientation provides evidence for rotational recrystallization. The lack of well-developed subgrains in plagioclase, growth of new unstrained grains along some grain boundaries between plagioclase and K-feldspar, and fine to very fine grained crystals that resemble chert, indicates migrational recrystallization in feldspar. In the North Hardscrabble area, the development of some quartz ribbons indicates easy (high-temperature) grain boundary migration in quartz (Passchier and Truow, 1996). Better subgrain development in feldspar and core and mantle structures indicates rotational recrystallization in feldspars. Williams Creek rocks have extensively developed quartz ribbons, with aspect ratios up to 10:1, sometimes displaying chessboard extinction, a strong lattice preferred orientation, up to 60-70% feldspar recrystallization and development of an S-C fabric indicating local mylonitization and the apparent highest degrees of strain in the field area.

Former melt is typically found on grain boundaries, triple junctions and adjacent to serrate-cuspate grain boundaries in these rocks, which is typical of melt microstructures attributed to granitic wet melting (Harte et al., 1991; Rosenberg and Riller, 2000; Sawyer, 2010). Because deformation occurred synchronously with melting, it appears that many of the melt microstructures have been overprinted by recrystallization. All of these rocks have evidence for former melt, but in many locations well-preserved melt pseudomorphs along a grain boundary transitions into an area that is pervasively recrystallized with abundant formation of new grains (see Figure 3.6B, G).

This association indicates that areas that contained melt were preferentially recrystallized, perhaps because they were rheologically weaker.

The southernmost Wet Mountains provide evidence for abundant melt in the system as indicated both by stromatic migmatites exposed in all rock types as well as widespread back-reaction between garnet and melt. Garnets in some of these rocks have an increase in Mn-content at their rims and are surrounded by envelopes of plagioclase/cordierite and biotite. This pattern of Mn-zoning, with Mn-rich rims, indicates garnets have been resorbed, and the envelope surrounding these garnets is comprised of the likely products of the garnet resorption reaction. These textures are quite different than the interpreted melt channels from Dawson Mountain, despite rocks in both areas providing evidence for biotite-dehydration melting. The lack of zoning in Dawson Mountain garnets indicates there was minimal reaction between garnet and melt, likely as a result of small volumes of melt moving through the rock. The well-developed Mn zoning in the garnets in the south combined with the textural appearance of poikloblastic, ragged, and embayed garnets surrounded by an envelope of plagioclase/cordierite and biotite, indicates significant melt-garnet interaction, likely due to abundant melt pooling in these rocks.

Across the Wet Mountains there appears to be a relationship between deformation and partial melting, with melt-rich areas localizing strain and highly strained locations preferentially melting. In the northern part of the range there are few textures indicative of in situ partial melting, the rocks have a low degree of recrystallization, low aspect ratios of quartz and feldspar grains, and a more widely spaced foliation than samples from the central/southern Wet Mountains.

At Dawson Mountain, the degree of partial melting and intensity of strain have increased substantially from the Five Points Deformation Zone, and here there is evidence for an association between deformation and partial melting. Coarse quartz grains surrounding garnet display chessboard extinction; this quartz is interpreted to represent crystallized leucosome and consequently deformation occurred after melting. Although this quartz must have been solid when the chessboard extinction formed,

deformation was localized within the area that had been molten. Melt channels at Dawson Mountain are found along grain boundaries and subgrain boundaries; the subgrain boundaries where partial melting occurred are found within the quartz grains that display chessboard extinction. Here, melting preferentially occurred along the same high-strain locations where deformation had previously been localized.

Within the southern Wet Mountains, particularly along the Williams Creek Road, where strain was the highest of any part of the field area, former melt is typically found in these rocks as thin films along grain boundaries. In many locations former melt, now K-feldspar is found along grain boundaries between plagioclase grains, or quartz and plagioclase and the crystals of plagioclase have very serrate/cuspate grain boundaries with low dihedral angles, suggesting these were areas where melting occurred. Some of these locations still show nicely preserved former melt, but others have undergone intense recrystallization, and there are abundant new fine grains of K-feldspar. Quartz ribbons, formed during easy (high-temperature) grain boundary migration, are present in several of these samples, and many of them contain former melt or have melt pseudomorphs along their grain boundaries. In some cases these quartz ribbons display chessboard extinction, and former melt is found along the subgrains within these ribbons, suggesting the intense deformation preferentially localized partial melting.

The above observations demonstrate that the products of partial melting (i.e. leucosomes, former melt films) are deformed and that deformed areas, on both the microscopic and field scale, are sites for partial melting. This association suggests a possible positive feedback loop where deformation is preferentially concentrated in melt-rich regions that are rheologically weaker and where increased deformation enhances the melting reaction. The former is generally accepted (Sawyer, 1994; Brown, 1994; Brown and Rushmer, 1997; Sawyer, 2001), and I present evidence in Chapter 5 that supports the role of lattice strain in promoting partial melting.

Although the intensity of strain appears to increase to the south and is localized in areas of partial melting, this effect may also be related to proximity to plutons and granitic dikes and veins. The samples collected in the Five Points Deformation Zone are

not close to any plutons, and they have few melt microstructures and are relatively low strain. Samples from Dawson Mountain are within the zone proposed to be affected by mid-crustal melt flow (Shaw et al., 2005), are adjacent to the Oak Creek pluton, and have tighter foliation spacing and higher aspect ratios of quartz and feldspar. Finally, rocks from the southernmost Wet Mountains are locally mylonitized, strongly recrystallized, have the highest aspect ratios for quartz and feldspar and a very tight spacing of the foliation. These rocks are adjacent to numerous magmatic bodies, ranging from pluton-scale, to veins and dikes of centimeter-meter scale. Thus the increases in intensity of strain from north to south may reflect localization of strain into areas that contain more former melt and crustal-scale magmatism. An increase in metamorphic grade correlates with the increase in degree of partial melting and plutonism and likely reflects proximity to a mid-crustal magma layer and associated steepened geothermal gradient as proposed by Shaw et al. (2005).

3.12 Correlations with Tectonic Models

Previous work on the Wet Mountains has focused on the larger tectonic picture of the area and has provided excellent timing constraints on magmatism in the area. Shaw et al. (2005) and Jones et al. (2010) have proposed a tectonic model for the area, with the northern Wet Mountains interpreted as upper crustal exposures and the southern Wet Mountains as lower crustal exposures (Figure 3.8). Jones et al. (2010) documented partitioned deformation, steep fabrics and discrete plutonism in the Northern Wet Mountains and correlated these with other upper crustal shear zones in Colorado. Shaw et al. (2005) propose a mid-crustal magma layer, which is coincident with the Oak Creek pluton in the central Wet Mountains, and numerous plutonic bodies and widespread lower crustal flow in the southern Wet Mountains.

These observations and the proposed tectonic model correlate well with observations based primarily on melt microstructures and detailed petrography of these rocks. In the northern Wet Mountains I documented the least strained rocks, rare melt pseudomorphs, and the lowest grade rocks of the area. Just north of the Oak Creek

pluton at Dawson Mountain we see relict melt channels in the rocks, consistent with a mid-crustal magma layer. In the southern Wet Mountains we see abundant evidence for melt in the system as evidenced by back-reaction between melt and garnet and abundant stromatic migmatites, consistent with widespread lower-crustal flow.

3.13 CONCLUSIONS

Samples collected from the Wet Mountains, from northwest to southeast, show an increase in metamorphic grade, intensity of strain, and volume of melt flowing through the rocks of the Wet Mountains. These processes of deformation and partial melting appear to enhance each other, with deformation localizing partial melting and the presence of melt localizing deformation, suggesting a positive feedback loop. The more deformed rocks provide more evidence for large volumes of melt in the system both by preserved former melt and textural and chemical evidence for garnet-melt interaction. Rocks containing more melt preferentially localize deformation into melt-rich areas as evidenced by chessboard extinction in quartz which represents crystallized leucosome and preferential recrystallization of former melt-rich locations, commonly along grain boundaries between feldspars. Analysis of detailed petrography and melt microstructures correlates well with larger scale plutonism and tectonic models for the Wet Mountains. In particular, the correlation between melt microstructures and larger granitic plutons, veins, and dikes suggests melt microstructures can be used as a proxy for crustal-scale melt flow.

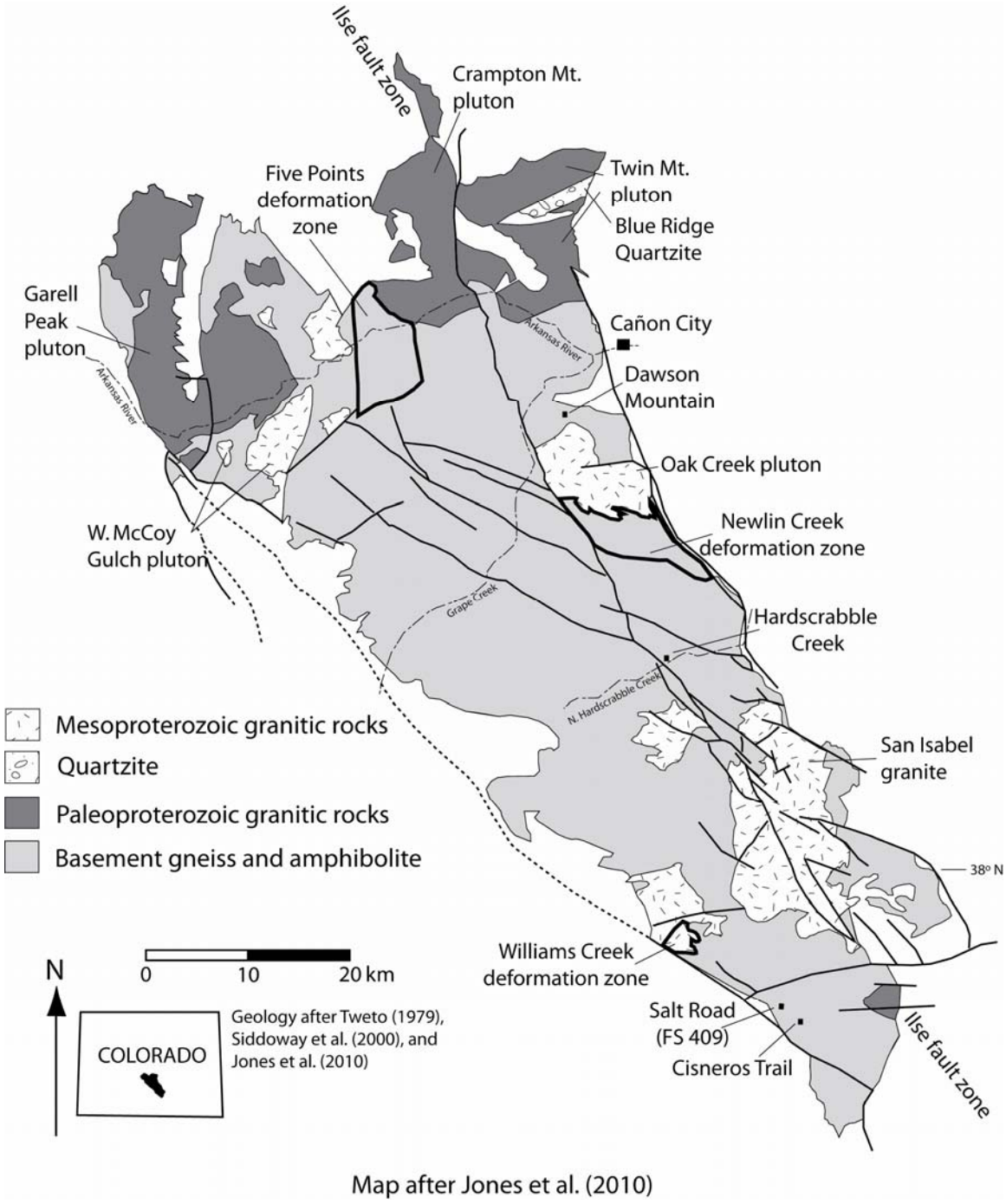

Figure 3.1. Geologic map of the Wet Mountains, central Colorado (after Jones et al., 2010). Areas represented with black squares and outlined in black represent locations where field work was conducted during this study.


gar
A
gar
gar
gar
B
C
pl
pl
pl
D
ksp
ksp
ksp
E
gar
gar
gar
F

Figure 3.2. Field photographs of typical exposures of rocks from each of the field areas, the degree of deformation, and textures associated with partial melting. A. Sparse leucocratic pods surrounding garnets. The long axes of the pods are parallel to lineations in the Five Points Deformation Zone. Foliation is defined by aligned biotite-rich layers alternating with quartzofeldspathic layers. Medium-grained muscovite gives the rock a sparkly appearance. B. Leucosomes of quartzofeldspathic material surrounding garnets, at an angle to foliation, Dawson Mountain. Millimeter-scale foliation is defined by alternating layers of quartzofeldspathic material and aligned biotite and sillimanite. C. Granitic gneisses in the Newlin Creek/Locke Mountain deformation zone with well-developed foliation that has been isoclinally folded. A pegmatite vein in lower part of the photo is sub-parallel to foliation. D. Foliation defined by layers of biotite and amphibole alternating with quartzofeldspathic material, North Hardscrabble Creek. Some quartzofeldspathic layers and feldspar megacrysts are boudinaged and feldspars are strung out parallel to foliation. E. Granitic gneisses with well-developed foliation defined by alternating layers of quartzofeldspathic material that contain K-feldspar augen and biotite or amphibole, Williams Creek. Development of a sheared fabric is indicated by foliation wrapping the K-feldspar augen and strung out feldspars. F. Metapelitic migmatite with pervasive leucosomes containing garnets, determined to be a product of partial melting, along the Cisneros Trail. Former melt is present parallel to foliation and at an angle to the dominant foliation. Garnets are present both within leucocratic layers and restitic material.

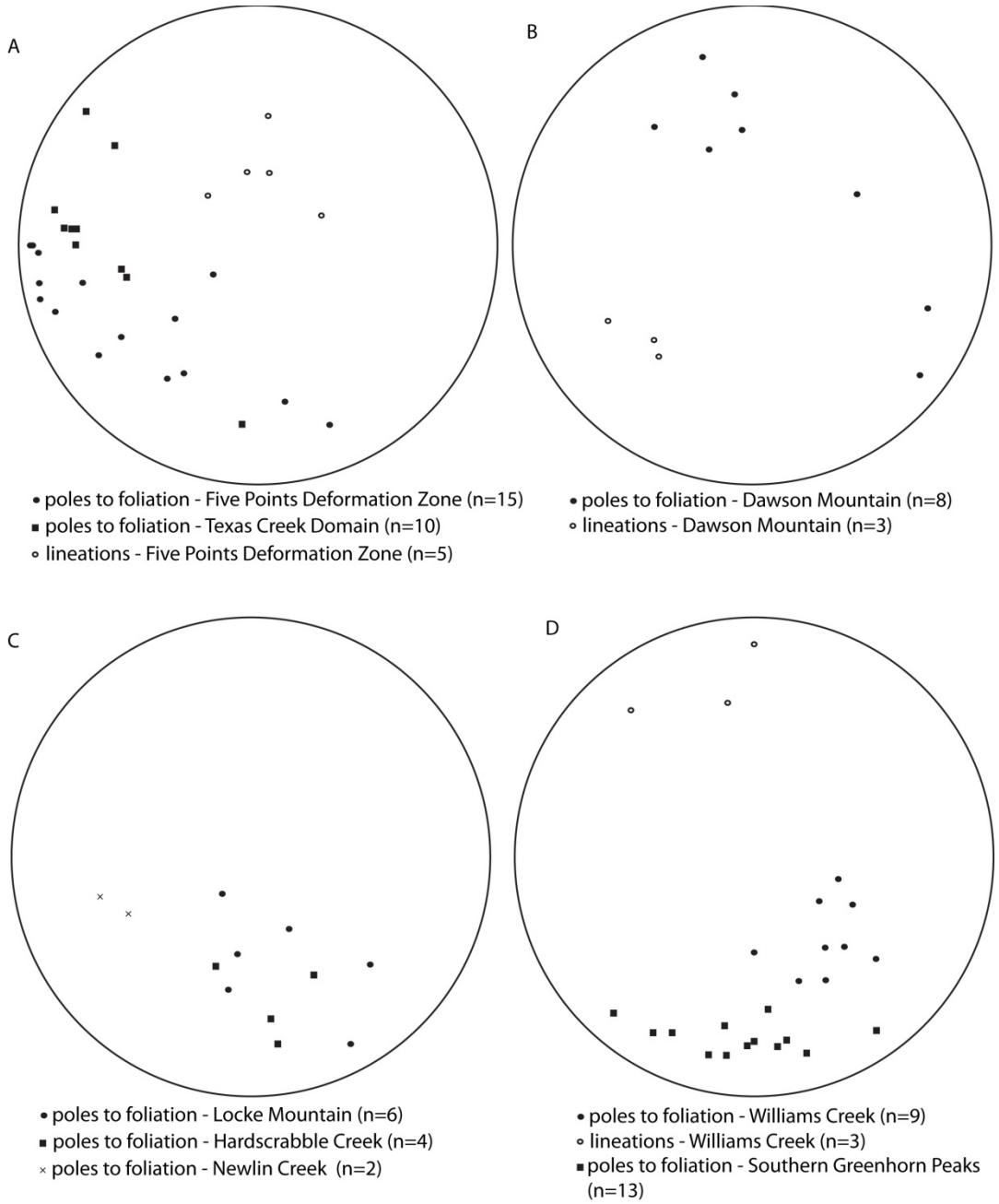

Figure 3.3. Equal area, lower hemisphere stereonets of S_2 foliation and L_2 lineations from all field areas. A. Poles to S_2 foliation from the Five Points Deformation Zone (filled circles) and the Texas Creek Domain (filled squares) and L_2 lineations from the Five Points Deformation Zone (open circles). B. Poles to S_2 foliation at Dawson Mountain (filled circles) and L_2 lineations (open circles). C. Poles to S_2 foliation at Newlin Creek (crosses), Locke Mountain (filled circles) and Hardscrabble Creek (filled squares). D. Poles to S_2 foliation at Williams Creek (filled circles) and Southern Greenhorn Peaks (filled squares) and L_2 lineations from Williams Creek (open circles).

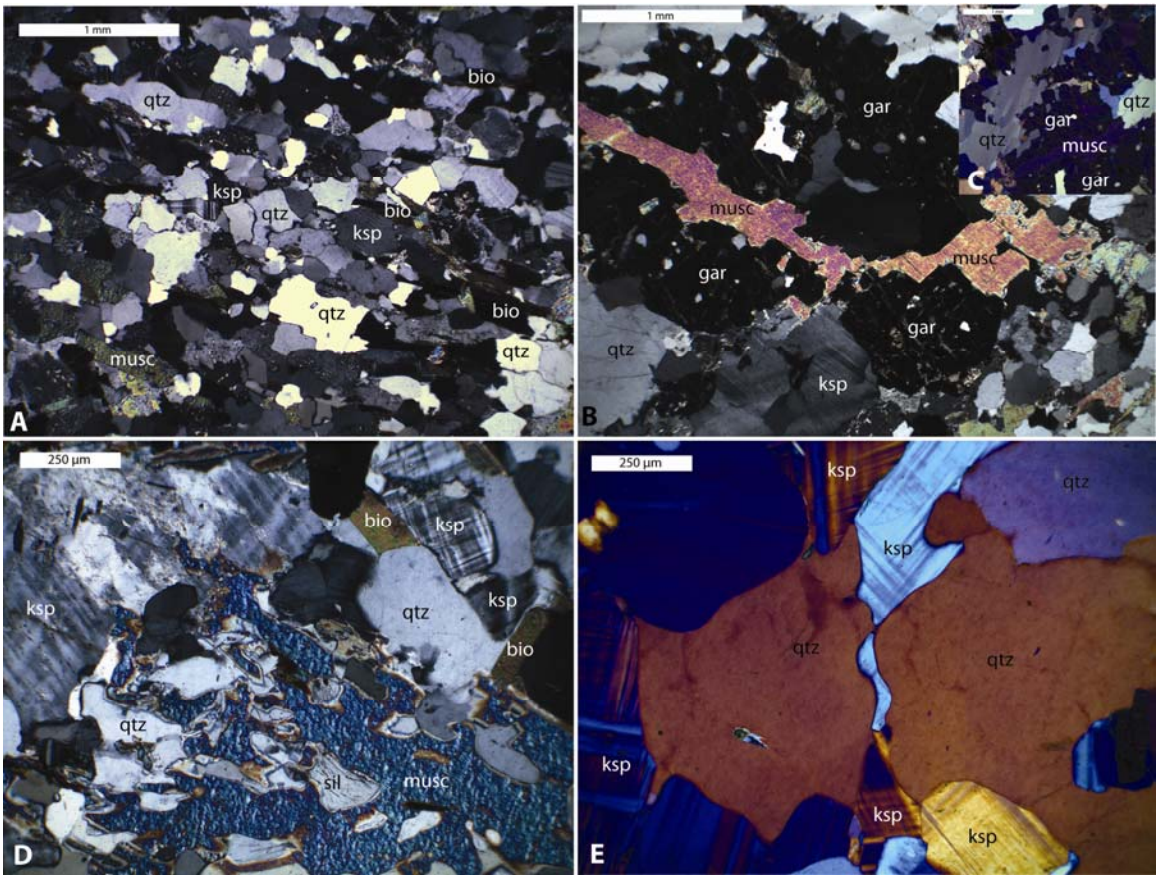

Figure 3.4. Photomicrographs from the Five Points Deformation Zone documenting microstructures, mineral assemblages and former melt textures. A. S_2 foliation defined by aligned biotite alternating with layers of elongated quartz and feldspar. Muscovite is also parallel to foliation and is coarser-grained than biotite. (Image in crossed-polars) B. Garnet with serrate and embayed margins crossed by muscovite in optical continuity. The surrounding material is composed of coarse grains of quartz and feldspar with local subgrain development. (Image in crossed-polars) C. Includes area shown in B, with gypsum plate, inserted to show well-developed subgrains within quartz surrounding the garnet. D. Coexisting muscovite, K-feldspar and sillimanite, indicating the second sillimanite isograd has been attained. Blebs of quartz within the muscovite and the overall embayed character of the muscovite grain indicate that partial melting has occurred (Sawyer, 1999; Waters, 2001). (Image in crossed-polars) E. Melt pseudomorph, now K-feldspar, interpreted based on its location between two quartz grains with rounded edges. (Image with gypsum plate)

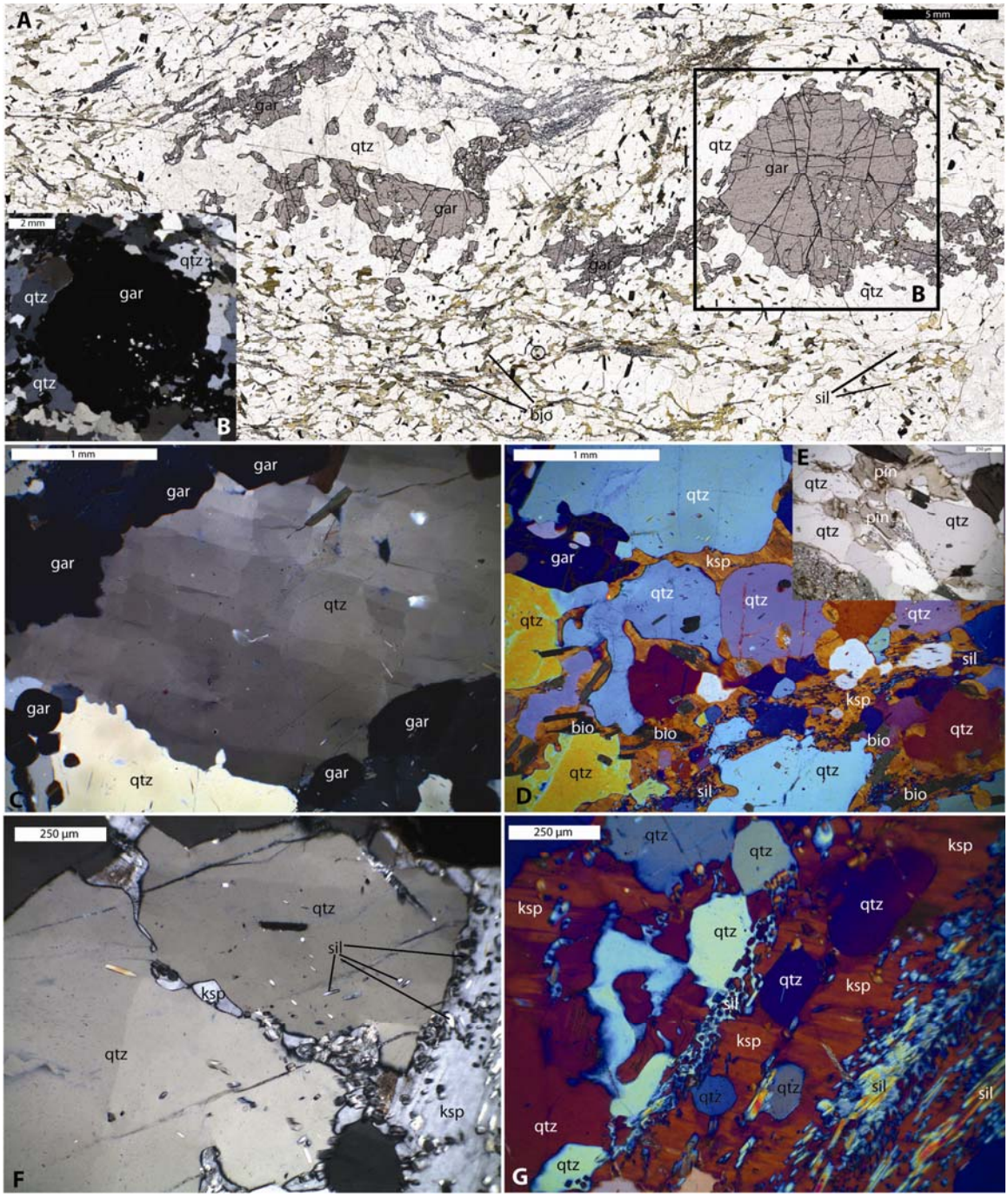

Figure 3.5. (continued on next page). Photomicrographs from Dawson Mountain illustrating the relative timing relationships between deformation and partial melting, characteristic mineral assemblages, and former melt textures. A. Plane-polarized image of thin section containing well-developed foliation, defined by alternating layers of biotite and sillimanite, and aligned quartz and feldspar. Somewhat embayed garnets, wrapped by the foliation, are surrounded by a leucosome that is void of biotite and

sillimanite. B. Boxed area within A in crossed polars. A very thin layer of plagioclase and K-feldspar is present upon some segments of the garnet grain boundary; evident as a narrow zone with gray extinction colors on the left side of the garnet. Garnet and rim are within an envelope of quartz, void of biotite and sillimanite. C. Close-up of quartz grain displaying chessboard extinction that is indicative of deformation at high temperature and represents crystallized leucosome (Waters, 2001; Barbey, 2007). (Image in crossed polars) D. Cuspate tapering grain boundary phase, which is interpreted as relict melt channels (orange) of perthitic K-feldspar and rimmed by plagioclase. Sillimanite is found within the interpreted melt channels, in addition to corroded biotite, which likely dehydrated to produce the melt. (Image with gypsum plate) E. Same textures from another part of this sample, but instead of K-feldspar as the dominant grain boundary phase, the phase is pinitized cordierite (yellow). (Image in plane-polarized light) F. K-feldspar containing inclusions of sillimanite, interpreted as a relict melt channel along a subgrain in quartz, indicating melting and melt migration occurred along the subgrain boundary. (Image in crossed polars) G. Close-up view of interpreted melt channel (entire field of view, orange) now composed of K-feldspar. As the melt crystallized, it broke down into some of its constituent components, and in some cases nucleated on pre-existing crystals. The quartz in particular can be seen in shades of light green-blue, and it appears to have nucleated onto the quartz crystals that were already present, because of the presence of a linear group of sillimanite crystals and optical continuity within all the quartz in contact with sillimanite. The rest of the former melt appears to have crystallized as K-feldspar and plagioclase. (Image with gypsum plate)

	Grt 1 rim	Grt 1 core	Grt 2 rim	Grt 2 core
Na_2O	0	0.08	0	0.09
CaO	0.41	0.60	0.42	0.42
K_2O	0.00	0	0.00	0.03
$Al2O_3$	21.39	21.89	21.70	21.89
SiO_2	37.12	37.58	37.53	36.68
MgO	4.69	4.79	4.56	4.40
FeO	35.48	35.61	35.96	36.16
TiO_2	0.00	0.01	0.00	0.01
MnO	0.50	0.52	0.57	0.59
Total	99.59	101.07	100.75	100.25
Na	0	0.012	0	0.013
Ca	0.035	0.051	0.035	0.036
K	0.000	0	0.000	0.003
Al	2.023	2.038	2.030	2.065
Si	2.978	2.968	2.978	2.936
Mg	0.561	0.564	0.539	0.525
Fe	2.38	2.352	2.386	2.421
Ti	0.000	0.001	0.000	0.000
Mn	0.034	0.035	0.039	0.040
Total	8.011	8.019	8.007	8.039
XCa	0.012	0.017	0.012	0.012
XMg	0.186	0.188	0.180	0.174
XFe	0.791	0.784	0.796	0.801
XMn	0.011	0.012	0.013	0.013

Table 3.1. Microprobe data of representative garnet composition in samples from Dawson Mountain.

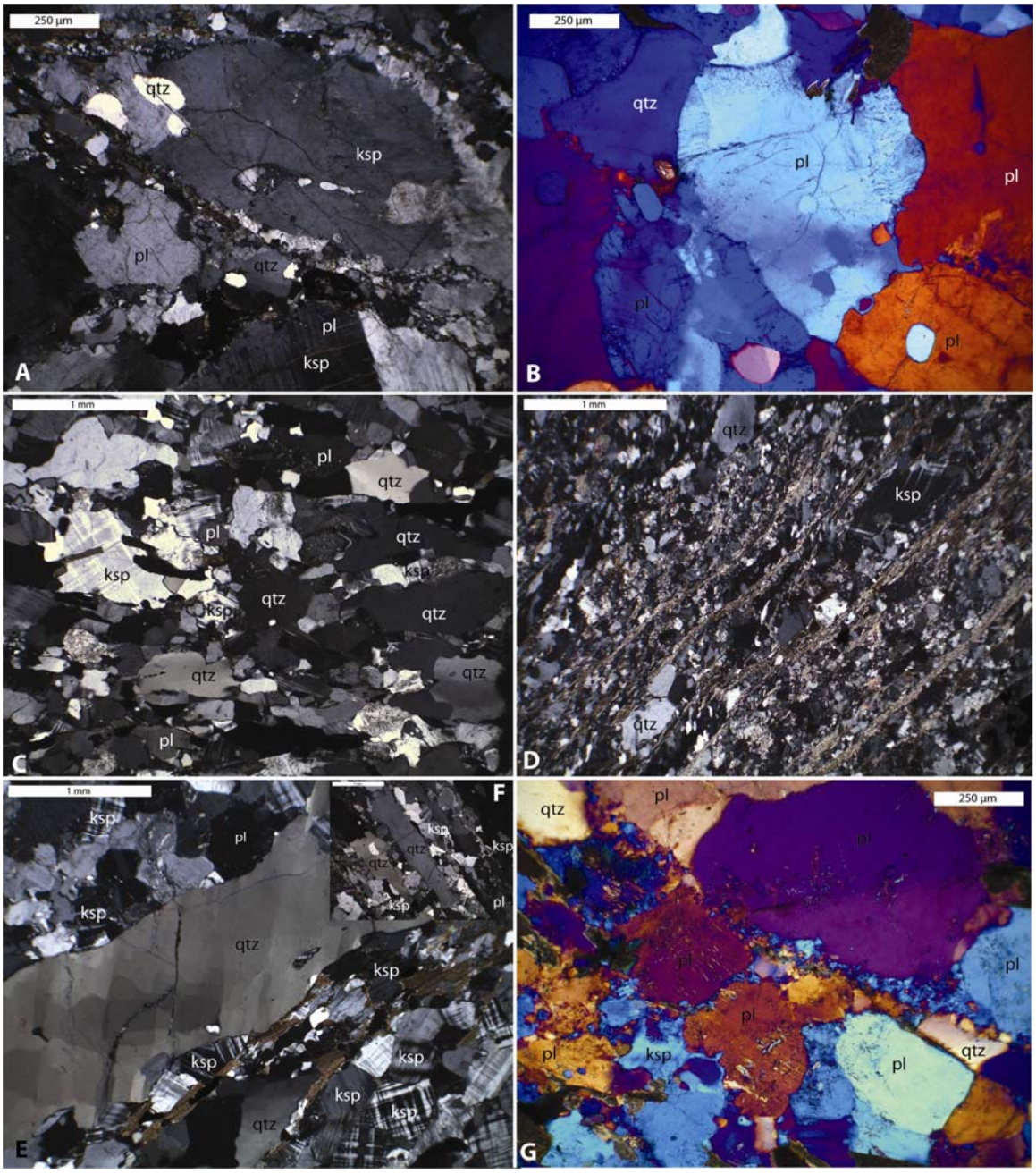

Figure 3.6 (continued on next page). Photomicrographs from the Newlin Creek/Locke Mountain deformation zone, Hardscrabble Creek and Williams Creek, all localities that have mineral associations indicative of fluid-present granitic melting. A. K-feldspar augen from the Newlin Creek/Locke Mountain deformation zone with myrmekite and fine-grained recrystallized quartz and feldspar, resembling chert in appearance, along the outside of the grain. (Image in crossed polars) B. Plagioclase grain (blue) from the Newlin Creek/Locke Mountain deformation zone with myrmekite developed on the right edge, serrate/cuspate grain boundaries and moat structures. Both are former melt textures

(Mehnert et al., 1973; Sawyer, 2001, 2008). (Image with gypsum plate) C. Well-developed foliation defined by elongate quartz and feldspar alternating with aligned biotite grains, in sample WMH103-1 from North Hardscrabble Creek. K-feldspar forms narrow grain boundary films, occupies the interstices at triple junctions, and has serrate/cuspate grain boundaries with reactant grains, a microstructure identified as a melt pseudomorph by Holness and Sawyer (2008). There is crude development of ribbon structure in quartz. (Image in crossed polars) D. Mylonite gneiss sample WMG112-1 from Williams Creek road, exhibiting pervasively recrystallized grains and well-developed core and mantle structure. (Image in crossed polars) E. Quartz ribbon with chessboard extinction, Williams Creek Road. New K-feldspar grains are all the same shape and size, indicating they formed during subgrain rotation recrystallization (Passchier and Truow, 1996). Small blebs of K-feldspar within quartz grains may represent former melt. (Image in crossed polars) F. Inset shows quartz ribbons and recrystallized feldspar, which is evidence of high-temperature grain boundary migration. (Image in crossed polars) G. Plagioclase grains with serrate/cuspate grain boundaries adjacent to K-feldspar. These areas of K-feldspar likely represent former melt, because of their serrate/cuspate shape and have been preferentially recrystallized. (Image with gypsum plate)

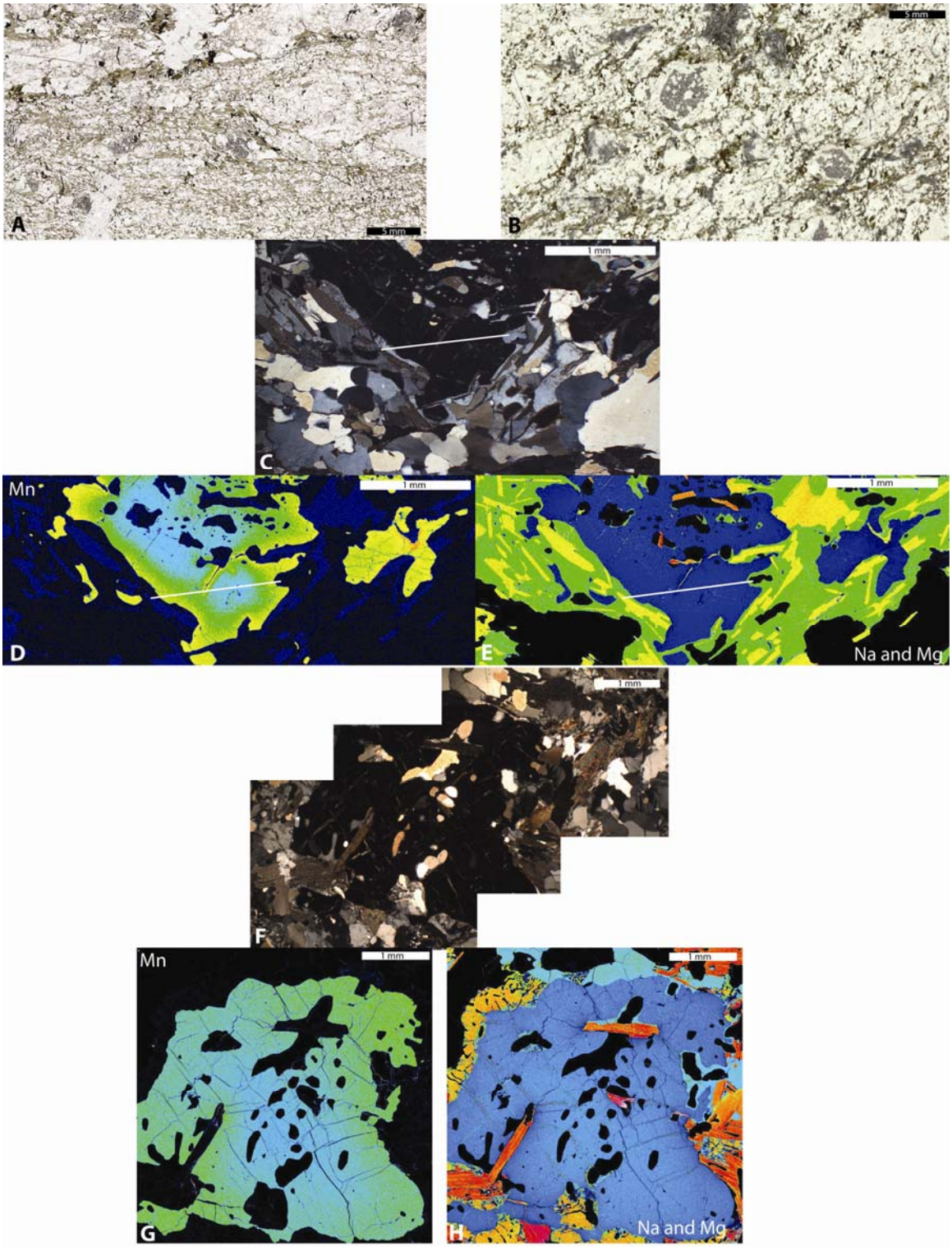
A
5 mm
B
5 mm
C
1 mm
Mn
D
1 mm
E
1 mm
Na and Mg
F
1 mm
Mn
G
1 mm
H
1 mm
Na and Mg

Figure 3.7. Photomicrographs and X-ray maps from garnets in the Southern Greenhorn Peaks. A. Thin section in plane-polarized light showing well-developed foliation defined by alternating layers of biotite-rich and quartzofeldspathic material. There is an absence of leucosome surrounding the garnets in this sample. B. Thin section in plane-polarized light that shows garnet surrounded by biotite-free leucosome. Foliation is defined by layers of biotite and sillimanite alternating with quartzofeldspathic material. The foliation wraps around garnets and cordierite, that likely rims garnet in the third dimension (see text for details). C. Poikiloblastic garnet from sample WMG123 that is surrounded by an envelope of plagioclase and biotite. White line represents the microprobe transect across the garnet, data tabulated in Table 3.2. Inclusions within the garnet are quartz rimmed by thin plagioclase between the quartz and garnet. (Image in crossed polars) D. Mn X-ray map of the garnet shown in C, with low Mn content in the core and high Mn content at the rims. Disaggregated parts of the garnet no longer attached to the main garnet have high Mn content. White line is the same as in C. E. Combined Na and Mg X-ray map of the area in C that shows the envelope of plagioclase (green) and biotite (yellow) surrounding the garnet, and plagioclase inclusions within the garnet (green). White line is the same as in C and D. F. Photomosaic of garnet in sample WMG117 surrounded by a narrow rim of plagioclase and biotite in the upper right, and cordierite and biotite in the lower left. Inclusions within the garnet are dominantly quartz with a thin rim of plagioclase. Where biotite inclusions are present, plagioclase on the grain boundary separates garnet from biotite. G. Mn X-ray map of the area in F, showing very slight increase in Mn content towards the rims of the garnet. This increase in Mn content appears to be more pronounced where garnet is adjacent to biotite, as opposed to cordierite or plagioclase. H. Combined Na and Mg X-ray map of the area in Figure F, which shows vermicular cordierite (yellow) on the left side and bottom and plagioclase (blue) on the top and right of the garnet. Slight Mg zoning is visible in the garnet with a decrease in Mg content at the rims, likely compensating for the increase in Mn content in these locations. The garnets for which compositional maps exist are very uniform with respect to Na and Mg, however.

Table 3.2: Microprobe data of garnet and biotite compositions in Southern Greenhorn Peaks rocks. Garnet data show representative analyses from a transect across the garnet shown in Figure 3.7C-E, and a garnet with no Mn zoning. Biotite data are from representative brown matrix biotite and green biotite from within the plagioclase-biotite envelope.

	Transect across garnet with Mn zoning								Transect across garnet with no Mn zoning						Brown Biotite			Green Biotite		
Na_2O	0.01	0.02	0.01	0.01	0.00	0.01	0.01	0.01	0.00	0.00	0.02	0.01	0.02	Na_2O	0.10	0.09	0.08	0.08	0.06	0.10
CaO	1.09	1.04	1.05	1.12	1.10	0.99	1.00	0.98	0.87	0.82	0.82	0.78	0.78	CaO	0.00	0.00	0.00	0.00	0.00	0.00
K_2O	0.01	0.00	0.01	0.01	0.00	0.27	0.01	0.01	0.01	0.00	0.02	0.00	0.01	K_2O	9.52	9.49	9.58	9.47	9.41	9.51
$Al2O_3$	20.88	20.99	21.12	21.18	21.14	21.56	21.14	21.02	21.15	21.31	21.32	21.42	21.14	$Al2O_3$	18.64	18.60	18.38	19.67	19.17	19.72
SiO_2	37.34	37.16	36.97	37.49	36.63	37.56	36.93	36.65	37.53	37.78	38.14	37.86	37.93	SiO_2	34.84	34.86	35.39	34.83	35.20	35.21
MgO	2.00	2.16	2.33	2.43	2.50	2.61	2.39	2.05	4.28	4.28	4.33	4.36	4.29	MgO	7.90	7.98	7.50	8.43	8.40	8.63
FeO	30.72	31.80	32.47	32.80	33.45	32.15	32.89	31.00	33.19	33.03	33.75	33.02	33.02	FeO	21.91	21.62	20.71	20.74	20.34	19.90
MnO	8.04	7.43	6.60	5.71	5.34	5.17	6.18	7.75	2.13	2.13	2.16	2.09	2.11	MnO	0.22	0.13	0.24	0.14	0.16	0.10
TiO_2	0.01	0.00	0.00	0.01	0.01	0.00	0.00	0.01	0.00	0.00	0.00	0.01	0.01	TiO_2	1.50	1.57	2.30	0.19	0.22	0.06
Total	100.08	100.59	100.55	100.77	100.17	100.32	100.56	99.48	99.15	99.34	100.55	99.54	99.30	Total	94.63	94.33	94.19	93.54	92.97	93.22
	Garnet calculated based on 12 Oxygens								Garnet calculated based on 12 Oxygens						Biotite calculated based on 22 Oxygens					
Na	0.001	0.002	0.001	0.002	0.000	0.001	0.002	0.002	0.000	0.000	0.003	0.001	0.003	Na	0.029	0.026	0.025	0.023	0.017	0.031
Ca	0.094	0.090	0.091	0.097	0.095	0.085	0.087	0.086	0.075	0.070	0.070	0.066	0.067	Ca	0.000	0.000	0.000	0.000	0.000	0.000
K	0.001	0.000	0.001	0.001	0.000	0.028	0.001	0.001	0.001	0.000	0.002	0.000	0.001	K	1.890	1.886	1.898	1.886	1.881	1.890
Al	1.992	1.997	2.010	2.003	2.020	2.038	2.012	2.021	2.003	2.010	1.992	2.016	1.995	Al	3.423	3.419	3.369	3.625	3.545	3.627
Si	3.022	2.999	2.985	3.008	2.969	3.012	2.982	2.990	3.016	3.024	3.024	3.023	3.036	Si	5.422	5.431	5.496	5.438	5.516	5.487
Mg	0.241	0.259	0.280	0.291	0.302	0.312	0.288	0.249	0.512	0.511	0.511	0.518	0.513	Mg	1.833	1.853	1.736	1.963	1.962	2.006
Fe	2.080	2.147	2.193	2.201	2.267	2.156	2.221	2.115	2.230	2.211	2.237	2.204	2.211	Fe	2.851	2.817	2.689	2.707	2.665	2.593
Mn	0.551	0.508	0.452	0.388	0.366	0.351	0.422	0.536	0.145	0.145	0.145	0.142	0.143	Mn	0.029	0.017	0.031	0.018	0.022	0.014
Ti	0.000	0.000	0.000	0.001	0.000	0.000	0.000	0.001	0.000	0.000	0.000	0.000	0.001	Ti	0.175	0.183	0.269	0.022	0.026	0.006
Total	7.982	8.003	8.012	7.991	8.021	7.983	8.014	8.000	7.983	7.971	7.983	7.970	7.968	Total	15.651	15.632	15.512	15.683	15.634	15.654
XCa	0.032	0.030	0.030	0.032	0.031	0.029	0.029	0.029	0.025	0.024	0.024	0.023	0.023	XMg	0.375	0.380	0.367	0.417	0.420	0.434
XMg	0.081	0.086	0.093	0.098	0.100	0.107	0.096	0.083	0.173	0.174	0.173	0.177	0.175	XFe	0.583	0.058	0.569	0.575	0.570	0.561
XFe	0.701	0.715	0.727	0.739	0.748	0.743	0.736	0.708	0.753	0.753	0.755	0.752	0.754	XTi	0.036	0.038	0.057	0.005	0.006	0.001
XMn	0.186	0.169	0.150	0.130	0.121	0.121	0.140	0.180	0.049	0.049	0.049	0.048	0.049							

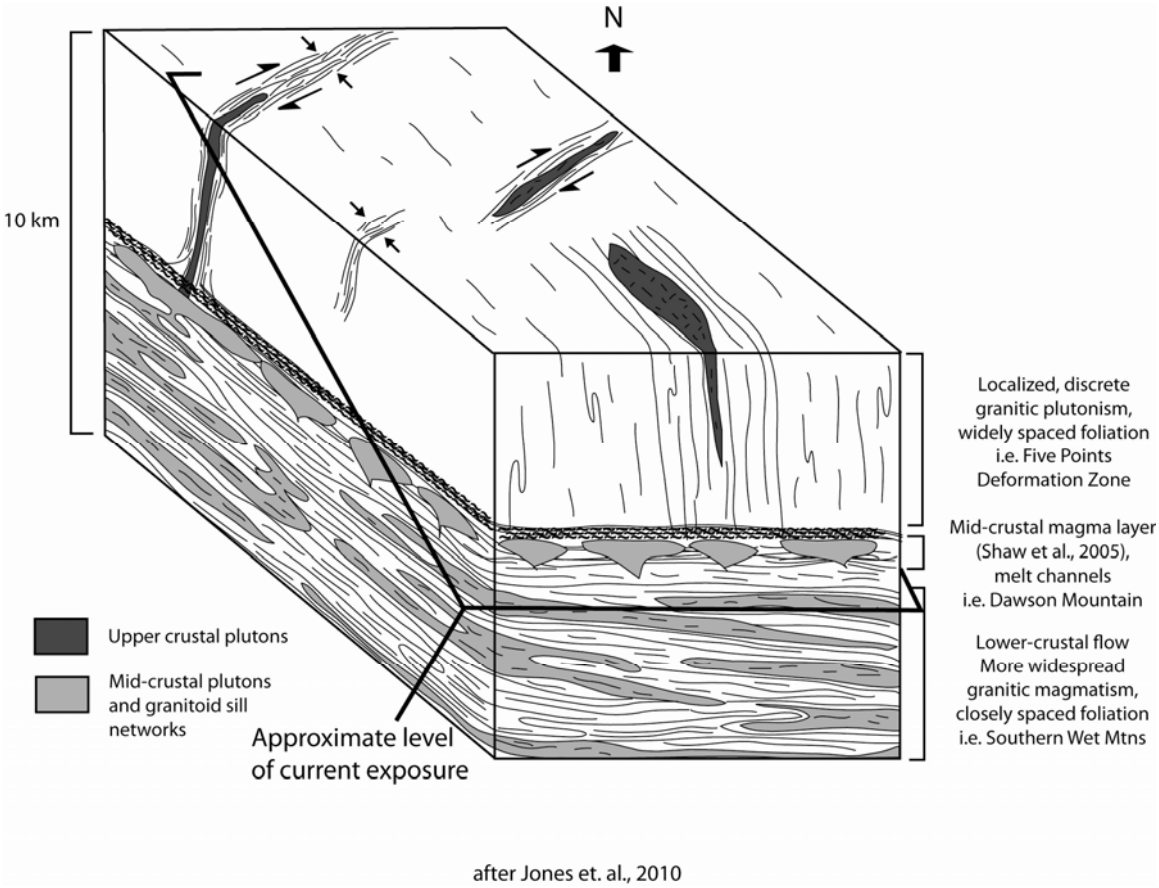

Figure 3.8. Tectonic block model of the Wet Mountains (after Jones et al., 2010). The top of the model (shown in white) represents upper crustal exposures, and Jones et al. (2010) document localized granitic plutonism and steeply-dipping fabrics, which are representative of relationships in the Five Points deformation zone. There are few melt microstructures, more widely-spaced foliations, and scant evidence for recrystallization within these, the lowest-grade rocks of this study. Shaw et al. (2005) and Jones et al. (2010) propose the area around the Oak Creek pluton represents a mid-crustal magma-rich layer and my observations of relict melt channels within samples from Dawson Mountain, in migmatites that have well-developed pervasive foliation, are consistent with that interpretation. In the Southern Wet Mountains, Jones et al. (2010) found evidence of lower crustal flow and distributed framework magmatism instead of discrete plutonism. My observations of extensive back-reaction with melt, abundant stromatic migmatites and the highest strain fabrics in the field area provide an excellent correlation.

Chapter 4: Geochemical evidence for fluid-saturated and -undersaturated partial melting during crustal extension in the Albany-Fraser Orogen, southwestern Australia

4.1 ABSTRACT

Five distinct generations of leucosomes and pegmatites from granulite-facies migmatites at Bremer Bay, part of the Biranup Complex of the Albany-Fraser Orogen, provide evidence for partial melting via fluid-saturated and -undersaturated biotite- and amphibole-dehydration. Leucosomes are associated with structures formed during bidirectional extension in an overall contractional regime and include foliation-parallel, cross-cutting, boudin neck and jumbled channelway leucosomes and late pegmatites. Earliest leucosomes are found parallel to the dominant migmatitic foliation and have the lowest SiO_2 and highest CaO, FeO and MgO contents of all of the leucosomes. Jumbled channelway leucosomes have a narrow range in SiO_2 content and have moderate to high CaO and low K_2O contents. Foliation-parallel and jumbled channelway leucosomes are interpreted to result from fluid-saturated or -undersaturated amphibole-dehydration melting and may contain accumulation of plagioclase. Cross-cutting leucosomes began forming just after the foliation-parallel leucosomes but continued forming throughout deformation, as evidenced by their broad compositional range, with some samples containing abundant plagioclase and others abundant K-feldspar. These samples likely represent a change from local fluid-saturated or -undersaturated amphibole-dehydration melting to distal fluid-undersaturated biotite-dehydration melting. Boudin-neck leucosomes have high SiO_2 and K_2O contents and also represent fluid-undersaturated biotite-dehydration melting. Pegmatites cross-cut all other structures and have a broad range in composition, with some plagioclase-rich and some K-feldspar-rich samples and can be separated into high and low Ba groups. The high Ba samples have a positive correlation with K_2O content and likely formed earlier than the low Ba samples.

4.2 INTRODUCTION

The structural evolution of migmatitic domains and differentiating between generations of partial melt can be quite enigmatic on the basis of field relationships or

petrographic analysis alone. In complexly deformed orogenic belts, migmatites are commonly found within a wide variety of structures, including foliation-parallel leucosomes, boudin neck leucosomes, shear zones containing leucosomes, and axial planar leucosomes (Mehnert, 1968; Brown, 1973; Hollister and Crawford, 1986; Brown, 1994, Sawyer, 1994). Although many mechanisms for melt segregation in actively deforming orogenic belts have been proposed, the mechanism of greatest importance is likely pressure gradients caused by differential stress (Brown et al., 1995; Vanderhaeghe, 2001). Differential stress causes melt to migrate into dilatant structures (Brown, 1994; Sawyer, 1994), but the timing of melt crystallization within several types of dilatant structures cannot be interpreted from field relationships alone. Although cross-cutting relationships between several generations of structures may be clear, the former melt located within these structures may have travelled along several interconnected conduits. As melt migrates through dilatant structures, different generations of melts may intermingle and during cooling, fractional crystallization or crystal accumulation may lead to modified melt compositions (Sawyer, 1998; Sawyer et al., 1999).

Whole rock geochemistry can be used to examine the relationship between a leucosome and the surrounding rock as well as between multiple generations of leucosomes. To fully determine the partial melting history of an area, it is necessary to know the composition of the protolith and of the melanosome and leucosome. In many migmatitic terranes, however, partial melting is so pervasive that pristine samples of protolith are lacking. Samples that appear to have escaped partial melting, are usually less-fertile compositions (Sawyer, 1998; 1999). These rocks do not have an appropriate composition to undergo melting at the same pressure and temperature conditions as the surrounding rocks. Analyzing a large suite of samples of various generations of leucosomes and associated melanosomes, and having petrographic constraints on the melting reactions, can provide a detailed picture of the melting process (Sawyer, 1998, 1999), particularly where leucosomes occupy a succession of generations of structures (Sawyer et al., 1999) or structural sites with distinct morphologies (Milord et al., 2001; Solar and Brown, 2001; Bhadra et al. 2007). Comparing the whole rock geochemistry

from the suite of leucosomes with compositions of experimentally-derived partial melts can also differentiate between specific types of melting reactions, including fluid-saturated and -undersaturated melting, muscovite, biotite, and amphibole dehydration melting and granite eutectic melting.

This chapter examines the petrographic relationships and whole rock geochemistry of leucosomes, their associated melanosomes, pegmatites and country rocks found at Bremer Bay, within the Biranup Complex of the Albany-Fraser Orogen. This area underwent protracted deformation in Proterozoic time, including three phases of bidirectional extension. Partial melting occurred throughout deformation (Barquero-Molina, 2009). Leucosomes are associated with a variety of structures, including foliations, shear zones, and boudins, and large, several meter wide, melt channels as well as late cross-cutting pegmatites. Major and trace element geochemistry from these leucosomes allows for differentiation of generations of melts and establishment of the chemical evolution of the melts. Pairing this geochemical analysis with the cross-cutting relationships and established structural and tectonic history of the Bremer Bay area allows for a more complete picture of the structural evolution and partial melting process, and provides better relative timing constraints on crystallization of these melts in relation to formation of the structures.

4.3 GEOLOGIC SETTING

The Albany-Fraser Orogen of southwestern Australia (Figure 4.1) is a Grenville-aged belt of rocks that experienced granulite facies deformation during the 1.3 Ga collision of the Western Australian Craton, the Northern Australian Craton, and the Mawson Craton of Australia and Antarctica, associated with assembly of the supercontinent Rodinia (Myers et al., 1996). The Albany-Fraser Orogen comprises two separate belts, the E-W striking Albany Mobile Belt and the NE-SW striking Fraser Mobile Belt, that are grouped together because of abundant felsic plutons metamorphosed to orthogneiss in both belts, the similarity in the overlying rocks, and their correlation along strike (Myers, 1990; Clark et al., 2000). U-Pb dating indicates that collision

occurred in two stages (Clark et al., 2000). Plutonism, deformation and metamorphism during Stage I lasted from 1345-1260 Ma and is attributed to closure of an ocean basin and collision of the Western Australian and Mawson Cratons, based on oceanic affinities of the Fraser Complex and detrital zircon ages of metasedimentary units (Clark et al., 2000; Fitzsimons, 2003). A period of tectonic quiescence followed, lasting approximately 45 my, and then during Stage II, from 1215-1140 Ma, reactivation of intracratonic structures occurred (Clark et al., 2000). More recent work, including structural mapping and geochronologic dating has suggested the Albany-Fraser Orogen is diachronous, wherein the eastern areas record deformation related to Stage I and II, and western portions of the orogen record deformation that occurred only during Stage II (Barquero-Molina, 2009).

The Albany Fraser Orogen is exposed along the coast of southwestern Australia. It is subdivided into four lithotectonic units on the basis of differences in structural style and aeromagnetic surveys: the Northern Foreland, the Biranup Complex, the Nornalup Complex, and the Fraser Complex (Figure 4.1) (Beeson et al., 1988; Myers, 1990; Whitaker, 1992, 1993). The Northern Foreland is composed of gneisses and dolerite dikes of the Archean Yilgarn Craton and metasedimentary rocks of the Mount Barren Group, Stirling Range Formation and Woodline Formation that were thrust northward over the Archean Yilgarn rocks (Myers, 1990). The Biranup Complex contains felsic orthogneisses with minor paragneisses and is interpreted to have been thrust over the southern margin of the Northern Foreland (Myers, 1990). The Nornalup Complex is comprised of orthogneisses and paragneisses that were thrust onto the Biranup Complex and is the southernmost of the four lithotectonic units (Myers, 1990). The Fraser Complex, which is only found in the eastern portion of the belt, is the most mafic of the lithotectonic units, comprising mafic granulites attributed to an ocean-arc origin because of subduction-related geochemical anomalies (Condie and Myers, 1999).

This study focuses on the rocks of the Biranup Complex at Bremer Bay (Figure 4.1, 4.2). The Biranup Complex includes the Dalyup Gneiss, which extends along the entire length of the complex, and the Coramup Gneiss, which is only present in the

western part of the complex (Spaggieri et al., 2008, 2009). The Coramup Gneiss is bounded by the Coramup and Heywood faults and is composed of both orthogneisses and paragneisses (Bodorkos and Clark, 2004a, b). The Dalyup Gneiss is present in the eastern portion of the Biranup Complex and contains granitic and rare mafic rocks that have been metamorphosed to granulite-facies conditions, likely during Stage I of the collision (Nelson et al., 1995). Rocks of the western Dalyup Gneiss are composed of heterogeneous orthogneisses with rare mafic rocks that have been metamorphosed to granulite-facies conditions and likely record only Stage II of collision (Beeson et al., 1988; Nelson et al., 1995; Barquero-Molina, 2009). These western rocks of the Dalyup Gneiss are present in the Bremer Bay area where a detailed petrographic and structural study was conducted by Barquero-Molina (2009); her structural history of the area provides the framework for the relative timing constraints between different generations of structures used in this study. In her detailed field study, mapping was conducted along the thirteen different headlands; the only exposures of rocks in the Bremer Bay area (Figure 4.2).

4.3.1 Structural History

Felsic-to-intermediate, migmatitic orthogneisses at Bremer Bay experienced granulite-facies metamorphism, and Barquero-Molina (2009) has defined eight different lithologies in this area, which are dominantly quartz monzonite/monzodiorite orthogneisses +/- orthopyroxene, clinopyroxene, biotite, amphibole and garnet. The rocks are all migmatitic and generally have a stromatic foliation defined by leucosome material, typically comprised of quartz, plagioclase and K-feldspar, alternating with more residual material with abundant mafic phases. In addition to foliation defined by leucosome material, leucosomes are found in the necks of boudins, at a high angle to and cross-cutting the foliation, and axial planar to folds. Additionally, late-stage pegmatites cross-cut all previous structures.

This area experienced a complicated structural history including three phases of bidirectional extension during a period of overall contraction (Barquero-Molina, 2009).

The relative timing of the structures as identified by Barquero-Molina (2009) is as follows: The early dominant migmatitic foliation (Figure 4.3A) is axial planar to early isoclinal folds that fold continuous bands of earlier leucosome material. This dominant migmatitic foliation is commonly discontinuous and is defined by both a compositional segregation of leucosome and residuum, and by alignment of platy and tabular minerals (Figure 4.3A). The early folding and formation of the associated dominant foliation was followed by three phases of bidirectional extension. Each of these phases resulted in the formation of orthogonal NE-SW and NW-SE boudins, which are interpreted to form synchronously (Figure 4.3B-E). All of the bidirectional extension phases are separated by a phase of folding (e.g. Figure 4.3C, D), related to either shearing or shortening, which allows them to be differentiated. Many of the boudin necks contain leucosome material. First generation boudins formed during the first phase of extension are typically quite small, generally centimeter to decimeter in size (Figure 4.3B, C); second generation boudins are intermediate in size, from less than a meter to several meters in scale (Figure 4.3D); and the final generation is defined by decameter-size boudins (Figure 4.3E). Shear bands are present throughout the area and range from several centimeters to a meter in length (Figure 4.3A, F). These shear bands commonly contain leucosome material and cut across the dominant migmatitic foliation, as well as some of the small and intermediate-scale boudins and folds. Their timing has not been definitely constrained, because it is unclear whether they all formed at the same time or throughout the deformational history. However, all shear bands clearly cut and thus postdate the dominant migmatitic foliation (Figure 4.3A, F). Channelways of former melt are found in several locations throughout the field area. These are interpreted as diatexite migmatites and are characterized by abundant leucosome material surrounding blocks of foliated, commonly folded and boudinaged mafic material that appear jumbled, “floating” in a sea of melt (Figure 4.3G). Timing constraints on these jumbled channelways are unclear, although they clearly postdate formation of the foliation and the early boudinage and folding. Finally, there are two generations of nearly perpendicular late pegmatites found

throughout the field area, which parallel the boudin orientations and cross-cut all other structures (Figure 4.3H, I).

Geochronologic data from country rock and leucosome material in the necks of boudins provide constraints on the timing of deformation and metamorphism. This data is reported in the dissertation of Barquero-Molina (2009), and individual ion-microprobe reports can be found in Bodorkos and Wingate (2008a, b, c, d, e, f). Three samples of country rock give a crystallization age for the orthogneiss protolith at approximately 1680 Ma (1680 +/- 7 Ma, 1670 +/- 12 Ma, and 1689 +/- 11 Ma). Two locations within the field area have boudin neck leucosomes that give igneous crystallization ages of 1178 +/- 3 Ma and 1187 +/- 5 Ma, and one unmetamorphosed boudin neck leucosome gives an igneous crystallization age of 1148 +/- 9 Ma. The boudin neck melt with an igneous crystallization age of 1187 +/- 5 Ma contains metamorphic zircons that give an age of 1172 +/- 16 Ma, which is interpreted to represent the high-grade metamorphic age. In the vicinity of the unmetamorphosed boudin neck melt, the high-grade metamorphism from country rock metamorphic zircons is dated at 1154 +/- 25 Ma. These dates have been interpreted to provide evidence for partial melting synchronous with the high-grade deformation in the region (Barquero-Molina, 2009).

4.4 Sample Description and Petrography

Samples for this study were divided into groups based on their relationship to the different structures. Brief descriptions of each sample type are provided below, and the samples are divided between country rocks, mafic samples (melanosome and mafic dikes), pegmatites and leucosomes (Figure 4.3). The leucosomes are subdivided into foliation-parallel leucosomes, boudin-neck leucosomes, cross-cutting leucosomes, and channelway leucosomes: diatexitic material encompassing mafic blocks (Figure 4.3A, B, C, E, F, G). Samples were collected on seven of the headlands (Figure 4.2). All sample compositions were normalized and plotted on a QAP diagram; because the focus of this study is on the leucosome material, the mafic rocks are plotted on the same diagram, although many of them contain 25-60% mafic minerals (Figure 4.4).

Four country rock samples were collected that have a well-developed foliation not defined by stromatic migmatites (i.e. do not contain segregations of leucosome and melanosome). In the field these rocks are identified as high-grade gneisses and do not macroscopically appear to contain relict melt. Country rock samples are primarily biotite-hornblende +/- clinopyroxene +/- orthopyroxene +/- ilmenite tonalitic, quartz monzodioritic or quartz monzonitic orthogneisses (Figure 4.4). However, because of the abundance of migmatites throughout the entire field area and their association with every type of structure, it is unlikely that these country rock samples were unaffected by the partial melting process. In thin section these samples contain former melt on grain boundaries and subgrain boundaries, serrate-cuspate grain boundaries and rounded reactant phases that are surrounded by very thin blebs of material, inferred to represent former melt. All these features are types of melt microstructures and indicate that country rock samples have undergone some degree of partial melting (Sawyer, 1999, 2001). Thus, the country rock samples may represent a bulk neosome composition.

Mafic samples are of two distinct types: some samples represent melanosome, the residual material that is associated with leucosomes, and others are mafic dikes or boudins, which do not appear to be associated with leucosome material (Figure 4.3A, B, C, G, J). Six samples of mafic dikes and boudins were sampled: orthopyroxene +/- biotite +/- hornblende +/- clinopyroxene quartz monzogabbroic, monzogabbroic or gabbroic orthogneisses (Figure 4.3C, J and 4.4). All of these samples have a foliation, ranging from poorly to well-defined. Nine samples of melanosome or residual material were sampled: biotite-orthopyroxene-hornblende-clinopyroxene quartz monzogabbroic or gabbroic orthogneisses (Figure 4.3A and Figure 4.4). Several samples are missing one of these mafic minerals, but most samples contain all four. One sample is far more aluminous than the others and is a spinel-biotite-garnet tonalitic orthogneiss. Most of these samples have a well-developed foliation defined by elongate mafic minerals alternating with aligned tabular quartzofeldspathic minerals; however one or two samples have a poorly-developed foliation with weak mineral alignment.

Five samples of foliation-parallel leucosomes were collected, each with an associated mafic melanosome (described above; Figure 4.3A). These former melts are all foliation parallel, and the foliation is defined by elongate quartzofeldspathic material and rare mafic minerals. The foliation-parallel leucosomes are the finest grained of all the leucosome samples. Three of the samples have at least 95% quartzofeldspathic minerals with the rest as biotite. The other two samples have up to 20% mafic minerals, including biotite, amphibole, clinopyroxene, and ilmenite. All samples are biotite tonalites, granodiorites or quartz monzodiorites (Figure 4.4). These foliation-parallel stromatic leucosomes define the foliation within the field area, and this foliation was determined to have formed during earliest deformation coincident with isoclinal folding (Barquero-Molina, 2009). Although leucosomes could have exploited these preexisting structures later during deformation, their somewhat discontinuous morphology and gradation with the melanosome material, suggests that they formed during in situ partial melting. Additionally the leucosomes and the minerals within them are deformed. Consequently, these foliation-parallel leucosomes are interpreted to be the earliest melts.

Leucosomes found in the necks of boudins (Figure 4.3B, E) also have relative timing constraints; the formation of the boudins postdates formation of the pervasive migmatitic foliation. Three samples from leucosomes in the necks of boudins were collected, including one from small decimeter-scale boudins, as well as two samples from intermediate meter-scale boudins. Leucosome-material from the intermediate scale boudins comes from boudins oriented in orthogonal directions to each other; one leucosome is from the NE-SW trending boudin, whereas the other sample is from the NW-SE trending boudin. All boudin neck leucosomes are coarse-grained and typically have a very poorly-developed foliation. These samples are hornblende +/- orthopyroxene +/- clinopyroxene granites or granodiorites (Figure 4.4). The boudin neck leucosomes cut across the dominant stromatic migmatitic foliation in the rocks, so they clearly postdate the foliation-parallel leucosomes. Despite the lack of well-developed foliation in these boudin neck leucosomes, the minerals are deformed with chessboard extinction in quartz, subgrains in feldspars, as well as continuous undulatory extinction in all

quartzofeldspathic minerals. Locally new dynamically recrystallized grains of feldspar are observed. Leucosomes within the boudin neck regions typically have a fairly sharp contact with the surrounding rock.

Cross-cutting leucosomes (Figure 4.3A, F) are found at a high-angle to the foliation and cut the foliation, clearly postdating it. The timing between their formation and that of the boudin neck leucosomes is unknown. Seven samples were collected from cross-cutting leucosomes; these leucosomes range from several centimeters to up to a meter in length and are medium to coarse-grained. All samples have a poorly to moderately developed foliation; it is better developed than the boudin neck leucosomes but not nearly as well-developed as in the foliation-parallel leucosomes. Cross-cutting leucosomes have a large range in composition from tonalite to granite (Figure 4.4). These leucosomes all contain less than 10% mafic minerals, but there is variability in mafic mineral abundance, including: biotite, hornblende, orthopyroxene, and clinopyroxene; one sample contains garnet.

The leucosomes forming the large (decameter-wide) channelways of former melt that surround mafic blocks are less well constrained in terms of time of formation (Figure 4.3G). Barquero-Molina (2009) described these channelways as areas of jumbled material, usually containing disaggregated mafic blocks floating in a matrix of monzogranitic orthogneiss. Many of the larger mafic blocks contain a foliation consistent in character, and locally orientation, with the foliation outside of these jumbled areas. These channelway units generally cross cut the dominant foliation and in most cases are not laterally continuous. These units are interpreted as channelways in different stages of development, on the basis of a few well defined melt channels that contain foliated, folded and boudinaged mafic layers. Thus it is likely that these channelways formed midway through or late in the deformational history. These areas may have had a high degree of melt infiltration, and locally material has been disaggregated, but some areas may be close to their original orientation. Four samples of these leucosomes were collected from around jumbled mafic blocks in different locations. All four of these leucosomes are very coarse-grained and do not contain a foliation. Within these samples,

the quartzofeldspathic minerals are deformed, with chessboard extinction in quartz, variable degrees of subgrain development in feldspar and continuous undulatory extinction in both minerals. These leucosomes are mostly granodiorites with one sample that is a tonalite (Figure 4.4). The leucosomes have a very low abundance of mafic minerals, with a range of 0-4%, including biotite, amphibole or clinopyroxene. The granodioritic sample with 57% quartz could likely be classified as a pegmatite, because of its very coarse grain size. However, because it appears to have the same relationship to the jumbled leucocratic channelways as the other leucosomes from this area, it is grouped with these former melts.

A variety of late pegmatites were sampled and are clearly constrained to be the latest group of former melts (Figure 4.3H, I). Previously the pegmatites have been grouped into two distinct groups in the field: intermediate composition pegmatites that were generally greenish in color and later cross-cutting felsic pegmatites that appeared pink in the field (Barquero-Molina, 2009). Pegmatitic samples do not display a foliation, but the minerals are slightly deformed, displaying undulatory extinction and some subgrain development in quartz and feldspar. Subgrains are ubiquitous in quartz but are only rarely developed in grains of K-feldspar. These samples have the broadest compositions ranging from tonalite to quartz syenite (Figure 4.4). Most of the pegmatites do not contain mafic minerals, but rare samples have less than 3% biotite, hornblende, orthopyroxene or clinopyroxene. Although the color of pegmatites in the field can be misleading in terms of their mineralogy because of a weathering patina, two distinct groups of pegmatites are observed: plagioclase-rich tonalites and K-feldspar-rich granites and quartz syenites (Figure 4.4). Many of the pegmatites appear to have two compositions, plagioclase-rich at the edges, and K-feldspar-rich in the center of the pegmatite (Figure 4.3I).

4.4.1 Metamorphic Reactions

Country rocks, mafic rocks and rare leucosomes contain orthopyroxene and clinopyroxene +/- amphibole +/- biotite. In many of the sampled rocks, the amphibole

and biotite appear retrogressed, they are commonly found rimming pyroxene and in some thin sections, pyroxene is rimmed by amphibole, which is in turn rimmed by biotite and some of this biotite is chloritized. These rocks experienced granulite-facies conditions and thus most of the original amphibole and biotite would have broken down to produce the granulite-facies mineral assemblage.

In samples of country rock as well as melanosome, grains of orthopyroxene and clinopyroxene commonly have small rims of material, now typically preserved as quartz, along their grain boundaries, particularly in locations with nicely faceted crystal faces on the pyroxene grains. These tiny quartz blebs are inferred to represent former melt that crystallized against the peritectic product of the melting reaction (Sawyer, 1999, 2001; Guernina and Sawyer, 2003). In addition to former melt in contact with peritectic phases, many grains of biotite are corroded and are surrounded by pools of former melt, now quartz, which are indicative of the breakdown of biotite to produce melt (Sawyer, 1999, 2001). Finally, many of the melanosomes and country rock samples contain ilmenite that is associated with the blebs of quartz, interpreted as former melt around grains of orthopyroxene. Grains of ilmenite are absent from the mafic dikes and boudins, which may indicate these rocks did not experience partial melting and did not have melt extracted from them. This association of ilmenite with orthopyroxene and with former melt suggests it is a result of the melting reaction. In granulite-facies rocks from the Ashuanipi terrane in northern Québec, these same relationships are seen between orthopyroxene, biotite and ilmenite and the interpreted reaction is,

Biotite + Quartz + Plagioclase +/- H_2O = Orthopyroxene + Ilmenite + Melt,

as a result of partial melting of metagraywackes (Sawyer, 1999, 2001; Guernina and Sawyer, 2003). These observations suggest that some of the melting in the area occurred via the breakdown of biotite with orthopyroxene as a product. The presence of orthopyroxene and ilmenite together with fine rims of former melt can be used to interpret which rocks have undergone partial melting, and because this mineral assemblage is only present in country rocks and residual mafic rocks it is assumed that the other mafic rocks were generally unaffected by partial melting.

The presence of relict melt along crystal faces of clinopyroxene and orthopyroxene suggests that biotite is not the only mineral that underwent dehydration to produce melt. These fine rims of interpreted former melt on both types of pyroxene provide evidence for amphibole-dehydration melting. Experimental studies of amphibole-dehydration melting (Waters, 1988; Patiño Douce and Beard, 1995) suggest a possible melting reaction is:

Hornblende + Quartz = Orthopyroxene + Clinopyroxene + Plagioclase +/- Oxide + Melt.

Patiño Douce and Beard (1995) also found that at pressures above 10 kbar, garnet also begins to be produced as a peritectic reaction product and simultaneously plagioclase becomes a reactant.

In the Bremer Bay rocks amphibole and garnet are not typically found together, and garnet is only found in rocks that appear to have skeletal or corroded biotite. This skeletal and corroded biotite texture is interpreted to result from biotite-breakdown, typically during dehydration melting (Sawyer, 1999, 2001). Thus, it seems likely that pressures in this area did not exceed 10 kbar during the partial melting process. Previous P-T estimates for the area suggest temperatures between 800-1000° C. Within the eastern portion of the Biranup Complex pressures have been estimated at only 0.5-0.6 GPa during Stage II collision (Bodorkos and Clark, 2004a). The western portion of the Biranup Complex, where Bremer Bay is located, was at higher temperatures than the eastern portion of the area, so it is probable that pressures were also higher, consistent with the granulite facies mineral assemblage in the Bremer Bay area.

Other experimental studies have found additional hornblende dehydration melting reactions, including:

Hornblende + Plagioclase = Clinopyroxene + Melt,

Hornblende + Plagioclase = Clinopyroxene + Al-Hornblende + Ca-Hornblende + Garnet + Orthopyroxene + Liquid (both reactions from: Wolf and Wyllie, 1991, 1994), and

$$\text{Quartz} + \text{Plagioclase}_1 + \text{Hornblende}_1 + H_2O = \text{Hornblende}_2 + \text{Plagioclase}_2 + \text{Melt}$$

$$\text{Quartz} + \text{Plagioclase}_1 + \text{Hornblende}_1 + H_2O = \text{Hornblende}_2 + \text{Plagioclase}_2 + \text{Orthopyroxene} + \text{Clinopyroxene} + \text{Melt}$$

(both reactions from: Hacker, 1990).

These reactions occur at temperatures ranging from 775-975 °C and pressures of approximately 10 kb, with the lower temperature end resulting from fluid-saturated melting and the higher temperature end representing both fluid-saturated and -undersaturated melting.

Although most of the rocks prepared for geochemical studies do not contain garnet, several lithologic units in the vicinity contain garnets (Barquero-Molina, 2009) and may provide evidence for an additional biotite-dehydration melting reaction. Along the Fisheries Bay Headland (Figure 4.2) one sample of melanosome and foliation-parallel leucosome contains garnet and small quantities of spinel. This lithology is far more aluminous than most of the lithologies which do not contain garnet, spinel, aluminosilicate or cordierite.

4.5 WHOLE ROCK GEOCHEMISTRY

4.5.1 Methods

Examples of samples described above were crushed and handpicked at the University of Texas at Austin, and only rock fragments that did not appear to be weathered, were selected for geochemical analysis. In many samples, the leucosome material was separated from the melanosome material, and each part of the sample was crushed separately. Additionally, material at the boundary between the leucosome and the melanosome was not included in the analyses. This exclusion of mixed material prevents anomalous enrichments or depletions in each portion of the migmatite, although information about mixing between leucosome and melanosome at their contacts is lost. Rock powders were sent to the Washington State University Geoanalytical Lab for whole rock geochemistry analysis At Washington State University 29 major, minor and trace elements were acquired by XRF and 27 trace elements including 14 REE were acquired via ICP-MS (Table 4.1).

4.5.2 Country Rocks

Country rocks have SiO_2 contents that range from 62-68 wt% and SiO_2 content increases with an associated decrease in FeO + MgO and K_2O; these samples have little variation in CaO content (Table 4.1, Figure 4.5). The country rocks generally plot within the field of leucosome material at the end closest to the mafic rock field (Figures 4.4 and 4.5). They have a moderately flat REE pattern, with some fractionation of LREE/HREE (La_N/Lu_N = 14.8-40.7), either a slight negative or flat Eu anomaly, Eu/Eu* = 0.65-0.97 and moderate total REE contents (ΣREE = 153-657) (Table 4.1, Figure 4.6A). La_N = La content (in ppm) divided by 0.33 and Lu_N = Lu content (in ppm) divided by 0.034. $Eu/Eu^* = Eu_N/(((Sm_N - Gd_N)/2)+Gd_N)$, where Eu_N = Eu content (in ppm) divided by 0.077, Sm_N = Sm content (in ppm) divided by 0.203 and Gd_N = Gd content (in ppm) divided by 0.276 (after Nakamura, 1974).

4.5.3 Mafic Rocks

Mafic rocks have SiO_2 contents that range from 44-65 wt% and SiO_2 content increases with decreasing FeO + MgO, and CaO; these samples have little variation in K_2O content (Table 4.1, Figure 4.5). The two different types of mafic rocks, melanosome and mafic boudins or dikes, are separated on these diagrams, but their compositions are quite similar and they all plot within the same region.

Mafic rocks have fairly flat REE patterns with little fractionation of LREE/HREE (La_N/Lu_N = 5-20.6), moderate total REE contents (ΣREE = 66-518) and have slight negative or flat Eu anomalies, with Eu/Eu* = 0.39-0.95, except for one sample with a positive Eu anomaly and Eu/Eu* = 2.1 (Table 4.1, Figure 4.7B-D). Mafic dikes and boudins have a broader range in sign and magnitude of Eu anomaly and flatter LREE patterns than melanosomes, which have less variation in the range of patterns (Figure 4.7B-D).

4.5.4 Leucosomes

Foliation-parallel leucosomes have the lowest SiO_2 contents, with a range from 62-71 wt% (Table 4.1, Figure 4.5). These SiO_2 contents overlap substantially with the

country rock samples but extend to higher values. Correlations between SiO_2 and the other oxides are similar in country rocks and foliation-parallel leucosomes. SiO_2 increases with a steep decrease in FeO + MgO, and a minor decrease in CaO; there is little correlation between SiO_2 and K_2O (Table 4.1, Figure 4.5). On the SiO_2 vs. K_2O and CaO diagrams the foliation-parallel leucosomes plot near the location of plagioclase, of a composition between albite and An_{50} (Figure 4.5A, B). Similarly, on the ternary diagram (Figure 4.4), the foliation-parallel leucosomes plot closer to the plagioclase apex, than any other group of leucosomes. Most of the foliation-parallel leucosomes plot in the field defined by experimentally produced fluid-saturated and -undersaturated amphibole-dehydration melting (Figure 4.4 and 4.5A, B). However, on any given SiO_2 vs. oxide plot, one or two foliation-parallel leucosomes do not plot near any experimentally-derived partial melts. On the ternary diagram (Figure 4.4), three of the foliation-parallel leucosomes plot at the very edge of the fluid-saturated and -undersaturated experimentally derived amphibole-dehydration partial melts.

The three boudin-neck leucosomes have a very narrow range in SiO_2 content, ranging from 70-75 wt% (Table 4.1, Figure 4.5). These leucosomes have nearly constant CaO and FeO + MgO with increasing SiO_2, but show a decrease in K_2O with increasing SiO_2 (Table 4.1, Figure 4.5). On the SiO_2 vs. CaO and K_2O diagrams, the boudin-neck leucosomes plot near the center of the triangle defined by quartz, plagioclase and K-feldspar (Figure 4.5A, B). These leucosomes plot primarily in the field of experimentally-produced fluid-undersaturated biotite-dehydration melting but slightly overlap the fields of fluid-undersaturated amphibole-dehydration partial melts. Depending on the specific diagram, they may also overlap several of the experimentally-produced fluid-saturated biotite-dehydration partial melts (Figure 4.4, 4.5A).

The diatexitic leucosomes from the jumbled channelways have a broader range in SiO_2 content than the boudin neck leucosomes, but the other trends are similar. Jumbled channelway leucosomes have a range of SiO_2 from 68-81 wt%, and with an increase in SiO_2 they show no change in FeO + MgO and K_2O, but an associated decrease in CaO (Table 4.1, Figure 4.5). It is important to note that three of the jumbled channelway

leucosomes plot together, with SiO_2 contents ranging from 67.5-72.5 wt%, whereas the fourth one is far more silica-rich (Figure 4.5). Jumbled channelway leucosomes are spread out along the plagioclase and quartz join on the ternary diagram and Harker diagrams; these leucosomes are quite low in K_2O. All four of these samples overlap the fields defined by experimentally-produced fluid-saturated and -undersaturated amphibole-dehydration partial melts (Figures 4.4 and 4.5).

The cross-cutting leucosomes have the broadest range in SiO_2 content of all of the former melts, ranging from 61-80 wt% (Table 4.1, Figure 4.5). These cross-cutting leucosomes do not all follow a single trendline on the Harker diagrams (Table 4.1, Figure 4.5). However, they do show a general decrease in FeO + MgO and CaO with increasing SiO_2 content and an increase in K_2O (Figure 4.5). Different samples within the cross-cutting leucosomes plot with different groups of the experimental partial melts. Two or three of the samples plot primarily in the fluid-undersaturated biotite-dehydration melting field, and the rest plot in the fluid-saturated and -undersaturated amphibole-dehydration melting field (Figures 4.4 and 4.5). However, two of the samples (BB1 and FMWM3-2A), the ones with the highest and lowest SiO_2 contents, do not plot near many of the experimentally-derived melts (Figures 4.4 and 4.5).

Leucosomes have more variation in their REE patterns than the mafic and country rocks, with increased fractionation between LREE and HREE (La_N/Lu_N = 0.3-316.1) and generally low total REE contents (ΣREE = 43-372) (Table 4.1, Figure 4.7A-E). Almost all of the leucosomes have a fairly pronounced positive Eu anomaly (Eu/Eu* = 1.20-8.19), but four samples have either a minor negative anomaly (Eu/Eu* = 0.43, 0.69) or no anomaly (Eu/Eu* = 1.02, 1.09) (Table 4.1, Figure 4.7A, C, D, E).

When the leucosomes are subdivided based on their structural type, some patterns emerge. The foliation-parallel leucosomes have either flat or positive Eu anomalies, and the boudin neck leucosomes have flat, or slightly positive or negative Eu anomalies. The channelway leucosomes and cross-cutting leucosomes have only positive Eu anomalies, with the exception of one cross-cutting leucosome that displays a very anomalous pattern, with a negative Eu anomaly and very high HREE concentrations (Figure 4.8A, B, D, E).

4.5.5 Pegmatites

Pegmatitic samples have a large range in SiO_2 contents, from 63-79 wt% (Table 4.1, Figure 4.5). The pegmatites have been divided into two groups with high and low Ba contents. Samples with low Ba have a range from 71-798 ppm, and high Ba samples have a range from 2121-5109 ppm (Table 4.1). Pegmatitic samples have broad ranges in CaO and K_2O and consequently do not show a correlation with increasing SiO_2, and have low values of FeO + MgO (Table 4.1, Figure 4.5). In the ternary diagram (Figure 4.4) and on the SiO_2 vs. K_2O Harker diagram (Figure 4.5A) many of the pegmatites plot along the join between quartz and K-feldspar, near the K-feldspar apex, or near the location of albite.

Pegmatitic samples have the widest range in REE patterns and have both the most positive and most negative Eu anomalies (Eu/Eu* = 0.09-35.97) (Table 4.1, Figure 4.7F). They tend to have low total REE contents (ΣREE = 9.1-239.6) and have large variability in fractionation between LREE and HREE (La_N/Lu_N = 1.2-241.1) (Table 4.1, Figure 4.7F). The high Ba samples do not fall into any clear patterns on the REE diagrams, but they all have a positive Eu anomaly, except one which has no Eu anomaly. Low Ba samples are split; three samples display a positive Eu anomaly and the other three have negative Eu anomalies. The three samples with negative Eu anomalies (FPG1, FPG3-G and FPG3-P) have high concentrations of U and Nb, and slightly higher concentrations of Ta, and they are all sourced from the same pegmatite. FPG1 is from the very tip of the pegmatite (sample taken near the I in Figure 4.3I) and FPG3-G and FPG3-P are from 20m away from the tip. FPG3-G is taken from the edge of the pegmatite and FPG3-P is taken from the core of the pegmatite. FPG3-G appears greenish in color and contains over 55% plagioclase and only 6% K-feldspar, whereas FPG3-P appears pinkish in color and contains less than 30% plagioclase, but 40% K-feldspar (Table 4.1, Figure 4.4).

Low Ba pegmatites are additionally low in Sr and Eu (Figure 4.8A, B). These low Ba samples have either very high or low K_2O contents, with three samples in each group (Figure 4.8C). Two of the low K_2O pegmatites also have negative Eu anomalies (FPG1 and FPG3-G) but the other low K_2O pegmatite has a positive Eu anomaly. The

high Ba pegmatites have high concentrations of Sr and Eu and all have intermediate to high amounts of K_2O (Figure 4.8).

4.6 DISCUSSION

Partial melting of granulite-facies orthogneisses within the Bremer Bay region of the Albany-Fraser Orogen of southwestern Australia has resulted in formation of four structurally distinct groups of leucosomes. In addition to structural differences between the groups, there are also differences in the major and trace element geochemical data for each of these leucosome types. Late pegmatites cross-cut all previous structures and have a distinct geochemical signature from the leucosomes. Whole rock geochemistry, in conjunction with structural and petrographic analysis, allows differentiation of the types of melting reactions that occurred and the processes that affected the partial melts during crystallization. Specifically, major and trace element geochemistry provides a distinction between fluid-saturated and -undersaturated partial melting, biotite- and amphibole-dehydration melting and whether the leucosomes may represent partial melts or crystal accumulations, as discussed below.

4.6.1 Leucosomes

4.6.1.1 Major and Trace Element Geochemistry

Foliation-parallel leucosomes are interpreted to have formed as a result of fluid-saturated or -undersaturated amphibole-dehydration melting, because most of the samples plot within the field defined by these experimental partial melts (Figures 4.4 and 4.5). The fields of experimental melts derived from fluid-saturated and -undersaturated amphibole-dehydration melting overlap each other greatly, and thus it is difficult to determine whether fluid was present when these leucosomes formed. Additionally, the foliation-parallel leucosomes have low SiO_2 and K_2O contents, high CaO and FeO+MgO concentrations, and contain abundant plagioclase. These characteristics are typical of partial melts that have been derived from fluid-fluxed melting (Patiño Douce and Harris, 1998). This may suggest the foliation-parallel leucosomes are more likely to be derived

from fluid-saturated than fluid-undersaturated amphibole-dehydration melting. Two or three of the foliation-parallel leucosomes are on the very outside of all of the fields defined by experimental partial melts (Figure 4.4), and consequently it seems likely that these leucosomes have some degree of plagioclase accumulation. Overall the major element compositions of the foliation-parallel leucosomes are consistent with formation as a result of amphibole-dehydration melting with or without fluids and during crystallization, some degree of plagioclase accumulation. The causes of accumulation of a particular type of mineral within the leucosome will be discussed later in the chapter.

Most of the jumbled channelway leucosomes plot in a similar position to the foliation-parallel leucosomes, within the field defined by experimentally-derived fluid-saturated and -undersaturated amphibole-dehydration partial melts (Figures 4.4 and 4.5). Differentiating between fluid-saturated and -undersaturated amphibole-dehydration melting is even more difficult with the channelway leucosomes than the foliation-parallel leucosomes. These samples all plot consistently within both experimental melting fields, whereas two of the foliation-parallel leucosomes plot in the fluid-undersaturated amphibole-dehydration melting field and do not overlap with fluid-saturated melting. One of the channelway leucosome samples plots away from the other three and has a much higher SiO_2 and lower CaO and Na_2O content (Table 4.1, Figures 4.4 and 4.5). This high SiO_2 sample likely represents an accumulation of quartz.

Cross-cutting leucosomes have the broadest range in composition of all the leucosomes, and they span the range of all the different types of experimentally-derived partial melts (Figures 4.4 and 4.5). This broad range suggests that although these leucosomes are found in a particular structural location, they formed from several different partial melting reactions. These cross-cutting leucosomes can be fairly evenly divided into three groups. The first group of three samples contains abundant plagioclase +/- quartz, and these samples plot within the fluid-saturated and -undersaturated amphibole-dehydration melting field. The second group contains two samples with more K-feldspar-rich compositions and plots at the intersection of all the fields of experimentally-derived melts (Figures 4.4 and 4.5). The last two samples of the cross-

cutting leucosomes have even more K-rich compositions and plot entirely within the field of fluid-undersaturated biotite-dehydration melting. Three of the cross-cutting leucosomes, two of the ones likely derived from amphibole-dehydration melting and one of the ones derived from biotite-dehydration melting have compositions that plot along the edges of the fields defined by these experimental melts, and these likely represent some degree of mineral accumulation. Each of the samples has an accumulation of a different mineral: plagioclase, quartz, and K-feldspar. Although these samples are not too distinct from the experimentally-derived melts, they are unlikely to represent pristine partial melts. In Figure 4.5A and B, these three samples plot on or close to the tie-lines connecting the end-member mineral compositions. This overlap between the leucosomes and end-member minerals also supports the interpretation that at least three of the cross-cutting leucosomes show some degree of accumulation.

The boudin neck leucosomes have the narrowest range in composition of all the leucosomes and are consistent with formation as a result of fluid-undersaturated biotite-dehydration melting. One of the boudin-neck leucosomes falls on the boundary between the fluid-undersaturated biotite-dehydration and amphibole-dehydration melting fields (Figures 4.4 and 4.5). Although it is possible that this sample may have been produced as a result of amphibole-dehydration, the sample has much lower CaO and K_2O and higher SiO_2 than other samples that are likely produced from breakdown of amphibole.

4.6.1.2 REE Geochemistry

Differences in the REE patterns within the group of foliation-parallel leucosomes appear to be related to the original source composition. The foliation-parallel leucosomes with the nearly flat Eu anomalies have melanosome pairs with a moderately negative Eu anomaly and higher overall REE contents, whereas the foliation-parallel leucosomes with positive Eu anomalies have melanosome pairs with generally less negative, nearly flat Eu anomalies and lower total REE contents (Figure 4.9, Table 4.1). Additionally, the two foliation-parallel leucosomes with nearly flat Eu anomalies have lower plagioclase contents than the samples with positive Eu anomalies, and because Eu preferentially

partitions into plagioclase, these results are consistent with accumulation of plagioclase in several of the foliation-parallel leucosomes. One of the foliation-parallel leucosomes with a positive Eu anomaly shows enrichment in HREEs (Figure 4.9B), which is attributed to small quantities of garnet in the leucosome.

Overall, the pattern of a positive Eu anomaly in all of the leucosomes (Figure 4.8) is distinct and generally attributed to accumulations of feldspar derived from primary melts (Sawyer, 2008). All of these samples have at least 38% feldspar, with some leucosomes having feldspar percentages of over 70%. The role of accessory phases has been proposed to effect trace element concentrations to a greater extent than major elements (Watt and Harley, 1993; Bea, 1996) and could also be a source of the difference in size and sign of the Eu anomalies in the leucosomes. In an example of positive Eu anomalies in leucosomes from Algeria, the positive Eu anomaly was attributed to depletion in LREEs and HREEs, relative to the associated melanosome (Barbey et al., 1989). Barbey et al. (1989) found that leucosomes were depleted in all REEs relative to the melanosomes, but less so in Eu than other elements. This result is consistent with many of the Bremer Bay leucosomes; the leucosome typically has a lower Eu content than the associated melanosome. Finally, it has been suggested that fluid-saturated or -undersaturated melting may lead to an associated positive or negative Eu anomaly (Harris and Inger, 1992; Cruciani et al., 2008). Plagioclase and quartz in the protolith will be consumed to a higher degree in fluid-saturated melting than fluid-undersaturated melting, and thus, the melt would be enriched in Eu relative to the other REEs (Harris and Inger, 1992; Patiño Douce and Harris, 1998). Differences in the size of the positive Eu anomaly likely reflect a complex history of partial melting and variable initial protolith compositions, but the overall presence of this positive Eu anomaly in nearly all of the leucosomes likely indicates some degree of accumulation of feldspar and possibly widespread fluid-saturated partial melting.

4.6.2 Pegmatites

4.6.2.1 Major and Trace Element Geochemistry

The wide range in pegmatite compositions results in the pegmatites plotting in three different groups (Figures 4.4 and 4.5). The three low Ba and K_2O pegmatites have high CaO + Na_2O contents and are tonalitic in composition. Two or three of the samples plot near the boudin-neck leucosomes and are granitic in composition with intermediate K_2O contents, and the remaining samples do not plot in any of the fields defined by experimentally derived melts (Figures 4.4 and 4.5). This broad compositional range of the pegmatites, and the fact that they do not plot together as a group, likely indicates that they represent somewhat extreme examples of mineral accumulation. Half of the pegmatites show K-feldspar accumulation, and another three have plagioclase and quartz accumulation. Remaining pegmatitic samples are fairly close to a granite eutectic composition (Figure 4.4) and may not represent much accumulation at all.

The more important observation within the pegmatite group is probably related to the high and low Ba contents of the samples. All of the high Ba pegmatites have a positive correlation with K_2O (Figure 4.8C, D). This result is expected, because Ba typically substitutes for K; the partition coefficient for Ba in K-feldspar ranges from 6-24 (Pearce and Norry, 1979; Nash and Crecraft, 1985). Samples with high Ba and a positive correlation with K_2O are likely to have been the earliest formed of the pegmatites. The K-feldspar could have preferentially incorporated Ba into its' crystal structure, and the remaining melt would be depleted in Ba. The pegmatites that formed later had lower concentrations of Ba, and the positive correlation between K_2O and Ba is not seen. Alternatively, the two groups of pegmatites may have had different magma sources. Either way, from field relationships, it is clear the high Ba samples formed earlier than the low Ba samples (e.g. Figure 4.3H).

4.6.2.2 REE Geochemistry

The presence of a positive or negative Eu anomaly does not correlate well with whether the pegmatites are plagioclase or K-feldspar rich, or whether they have high or

low Ba contents. One pegmatite sample (FPG3) that was separated into constituent intermediate (exterior) and felsic (interior) components has a negative Eu anomaly for both components (Table 4.1). However, the two distinct portions of the pegmatite have a clear difference in composition, with the felsic component (FPG3-P) containing 3.63 wt% Na_2O + CaO and 6.52 wt% K_2O, whereas the intermediate component (FPG3-G) contains 7.32 wt% Na_2O + CaO and 1.04 wt% K_2O (Table 4.1). The size of the negative Eu anomaly does differ between the separate portions of the pegmatite, with a very large negative anomaly (Eu/Eu* = 0.1) in the felsic portion and a slightly smaller negative anomaly (Eu/Eu* = 0.5) in the intermediate part. The other pegmatite sample, FPG1, which has a similar sized negative Eu anomaly to FPG3-G, comes from another location along the same pegmatitic dike (Figure 4.3H, I). Thus, it seems quite likely that this negative Eu anomaly in all of these samples could possibly be attributed to an accessory phase present within this particular pegmatite dike (Watt and Harley, 1993; Bea, 1996). All three of the pegmatites with negative Eu anomalies have a substantially higher U content than any of the other pegmatites (Table 4.1). Many accessory minerals, including monazite, zircon, apatite, tourmaline and uraninite have negative Eu anomalies, and if these phases are abundant in the pegmatite, they could be the source of the negative Eu anomaly. All of the other pegmatites have positive Eu anomalies which is consistent with their high feldspar contents.

4.6.3 Summary and Relative Timing

Foliation-parallel leucosomes are the earliest formed leucosomes and are likely a result of fluid-saturated or -undersaturated amphibole-dehydration melting. Some of the cross-cutting leucosomes plot near the foliation-parallel leucosomes and are also consistent with derivation from fluid-saturated or -undersaturated amphibole-dehydration melting. The other half of the cross-cutting leucosomes, plot at the intersection of all the fields defined by experimental melts or within the fluid-undersaturated biotite-dehydration melting field. This difference may suggest that some of the leucosome material that cuts across the foliation has the same amphibole-rich source as the foliation-

parallel leucosomes. The cross-cutting leucosomes may represent a higher degree of mobilization of the leucosome material. Cross-cutting leucosomes that are higher in K_2O and plot close to or within the field of biotite-dehydration melting are likely to have biotite-rich protoliths.

The channelway leucosomes also plot primarily within the fluid-saturated or -undersaturated amphibole-dehydration melting fields. This result could indicate that they formed relatively early in the partial melting history, because most of the other leucosomes that formed as a result of fluid-saturated or -undersaturated amphibole-dehydration melting formed early. Alternatively, if these channelway leucosomes acted as large conduits for melt transport, when they began crystallizing, the larger crystals could have been trapped and accumulated at one crustal level while smaller crystals may have moved further. Additionally, some material in the leucosome may have crystallized from a solute-rich fluid, instead of partial melts. Either of these last two possibilities would suggest the channelways acted as larger conduits for melt transport and support late formation of the channels. Dating of these channelway leucosomes would lead to better constraints on when these leucosomes formed relative to the other leucosomes that plot within the fluid-saturated or -undersaturated amphibole-dehydration melting field.

The boudin neck leucosomes are the only group that plot entirely within or on the edge of the fluid-undersaturated biotite-dehydration melting field. One sample does plot within the fluid-undersaturated amphibole-dehydration melting field, but very close to the boundary with fluid-undersaturated biotite-dehydration melting. The timing constraints on these leucosomes are difficult to identify, but based on field relationships, they formed after the foliation-parallel leucosomes. One of the boudin neck leucosomes is from a small-scale boudin, only several cm in diameter, and the other two are from intermediate-scale boudins. The boudin neck leucosome from the small-scale boudin does not contain biotite, and neither does the surrounding rock, which may suggest that the surrounding rock underwent in situ biotite-dehydration melting to produce the leucosome material in the boudin neck. The intermediate-scale boudins do not show the same relationship;

immediately adjacent rocks contain both biotite and amphibole and these boudin neck leucosomes may represent a nearby biotite-rich source, not sampled in this study.

Difficulty in differentiation between fluid-saturated and -undersaturated amphibole-dehydration melting, makes piecing together the exact melting history a bit tenuous. However, previous work on distinguishing fluid-saturated and -undersaturated melting, indicates fluid-saturated partial melting may be characterized by low K_2O contents, high Na_2O/K_2O, low Rb/Sr, high Sr/Ba and a positive Eu anomaly (Harris and Inger, 1992; Harris et al., 1993; Patiño Douce and Harris, 1998). It is important to note that these studies were primarily focused on muscovite- +/- biotite-dehydration melting. Conrad et al., (1988) conducted fluid-saturated and -undersaturated experiments on amphibole- +/- biotite-dehydration melting and found high aH_2O partial melts contain abundant plagioclase and low aH_2O melts have much more K-feldspar. Consequently, it seems that similar results may occur when fluid-saturated melting occurs in muscovite, biotite and amphibole. The samples that plot within both fluid-saturated and -undersaturated amphibole-dehydration melting fields are characterized by low K_2O contents, high Na_2O/K_2O, low Rb/Sr, and high Sr/Ba, and thus they may be more likely to have formed in a fluid-saturated regime.

The Bremer Bay leucosomes that plot within the fluid-saturated or -undersaturated amphibole-dehydration melting field have major and trace element geochemistry consistent with observations from the previous experimental studies (Conrad et al., 1988; Harris and Inger, 1992; Harris et al., 1993; Patiño Douce and Harris, 1998). The foliation-parallel leucosomes, half of the cross-cutting leucosomes and the channelway leucosomes all contain abundant plagioclase, have high Na_2O/K_2O ratios, even higher $CaO+Na_2O/K_2O$ ratios, and lower Rb/Sr and higher Sr/Ba ratios than the other leucosomes (Table 4.2). The boudin neck leucosomes and half of the cross-cutting leucosomes show the opposite patterns and have much higher Ba contents than the likely fluid-fluxed leucosomes (Figure 4.8D, Table 4.2). A positive Eu anomaly is found in nearly all of the leucosomes, thus it does not appear to be a good way of distinguishing fluid-saturated and -undersaturated melting in these samples. It is worth noting that the

boudin neck leucosomes are likely produced by fluid-undersaturated biotite-dehydration melting and do not have a positive Eu anomaly; they have a fairly flat REE pattern. But, all of the cross-cutting leucosomes have a positive Eu anomaly and some of the most granitic samples, have the largest positive Eu anomaly. Thus, the flat patterns of the boudin neck leucosomes, and two of the foliation-parallel leucosomes are likely related to the protolith composition, and not to the type of melting reaction that occurred.

Pegmatites can be divided into high and low Ba groups, and the high Ba group that shows a strong correlation with K_2O content likely formed earlier than the low Ba group. This distinction is consistent with cross-cutting field relationships. However, the major element chemistry of the pegmatites is incredibly diverse, and the plagioclase or K-feldspar content of a given pegmatite does not seem to correlate with timing of crystallization. The pegmatites are likely to represent high degrees of crystal accumulation, either plagioclase or K-feldspar, or they could represent crystallization of some material from solute-rich fluids, or both. The pegmatites clearly postdate the other leucosomes in the field area, and some of them are not deformed, suggesting that they have formed at the end of deformation, and possibly metamorphism.

4.6.4 Sample Bias and Accumulation

When samples were prepared for geochemistry, care was taken to avoid the weathered exterior. In samples that were separated into two parts (e.g. melanosome and leucosome or intermediate and felsic pegmatites), the contact between the two portions of the sample was avoided. This method of sample preparation may have led to a bias in the sample, particularly if the composition of the sample changed drastically at the boundary or if smaller crystals were present on the boundary. Furthermore, the grain size of the sample may bias the sample if parts of larger grains are included or excluded during preparation. The pegmatites may have been affected strongly by these issues, as well as the two samples with particularly quartz-rich compositions: one cross-cutting leucosome and one channelway leucosome.

Both of the leucosome samples that plot near the boundary between granodiorite and quartz-rich granitoid (Figure 4.4) are from rocks that were separated into two and three different samples. The cross-cutting leucosome is from a sample that also had a foliation-parallel leucosome and a melanosome. The channelway leucosome comes from a sample with a melanosome pair. Consequently, any boundary material between the different samples was avoided and the sample size was small. As a result, these two samples may have anomalously high quartz components as a result of sample separation. These samples may appear to be more strongly cumulate than other samples within the same leucosome group. The same process may have affected some of the other leucosomes that plot on the boundary of the fields defined by different types of experimentally-derived partial melts. However, some of the samples that plot on the edges of these fields, may in fact represent mineral accumulations, indicative of melt loss from the system.

4.6.5 Tectonic Setting

The geochemistry of the leucosomes and pegmatites is consistent with the previous tectonic model proposed for the area, but there is no definitive geochemical evidence that supports the model. Barquero-Molina (2009) suggested the granulite-facies migmatites, found at Bremer Bay in the Biranup Complex, located in the Albany-Fraser Belt of southwestern Australia, have undergone partial melting synchronous with three phases of bidirectional extension that alternate with contractional phases of deformation. This granulite-facies metamorphism and associated deformation is related to continent-continent collision during Stage II of the Albany-Fraser Orogeny, and the source of heat for metamorphism and partial melting has been attributed to slab breakoff and asthenospheric upwelling (Barquero-Molina, 2009).

The early partial melting, characterized by foliation-parallel and some cross-cutting leucosomes is likely related to fluid-saturated dehydration melting. Fluid-undersaturated dehydration melting cannot be eliminated as a possibility, but fluid-saturated amphibole-dehydration melting is consistent with the chemistry of these early

leucosomes. It has been suggested that fluid-saturated partial melting may occur early in the prograde metamorphic history, during the transition from amphibolite-granulite facies metamorphism (Patiño Douce and Harris, 1998; Fornelli et al, 2002; Cruciani et al., 2008), and these leucosomes may have formed during collision. During slab-breakoff and asthenospheric upwelling and the associated bidirectional extension, fluid-undersaturated biotite-dehydration occurred, producing the rest of the cross-cutting leucosomes and the intermediate-scale boudin neck leucosomes. Finally, after slab-breakoff and asthenospheric upwelling, during late-stage crystallization, the pegmatites were produced. Further geochemical and isotopic analyses from rocks at Bremer Bay or in other locations in the western Albany-Fraser Orogen are needed to place tighter constraints on the timing of partial melting and the precise tectonic setting.

4.7 CONCLUSIONS

Within granulite-facies migmatites located at Bremer Bay, southwestern Australia, five distinct groups of leucosomes and pegmatites can be distinguished. Whole rock geochemistry combined with a previously interpreted structural history of the area provides evidence for the metamorphic reactions and relative timing of leucosome crystallization.

Foliation-parallel leucosomes formed first and have the most calcic, plagioclase-rich compositions, consistent with either fluid-saturated or -undersaturated amphibole-dehydration melting. Channelway leucosomes have moderately high SiO_2 contents, high CaO and low K_2O. These leucosomes also plot within the fluid-saturated or -undersaturated amphibole-dehydration melting field. Cross-cutting leucosomes began forming just after the foliation-parallel leucosomes and outlasted them, as evidenced by their range in composition from calcic with relatively low SiO_2 contents, to highly silicic with abundant K-feldspar. These cross-cutting leucosomes may reflect a transition from fluid-saturated amphibole-dehydration partial melting to a more biotite-rich protolith undergoing fluid-undersaturated biotite-dehydration melting. Boudin neck leucosomes have fairly high SiO_2 and high K_2O contents and are consistent with formation as a result

of biotite-dehydration melting. Pegmatites cross-cut all other leucosomes and have a range in composition, from very calcic to very potassic, but can be divided into high and low Ba samples. High Ba samples have a positive correlation with K_2O and are interpreted to form before the low Ba pegmatites. The partial melting at Bremer Bay occurred via both fluid-saturated and -undersaturated partial melting, related to both biotite- and amphibole-dehydration.

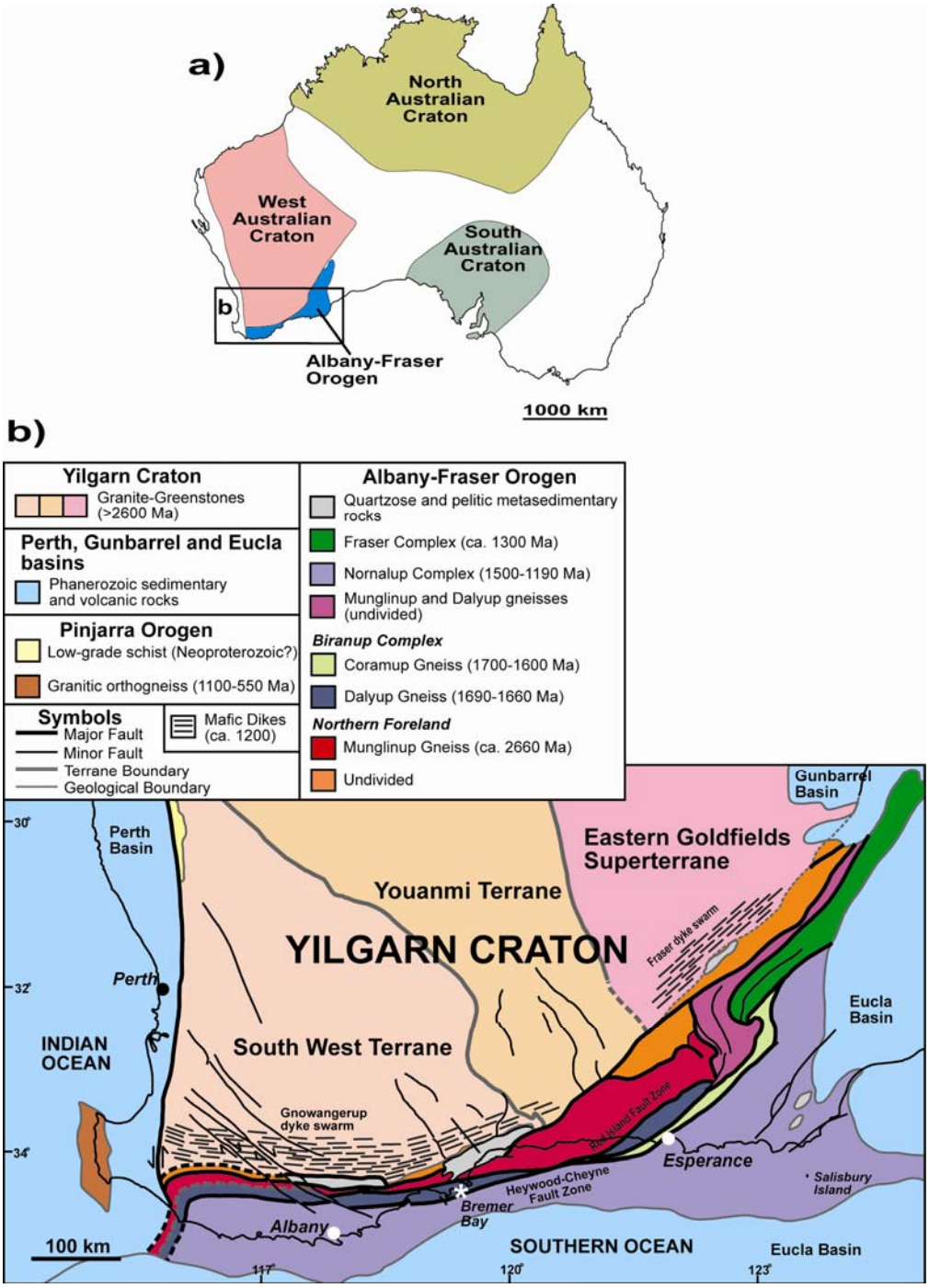

Figure 4.1. Geologic map of southwestern Australia (modified from Spaggieri et al., 2009 and Barqero-Molina, 2009). A. Map of Australia, showing locations of Archean cratons and the Albany-Fraser Orogen. B. Detailed map of the Albany-Fraser Orogen showing the different complexes within the orogen and adjacent geologic units. Bremer Bay is marked with an asterisk.

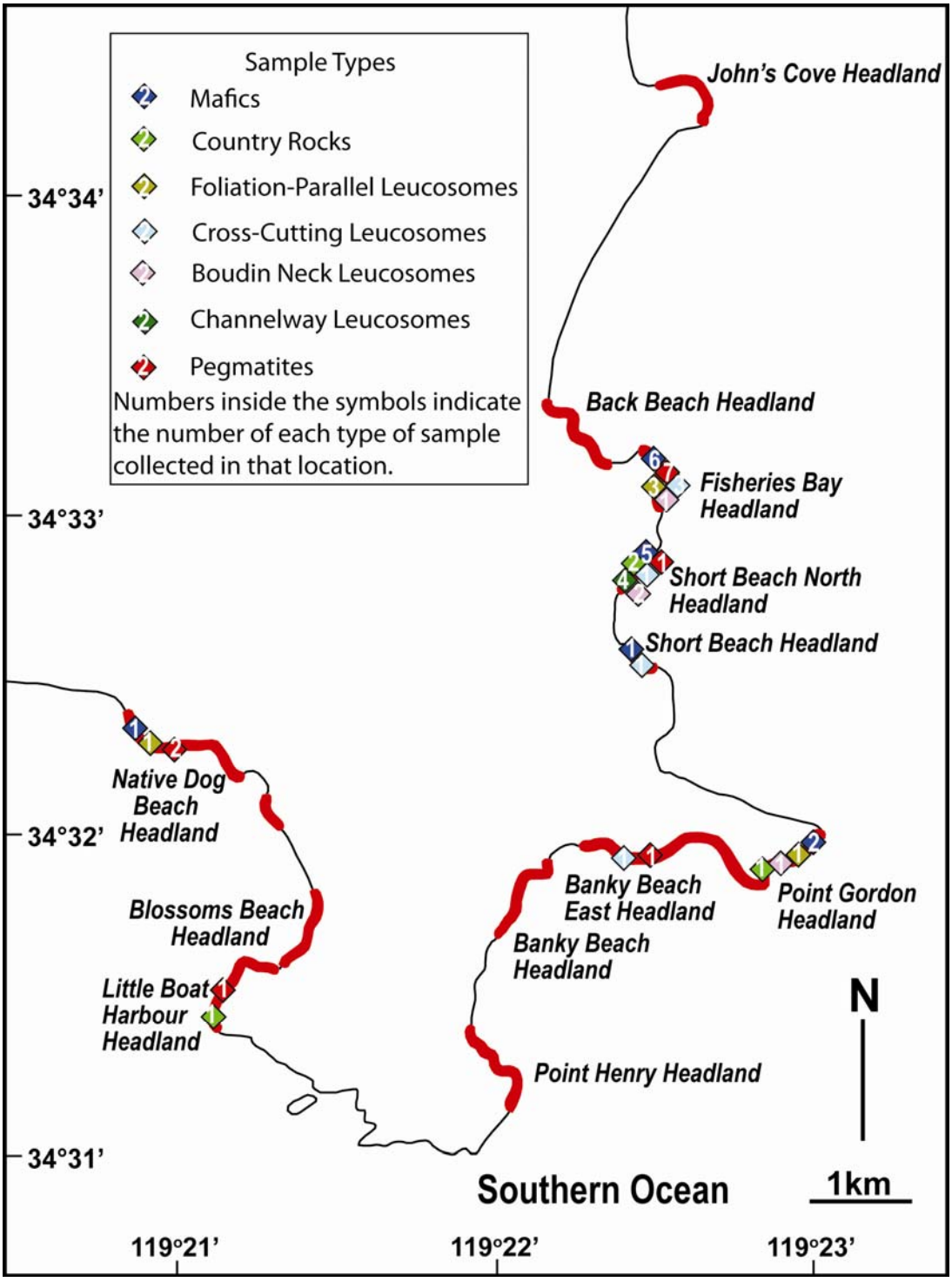

Figure 4.2. Map of the Bremer Bay peninsula (after Barquero-Molina, 2009). Each headland is marked in red and the type of sample and number of samples collected at each locality, are indicated.

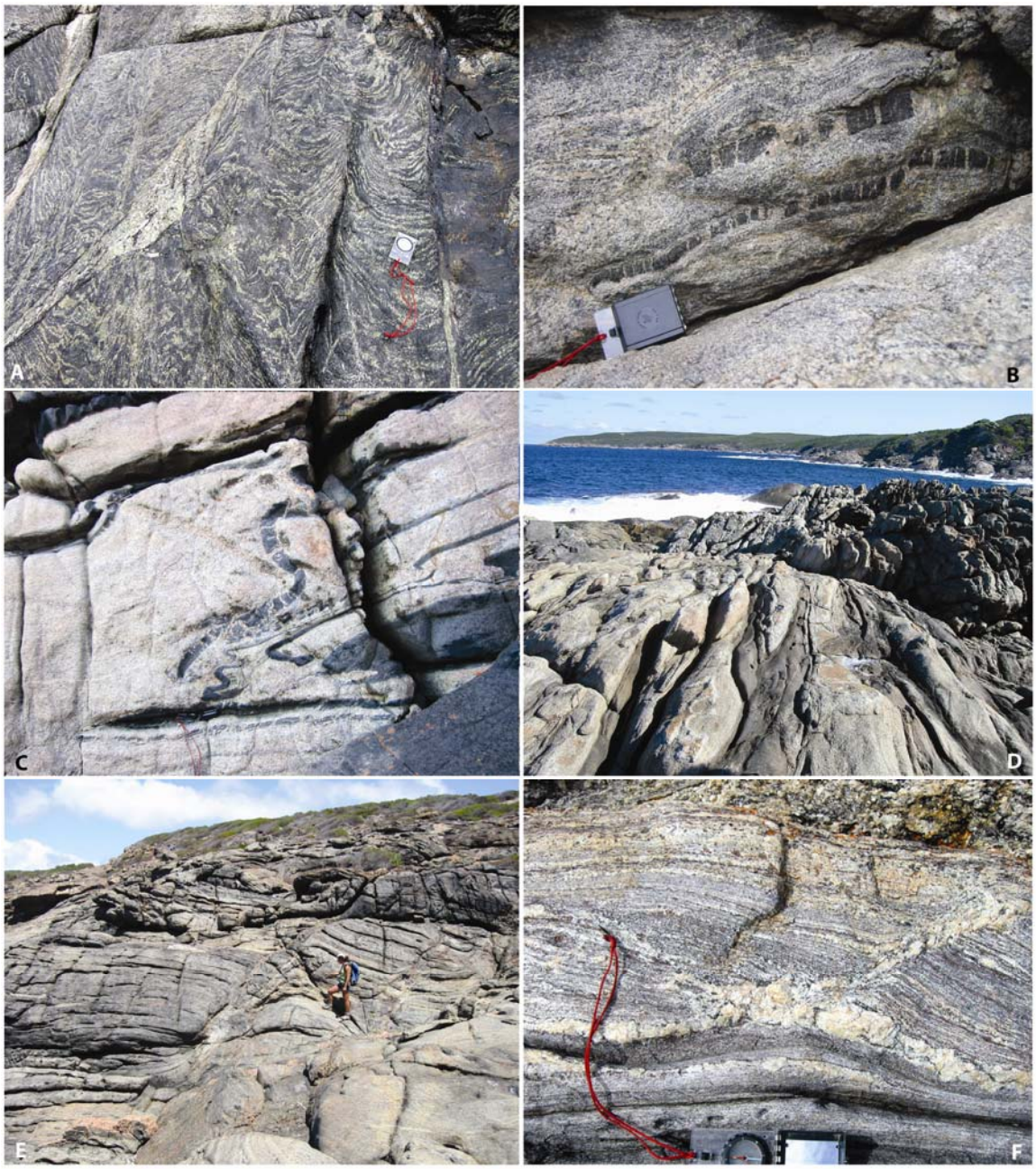

Figure 4.3. (continued on next page). Field photographs of structures and associated leucosomes. A. Characteristic stromatic migmatitic foliation seen throughout the field area. The foliation-parallel leucosomes appear greenish in color and have been folded. The melanosome is located in between these foliation-parallel leucosomes. Several cross-cutting leucosomes are at a high angle to the foliation. B. Small-scale boudins formed during the first bidirectional extension phase. Note the presence of leucosome material in the necks of these square boudins.

C. Trains of small-scale boudins that have been folded along with the foliation. These folds formed after the first phase of bidirectional extension. D. Intermediate-sized boudins, formed during the second phase of bidirectional extension. Compass is resting on earlier folds (same generation as those in C) that have been boudinaged by this second phase of extension. E. Decameter scale boudins formed during the last phase of bidirectional extension. Leucosome material is present within the necks of these boudins. F. Cross-cutting shear band in one of the more aluminous, garnet-bearing units. This shear band contains leucocratic material which cross-cuts the dominant migmatitic foliation. G. Jumbled channelway leucosome that contains isolated mafic blocks and discontinuous layering. H. Two late pegmatites. The pegmatite that extends horizontally across the photograph is cross-cut by the younger felsic pink pegmatite (vertical). I. An example of a pegmatite that appears greenish on the outside and is pink in the interior. This pegmatite is the same pegmatite as the pink pegmatite (vertical) in photo H, near the tip of the pegmatite. J. Mafic dike that is not associated with any of the leucosomes. This sample was collected to provide a comparison to the samples of melanosome, which likely have had melt extracted from them.

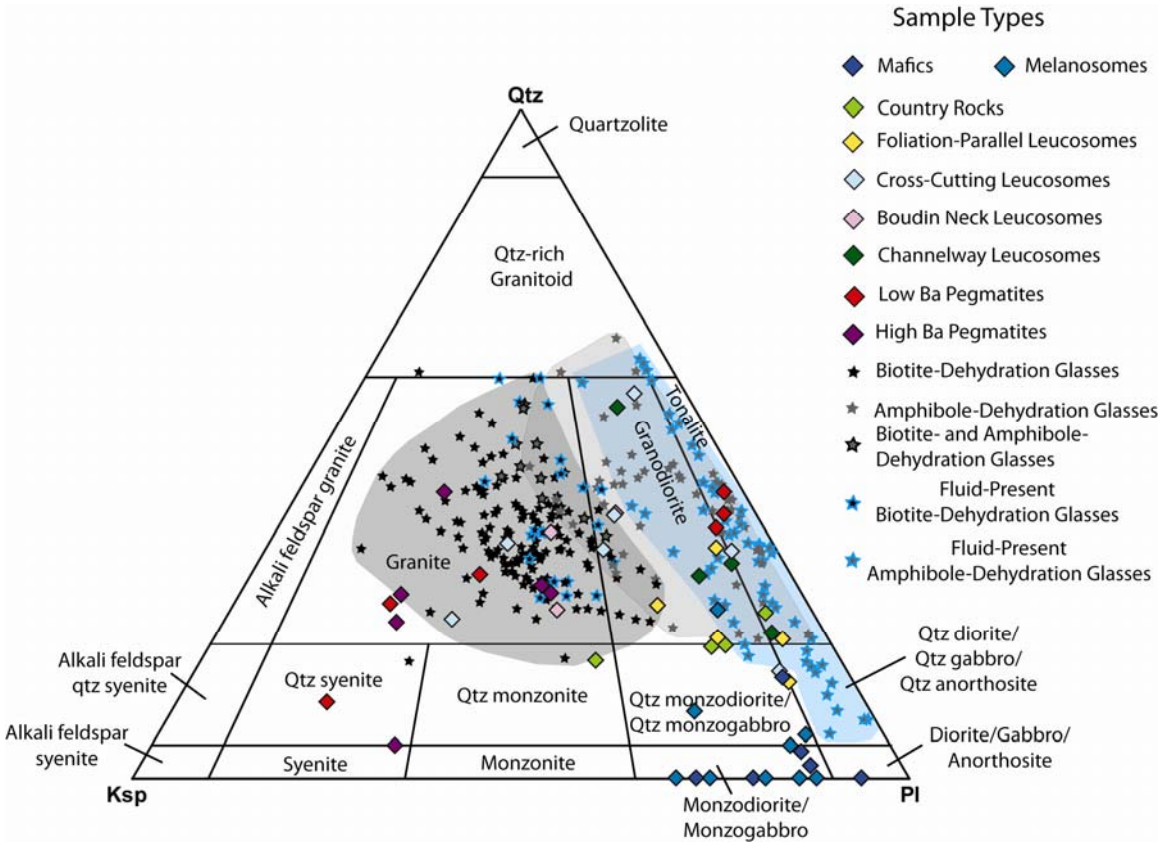

Figure 4.4. Quartz-Alkali Feldspar-Plagioclase (QAP) diagram with normative mineralogy from all samples. Experimental data from biotite-dehydration (Castro et al., 1999, 2000; Gardien et al., 1995, 2000; Koester et al., 2002; Le Breton and Thompson, 1988; Montel and Vielzeuf, 1997; Patiño Douce and Johnston, 1991; Patiño Douce and Beard, 1995, 1996; Patiño Douce and Harris, 1998; Pickering and Johnston, 1991; Singh and Johannes, 1996; Skjerlie and Johnston, 1992; Skjerlie et al., 1993; Tropper et al., 2005; Vielzeuf and Holloway, 1988) and amphibole-dehydration melting (Beard and Lofgren, 1991; Getsinger et al., 2009; Hacker, 1990; Koepke et al., 2004; Patiño Douce and Beard, 1995; Prouteau et al., 1999; Rapp et al., 1991; Rushmer, 1991, 1993; Selbekk and Skjerlie, 2002 Skjerlie and Johnston, 1992, 1996; Skjerlie and Patiño Douce, 1995; Springer and Seck, 1997; Wolf and Wyllie, 1991, 1994). Interpreted fields of experimental partial melts are outlined. Fluid-undersaturated biotite-dehydration melting is colored in dark gray, fluid-undersaturated amphibole-dehydration melting is light gray and fluid-saturated amphibole-dehydration melting is shown in light blue.

Table 4.1: Whole rock geochemical data for all samples.

	Country Rocks				Mafic Rocks - non Melanosomes						Mafic Rocks - Melanosomes								
Sample:	LBH2	PG2	SB10	SB12	FMR2	PG4-B	SB4	SB7	SBGU7	SBGU8	FBH8	FMB3-B	FMWM1-B	FMWM2-B	FMWM3-B	NDB1	PG1-B	SB14-B	SBGU3-B
wt %																			
SiO_2	61.40	67.66	63.21	63.63	49.00	55.05	53.07	54.48	59.85	48.66	44.19	49.29	52.59	51.23	52.16	53.06	45.48	60.85	48.00
TiO_2	1.30	0.23	0.65	0.74	0.96	0.67	0.24	0.88	0.17	0.28	1.15	1.42	1.52	1.03	1.70	2.47	1.70	1.20	0.45
Al_2O_3	15.98	16.50	16.46	16.81	17.10	16.26	14.16	16.73	13.53	12.31	25.34	13.32	14.29	12.45	15.76	15.26	12.00	15.12	13.16
FeO_T	5.85	3.08	5.67	5.10	9.78	7.49	6.74	8.30	8.64	8.68	14.35	13.10	10.72	11.08	12.94	11.15	16.95	7.99	10.78
MnO	0.10	0.08	0.12	0.06	0.18	0.15	0.17	0.17	0.20	0.18	0.36	0.23	0.19	0.18	0.26	0.20	0.31	0.14	0.19
MgO	1.60	1.05	1.97	1.72	8.24	4.78	10.23	4.53	8.22	14.58	4.43	8.97	5.51	10.13	5.32	3.34	7.14	3.60	12.10
CaO	4.40	4.57	4.60	4.37	9.73	7.68	9.78	7.39	4.54	10.49	2.91	8.00	7.96	8.45	6.51	7.20	9.81	6.10	9.29
Na_2O	3.07	5.16	4.14	4.44	2.94	4.50	2.98	4.12	3.73	1.53	3.43	2.33	3.50	2.82	3.33	2.95	2.97	2.81	2.41
K_2O	4.36	0.96	2.19	1.97	0.62	1.32	1.87	1.37	0.95	2.05	3.03	2.21	1.28	0.95	1.07	2.52	1.03	1.51	1.51
P_2O_5	0.39	0.12	0.23	0.24	0.13	0.13	0.04	0.23	0.01	0.08	0.05	0.21	0.25	0.14	0.39	0.73	0.15	0.28	0.09
LOI	0.31	0.78	0.57	0.31	0.68	0.78	0.44	0.88	0.16	0.45	-0.51	0.21	1.25	0.78	-0.26	0.07	0.27	0.10	0.77
Total	98.45	99.41	99.24	99.07	98.67	98.03	99.29	98.22	99.84	98.85	99.24	99.08	97.80	98.45	99.44	98.88	97.54	99.61	97.98
ppm																			
Ni	3	2	9	3	88	30	187	41	136	311	102	205	26	315	42	13	53	54	273
Cr	8	21	15	9	242	99	308	68	150	493	165	594	93	490	214	21	133	163	474
V	86	55	91	75	178	154	69	151	39	98	174	215	188	193	245	172	353	138	105
Ga	23	20	19	22	18	22	13	23	17	13	34	21	21	16	22	25	26	19	17
Cu	12	2	16	28	29	49	11	38	18	30	4	25	19	24	39	17	54	29	47
Zn	99	33	67	65	88	94	90	100	145	88	423	181	119	163	153	150	218	101	143
La	99.73	35.36	32.67	47.24	11.72	48.01	19.42	74.67	19.26	18.49	68.88	21.19	56.33	32.11	35.82	99.73	51.61	39.40	47.76
Ce	229.73	66.51	64.71	91.97	25.18	120.14	42.31	192.24	27.03	42.08	128.98	52.48	157.91	78.60	83.12	229.73	148.30	95.92	120.35
Pr	27.51	7.39	8.59	10.53	3.16	15.94	5.61	26.39	2.61	5.58	13.68	7.41	20.59	9.97	10.61	27.51	20.22	12.21	15.18
Nd	104.34	26.94	36.27	39.94	12.92	63.05	21.51	108.88	8.57	21.68	47.11	32.00	80.29	38.63	43.12	104.34	80.93	50.43	57.23
Sm	17.79	5.00	7.78	6.56	3.24	12.75	4.22	23.04	1.46	4.12	8.05	7.53	16.48	7.55	9.43	17.79	17.77	11.01	11.20
Eu	3.63	1.42	1.59	1.84	1.15	2.12	1.08	2.68	0.97	1.16	2.00	1.63	2.91	2.17	2.07	3.63	3.44	1.90	2.03
Gd	13.09	3.76	6.27	4.65	3.71	9.78	3.34	18.20	1.24	3.16	5.79	7.32	13.69	6.52	8.68	13.09	14.84	9.62	8.79
Tb	1.84	0.53	0.83	0.60	0.67	1.44	0.52	2.71	0.20	0.45	0.82	1.16	2.18	0.96	1.38	1.84	2.30	1.53	1.36
Dy	9.93	2.80	4.42	3.11	4.46	8.20	3.05	15.18	1.35	2.51	4.65	6.88	12.84	5.20	8.48	9.93	13.46	9.04	7.79
Ho	1.79	0.53	0.81	0.59	0.93	1.60	0.61	2.88	0.31	0.47	0.92	1.34	2.51	0.94	1.74	1.79	2.62	1.78	1.52
Er	4.40	1.35	1.98	1.46	2.54	4.24	1.66	7.40	1.01	1.22	2.49	3.46	6.59	2.31	4.84	4.40	7.09	4.68	4.08
Tm	0.59	0.18	0.26	0.19	0.37	0.61	0.24	0.99	0.19	0.18	0.37	0.48	0.96	0.30	0.72	0.59	1.01	0.64	0.61
Yb	3.42	1.05	1.52	1.10	2.28	3.81	1.55	5.67	1.56	1.08	2.43	2.89	5.77	1.70	4.61	3.42	6.18	3.79	3.63
Lu	0.50	0.16	0.23	0.18	0.36	0.59	0.24	0.83	0.28	0.17	0.40	0.43	0.87	0.25	0.74	0.50	0.94	0.59	0.55
Ba	1293	253	846	1171	230	318	381	338	221	257	1202	433	259	259	313	1293	174	381	260
Th	3.73	0.61	0.70	1.59	1.72	2.02	4.18	5.05	2.41	2.24	17.45	1.01	1.81	0.95	3.19	3.73	0.61	0.83	1.74
Nb	25.97	2.17	5.74	5.72	3.10	10.33	3.98	10.93	1.21	2.43	15.72	10.25	14.51	9.46	14.90	25.97	24.90	11.80	9.14
Yb	46.37	13.53	19.68	13.99	22.79	42.27	16.05	71.48	8.23	12.32	22.48	33.48	64.83	23.09	45.23	46.37	68.63	44.35	39.71
Hf	11.76	2.42	5.24	6.84	1.88	3.44	1.72	2.73	32.27	1.09	5.07	3.56	4.41	1.91	6.54	11.76	2.97	7.09	1.42
Ta	1.40	0.09	0.30	0.23	0.21	0.59	0.30	0.50	0.07	0.14	1.43	0.68	0.75	0.49	0.93	1.40	0.85	0.54	0.49
U	0.39	0.31	0.23	0.25	0.52	0.21	0.33	0.31	0.89	0.51	0.89	0.25	0.13	0.13	0.40	0.39	0.09	0.18	0.65
Pb	14.57	10.97	10.15	10.36	3.77	9.83	8.50	9.89	7.45	4.55	24.37	6.34	7.68	6.82	8.12	14.57	6.70	10.21	6.02
Rb	60.4	18.3	49.8	37.6	13.6	20.0	82.7	22.6	11.8	103.6	136.7	134.2	9.6	11.8	35.9	60.4	7.5	48.3	60.7
Cs	0.10	0.19	0.09	0.04	0.13	0.12	1.59	0.08	0.06	3.49	3.69	3.19	0.05	0.04	0.55	0.10	0.03	0.16	0.98
Sr	536	585	483	662	338	441	380	496	430	273	208	189	318	226	291	536	251	257	213
Sc	24.0	9.8	17.6	11.4	25.6	28.5	27.6	38.1	17.4	28.8	30.3	32.7	32.4	22.6	41.1	24.0	52.3	27.0	35.4
Zr	525	85	222	265	62	116	58	74	1400	42	176	130	163	56	252	525	87	289	45
Eu/Eu*	0.65	0.96	0.68	0.97	1.02	0.56	0.85	0.39	2.16	0.95	0.86	0.67	0.58	0.93	0.69	0.70	0.63	0.55	0.61
ΣREE	518.27	152.97	167.92	209.95	72.68	292.27	105.36	481.77	66.04	102.36	286.57	146.21	379.92	187.23	215.36	518.27	370.70	242.54	282.07
$(La/Lu)_N$	40.66	22.83	14.76	27.31	3.39	8.38	8.37	9.26	7.14	10.98	17.72	5.03	6.65	13.12	5.00	20.56	5.67	6.91	8.90

Table 4.1 continued

	Foliation-Parallel Leucosomes					Cross-Cutting Leucosomes							Boudin Neck Leucosomes			Jumbled Channelway Leucosomes			
Sample:	FBH8-M	FMWM2-A	FMWM3-A	NDB1-P	PG1-A	BB1	FBH9	FMB3-A	FMWM1-A	FMWM3-2A	SB8	SB14-A	PG4-A	SB2	SB5	SBGU2	SBGU3-A	SBGU4	SBGU5
wt %																			
SiO_2	66.52	65.76	70.72	62.00	61.79	61.18	70.95	72.17	64.64	79.37	70.71	73.13	68.96	73.96	74.35	69.41	80.22	67.60	72.29
TiO_2	0.20	0.26	0.12	1.53	0.49	0.07	0.37	0.17	0.21	0.09	0.04	0.16	0.38	0.13	0.08	0.19	0.24	0.02	0.02
Al_2O_3	17.55	19.19	16.92	14.37	17.46	18.75	14.17	14.27	19.10	10.81	15.34	14.03	14.90	13.10	13.33	15.37	9.93	19.26	16.57
FeO_T	2.77	1.14	0.92	8.37	4.70	9.31	2.58	1.80	2.04	1.33	0.47	0.99	2.64	1.59	1.43	1.75	1.52	0.56	0.61
MnO	0.08	0.01	0.02	0.17	0.09	0.47	0.07	0.03	0.05	0.03	0.01	0.02	0.05	0.02	0.03	0.03	0.04	0.01	0.01
MgO	0.88	0.83	0.35	2.33	1.81	1.51	1.11	0.83	0.78	0.51	0.14	0.38	0.88	0.79	0.90	1.86	0.87	0.36	0.32
CaO	3.51	5.45	5.05	4.78	5.59	4.89	3.05	3.36	4.81	2.53	1.28	2.56	2.36	2.15	2.67	4.14	2.44	4.87	4.15
Na_2O	4.98	5.04	3.69	2.93	5.25	2.61	3.06	2.73	5.62	2.50	2.66	2.07	3.35	2.75	3.20	4.01	2.59	5.34	4.65
K_2O	2.15	0.94	1.21	2.55	1.17	0.76	3.39	2.84	1.37	1.07	7.59	5.44	5.00	4.35	2.89	1.81	1.56	1.14	1.12
P_2O_5	0.03	0.03	0.04	0.44	0.24	0.01	0.10	0.05	0.18	0.01	0.07	0.04	0.17	0.02	0.04	0.06	0.01	0.01	0.02
LOI	0.98	1.30	0.51	0.11	1.24	0.14	0.70	1.28	0.92	0.88	0.45	0.37	0.76	0.55	0.61	0.57	0.62	0.58	0.56
Total	98.67	98.66	99.03	99.46	98.58	99.56	98.84	98.24	98.80	98.26	98.30	98.82	98.70	98.87	98.92	98.60	99.44	99.17	99.75
ppm																			
Ni	17	33	2	7	6	6	15	13	5	3	5	4	5	22	17	46	23	3	2
Cr	33	17	9	13	15	86	31	21	6	11	6	14	11	26	25	42	34	5	4
V	40	34	8	93	80	51	43	18	17	10	6	13	42	14	9	16	21	1	1
Ga	19	22	17	19	21	18	14	15	23	13	12	13	15	15	15	16	12	17	18
Cu	20	3	5	10	9	9	10	7	11	12	3	4	8	13	3	16	6	1	1
Zn	34	17	14	123	57	30	33	12	31	14	5	13	30	21	22	23	23	3	4
La	21.48	27.43	17.31	53.00	40.09	31.89	24.24	12.12	30.36	12.62	25.22	13.97	39.52	45.88	40.48	44.94	16.40	31.17	30.67
Ce	33.89	36.14	24.56	105.63	75.67	54.43	39.93	17.96	52.67	19.09	35.60	18.54	73.09	92.11	67.67	66.75	25.52	43.02	40.30
Pr	3.35	3.09	2.10	11.52	8.41	5.63	4.28	1.72	5.42	1.82	3.42	1.62	8.01	10.23	7.27	6.15	2.76	3.75	3.32
Nd	10.49	9.48	6.07	41.36	30.54	19.58	14.78	5.58	17.86	5.80	10.65	4.93	28.50	35.76	24.25	17.93	9.72	10.10	8.36
Sm	1.60	1.00	0.67	6.65	5.34	7.31	2.34	0.82	2.64	0.91	1.48	0.67	4.61	6.74	3.89	1.86	1.77	0.99	0.74
Eu	1.43	1.69	1.41	2.34	1.73	1.76	1.52	1.35	1.66	0.92	1.29	1.59	1.78	1.36	1.15	0.99	0.83	1.43	1.15
Gd	1.68	0.55	0.45	4.91	4.06	19.23	1.69	0.66	1.91	0.67	0.98	0.49	3.14	5.05	2.79	1.05	1.40	0.56	0.35
Tb	0.38	0.05	0.06	0.69	0.55	6.01	0.22	0.09	0.26	0.10	0.13	0.07	0.40	0.78	0.42	0.12	0.21	0.06	0.05
Dy	2.96	0.22	0.32	3.80	2.88	58.01	1.21	0.52	1.37	0.64	0.64	0.38	2.10	4.47	2.35	0.62	1.18	0.27	0.20
Ho	0.72	0.04	0.06	0.68	0.53	16.72	0.23	0.10	0.26	0.13	0.11	0.08	0.39	0.86	0.46	0.12	0.23	0.05	0.03
Er	2.10	0.11	0.17	1.85	1.38	58.70	0.59	0.26	0.65	0.37	0.29	0.22	0.95	2.29	1.25	0.34	0.59	0.10	0.09
Tm	0.33	0.02	0.02	0.26	0.19	10.12	0.09	0.03	0.09	0.06	0.04	0.03	0.14	0.33	0.18	0.06	0.08	0.01	0.01
Yb	2.07	0.13	0.16	1.64	1.12	70.50	0.56	0.21	0.54	0.38	0.25	0.23	0.82	2.05	1.13	0.41	0.51	0.07	0.09
Lu	0.33	0.03	0.03	0.26	0.18	11.95	0.10	0.03	0.09	0.06	0.04	0.04	0.13	0.32	0.18	0.07	0.08	0.01	0.01
Ba	443	495	387	1338	323	86	1646	820	500	305	2253	1750	2156	1345	1006	576	555	310	202
Th	0.55	3.40	0.25	3.21	0.49	7.81	0.71	0.42	0.99	4.06	3.12	0.18	1.43	19.23	11.68	13.09	0.40	1.72	0.68
Nb	1.52	1.30	1.06	16.56	5.27	1.43	3.89	1.26	2.64	0.88	0.98	1.90	5.24	5.83	2.17	1.81	2.68	0.18	0.16
Yb	19.01	1.06	1.69	18.40	13.58	442.46	5.91	2.56	7.00	3.26	3.29	2.10	10.23	22.57	11.97	3.25	5.59	1.17	0.99
Hf	1.87	5.02	0.53	9.05	5.13	33.51	3.93	1.67	1.38	3.51	2.56	1.81	7.53	5.36	7.10	4.79	1.63	0.19	0.07
Ta	0.11	0.04	0.10	1.14	0.20	0.21	0.20	0.12	0.14	0.08	0.15	0.13	0.20	0.76	0.18	0.10	0.15	0.04	0.04
U	0.16	0.28	0.03	0.62	0.19	1.11	0.33	0.12	0.08	0.20	0.81	0.25	0.31	5.65	0.64	0.38	0.14	0.18	0.06
Pb	20.31	11.99	8.55	16.39	10.22	14.22	13.27	10.21	10.72	5.34	32.68	17.18	18.14	20.76	13.79	9.82	9.15	10.35	12.19
Rb	37.6	16.1	34.5	69.0	13.2	24.0	83.3	83.5	11.9	31.2	299.4	174.0	147.5	168.9	86.6	43.9	54.3	13.8	18.7
Cs	0.23	0.08	0.23	0.26	0.28	0.40	0.34	0.54	0.03	0.16	0.96	0.34	0.43	2.19	0.32	0.11	0.61	0.02	0.05
Sr	515	571	345	520	577	185	438	308	573	244	621	320	653	352	358	566	280	675	404
Sc	7.2	2.0	1.5	11.0	10.9	69.7	6.2	1.9	2.4	3.0	0.5	1.9	4.0	6.8	4.7	2.8	3.3	0.1	0.3
Zr	67	180	20	390	202	1316	159	70	57	153	98	73	308	179	278	178	66	7	2
Eu/Eu*	2.66	6.35	7.38	1.20	1.09	0.43	2.24	5.45	2.16	3.47	3.10	8.19	1.35	0.69	1.02	5.38	1.57	5.38	6.05
ΣREE	82.80	79.98	53.40	234.60	172.66	371.84	91.77	41.46	115.76	43.57	80.15	42.85	163.57	208.22	153.47	141.41	61.28	91.59	85.38
$(La/Lu)_N$	6.76	101.47	67.93	21.15	23.23	0.27	26.20	37.93	36.30	21.33	67.09	34.41	30.66	14.96	23.27	67.99	21.73	316.13	235.34

Table 4.1 continued

	Pegmatites											
Sample:	BBEH-4	FBWM1	FPG1	FPG3-G	FPG3-P	FPG4	FPG5	FPG6	LBH2-A	NDBPD1-GA	NDBPD1-PA	SB11
wt %												
SiO_2	68.17	70.95	76.48	75.93	74.05	62.23	73.80	71.71	77.63	73.40	71.78	71.22
TiO_2	0.01	0.10	0.07	0.02	0.06	0.04	0.03	0.03	0.18	0.25	0.05	0.13
Al_2O_3	16.56	15.06	14.00	14.05	13.31	16.72	14.31	15.02	11.15	14.43	14.45	15.78
FeO_T	0.12	1.87	1.15	0.38	0.98	4.19	0.17	0.47	0.84	2.93	0.98	0.41
MnO	0.00	0.03	0.02	0.01	0.01	0.12	0.00	0.01	0.01	0.03	0.01	0.00
MgO	0.01	0.81	0.19	0.11	0.08	2.50	0.03	0.13	0.15	0.24	0.07	0.09
CaO	0.14	2.01	2.29	1.87	0.48	1.08	0.29	0.39	0.92	4.04	0.79	2.25
Na_2O	2.17	3.17	5.12	5.36	3.10	2.58	2.26	2.34	1.62	3.71	1.86	3.34
K_2O	11.45	5.09	0.69	1.03	6.42	9.12	8.48	8.82	5.89	0.42	8.67	5.20
P_2O_5	0.01	0.13	0.03	0.01	0.03	0.02	0.01	0.01	0.03	0.01	0.01	0.06
LOI	0.22	0.90	0.54	0.50	0.31	0.44	0.36	0.50	0.27	0.54	0.54	0.39
Total	98.64	99.22	100.04	98.77	98.53	98.61	99.38	98.93	98.40	99.46	98.67	98.47
ppm												
Ni	3	6	0	3	4	18	0	5	1	0	0	3
Cr	5	11	6	4	5	23	3	3	5	2	4	7
V	0	15	8	3	4	11	2	2	11	19	3	9
Ga	19	15	38	42	46	14	12	14	11	23	15	16
Cu	1	10	3	4	3	36	0	20	2	2	1	2
Zn	1	19	25	6	7	73	3	16	12	46	17	7
La	1.27	31.93	13.85	9.04	36.24	18.14	11.47	13.25	76.98	25.17	15.05	19.64
Ce	2.73	64.28	27.93	17.46	97.08	20.72	10.67	13.81	119.93	33.43	17.94	28.88
Pr	0.22	8.02	2.99	1.89	11.34	1.69	0.65	0.98	10.06	2.99	1.55	3.07
Nd	0.77	31.15	9.52	5.49	34.32	4.84	1.46	2.44	26.90	8.57	4.40	10.48
Sm	0.29	6.21	2.98	1.73	12.68	0.70	0.22	0.36	2.09	1.04	0.50	1.67
Eu	0.72	1.90	0.48	0.29	0.33	2.03	2.13	2.23	1.79	1.07	1.26	1.81
Gd	0.56	4.79	2.83	1.60	10.55	0.59	0.13	0.21	0.85	0.69	0.28	1.26
Tb	0.12	0.71	0.51	0.33	2.22	0.11	0.01	0.02	0.09	0.09	0.03	0.16
Dy	0.86	4.05	2.34	1.63	9.98	0.78	0.06	0.12	0.39	0.47	0.14	0.86
Ho	0.18	0.77	0.28	0.21	1.09	0.18	0.01	0.02	0.07	0.09	0.02	0.16
Er	0.53	2.00	0.49	0.40	1.81	0.56	0.03	0.06	0.16	0.22	0.06	0.38
Tm	0.09	0.28	0.05	0.05	0.20	0.10	0.01	0.01	0.03	0.03	0.01	0.05
Yb	0.65	1.70	0.26	0.24	0.99	0.73	0.04	0.07	0.20	0.20	0.04	0.26
Lu	0.11	0.25	0.04	0.03	0.12	0.13	0.01	0.01	0.03	0.03	0.01	0.04
Ba	798	2121	71	29	126	5176	4740	5109	2518	38	708	3256
Th	1.43	5.13	7.59	3.37	42.24	1.11	0.16	0.61	20.93	2.74	3.71	0.21
Nb	0.91	2.45	24.20	21.57	345.25	0.31	0.14	0.33	2.40	5.25	0.40	1.35
Yb	7.23	19.83	8.04	5.91	24.39	4.61	0.35	0.66	1.69	2.22	0.69	3.99
Hf	0.12	1.95	2.13	0.36	6.30	0.33	0.03	0.35	4.34	0.24	0.12	0.22
Ta	0.06	0.13	1.38	1.29	24.25	0.04	0.01	0.03	0.15	0.90	0.07	0.10
U	0.21	0.53	36.32	13.04	140.72	0.23	0.10	0.17	0.37	0.41	0.23	0.09
Pb	42.49	19.07	16.51	9.63	32.27	26.31	21.12	32.73	30.34	13.11	49.24	14.37
Rb	1102.0	142.7	83.7	119.7	1034.3	241.4	227.1	237.7	187.7	26.8	449.5	128.5
Cs	5.73	0.69	2.72	1.18	8.98	0.77	0.31	0.35	0.46	0.45	1.47	0.13
Sr	191	456	184	91	56	608	532	555	414	223	220	529
Sc	0.4	5.2	1.0	0.5	2.8	8.6	0.4	0.4	1.1	1.1	0.2	1.1
Zr	3	76	46	9	111	12	1	14	166	6	4	10
Eu/Eu*	5.42	1.03	0.50	0.52	0.09	9.45	35.97	22.65	3.48	3.65	9.38	3.68
ΣREE	9.11	158.06	64.55	40.38	218.95	51.29	26.90	33.61	239.56	74.09	41.29	68.70
$(La/Lu)_N$	1.17	12.90	37.36	27.77	30.89	14.87	119.74	197.76	241.13	84.25	217.09	50.30

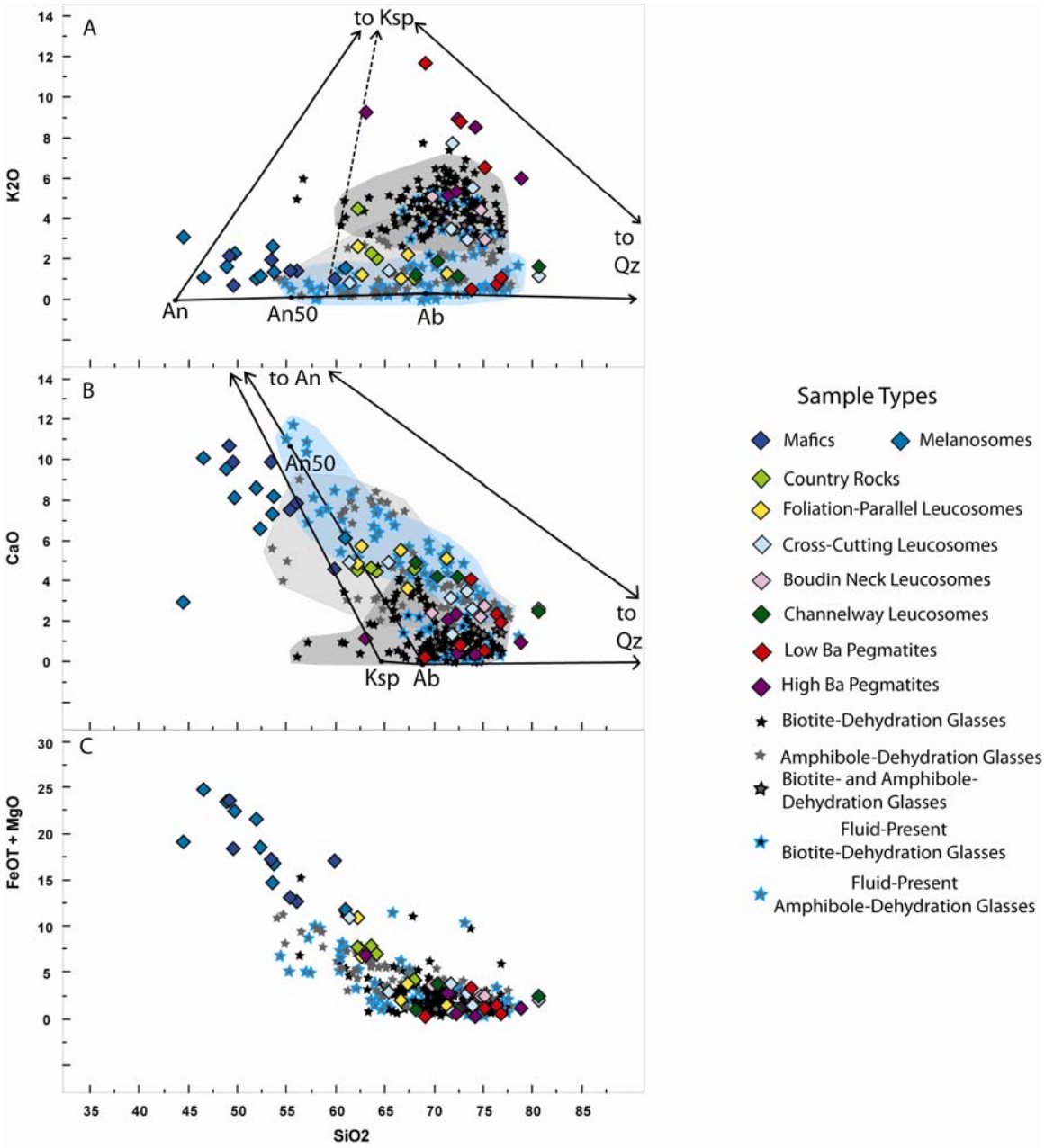

Figure 4.5. Harker diagrams showing compositional trends from all whole rock geochemistry samples. Experimental data (stars) and fields representing experimental melts come from the same datasets referenced in Figure 4.4. A and B have mineral compositions plotted for comparison with the experimental and whole rock geochemical data. K-feldspar and quartz plot off the diagram, so arrows are used to indicate their positions relative to the other feldspars. Samples from the Bremer Bay area that fall near mineral apices or along tie-lines between phases may represent mineral accumulations.

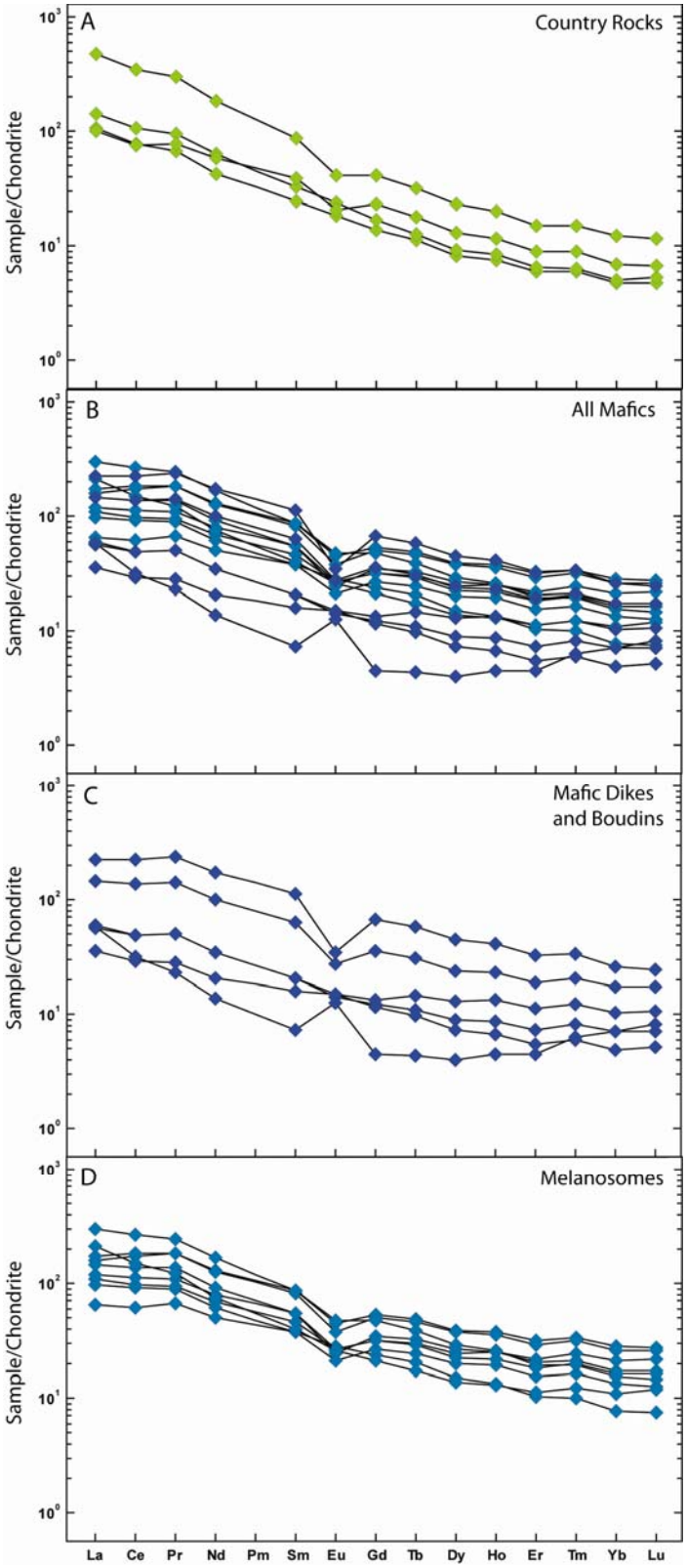
A
Country Rocks
B
All Mafics
C
Mafic Dikes
and Boudins
D
Melanosomes
Sample/Chondrite
La
Ce
Pr
Nd
Pm
Sm
Eu
Gd
Tb
Dy
Ho
Er
Tm
Yb
Lu

Figure 4.6. Rare earth element diagrams with country rock and mafic samples normalized to chondrite. Normalized to values of Nakamura (1974). Country rock samples have fairly flat REE patterns flat to slightly negative Eu anomalies. Melanosome samples have negative Eu anomalies and similar patterns to each other, whereas mafic rocks that do not have an associated leucosome have positive, flat or negative Eu anomalies and a wider range of REE profiles.

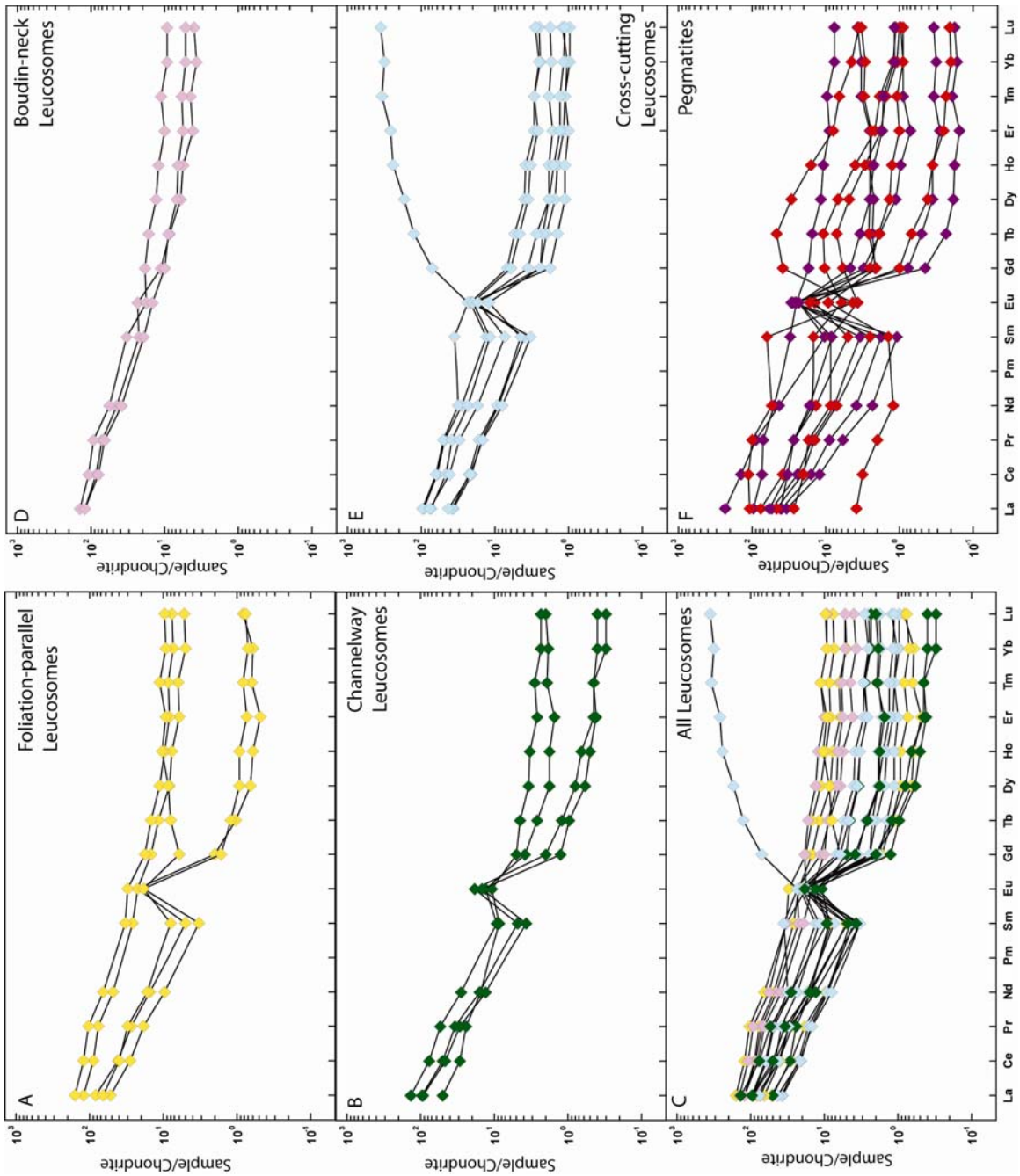

Figure 4.7. Rare earth element diagrams with leucosome and pegmatite sample normalized to chondrite. Normalized to values of Nakamura (1974). Most of the leucosomes have a positive Eu anomaly; only four samples have a slight negative Eu anomaly or no anomaly. Pegmatitic samples have a wide range in patterns and Ba content (the purple vs. red color) does not correlate with REE patterns.

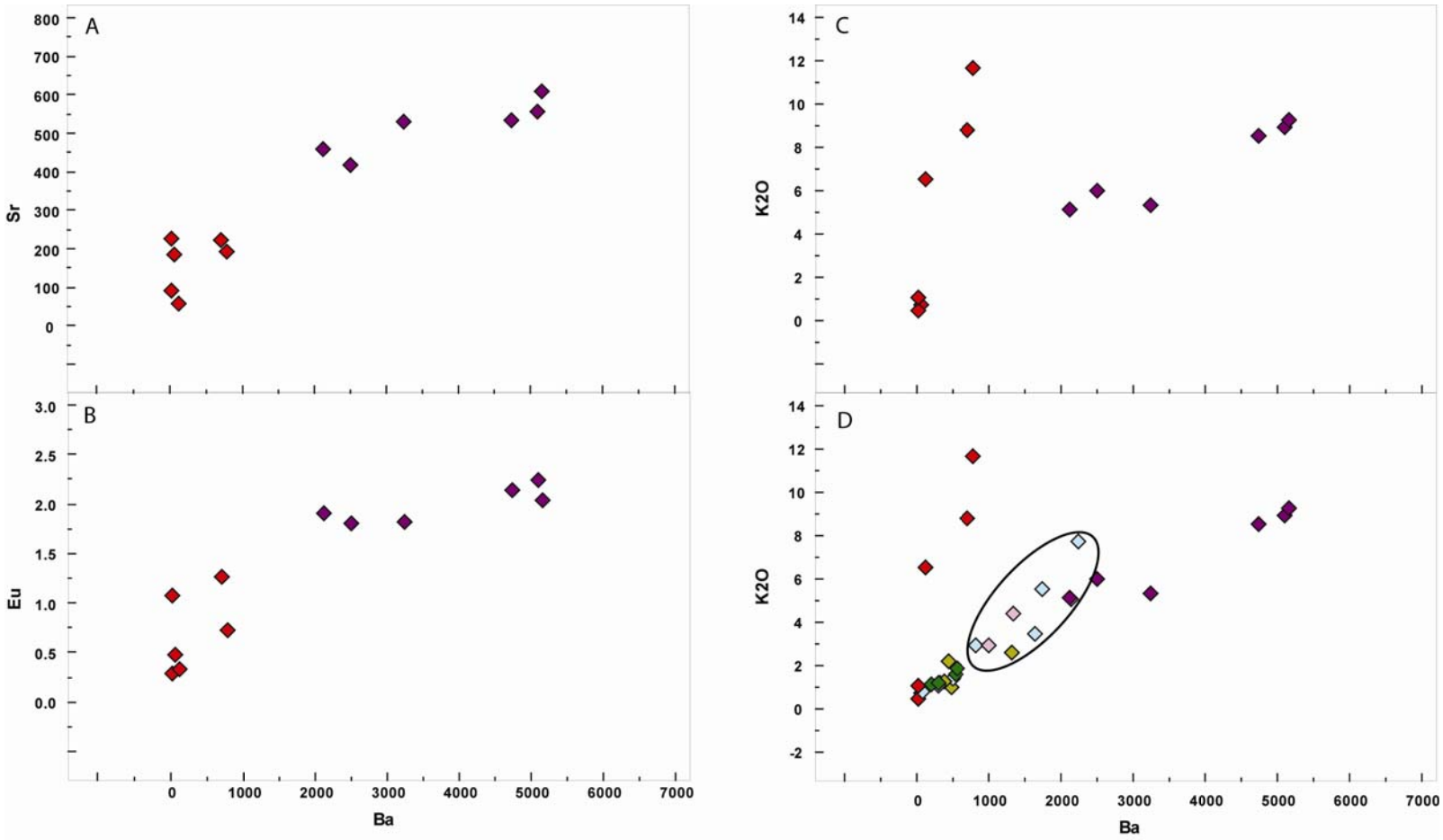
A
Sr
800
700
600
500
400
300
200
100
0
B
Eu
3.0
2.5
2.0
1.5
1.0
0.5
0.0
0
1000
2000
3000
4000
5000
6000
7000
Ba
C
K2O
14
12
10
8
6
4
2
0
D
K2O
14
12
10
8
6
4
2
0
-2
0
1000
2000
3000
4000
5000
6000
7000
Ba

Figure 4.8. A-C. Plots of Ba vs. Sr, Eu and K_2O for the pegmatites. Pegmatites can be broken into low and high Ba groups. D. Plot of Ba vs. K_2O for leucosomes and pegmatites. The high Ba leucosomes are circled and these are the group of leucosomes that do not overlap the field of experimental melts derived from fluid-saturated melting.

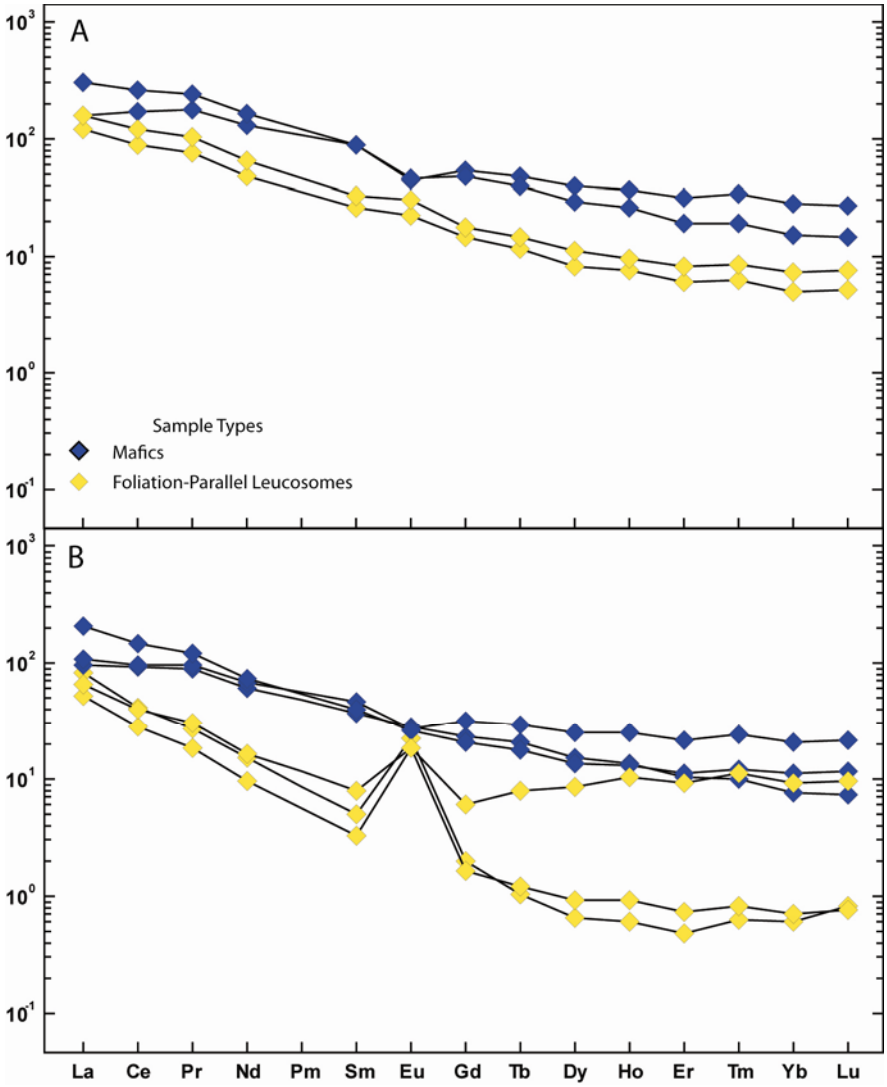

Figure 4.9. Rare earth element diagrams with foliation-parallel leucosome and melanosome pairs normalized to chondrite. A. Two of the foliation-parallel leucosomes have no Eu anomaly and their melanosome pairs have a negative Eu anomaly. B. Three of the foliation-parallel leucosomes have a positive Eu anomaly and their melanosome pairs have no Eu anomaly. Note all of the melanosome pairs have higher Eu concentrations than their associated leucosome. Normalized to values of Nakamura (1974).

Table 4.2: Values of selected elements, elemental ratios and normative quartz-plagioclase-K-feldspar percentages for the leucosomes. Each leucosome is categorized as fluid-present, fluid-absent or borderline based on where it plots on Harker and QAP norm diagrams.

	Foliation-Parallel Leucosomes					Cross-Cutting Leucosomes							Boudin Neck Leucosomes			Jumbled Channelway Leucosomes			
Sample:	FBH8-M	FMWM2-A	FMWM3-A	NDB1-P	PG1-A	BB1	FBH9	FMB3-A	FMWM1-A	FMWM3-2A	SB8	SB14-A	PG4-A	SB2	SB5	SBGU2	SBGU3-A	SBGU4	SBGU5
Fluid	Present	Present	Present	Borderline	Present	Present	Absent	Absent	Present	Present	Absent	Absent	Absent	Absent	Absent	Present	Present	Present	Present
CaO (wt %)	3.55	5.52	5.10	4.80	5.67	4.91	3.08	3.42	4.87	2.58	1.30	2.59	2.39	2.18	2.70	4.19	2.46	4.91	4.16
Na2O (wt %)	5.05	5.10	3.72	2.94	5.33	2.62	3.09	2.78	5.69	2.54	2.71	2.09	3.40	2.78	3.23	4.06	2.61	5.39	4.66
K2O (wt %)	2.18	0.96	1.23	2.56	1.19	0.76	3.43	2.89	1.39	1.09	7.72	5.50	5.06	4.40	2.92	1.83	1.57	1.15	1.12
Na2O/K2O	2.32	5.31	3.04	1.15	4.48	3.44	0.90	0.96	4.10	2.33	0.35	0.38	0.67	0.63	1.11	2.22	1.66	4.69	4.16
(CaO+Na2O)/K2O	3.95	11.06	7.20	3.03	9.24	9.90	1.80	2.14	7.61	4.69	0.52	0.85	1.14	1.13	2.03	4.51	3.23	8.97	7.87
Rb/Sr	0.07	0.03	0.10	0.13	0.02	0.13	0.19	0.27	0.02	0.13	0.48	0.54	0.23	0.48	0.24	0.08	0.19	0.02	0.05
Sr/Ba	1.16	1.15	0.89	0.39	1.79	2.15	0.27	0.37	1.15	0.80	0.28	0.18	0.30	0.26	0.36	0.98	0.51	2.17	2.00
Pl Norm (%)	61.16	70.81	56.58	46.00	68.48	49.80	41.13	40.36	71.98	34.43	28.64	29.98	39.80	34.22	40.62	53.94	33.22	70.03	59.99
Qtz Norm (%)	20.03	20.28	33.78	21.91	12.78	28.19	32.29	37.59	15.33	55.73	23.39	34.44	24.05	35.51	37.87	28.35	53.30	21.29	31.68
Ksp Norm (%)	13.61	5.96	7.62	16.72	7.59	5.06	21.35	17.94	8.65	6.76	46.72	33.65	31.30	27.05	18.02	11.42	9.72	7.09	6.90

Chapter 5: The role of lattice strain in partial melting

5.1 ABSTRACT

Evidence for partial melting along subgrain boundaries, areas of high dislocation density, in quartz and plagioclase is documented for rocks from the Wet Mountains of central Colorado, the Lost Creek Gneiss of the Llano Uplift, central Texas and the Albany-Fraser Orogen, southwestern Australia. Domains of quartz or plagioclase crystals along subgrain boundaries are preferentially involved in the partial melting reaction over unstrained domains of these minerals, indicating more favorable conditions for melting along more strained areas of a crystal lattice. Microstructural evidence for former partial melt in migmatites includes melt pseudomorphs along grain boundaries and at triple junctions and serrate/cuspate grain boundaries with low dihedral angles between inferred former melt and solid material. The material along subgrain boundaries in quartz and plagioclase has the same morphology as melt pseudomorphs present along grain boundaries and is commonly laterally continuous with this former grain boundary melt. This similarity and continuity indicates the material along subgrain boundaries can also be categorized as melt pseudomorphs. Subgrain boundaries consist of arrays of dislocations within a crystal lattice, and unlike fractures, would not act as conduits for melt migration. Instead, the presence of this former melt along subgrain boundaries requires that partial melting occurred in these locations. Melt pseudomorphs are interpreted to have formed along subgrain boundaries by preferential melting in these locations because it is kinetically more favorable for melting reactions to occur in these high-strain locations. For these rocks that involve multicomponent systems, the primary cause for preferential melting in high strain locations is enhanced diffusion rates along the subgrain boundary because of pipe diffusion or water associated with dislocations. Other mechanisms related to a lowering of the activation energy needed to cause partial melting, which have been proposed for phase transformations in the material and physical sciences, are likely to have only a very minor contribution to the melting process.

5.2 INTRODUCTION

In the last 35 years great strides have been made on understanding the role of strain in promoting metamorphic reaction. Internal plastic strain of crystal lattices induces dislocations which may form tangles or migrate to form walls of dislocations, depending primarily on the rate of diffusion relative to the rate of strain. In either case, dislocations are concentrated near the grain boundaries. With increased strain and/or temperature, dynamic recrystallization may occur 1) through subgrain rotation recrystallization as walls of dislocations transition from subgrain to discrete grain boundaries as a result of further migration of dislocations into walls, or 2) through migration of grain boundaries of less strained grains into more strained grains. Both of these processes lower the stored lattice strain energy and lead to formation of new strain-free grains with most remaining dislocations at the grain boundaries (Poirier, 1985). Highly strained locations are seen to promote reaction due to a decrease in grain size caused by dynamic recrystallization; this decrease in grain size leads to increased rates of diffusion, as well as more surface area for reactions to occur, and associated increases in reaction rates (Wintsch, 1975; White, 1975; Kerrich et al., 1977; Brodie and Rutter, 1985; Yund and Tullis, 1991).

Many processes involving internal plastic strain have been shown to increase reaction rates as a result of enhanced diffusion rates. More highly strained locations have increased dislocation density, finer grain size, and enhanced diffusion rates; the latter has been attributed to pipe diffusion along linear diffusion arrays (Smoluchowski, 1952; Luther, 1965; Yurimoto and Nagasawa, 1989). Dislocations commonly have water bonded to the crystal lattice, which appears in the Transmission Electron Microscope (TEM) as water bubbles located at dislocations; this presence of water also has been proposed to enhance diffusion rates (Green and Radcliffe, 1975; McLaren et al., 1983; Kronenberg et al., 1986, 1990). Other authors have identified enhanced fluid flow in highly deformed locations, and the fluids promoted metamorphic reactions as a result of increases in diffusion rates (Etheridge et al., 1984). Strain solution, a process where more highly strained locations are preferentially dissolved, has also been proposed to

increase chemical potential gradients of dissolved species resulting in an associated increase in reaction rates (Wintsch and Dunning, 1985).

An energetic contribution to the reaction from the stored strain energy in dislocations has been proposed, and experiments indicate preferential localization of reaction into very highly strained minerals (Green, 1972). In an experiment by Green (1972), flint was experimentally deformed and areas that were more highly strained preferentially transformed to coesite. Coesite formed at temperatures as low as 450° C and pressures of 1.0 GPa, conditions far lower than coesite stability; therefore coesite was determined to have formed metastably. These lower temperature and pressure conditions were attributed to a contribution from stored strain energy of at least 1200-4100 J/mol, as this is the difference in free energy of strain free quartz and coesite.

Subsequent studies have suggested that naturally deformed rocks are unlikely to have dislocation densities higher than 10^9 cm^{-2}, which would contribute only about 3 J/mol (Knipe and White, 1979; Wintsch and Dunning, 1985), an amount of energy unlikely to noticeably affect reaction rates. However, dislocation densities are typically higher within dislocation tangles, pileups, and subgrain boundaries, with densities that may be higher than 10^{11} cm^{-2} (Wintsch and Dunning, 1985). At sites with dislocation densities this high, the energetic input from dislocations becomes significant, with values proposed to range from 100-600 J/mol for densities of 10^{11} cm^{-2} and 1400-3000 J/mol for densities of 10^{12} cm^{-2} (Wintsch and Dunning, 1985). Although dislocation densities this high will persist to high temperatures consistent with partial melting, they form at subsolidus conditions (Passchier and Trouw, 1996; Vernon, 2004).

Any metamorphic reaction will only occur when the activation energy required to make a reaction occur, is overstepped. The reactant minerals have a specific free energy and the product minerals, or melt, have a lower free energy at that temperature and pressure condition, but activation energy is required to allow the reaction to occur. Highly strained minerals will have a higher free energy than unstrained (or less strained) minerals; therefore strained reactants will require a smaller contribution from activation

energy than unstrained minerals, and consequently strained reactants should react more rapidly than less strained reactants (Hand and Dirks, 1992) (Figure 5.1).

Partial melting reactions typically occur along interfaces or surfaces, such as grain boundaries, because interfaces are locations where reactant minerals +/- fluids are in contact with each other. Reactions could also occur along subgrain boundaries, another form of interface, if the reactant phases are present. However, in addition to being interfaces, grain and subgrain boundaries are high strain locations with high dislocation densities. Studies of melting in simpler systems, such as monomineralic substances or even single crystals, have also found that melting occurs along grain boundaries or along surfaces (Dash et al., 1999 and references therein; Alsayed et al., 2005; Mei and Lu, 2007 and references therein; Han et al., 2010). Within the material-science, physics, metallurgical and geological communities, the process of melting has been studied intensely, but this process is still not fully understood.

Within material science and metallurgy the role of strain in melting of one-component systems has been established, and experiments and molecular dynamics simulations showing preferential melting at high strain locations have been conducted on metals and colloidal silica (Lutsko et al., 1989; Tartaglino and Tosatti, 2003; Alsayed et al., 2005; Sirong et al., 2006; Han et al., 2010). Until recently, the geological community had not considered the role of strain in partial melting. Hand and Dirks (1992) proposed that melting preferentially occurred in crenulated regions of the Napperby Gneiss, northern Australia because of increased stored strain energy, surface free energy and smaller grain size. More recently an experimental study on melting in strained metapelites concluded that more melting occurred in more highly strained locations, possibly caused by smaller grain size, shear heating, or chemical or thermal effects from changes in mean stress during melting (Misra et al., 2009).

In this study I investigated the role of strain in preferentially inducing melting in locations of high dislocation density, specifically along subgrain boundaries in quartz and plagioclase grains. Below I give background on the role of strain and dislocations in melting of one-component systems from the material, physical science and metallurgical

literature and briefly discuss melt microstructures attributed to identification of former melt. I also provide evidence from samples taken from three different field areas of melting along subgrain boundaries in quartz and plagioclase, and conclude with a discussion of the role of strain in partial melting along subgrain boundaries in geologic materials.

5.3 THE MELTING PROCESS AND THE ROLE OF STRAIN

In material science and metallurgy, the role of strain in melting has been investigated extensively where only a single phase is involved and the actual melting process is a true phase transformation of solid to liquid. Melting can be thought of in a thermodynamic context where the melting temperature, at a given pressure, is a point where the free energy of the solid and liquid are equal.

Experiments have shown that the location where melting typically occurs is along surfaces or interfaces, such as a free surface, if a single crystal is being considered, or a grain boundary when there is more than one crystal (Dash, 1999 and references therein; Mei and Lu, 2007 and references therein). Other theories have suggested that melting preferentially occurs in areas with high defect density, including dislocations, stacking faults, vacancies and impurities (Mott, 1950; Mizushima, 1960; Ookawa, 1960; Kuhlmann-Wilsdorf; 1965). Many studies have specifically investigated premelting, a process where melting begins below the thermodynamically calculated melting temperature (Pluis et al., 1987; Mei and Lu, 2007 and references therein). Recently several studies have looked at both interfaces and defects, by looking at the role of strain in preferential melting along grain boundaries, subgrain boundaries or strained surfaces (Tartaglino and Tosatti, 2003; Alsayed et al., 2005; Han et al., 2010).

Alsayed et al. (2005) conducted an experimental study on colloidal silica gels, where they found that premelting preferentially occurred along grain boundaries, and in regions that did not contain or were far from grain boundaries, premelting preferentially occurred along partial dislocations. Colloidal silica gels studied by Alsayed et al. (2005) melt at fairly low temperatures of 28° C, and consequently they can be heated under the

microscope and their motions can be tracked. This approach has allowed close observation of the particles when they reach their melting point. However, many other substances, such as metals and geologic materials have much higher melting temperatures, and consequently it is difficult to conduct experiments on these substances. It is not possible to watch melting occur or to capture it on camera. As a result, molecular dynamics simulations have provided an alternate strategy for analyzing the role of strain on the melting process in materials that melt at higher temperatures.

One molecular dynamics simulation evaluated differences in surface melting between strained and unstrained Al (Tartaglino and Tosatti, 2003), whereas another compared melting of Cu at a low and a high energy grain boundary (Han et al., 2010). Both of these studies found that more highly strained, higher energy locations melt at lower temperatures than unstrained or lower energy regions. Tartaglino and Tosatti (2003) looked at Al crystals strained in compression and tension and found that although both of these melted at lower temperatures than an unstrained crystal, crystals in tension melted at lower temperatures than the compressed samples. The Han et al. (2010) study showed that high energy grain boundaries undergo premelting, whereas the low energy grain boundaries melt at the bulk melting temperature.

These three studies (Tartaglino and Tosatti, 2003; Alsayed et al., 2005; Han et al., 2010) provide compelling evidence that more highly strained regions preferentially undergo melting. Geological systems are far more complex, however, because they are multicomponent systems. In metamorphic petrology, melting is commonly considered a reaction, where solid reactants +/- fluids react to form a liquid product +/- solid products. Multiple phases undergo eutectic melting, instead of a simple phase transformation. Although geological systems are far more complicated, the role of strain still needs to be considered in partial melting of rocks. In fact, in some rocks, there is a higher degree of anisotropy than in the systems considered by material science and metallurgy, and thus the role of strain could be enhanced in some grain-grain interactions.

5.4 GEOLOGIC SETTINGS

Samples for this study were taken from the three field areas described in Chapters 2-4: the Wet Mountains of central Colorado, the Llano Uplift of central Texas and the Albany-Fraser Belt of southwestern Australia. A more in depth field description is given for each of these locations in Chapters 2-4. Each field location has different lithologies, and these compositional differences affect the types of partial melting reactions occurring in each rock. Understanding the reactions that have occurred in each location is fundamental for understanding where melting occurred within the rock. Melting reactions in the Wet Mountains were dominantly biotite-dehydration and granite wet melting reactions, with rare muscovite-dehydration melting. Rocks have a range of compositions, but granitic and metapelitic gneisses are the lithologies that provide the best evidence for partial melting. Granitic gneisses of the Lost Creek Gneiss of the western Llano Uplift experienced granite wet melting. In the Albany-Fraser Belt, melt was produced primarily through fluid-saturated and -undersaturated biotite- and amphibole-dehydration melting. The most common rock types are quartz monzonitic, quartz dioritic, granodioritic and tonalitic orthogneisses. Despite differences in lithologies and melting reactions in these three diverse locations, thin sections from each location preserve textures attributed to the former presence of melt.

5.5 MICROSTRUCTURES AND PETROGRAPHY

The presence of former melt in thin section is typically inferred from textural relationships between reactant minerals and characteristic shapes and spatial locations of former melt. In areas that have undergone granitic wet melting, the presence of small blebs of material along unlike grain boundaries, serrate and cuspate grain boundaries with low dihedral angles between former melt and adjacent minerals, and the string-of-beads texture, with small blebs of former melt of different compositions along grain boundaries, are all characteristic of melt pseudomorphs (Harte et al., 1991; Sawyer, 1999; Rosenberg and Riller, 2000; Sawyer, 2001; Holness and Isherwood, 2003; Holness and Sawyer, 2008). Rocks that have undergone dehydration melting will typically display corroded and skeletal reactant minerals, commonly associated with films of former melt adjacent

to these grains, and peritectic products of melting, typically with euhedral crystal faces, surrounded by an envelope of material that represents former melt (Sawyer, 1999; Sawyer, 2001; Waters, 2001; Barbey, 2007; Holness and Sawyer, 2008).

Subgrain boundaries can be identified in thin section, under crossed-polars, by a sharp change in extinction across a boundary that is not a fracture within a larger grain. In plane-polarized light, the subgrain boundary is not visible. Fractures are visible in both crossed-polars and plane light, however, and a change in extinction may be observed. Changes in extinction in crossed polarized light that are associated with fluid inclusions in plane-polarized light, likely represent healed fractures and not subgrain boundaries.

Previous workers have not described the presence of melt pseudomorphs along subgrain boundaries. However, I have observed blebs of material along subgrain boundaries that have a similar morphology and texture to melt pseudomorphs along grain boundaries with serrate/cuspate grain boundaries and low solid-solid dihedral angles, which I infer to be former melt. Additionally, this material inferred to be former melt along subgrain boundaries commonly maintains a physical connection with similar material along grain boundaries. Consequently, I propose that in addition to previously described melt microstructures, the presence of blebs of material along subgrain boundaries, having a different composition than the host mineral, and low solid-solid and solid-melt dihedral angles, be considered as a new melt microstructure.

5.5.1 Wet Mountains, central Colorado

Samples from the Wet Mountains provide evidence for syndeformational partial melting, resulting in the deformation of and formation of former melt preferentially in deformed locations. Melt pseudomorphs are interpreted in these rocks based on serrate and cuspate grain boundaries with low dihedral angles between inferred former melt and adjacent minerals, thin films of inferred melt pseudomorphs along unlike grain boundaries, and skeletal or corroded reactant minerals (Harte et al., 1991; Sawyer, 1999; Rosenberg and Riller, 2000; Holness and Sawyer, 2008). Morphological and textural

similarities between inferred former melt on grain boundaries and subgrain boundaries, suggests thin films of material along subgrain boundaries, are also melt pseudomorphs. Former melt preserved along subgrain boundaries is found primarily in quartz with only several examples of former melt within plagioclase grains.

Most melt pseudomorphs from the Wet Mountains are now comprised of K-feldspar; in some locations this K-feldspar is rimmed by plagioclase. However, all of the melt pseudomorphs preserved along subgrain boundaries in quartz and plagioclase is K-feldspar, which is also locally rimmed by plagioclase. These melt pseudomorphs are preserved as K-feldspar because the quartz component of the melt crystallized onto pre-existing quartz grains and the plagioclase component either crystallized onto pre-existing plagioclase grains or is present as the plagioclase rimming the K-feldspar (Harte et al., 1991; Rosenberg and Riller, 2000; Holness and Sawyer, 2008). Metapelitic rocks do not contain significant amounts of plagioclase, and consequently none of the plagioclase grains contain former melt on their subgrain boundaries. Granitic gneisses preserve melt pseudomorphs along subgrain boundaries in quartz and plagioclase in relatively equal amounts. However, many more melt pseudomorphs are present along grain boundaries than subgrain boundaries; the amount of former melt located along subgrain boundaries is likely less than 5% of the total amount of former melt in these rocks.

Former melt along subgrain boundaries in quartz grains from metapelitic rocks extend partway to all the way along the subgrain boundary (Figure 5.2A-C). The blebs of former melt are either pointed or rounded at the tip with an overall cuspate shape and have variable thickness, from 20-200 μm along their lengths (Figure 5.2A-C). Along some subgrain boundaries, the blebs of former melt may be discontinuous, but still share the same optic orientation, suggesting they are connected in the third dimension (Figure 5.2B). Grains of sillimanite are present within some of the melt pseudomorphs found along subgrain boundaries (Figure 5.2B), and are interpreted to have coarsened in the presence of melt due to enhanced diffusion. The photomicrograph in Figure 5.2C is an example where melting is interpreted to have occurred all the way along the subgrain boundary, resulting in two separate quartz grains with former melt along their boundary.

The low angle grain boundary seen today is inferred to represent a former subgrain boundary that formed because of partial melting across this boundary.

Most of the examples of former melt along subgrain boundaries from the metapelites are laterally continuous with melt pseudomorphs present along the grain boundaries (Figure 5.2B, C). This continuity provides strong evidence that the material present along the subgrain boundaries is indeed former melt. In Figure 5.2A the former melt is not continuous with inferred former melt along grain boundaries, but it is in the same optic orientation, as evidenced by the same blue color of the K-feldspar throughout the photomicrograph, suggesting a connection in the third dimension. The melt pseudomorphs along subgrain and grain boundaries have similar morphologies. Both have variations in width along the length of the former melt, ranging from 20-200 μm in width, with several examples of discontinuous blebs of material, and they both have rounded or pointed tips. They are compositionally the same, composed of K-feldspar +/- a rim of plagioclase and there are examples of both types of former melt along subgrain and grain boundaries that contain sillimanite inclusions.

Former melt along subgrain boundaries in quartz from granitic gneisses has a different morphology (Figure 5.2D). In these rocks, melt pseudomorphs along subgrain boundaries are much thinner, not more than 10-30 μm in width, only extend a short distance into the quartz grain and have only minor variations in thickness along their width (Figure 5.2D). Within these rocks the former melt along subgrain boundaries may or may not be laterally continuous with melt pseudomorphs along grain boundaries. Former melt preserved along subgrain boundaries in plagioclase is morphologically similar to former melt along subgrain boundaries in quartz from the granitic gneisses. Within plagioclase grains the former melt does not extend very far into the crystal, it may be discontinuous and it is very thin, commonly less than 10 μm in width (Figure 5.2E). This former melt is interconnected and optically continuous with former melt along the grain boundary and has an angular morphology with pointed tips (Figure 5.2E).

In granitic gneisses, the former melt on grain boundaries is morphologically similar to melt pseudomorphs along subgrain boundaries in both quartz and plagioclase.

Melt pseudomorphs along grain boundaries in granitic gneisses are not typically more than 50 μm in width and have very little variation in thickness along their length. Additionally, no laterally continuous, several centimeter long melt pseudomorphs (inferred melt channelways) are preserved in the granitic gneisses as they are in the metapelitic rocks (see Chapter 3). Former melt along grain boundaries is less abundant than in metapelitic rocks. This difference is consistent with less abundant melt pseudomorphs along subgrain boundaries in these samples. Granitic gneisses may contain fewer melt pseudomorphs because the minerals present in these samples: quartz, plagioclase, and K-feldspar, acted as nucleation sites for the melt present in the sample, upon crystallization. Because there were already abundant quartz, plagioclase and K-feldspar grains, melt would have preferentially crystallized onto these pre-existing grains and fewer melt pseudomorphs would form along grain boundaries, or subgrain boundaries.

5.5.2 Lost Creek Gneiss, Llano Uplift, central Texas

Samples from the Lost Creek Gneiss provide evidence for partial melting during very latest deformation, and melting likely continued after deformation had ceased. Melt pseudomorphs are interpreted in these rocks based on the abundance of serrate/cuspate grain boundaries and films of interpreted former melt between unlike phases on grain boundaries (Harte et al., 1991; Sawyer, 1999; Rosenberg and Riller, 2000; Holness and Sawyer, 2008). Within these rocks melt pseudomorphs preserved on subgrain boundaries in both quartz and plagioclase (Figure 5.3) are interpreted based on their textural similarities and lateral continuity with melt pseudomorphs on grain boundaries. Most of the former melt in Lost Creek Gneiss samples is now preserved as K-feldspar, and this phase is generally seen along subgrain boundaries in quartz and plagioclase, even within the same thin section. Former melt is not preferentially found in one mineral versus the other; equal abundances of former melt occur along subgrain boundaries in both minerals.

Many of the coarse quartz grains display chessboard extinction, and blebs of K-feldspar are located along one specific subgrain orientation, either the *a*- or *c*-axis, within quartz grains (Figure 5.3A, B). In a few cases, former melt follows both orientations, and the melt pseudomorph forms a diamond shape with curved boundaries and cuspate morphologies (Figure 5.3A). Former melt is not found along the entire length of the subgrain and commonly is seen along the part of the subgrain that intersects the grain boundary, which may also contain former melt (Figure 5.3A, B). Former melt may only be present at the intersection of the grain and subgrain boundary because melting may not have occurred along the entire length of the subgrain. Melt pseudomorphs within quartz are as wide as 100 μm across and extend along the subgrain boundary for up to 1 mm (Figure 5.3A, B). These films of former melt typically end in a point and are cuspate-shaped (Figure 5.3A), but rare examples show a less angular shape and a rounded tip (Figure 5.3B).

Plagioclase grains typically have melt pseudomorphs along several parallel subgrain boundaries (Figure 5.3C, D) or along subgrain boundaries in multiple orientations within the same grain (Figure 5.3E), locally outlining most of the subgrain (Figure 5.3D). In many cases melt pseudomorphs are seen as discontinuous blebs of former melt along an individual subgrain boundary (Figure 5.3C, D). These blebs of former melt are 10-30 μm in width and are 100-200 μm in length; they display only minor variations in thickness along the length of the melt pseudomorph. Many of these melt pseudomorphs have rounded or square tips (Figure 5.3C, D), although rare blebs do have pointed tips (Figure 5.3E). Within plagioclase grains it is usually difficult to determine the composition of the melt pseudomorph because the blebs of former melt are so fine-grained.

The other melt microstructures within the Lost Creek Gneiss rocks, not located on subgrain boundaries, are morphologically similar to the former melt found along subgrain boundaries in these same samples. Melt pseudomorphs along grain boundaries are 10-100 μm in width and may only extend for several hundred μm; this material may not wet the entire grain boundary between two minerals. At triple or quadruple junctions there are

commonly larger pools of former melt that may extend for up to 500 μm in width, and these have cuspate edges. The former melt along grain boundaries has pointed, rounded and square-shaped tips, all of the morphologies seen in the former melt along subgrain boundaries.

5.5.3 Albany Fraser Orogen, southwestern Australia

Rocks of the Albany-Fraser Orogen provide evidence for partial melting during deformation with leucocratic material associated with all structures, including foliations, fold hinges, necks of boudins, shear bands, and melt channels. Melt pseudomorphs are interpreted on the basis of their serrate/cuspate shape, presence along grain boundaries between unlike phases and in areas where skeletal or corroded grains of biotite or amphibole are present (Harte et al., 1991; Sawyer, 1999, Rosenberg and Riller, 2000; Holness and Sawyer, 2008). In these rocks, melt pseudomorphs are preserved as quartz, plagioclase or K-feldspar, but most commonly as either quartz or K-feldspar. Former melt is typically found as the phase that is least abundant of the quartzofeldspathic phases, in terms of modal mineralogy (Harte et al., 1991; Rosenberg and Riller, 2000). Because the rocks are fairly plagioclase-rich, the other two phases make up the majority of the melt pseudomorphs. In these plagioclase-rich rocks the plagioclase component of the melt preferentially nucleated and crystallized onto pre-existing plagioclase grains. The remaining quartz and K-feldspar components of the melt could crystallize onto any pre-existing grains of quartz or K-feldspar, but because these two minerals were not abundant, the remaining melt preferentially formed quartz or K-feldspar melt pseudomorphs. Former melt is found in roughly equal proportions along subgrain boundaries in both plagioclase and quartz.

Former melt preserved along subgrain boundaries in both plagioclase and quartz grains, is typically found at the edges of the grains, with former melt only along small segments of subgrain boundaries (Figure 5.4A-D). Melt pseudomorphs in both quartz and plagioclase are very thin, not more than 20-30 μm in width (Figure 5.4A-D). These melt pseudomorphs along subgrain boundaries are commonly optically and laterally

continuous former melt on grain boundaries (Figure 5.4A-D). Melt pseudomorphs typically have pointed or square tips, a cuspate shape and have almost no lateral variations changes in thickness.

Most of the former melt in samples from the Albany-Fraser Belt is found along grain boundaries and it has the same thin (20-60 μm in width) morphology as that seen along subgrain boundaries. Melt pseudomorphs along grain boundaries usually have pointed tips, minor lateral changes in thickness and do not form larger pools at triple junctions. Pseudomorphs of melt along subgrain boundaries are fairly rare in these rocks; the other two locations have many more examples of former melt along subgrain boundaries.

5.5.4 Summary of Observations and Comparison of the Areas

Rocks from three different field areas have experienced partial melting, via a variety of different reactions. All preserve former melt along subgrain boundaries in plagioclase and quartz. The lengths and widths of former melt along subgrain boundaries vary by location and the type of mineral containing the melt pseudomorph. None of the samples have former melt present along subgrain boundaries in K-feldspar and there are likely two main reasons. First of all, K-feldspar is less abundant than both quartz and plagioclase in all of the rocks. As a result, the melt will not be able to crystallize and nucleate onto as many pre-existing grains of K-feldspar as quartz or plagioclase grains. Melt pseudomorphs will therefore be more likely to be composed of K-feldspar, rather than the other minerals that made up a larger volume percent of the original rock. Secondly, in these particular samples, very few grains of K-feldspar containing subgrains were identified.

The Albany-Fraser Belt samples and samples from the Wet Mountains with plagioclase grains hosting the former melt contain less abundant, thinner and shorter melt pseudomorphs along subgrain boundaries, than the other samples. Melt pseudomorphs are present only at the edges of mineral grains where subgrains and grain boundaries intersect and in these locations they are very thin and only extend for short distances.

Melt pseudomorphs along subgrain boundaries in both plagioclase and quartz from the Lost Creek Gneiss are 10-100 μm thick, discontinuous within some samples, and extend for 500-1000 μm, with some lateral variations in width. Samples from metapelitic rocks of the Wet Mountains provide abundant evidence for melting along subgrain boundaries, with several examples of melting nearly or all the way across a quartz grain, and development of new grains separated by a narrow channel of former melt. Within these samples, the melt pseudomorphs along subgrain boundaries have greater widths and lengths than seen in any of the other rock types.

5.6 DISCUSSION

The presence of former melt along subgrain boundaries in quartz and plagioclase in rocks from three diverse field locations indicates partial melting along subgrain boundaries is common in migmatitic terranes. These three field locations were each chosen to investigate the role of strain in preferentially inducing melting on the scale of centimeters to kilometers, as well as on the microscopic scale, and all samples display melt pseudomorphs on subgrain boundaries. The presence of former melt along subgrain boundaries has not been previously documented, but its presence indicates a link between the partial melting process and internal plastic strain.

In migmatitic terranes, the presence of leucosome material along foliation surfaces, axial planes of folds, in the necks of boudins and shear zones has typically been interpreted as exploitation of pre-existing structures as melt conduits (Sawyer, 1994; Brown, 1994). This melt migration is generally attributed to stress or pressure gradients (Robin, 1979; Stevenson, 1989; Cooper, 1990; Sawyer, 1994; Collins and Sawyer, 1996; Marchildon and Brown, 2001; Mancktelow, 2002), buoyancy flow driven by gravity (McKenzie, 1984; Wolf and Wyllie, 1991), and volume change associated with melting reactions (Wickham, 1987; Beckerman and Viskanta, 1988; Davidson et al., 1994; Brown et al., 1995).

In the case of former melt found along subgrain boundaries, it is highly unlikely that melt could exploit these boundaries only as a conduit. Subgrain boundaries are

planar arrangements of dislocations within a crystal lattice; atoms are still bonded across these boundaries. Diffusion of atoms or ions along subgrain boundaries can occur preferentially in areas of high dislocation density, commonly referred to as pipe diffusion (Smoluchowski, 1952; Luther, 1965; Yurimoto and Nagasawa, 1989). Melt, however, cannot migrate along the subgrain boundaries without disruption of the lattice through actual melting along this boundary. If the host grain was not being progressively melted, there would be a space problem. If volume changes associated with melting reactions caused fracturing, it is possible that fractures would nucleate on pre-existing subgrain boundaries. In this case melt possibly could migrate into these composite subgrain boundaries/fractures. However, all of the subgrain boundaries that contain former melt were also viewed in plane polarized light to make sure that they were truly subgrain boundaries and not fracture surfaces. None of these surfaces are fractures or even annealed fractures; subgrain boundaries are not coincident with fluid inclusion planes. The presence of former melt on subgrain boundaries therefore cannot be interpreted to be a result of differential stress causing the melt to migrate with subsequent destruction of the microstructure. To preserve melt along these subgrain boundaries, the host mineral must have been melted.

All of the melting reactions that occurred in these rocks require multiple reactants to produce melt +/- a peritectic phase. For the reactions to occur, all of these reactants must be present, and in close enough proximity to each other to allow the reaction to proceed. Therefore, melting along the subgrain boundary does not occur in isolation from the rest of the system. Melting of the host grain must occur synchronously with melting in the rest of the rock, most likely along the adjacent grain boundary. This requirement explains two observations from these rocks: 1) melt pseudomorphs along subgrain boundaries are optically and laterally continuous with former melt along adjacent grain boundaries, and 2) the compositions of the former melt and the host grain differ. Former melt crystallizes as a monomineralic film, with the single phase equivalent to the least abundant phase in a sample. Melt pseudomorphs along subgrains are connected with former melt along grain boundaries, and the composition of these melt

pseudomorphs along subgrain boundaries is also the modally least abundant phase of the quartzofeldspathic minerals. The latter is a result of the other components of the melt nucleating and crystallizing onto the modally more abundant minerals (Harte et al., 1991; Rosenberg and Riller, 2000; Holness and Sawyer, 2008). In fact, if a host quartz grain melted along subgrain boundaries in isolation from the rest of the rock, the composition of the melt would have to be the same as the host. Thus the former melt would not be optically distinguishable from the host mineral, unless impurities were present or accumulated at the subgrain boundary.

The observation that former melt along subgrain boundaries is commonly laterally continuous with former melt along grain boundaries, and that it has a different composition than the host mineral, provides additional support for the interpretation that the material on the subgrain boundaries is indeed a melt pseudomorph. Previously, I described their textural and morphological similarity to other melt microstructures, such as former melt on grain boundaries and serrate or cuspate grain boundaries; these have been interpreted to represent melt pseudomorphs (Harte et al., 1991; Sawyer, 1999, Rosenberg and Riller, 2000; Sawyer, 2001; Holness and Sawyer, 2008). All of these criteria combined together provide strong support for subgrain boundaries in quartz and plagioclase being preferentially consumed in partial melting reactions because they are more highly strained locations. Melting preferentially of these highly strained minerals is a local phenomenon; the overall degree of strain in an outcrop or hand sample is unlikely to affect the degree of melting along a subgrain boundary. Only the presence or absence of a subgrain boundary and the dislocation density of that subgrain boundary is likely to affect whether melting occurs.

5.6.1 Mechanisms of Strain-Induced Melting

The evidence I have presented that documents partial melting has occurred preferentially along subgrain boundaries indicates that melting is somehow related to higher strains along subgrain boundaries. There are three possible ways that strain could contribute to preferential melting in such high-strain locations: 1) the activation energy

required for partial melting is lower because of a contribution from stored strain energy (Hand and Dirks, 1992); 2) less energy is needed to melt in this location because of an increased abundance of weakened bonds along the subgrain boundary; and 3) enhanced diffusion rates along the subgrain boundary occur because of pipe diffusion or interstitial hydrogen or hydroxyl groups preferentially located at dislocations (Smoluchowski, 1952; Luther, 1965; McLaren et al., 1983; Yurimoto and Nagasawa, 1989; Kronenberg et al., 1986, 1990). The first two cases are similar because both assume the partial melting reaction occurs preferentially in more highly-strained locations because less energy is needed.

As mentioned in the introduction, the contribution from stored strain energy within the mineral lattice, relative to the free energy of reactants, is small (Green, 1972; Wintsch and Dunning, 1985). This small difference has led to the suggestion that stored strain energy does not contribute in a geochemically relevant way to metamorphic reactions (Wintsch and Dunning, 1985). However, if we consider a subgrain boundary in quartz that has a dislocation density of 10^{11} cm^{-2}, the contribution to the free energy of quartz will be approximately 0.1-0.6 kJ/mol (Wintsch and Dunning, 1985; Liu et al., 1995). An order of magnitude increase in density of dislocations will also contribute an order of magnitude increase in energy, with estimates of 2.9-4.2 kJ/mol (Green, 1972; Wintsch and Dunning, 1985). Typical activation energies for diffusion in hydrous melts have been estimated at approximately 150-300 kJ/mol (Rubie and Brearley, 1990). Although activation energies for diffusion in melts are not the same as activation energies for a partial melting reaction, they may be approximately the same magnitude. It is clear that the energy differences between stored strain energy and activation energy for diffusion is a difference of four orders of magnitude, three if dislocation densities of 10^{12} cm^{-2} are considered. Although there is in fact a minor contribution from the stored strain energy, the additional energetic contribution is unlikely to significantly affect reaction rates of partial melting along subgrain boundaries on its own.

Dislocations are areas where the crystal lattice is distorted and planes or half-planes of atoms are missing or added or the lattice is twisted along screw dislocations.

As a result there are large numbers of stretched and weakened bonds. Areas of high dislocation density are therefore likely to have higher numbers of weakened bonds than the rest of a mineral's crystal lattice. The melting process involves the weakening of bonds and disruption of the crystal lattice, and consequently, it would require less additional thermal input to weaken the bonds in deformed areas that already have high numbers of weak bonds. How much contribution this mechanism would have in causing partial melting is difficult to quantify, but most likely is similar in magnitude to the former, in that they both rely on needing less activation energy for reaction.

Both of the above mechanisms are viable explanations for single component systems where melting is fundamentally a phase transformation, such as those studied in the material and physical sciences literature described in the introduction. But in a multicomponent system for eutectic melting to occur, it is necessary for there to be communication between the phases undergoing melting and transport of the reactants from non-adjacent sites. Thus the presence of former melt along subgrain boundaries requires that diffusion along subgrain boundaries has occurred.

Enhanced rates of diffusion in highly strained locations have been proposed as a result of either pipe diffusion along dislocation cores, increased diffusion along planar dislocations, such as subgrain boundaries (Smoluchowski, 1952; Luther, 1965; Yurimoto and Nagasawa, 1989), or increased concentrations of water associated with dislocations (Green and Radcliffe, 1975; McLaren et al., 1983; Kronenberg et al., 1986, 1990). All of these could lead to rapid transport of reactants along subgrain boundaries, allowing and enhancing melting along subgrain boundaries, which also are energetically susceptible to melting.

Images of dislocations within grains of quartz, taken in the TEM, show water bubbles present at the ends of dislocations and strings of water bubbles present along subgrain and grain boundaries (McLaren et al., 1983). These water bubbles have been interpreted to form initially as interstitial H^+ defects and as heating occurred they have coalesced into bubbles (McLaren et al., 1983). Although the amount of water present along subgrain boundaries is probably small, it should enhance diffusion and could be a

minor source of some of the water needed for the partial melting reaction to occur. Experimental studies on water content in quartz indicate a range of water quantities of 20-600 ppm by weight, with more deformed samples containing higher water contents (Kronenberg and Wolf, 1990; Stipp et al., 2006; Gleason et al., 2008). This amount is not enough water to allow the partial melting reaction to occur, as several weight percent is required (Tuttle and Bowen, 1958; Luth et al., 1964), but it could provide a small amount. The rest of the water needed for the reaction to occur would likely be contributed via the grain boundaries. Viewing these samples under the TEM could verify whether there is water associated with dislocations along these subgrains.

Thus, preferential melting along subgrain boundaries in quartz and plagioclase can be explained in two ways. Pipe diffusion along subgrains would lead to more material, in the form of ions, being brought into the subgrain boundary and melting would then proceed preferentially in these locations. The presence of water associated with dislocations in a subgrain boundary could contribute water to the melting reaction or enhance reaction rates, also allowing melting preferentially along subgrain boundaries.

Strain can contribute to partial melting along subgrain boundaries in all the ways described above, however, the last: enhanced diffusion rates and water associated with dislocations, is likely to have the most significant effect. Even though the contribution from stored strain energy is quite small, it is likely to provide a small input and should not be dismissed entirely as one of the potential effects of strain on melting and metamorphic reaction. Further experimental work is needed to provide better quantitative constraints on the potential contributions of weakened bonds and enhanced diffusion rates.

Enhanced diffusion rates in more strained areas have been proposed to explain greater extent of reaction in highly deformed regions. This relationship could be related to recrystallization and the subsequent finer grain size, which increases the number of diffusion pathways as well as the amount of surface area on which the reaction can occur (White, 1975; Wintsch, 1975; Kerrich et al., 1977; Brodie and Rutter, 1985; Yund and Tullis, 1991). Subgrains subdivide larger grains. Their presence also increases the

number of diffusion pathways within the crystal, which enhances diffusion, and thereby melt reactions, and the amount of crystal lattice (i.e. subgrain boundaries) that is in contact with the needed reactants, and is energetically susceptible to melting. These factors together can lead to enhanced melting in deformed areas.

5.6.2 Initiation of Melting Along Subgrain Boundaries

The process of melting along subgrain boundaries likely begins with partial melting along triple junctions of reactant grains. For purposes of simplification, I will consider the partial melting process in a granitic gneiss, where melting occurs via the reaction,

$$\text{Quartz} + \text{Plagioclase} + \text{K-feldspar} + H_2O = \text{Melt}.$$

This process of partial melting along subgrain boundaries is illustrated in a schematic diagram (Figure 5.5). The purpose of Figure 5.5 is to illustrate the timing of melting along subgrain boundaries relative to melting along grain boundaries and triple junctions and as a point of comparison for the actual photomicrographs from the three different field areas.

Figure 5.5A is a schematic diagram of a photomicrograph, in crossed polars, of deformed granitic gneiss with elongate quartz and feldspar grains defining a foliation. On the middle left side of Figure 5.5A, an elongate grain of quartz has a change in extinction along its length; these extinction changes represent subgrains. In Figure 5.5A, the outline of a triple junction is highlighted, where plagioclase, K-feldspar and deformed quartz (+ H_2O) are present. Experimental studies of partial melting have shown that triple junctions are the locations where melting typically occurs first, because the reactant grains are in contact (Mehnert et al., 1973). Melting will occur along many triple junctions in a rock as the melting temperature is reached, but for the purposes of this diagram, the process of melting will only be considered at one location. Figure 5.5B is the area shown within the box in Figure 5.5A, and is an enlarged view of the triple junction between K-feldspar, plagioclase and deformed quartz.

The rest of Figure 5.5 represents progressive time steps with an increase in the degree of partial melting, until Figure 5.5F, which represents crystallization. In Figure 5.5C melting has begun at the triple junction and along the subgrain boundary, and the melt/solid interfaces have a cuspate shape because the minerals are melting and their boundaries are becoming rounded (Mehnert et al., 1973). The more highly strained quartz present along the subgrain boundary is the source of quartz for this partial melting reaction (Figure 5.5C). Figure 5.5C can be compared with photomicrographs from the Wet Mountains and the Albany-Fraser Belt, where melting along the subgrain boundary has only occurred at the edge of the grain (Figure 5.2E, and 5.4).

Continued melting leads to wetting of additional grain boundaries, progressive melting of reactant minerals, and continued melting along the subgrain boundary and other parallel subgrain boundaries within the deformed quartz (Figure 5.5D). Melting has progressed sufficiently to have melting all the way across the subgrain boundary, and Figure 5.5E illustrates two quartz grains separated by a thin film of melt. Figure 5.5E can be compared with Figure 5.2C, where two quartz grains that appear to have a slight difference in orientation are separated by a thin film of former melt. Figure 5.5F indicates preservation of this texture during crystallization, and former melt along subgrain boundaries is interconnected with former melt along the adjacent grain boundaries. The shaded areas on the edge of mineral grains are locations that have developed overgrowths due to nucleation and crystallization of the melt onto pre-existing grains. Melt pseudomorphs are preserved on grain boundaries and subgrain boundaries, as quartz and K-feldspar; the pseudomorphs are preserved as these minerals because they are the modally least abundant phases.

Figure 5.5 illustrates that the subgrain boundary is still connected, via the partial melt, to the other reactant phases that are melting, and consequently eutectic melting can still occur, with the deformed quartz grain and the K-feldspar and plagioclase grains all continuing to melt. Figures 5.5D and 5.5E show a number of the same features seen in Figures 5.2, 5.3, and 5.4; illustrating that samples from the Wet Mountains, Lost Creek Gneiss and Albany-Fraser Belt represent different degrees of partial melting along

subgrain boundaries, with some incipient textures and several examples of nearly or complete melting across a subgrain boundary.

5.7 CONCLUSIONS

Former melt is found along subgrain boundaries in quartz and plagioclase from three field locations: the Wet Mountains of central Colorado, the Lost Creek Gneiss of the Llano Uplift, central Texas and the Albany-Fraser Belt of southwestern Australia. The material found along subgrain boundaries is determined to be former melt on the basis of its textural and morphological similarity to former melt seen on grain boundaries and because it is commonly laterally and optically continuous with melt pseudomorphs on grain boundaries. Consequently, former melt located along subgrain boundaries, should be categorized as a new melt microstructure.

The presence of this former melt along subgrain boundaries indicates that partial melting occurred preferentially in high-strain locations. Melt pseudomorphs present along subgrain boundaries must have formed as a result of partial melting along subgrain boundaries; subgrain boundaries are not open conduits, so melt could not migrate into these locations without melting the host mineral. Three explanations for the role of strain in preferentially causing partial melting are, in decreasing order of importance: 1) enhanced diffusion rates along the subgrain boundary because of pipe diffusion or water bubbles located at dislocations, 2) an increased abundance of weakened bonds located within the subgrain boundary requiring less energy to weaken the remaining bonds, and 3) a lowering of the activation energy needed to cause reaction by contribution from stored strain energy. For multicomponent geologic materials, diffusion along the subgrain boundaries is needed to transport the reactants, and enhanced diffusion rates along subgrain boundaries will favor preferential melting. The contribution of the latter two mechanisms are likely very minor, and the primary reason that melting occurs along subgrain boundaries is because of enhanced diffusion rates and a potential input from water associated with dislocations. The role of lattice strain in enhancing partial melting in a deformed region is most likely a combination of enhanced diffusion rates and more

crystal lattice being in contact with the needed reactants for melting and energetically susceptible to melting.

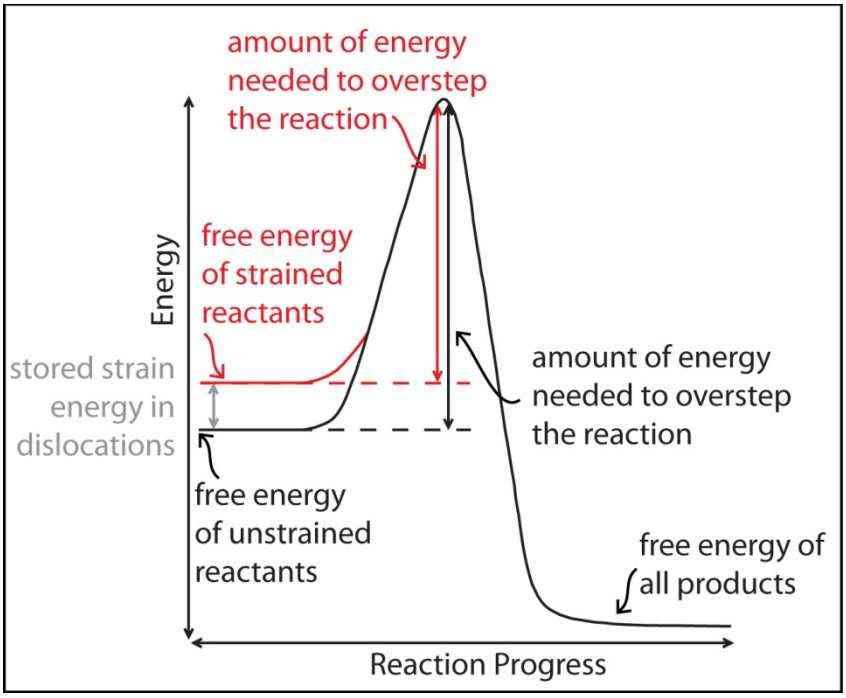

Figure 5.1. Graph of reaction progress versus energy illustrating the activation energy needed for a reaction to occur for strained and unstrained reactants (modified from Hand and Dirks, 1992). The free energy of unstrained reactants is lower than strained reactants and thus less energy is required to overstep the reaction for strained reactants.

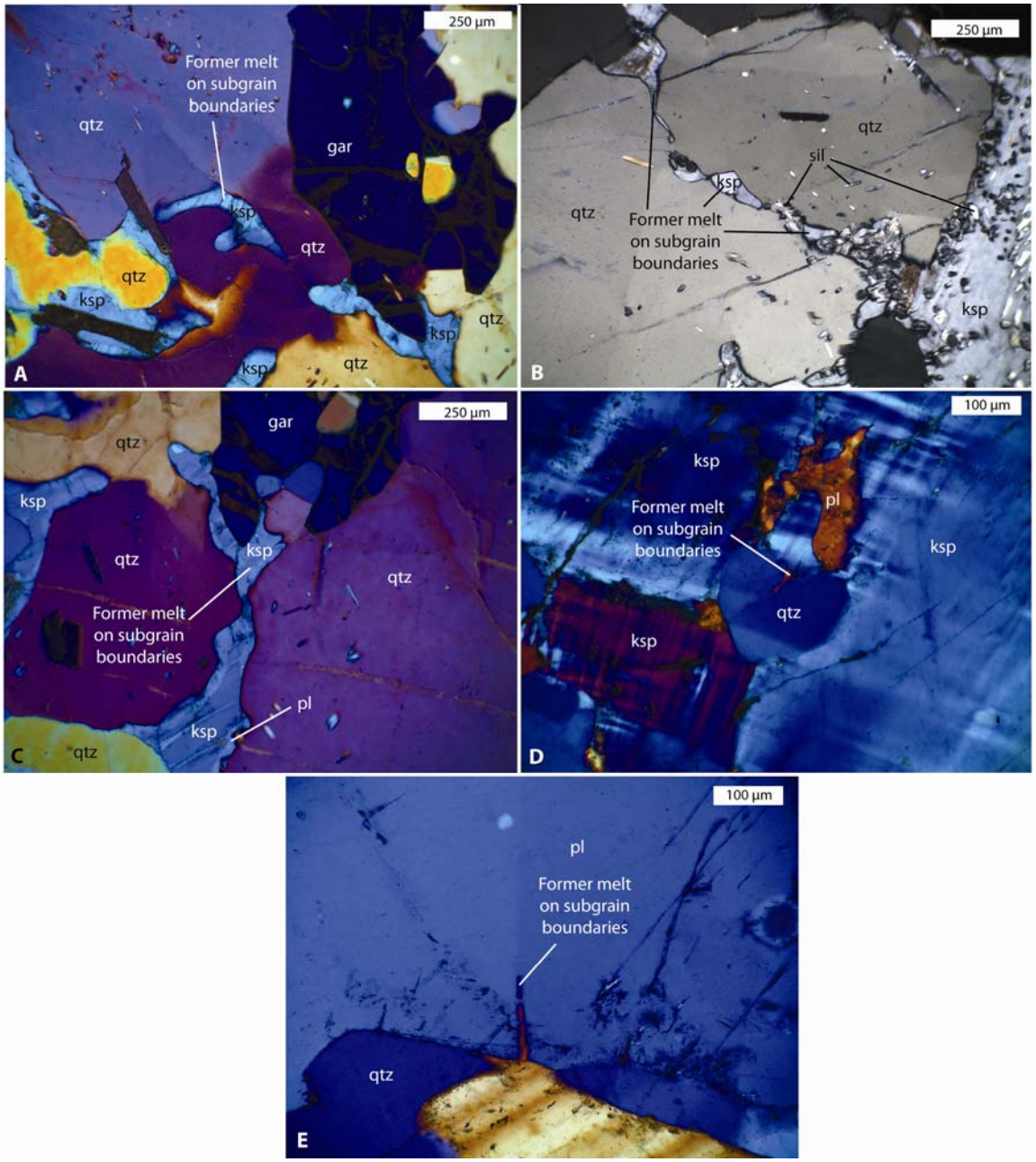

Figure 5.2. (continued on next page). Photomicrographs of former melt along subgrain boundaries in rocks from the Wet Mountains, central Colorado. (All images in crossed polars; all but B with gypsum plate.) A. Former melt, now K-feldspar (blue) formed through biotite-dehydration melting, along subgrain boundary in quartz (blue/purple). This former melt is not quite continuous with former melt along the grain boundary between quartz and biotite, but has the same optic orientation. Although there is a lack of visible continuity between former melt on the grain and subgrain boundary, it may be continuous in the third dimension. Former melt is up to 100 µm in width and has pointed

tips along the subgrain boundary. Some of the plagioclase component of the melt is found as a thin rim of material on the edge of the K-feldspar melt pseudomorph and the rest of it likely crystallized on plagioclase grains present in the third dimension of the rock (not visible in this image). B. Former melt, now K-feldspar, with inclusions of sillimanite, along subgrain boundary in quartz. Former melt is nearly continuous along the subgrain boundary and ranges from 10-75 μm in width. C. Former melt, now K-feldspar with plagioclase rims (blue) along a subgrain boundary in quartz. This melt pseudomorph extends all the way across the subgrain boundary, and there are now two grains of quartz separated by the former melt. D. Former melt (orange) along subgrain boundary in quartz (blue). Former melt is very thin, less than 10 μm in width, is only present at the interface between the grain and subgrain boundary and does not extend very far into the quartz crystal. E. Former melt, now K-feldspar (orange) along subgrain boundary in plagioclase (blue). This melt pseudomorph is only present at the edge of the subgrain boundary, is less than 10 μm in width, and is discontinuous.

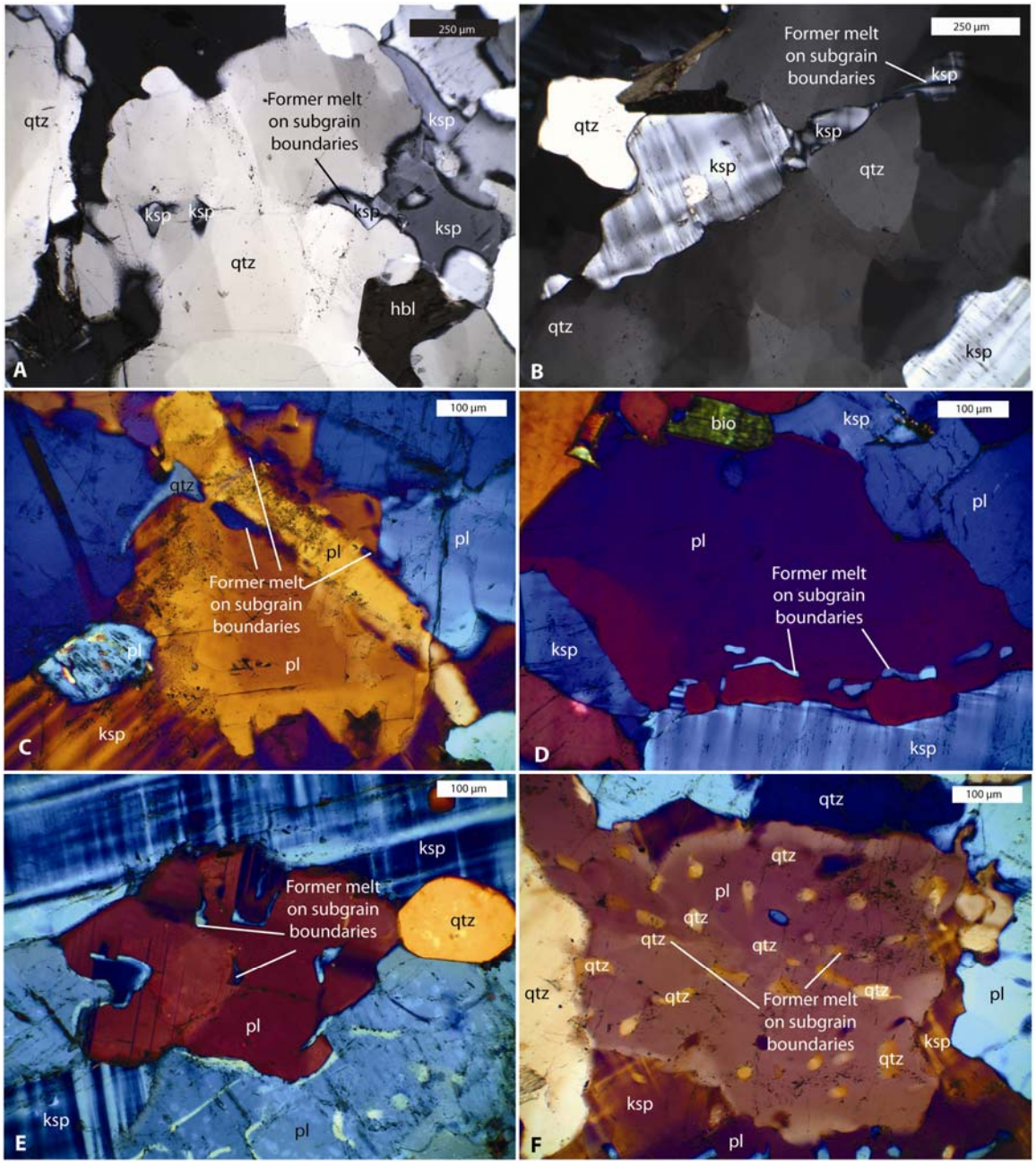

Figure 5.3. (continued on next page). Photomicrographs of former melt along subgrain boundaries in rocks from the Lost Creek Gneiss, of the Llano Uplift, central Texas. (All images taken in crossed polars; all but A & B with gypsum plate.) A. Former melt, now K-feldspar (gray), on subgrain boundaries in quartz. Former melt is found along the edge of the subgrain boundary near the grain boundary, and there are also isolated blebs of former melt within the interior of the quartz grain along the subgrain boundary. All of the former melt has a cuspate shape and is 50-75 µm in width. B. Former melt, now K-feldspar (displays microcline twinning), along subgrain boundary in quartz. Former melt

is connected to a larger melt pseudomorph along the grain boundary. The former melt along the subgrain boundary has a rounded tip and variable thickness, up to 100 μm, along its length. C. Former melt (blue), now quartz, along subgrain boundary in plagioclase (orange). This melt pseudomorph is mostly discontinuous and is seen as blebs along two parallel subgrain boundaries. These blebs have rounded tips and are 10-30 μm in width. D. Former melt (blue), now K-feldspar, along subgrain boundaries in plagioclase (purple). This melt pseudomorph is discontinuous, with rounded tips and is less than 20 μm in width. E. Melt pseudomorph (blue), now quartz, along subgrain boundaries in plagioclase (pink). Former melt forms discontinuous blebs, is 10-20 μm in width, and is found primarily in the interior of the grain.

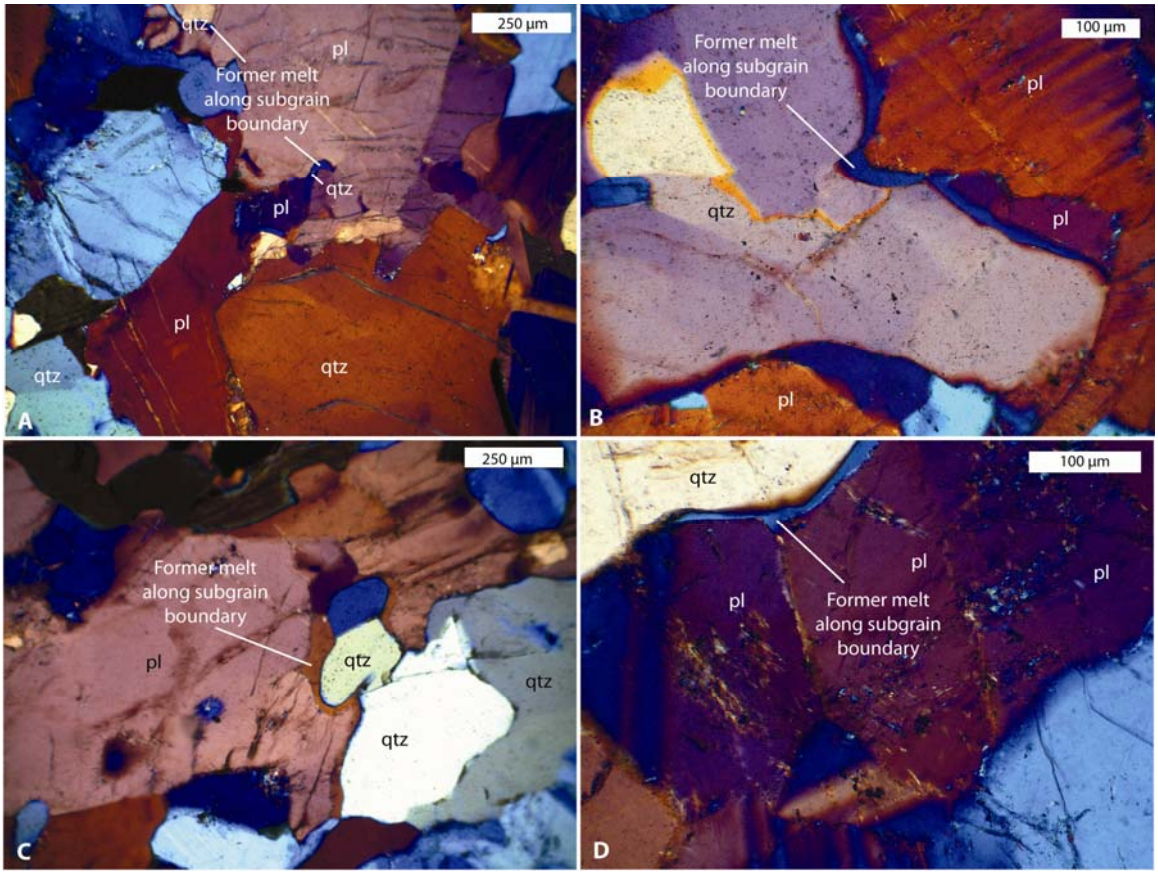

Figure 5.4. Photomicrographs of melt pseudomorphs along subgrain boundaries in rocks from the Albany-Fraser Belt, southwestern Australia. All photomicrographs are in crossed polars with the gypsum plate inserted. A. Plagioclase grain shown in pink, in the top center of the image, with a subgrain boundary that can be seen in darker purple, at bottom of plagioclase grain. Along the subgrain boundary is former melt, likely quartz, blue in color. At the top of the image is another subgrain boundary in the same plagioclase grain, also with former melt, now quartz, along the boundary. Both of these melt pseudomorphs are quite thin, only 20-30 µm in width, and are also present at the edge of the plagioclase grains, on the plagioclase-quartz boundary. B. Former melt (blue), now K-feldspar, along a grain boundary between quartz and plagioclase. This former melt extends a very slight distance into the quartz grain along a subgrain boundary, and is very thin, only 30 µm in width. C. A melt pseudomorph, seen in orange in the center of the image, with a cuspate shape against a subgrain boundary in plagioclase (pink). This former melt is now comprised of K-feldspar and is laterally continuous with former melt along the grain boundary between quartz and plagioclase. D. Former melt (blue), along a grain boundary between plagioclase and quartz. This melt pseudomorph is now K-feldspar, is 10 µm in width, and is also present along the subgrain boundary in plagioclase.

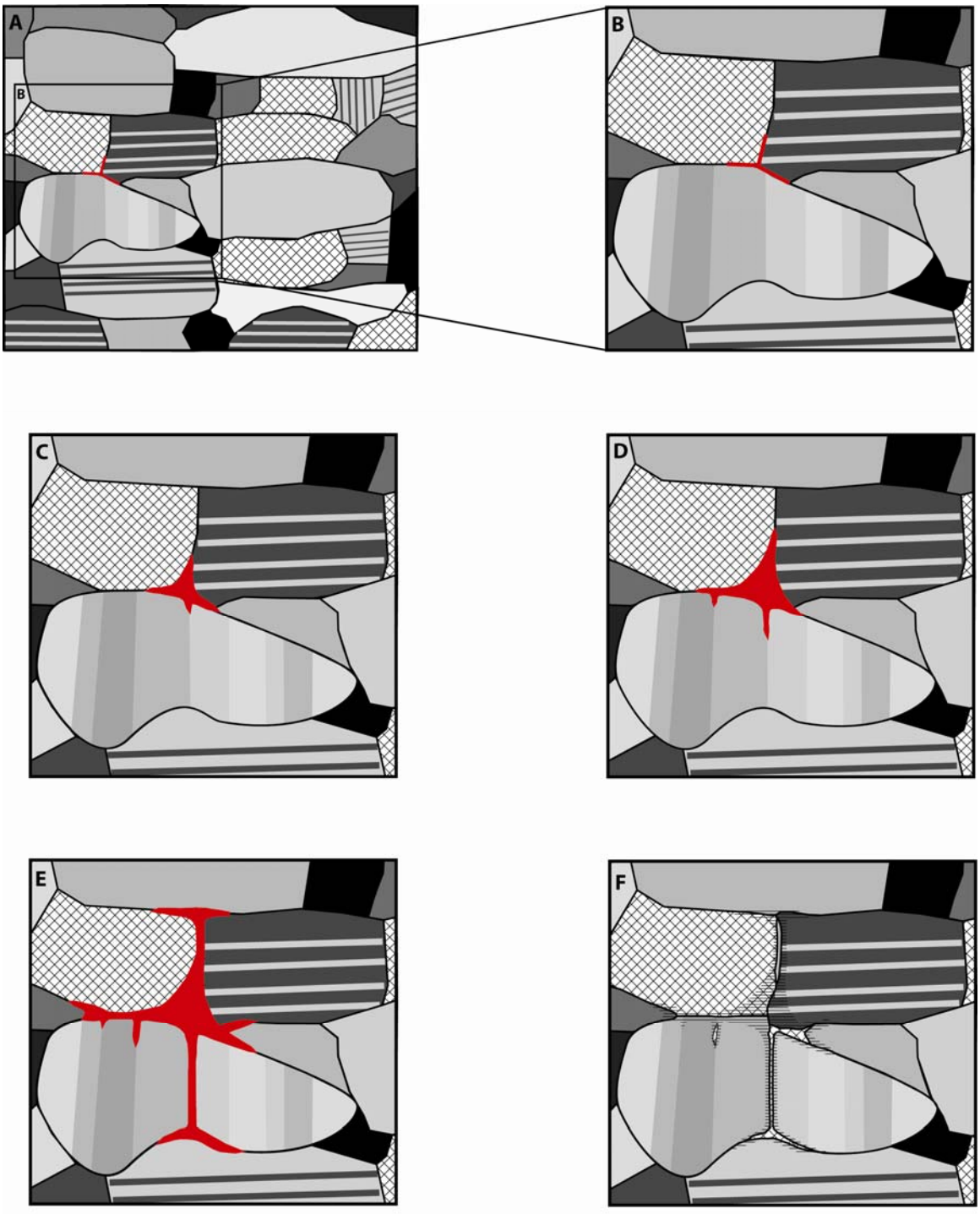

Figure 5.5. (continued on next page). Schematic diagram of a photomicrograph in crossed-polars, illustrating the model for partial melting along subgrain boundaries. Each image C-E represents a successive time-step in the partial melting process. A. Deformed granitic gneiss with elongate quartz and feldspars, defining a foliation. Cross-hatched

pattern represents microcline, grains with parallel lines represent albite twinned plagioclase and solid grains represent different optic orientations of quartz grains. The central left elongate quartz grain with the vertical bands of shading, represents a grain of quartz with subgrains. The box in A is the area shown in B and all subsequent diagrams. B. A triple junction between deformed quartz, plagioclase and K-feldspar where melting could begin at sufficiently high temperature and pressure. C. Partial melting (melt shown in red) has begun at this triple junction and reactant grains start to form rounded edges as a result of melting of the grains. Melting in quartz has preferentially begun along the subgrain boundary, the most highly strained part of the grain. D. Partial melting has progressed along the triple junction and melt is now present further along the grain and subgrain boundaries. A second subgrain boundary, parallel to the first has also started melting. Reactant grains continue to have rounded edges and previously dry grain boundaries are now wetted. E. Melting has progressed significantly and the deformed quartz grain has now been melted entirely through, forming two separate quartz grains. There is also melt present on many previously dry grain and subgrain boundaries and reactant grains continue to form rounded edges as they are melted. F. Crystallization. The shaded edges of mineral grains indicate new material, formerly melt, has nucleated and crystallized onto these pre-existing grains. After crystallization the original deformed quartz grain is preserved as two separate quartz grains with a slight difference in optic orientation and they are separated by a film of former melt. Melt pseudomorphs are preserved on grain and subgrain boundaries as the modally least abundant mineral at that location. One of the subgrain boundary melt pseudomorphs is connected to a grain boundary pseudomorph, whereas the other one exists as an isolated film of K-feldspar.

References

Allibone, A.H. and Norris, R.J., 1992, Segregation of leucogranite plutons during syn-anatectic deformation: an example from the Taylor Valley, Antarctica: Journal of Metamorphic Geology, v. 10, p. 589-600.

Alsayed, A. M., Islam, M. F., Zhang, J., Collings, P. J., and Yodh, A. G., 2005, Premelting at defects within bulk colloidal crystals: Science, v. 309, p. 1207-1210.

Barbey, P., Bertrand, J-M., Angoua, S., and Dautel, D., 1989, Petrology and U/Pb geochronology of the Telohat migmatites, Aleksod, central Hoggar, Algeria: Contributions to Mineralogy and Petrology, v. 101, p. 207-219.

Barbey, P., 2007, Diffusion-controlled biotite breakdown reaction textures at the solid/liquid transition in the continental crust: Contributions to Mineralogy and Petrology, v. 154, p. 707-716.

Barker, D.S., and Reed, R.M., 2010, Proterozoic granites of the Llano Uplift, Texas: A collision-related suite containing rapakivi and topaz granites: Geological Society of America Bulletin, v. 122, p. 253-264.

Barquero-Molina, M., 2009, Kinematics of Bidirectional extension and coeval NW-directed contraction in orthogneisses of the Biranup Complex, Albany-Fraser Orogen, southwestern Australia [Ph.D. dissertation]: Austin, University of Texas at Austin, 205 p.

Bea, F. 1996, Residence of REE, Y, Th, and U in granites and crustal protoliths: implications for the chemistry of crustal melts: Journal of Petrology, v. 37, p. 521-552.

Beard, J.S., and Lofgren, G.E., 1991, Dehydration melting and water-saturated melting of basaltic and andesitic greenstones and amphibolites at 1, 3, and 6.9 kb: Journal of Petrology, v. 32, p. 365-401.

Becke, F., 1908, Über myrmekite: Schweizerische Mineralogische und Petrographisce Mitteilungen, v. 27, p. 377-390.

Beckerman, C., and Viskanta, R., 1988, Natural convection solid/liquid phase change in porous media: International Journal of Heat and Mass Transfer, v. 3, p. 35-46.

Beeson, J., Delor, C.P., and Harris, L.B., 1988, A structural and metamorphic traverse across the Albany Mobile Belt, Western Australia: Precambrian Research, v. 40/41, p. 117-136.

Bhadra, S., Das, S. and Bhattacharya, A., 2007, Shear zone-hosted migmatites (Eastern India): the role of dynamic melting in the generation of REE-depleted felsic melts, and implications for disequilibrium melting: Journal of Petrology, v. 48, p. 435-457.

Bickford, M.E., Cullers, R.L., Shuster, R.D., Premo, R.L., and Van Schmus, W.R., 1989, U-Pb zircon geochronology of Proterozoic and Cambrian plutons in the Wet Mountains and southern Front Range, in Grambling, J.A., and Tewksbury, B.J., eds., Proterozoic Geology of the Southern Rocky Mountains: Geological Society of America Special Paper 235, p. 49-64.

Bodorkos, S. and Clark, D.J., 2004a, Evolution of a crustal-scale transpressive shear zone in the Albany-Fraser Orogen, SW Australia: 1. P-T conditions of Mesoproterozoic metamorphism in the Coramup Gneiss: Journal of Metamorphic Geology, v. 22, p. 691-711.

Bodorkos, S. and Clark, D.J., 2004b, Evolution of a crustal-scale transpressive shear zone in the Albany-Fraser Orogen, SW Australia: 2. Tectonic history of the Coramup Gneiss and a kinematic framework for Mesoproterozoic collision of the West Australian and Mawson cratons: Journal of Metamorphic Geology, v. 22, p. 713-731.

Bodorkos, S., and Wingate, M.T.D., 2008a, 184119: monzogranitic gneiss, Point Henry; Geochronologic dataset 699. *In*: Compilation of geochronology data: Geological Survey of Western Australia.

Bodorkos, S., and Wingate, M.T.D., 2008b, 184307: pegmatitic granodiorite, Point Henry; Geochronologic dataset 706. *In*: Compilation of geochronology data: Geological Survey of Western Australia.

Bodorkos, S., and Wingate, M.T.D., 2008c, 184310: leucocratic granodiorite, Fisheries Bay headland; Geochronologic dataset 707. *In*: Compilation of geochronology data: Geological Survey of Western Australia.

Bodorkos, S., and Wingate, M.T.D., 2008d, 184311: orthopyroxene-clinopyroxene orthogneiss, Fisheries Bay headland; Geochronologic dataset 708. *In*: Compilation of geochronology data: Geological Survey of Western Australia.

Bodorkos, S., and Wingate, M.T.D., 2008e, 184312: granodioritic gneiss, Short Beach headland; Geochronologic dataset 709. *In*: Compilation of geochronology data: Geological Survey of Western Australia.

Bodorkos, S., and Wingate, M.T.D., 2008f, 184326: pegmatitic leucogranite, Short Beach headland; Geochronologic dataset 711. *In*: Compilation of geochronology data: Geological Survey of Western Australia.

Brock, M.R., and Singewald, Q.D., 1968, Geologic map of the Mount Tyndall quadrangle, Custer County, Colorado: U.S. Geological Survey Geologic Quadrangle Map GQ-596, scale 1:24,000.

Brodie, K.H. and Rutter, E.H., 1985, On the relationship between deformation and metamorphism with special reference to the behavior of basic rocks. *in:* Thompson, A.B. and Rubie D.C., eds., Metamorphic reactions: kinetics, textures, and deformation: Berlin, Springer, p. 138-179.

Brown, M., 1973, The definition of metatexis, diatexis and migmatite: Proceedings of the Geologists' Association, v. 84, p. 371-382.

Brown, M., 1994, The generation, segregation, ascent and emplacement of granite magma: the migmatite-to-crustally-derived granite connection in thickened orogens: Earth-Science Reviews, v. 36, p. 83-130.

Brown, M. and Rushmer, T., 1997, The role of deformation in the movement of granite melt: views from the laboratory and the field: In: Holness, M.B. (ed.), *Deformation-enhanced Fluid Transport in the Earth's Crust and Mantle*, The Mineralogical Society Series 8, Chapman and Hall, London, p. 111-144.

Brown, M. and Solar, G.S., 1998, Shear zone systems and melts: Feedback relations and self-organization in orogenic belts: Journal of Structural Geology, v. 20, p. 211-227.

Brown, M., Averkin, Y., McLellan, E., and Sawyer, E., 1995, Melt segregation in migmatites: Journal of Geophysical Research, v. 100, p. 15,655-15,679.

Büsch, W., Schneider, G. and Mehnert, K.R., 1974, Initial melting at grain boundaries. Part II: Melting in rocks of granodioritic, quartz dioritic and tonalitic composition: Neues Jahrbuch Fur Mineralogie Monatschefte, v. 8, p. 345-370.

Carlson, W.D., 1998, Petrologic constraints on the tectonic evolution of the Llano Uplift. *In*. J.P. Hogan and M.C. Gilbert, (eds.), *Basement Tectonics*, v. 12, p. 3-27, Kluwer, Dordrecht.

Carlson, W.D., Anderson, S.D., Mosher, S., Davidow, J.S., Crawford, W.D., and Lane, E.D., 2007, High-pressure metamorphism in the Texas Grenville orogen: Mesoproterozoic subduction of the southern Laurentian continental margin: International Geology Review, v. 49, p. 99-119.

Carstens, H., 1967, Exsolution in ternary feldspars. II. Intergranular precipitation in alkali feldspar containing calcium in solid solution: Contributions to Mineralogy and Petrology, v. 14, p. 316-320.

Castro, A., Patiño Douce, A.E., Corretgé, L.G., de la Rosa, J.D., El-Biad, M., and El-Hmidi, H., 1999, Origin of peraluminous granites and granodiorites, Iberian Massif, Spain: an experimental test of granite petrogenesis: Contributions to Mineralogy and Petrology, v. 135, p. 255-276.

Castro, A., Corretgé, L.G., El-Biad., M., El-Hmidi, H., Fernández, C. and Patiño Douce, A.E., 2000, Experimental constraints on Hercynian anatexis in the Iberian Massif, Spain: Journal of Petrology, v. 41, p. 1471-1488.

Clark, D.J., Hensen, B.J., and Kinny, P.D., 2000, Geochronological constraints for a two-stage history of the Albany-Fraser Orogen, western Australia: Precambrian Research, v. 102, p. 155-183.

Collins, W. J., and Sawyer, E., 1996, Pervasive granitoid magma transfer through the lower-middle crust during non-coaxial compressional deformation: Journal of Metamorphic Geology, 14, 565-579.

Condie, K.C., and Myers, J.S., 1999, Mesoproterozoic Fraser Complex: geochemical evidence for multiple subduction-related sources of lower crustal rocks in the Albany-Fraser Orogen, Western Australia: Australian Journal of Earth Sciences, v. 46, p. 875-882.

Conrad, W.K., Nicholls, I.A., and Wall, V.J., 1988, Water-saturated and –undersaturated melting of metaluminous and peraluminous crustal compositions at 10 kb evidence for the origin of silicic magmas in the Taupo Volcanic Zone, New Zealand, and other occurrences: Journal of Petrology, v. 29, p. 765-803.

Cooper, R.F., 1990, Differential stress induced melt migration: an experimental approach: Journal of Geophysical Research, v. 95, p. 6979-6992.

Cruciani, G., Franceschelli, M., Elter, F.M., Puxeddo, M., and Utzeri, D., 2008, Petrogenesis of Al-silicate-bearing trondhjemitic migmatites from NE Sardinia, Italy: Lithos, v. 102, p.554-574.

Cullers, R.L., Stone, J., Anderson, J.L., Sassarini, N., and Bickford, M.E., 1993, Petrogenesis of Mesoproterozoic Oak Creek and West McCoy Gulch plutons, Colorado: an example of cumulate unmixing of a mid-crustal, two-mica granite of anorogenic affinity: Precambrian Research, v. 62, p. 139-169.

Dash, J.G., 1999, History of the search for continuous melting: Reviews of Modern Physics, v. 71, p. 1737-1743.

Davidson, C., Schmid, S.M. and Hollister, L.S., 1994, Role of melt during deformation in the deep crust: TERRA Nova, v. 6, p. 133-142.

Dean, R.L., Andronicos, C., Siddoway, C. and Ray, J., 2002, Syntectonic emplacement of the 1.44 Ga Oak Creek pluton, Wet Mountains, Colorado: Geological Society of America Abstracts with Programs, v. 34, no. 6, p. 243.

Etheridge, M.A., Wall, V.J., Cox, S.F., and Vernon, R.H., 1984, High fluid pressures during regional metamorphism and deformation: Implications for mass transport and deformation mechanisms: Journal of Geophysical Research, v. 89, p. 4344-4358.

Fitzsimons, I.C.W., 2003, Proterozoic basement provinces of southern and southwestern Australia, and their correlation with Antarctica. *In*: Yoshida, M. Windley, B.F. and Dasgupta, S. (Eds.), Proterozoic East Gondwana: Supercontinent Assembly and Breakup. Geological Society of London Publication, v. 206, p. 93-130.

Fornelli, A. Piccarreta, G., Del Moro, A., and Acquafredda, P., 2002, Multi-stage melting in the lower crust of the Serre (southern Italy): Journal of Petrology, v. 43, p.2191-2217.

Fyfe, W.S., Flinn, D., and Nicolas, A., 1976, Chemical aspects of rock deformation: Philosophical Transactions of the Royal Society of London. Series A, v. 283A, p. 221-228.

Gardien, V., Thompson, A.B., Grujic, D. and Ulmer, P., 1995, Experimental melting of biotite + plagioclase + quartz +/- muscovite assemblages and implications for crustal melting: Journal of Geophysical Research, v. 100, B8, p. 15581-15591.

Gardien, V., Thompson, A.B., and Ulmer, P., 2000, Melting of biotite + plagioclase + quartz gneisses: the role of H_2O in the stability of amphibole: Journal of Petrology, v. 41, p. 651-666.

Garrison, J.R., Jr., 1981, Coal Creek serpentinite, Llano Uplift, Texas: A fragment of an incomplete Precambrian ophiolite: Geology, v. 9, p. 361-374.

Getsinger, A., Rushmer, T., Jackson, M.D., and Baker, D., 2009, Generating high-Mg numbers and chemical diversity in tonalite-trondjhemite-granodiorite (TTG) magmas during melting and melt segregation in the continental crust: Journal of Petrology, v. 50, p. 1935-1954.

Givot, R.M., and Siddoway, C.S., 1998, Deformation of mid-Proterozoic metamorphic rocks, Five Points Gulch shear zone, Colorado: Geological Society of America Abstracts with Programs, v. 30, no. 6, p. 9.

Gleason, G.C. and DeSisto, S., 2008, A natural example of crystal-plastic deformation enhancing the incorporation of water into quartz: Tectonophysics, v. 446, p. 16-30.

Green, H.W., II, 1972, Metastable growth of coesite in highly strained quartz: Journal of Geophysical Research, v. 77, p. 2478-2482.

Green, H.W., and Radcliffe, S.V., 1975, Fluid precipitates in rocks from the earth's mantle: Geological Society of America Bulletin, v. 86, p. 846-852.

Guernina, S. and Sawyer, E.W., 2003, Large-scale melt-depletion in granulite terranes: an example from the Archean Ashuanipi Subprovince of Quebec: Journal of Metamorphic Geology, v. 21, p. 181-201.

Hacker, B.R., 1990, Amphibolite-facies-to-granulite-facies reactions in experimentally deformed, unpowdered amphibolite: American Mineralogist, v. 75, p. 1349-1361.

Han, L., An, Q., Fu, R., Zheng, L., and Luo, S., 2010, Local and bulk melting of Cu at grain boundaries: Physica B, v. 405, p. 748-753.

Hand, M. and Dirks, P.H.G.M., 1992, The influence of deformation on the formation of axial-planar leucosomes and the segregation of small melt bodies within the migmatitic Napperby Gneiss, Central Australia: Journal of Structural Geology, v. 14, p. 591-604.

Harris, N.B.W., and Inger, S., 1992, Trace element modeling of pelite-derived granites: Contributions to Mineralogy and Petrology, v. 110, p. 46-56.

Harris, N., and Inger, S., and Massey, J., 1993, The role of fluids in the formation of High Himalayan leucogranites. In: Treloar, P.J., Searle, M.P., eds., *Himalayan Tectonics*. Geological Society, London, Special Publication 74, p. 391-400.

Harte, B., Pattison, D.R.M. and Linklater, C.M., 1991, Field relations and petrography of partially melted pelitic and semi-pelitic rocks. In: Voll, G., Töpel, J., Pattison, D.R.M. and Seifert, F., eds., *Equilibrium and Kinetics in Contact Metamorphism, The Ballachulish igneous complex and its aureole*: Springer-Verlag, Berlin and Heidelberg, p. 182-210.

Hasalová, P., Schulmann, K., Lexa, O., Štípská, P., Hrouda, F., Ulrich, S., Haloda, J. and Týcová, P., 2008, Origin of migmatites by deformation-enhanced melt infiltration of orthogneiss: a new model based on quantitative microstructural analysis: Journal of Metamorphic Geology, v. 26, p. 29-53.

Hibbard, M.J., 1979, Myrmekite as a marker between preaqueous and postaqueous phase saturation in granitic systems: GSA Bulletin, v. 90, p. 1047-1062.

Hoh, A.M., 2000, Deformational history of the Valley Spring Domain in the northeastern Llano Uplift, Devils Waterhole, Inks Lake State Park, Burnet County, Texas [Master's thesis]: Austin, University of Texas at Austin, 140 p.

Hollister, L.S., and Crawford, M.L., 1986, Melt-enhanced deformation: A major tectonic process: Geology, v. 14, p. 558-561.

Holness, M. B., 2008, Decoding Migmatite Microstructures. In: Working with Migmatites. Short Course, 38. Mineralogical Association of Canada, Québec, Québec, pp. 57-76.

Holness, M.B. and Isherwood, C., 2003, The aureole of the Rum Tertiary Igneous Complex, Inner Hebrides, Scotland: Journal of the Geological Society, London, v. 160, p. 15-27.

Holness, M.B. and Sawyer, E.W., 2008, On the pseudomorphing of melt-filled pores during the crystallization of migmatites: Journal of Petrology, v. 49, p. 1343-1363.

Huang, W.L., and Wyllie, P.J., 1975, Melting reactions in the system $NaAlSi_3O_8$ – $KAlSi_3O_8$ – SiO_2 to 35 kilobars, dry and with excess water: Journal of Geology, v. 83, p. 737-748.

Hunt, B.B., 2000, Mesoproterozoic structural evolution and lithologic investigation of the western Llano Uplift, Mason County, central Texas [Master's thesis]: Austin, University of Texas at Austin, 139 p.

Johannes, W., 1983, On the origin of layered migmatites: In: *Migmatites, Melting and Metamorphism* (eds. Atherton, M.P. and Gribble, C.D.), p. 234-248, Shiva Publishing, Nantwich, UK.

Jones, J.V., 2005, Proterozoic tectonic evolution of southern Laurentia: new constraints from field studies and geochronology in southeastern Colorado and northern New Mexico, USA [PhD dissertation]: Austin, University of Texas at Austin, 204 p.

Jones, J.V., Siddoway, C.S., and Connelly, J.N., 2010, Characteristics and implications of ca. 1.5 Ga deformation across a Proterozoic mid-crustal section, Wet Mountains, Colorado, USA: Lithosphere, v. 2, no. 2, p. 119-135.

Jurewicz, S.R. and Watson, E.B., 1984, Distribution of partial melt in a felsic system: the importance of surface energy: Contributions to Mineralogy and Petrology, v. 85, v. 25-29.

Jurewicz, S.R. and Watson, E. B., 1985, The distribution of partial melt in a granitic system: the application of liquid phase sintering theory: Geochimica et Cosmochimica Acta, v. 49, p. 1109-1121.

Kerrich, R., Fyfe, W.S., Gorman, B.E. and Allison, I., 1977, Local modification of rock chemistry by deformation: Contributions to Mineralogy and Petrology, v. 65, p. 183-190.

Koepke, J., Feig, S.T., Snow, J., and Freise, M., 2004, Petrogenesis of oceanic plagiogranites by partial melting of gabbros: an experimental study: Contributions to Mineralogy and Petrology, v. 146, p. 414-432.

Koester, E., Pawley, A.R., Fernandes, L.A.D., Porcher, C.C., and Soliani, E., Jr., 2002, Experimental melting of cordierite gneiss and the petrogenesis of syntranscurrent peraluminous granites in southern Brazil: Journal of Petrology, v. 43, p. 1494-1616.

Knipe, R.J., and White, S.H., 1979, Deformation in low grade shear zones in the Old Red Sandstone, S. W. Wales: Journal of Structural Geology, v. 1, p. 53-66.

Kriegsman, L.M. and Álvarez-Valero, A.M., 2010, Melt-producing versus melt-consuming reactions in pelitic xenoliths and migmatites: Lithos, v. 116, p. 310-320.

Kronenberg, A.K., and Wolf, G.H., 1990, Fourier transform infrared spectroscopy determinations of intragranular water content in quartz-bearing rocks: implications for hydrolytic weakening in the laboratory and within the earth: Tectonophysics, v. 172, p. 255-271.

Kronenberg, A.K., Kirby, S.H., Aines, R.D., and Rossman, G.R., 1986, Solubility and diffusional uptake of hydrogen in quartz at high water pressures: Implications for hydrolytic weakening: Journal of Geophysical Research, v. 91, p. 12, 723-12,744.

Kronenberg, A.K., Segall, P. and Wolf, G.H., 1990, Hydrolitic weakening and penetrative deformation within a natural shear zone. In: Duba, A.G., Durham, W.B., Handin, J.W., Wang, H.F., (eds.), The Brittle-Ductile Transition in Rocks: the Heard Volume. American Geophysical Union Monograph, v. 56, p. 21-36.

Kruhl, J.H., 1996, Prism- and basal-plane parallel subgrain boundaries in quartz: a microstructural geothermobarometer: Journal of Metamorphic Geology, v. 14, p. 581-589.

Kuhlmann-Wilsdorf, D., 1965, Theory of melting: Physical Review, v. 140, p. A1599-1610.

Lanzirotti, A., 1988, Geology and geochemistry of a Proterozoic supracrustal and intrusive sequence in the central Wet Mountains, Colorado [Master's thesis]: Socorro, New Mexico Institute of Mining and Technology, 164 p.

Lanzirotti, A. and Condie, K.C., 1988, Origin and tectonic significance of early Proterozoic leucogranites and high-pressure granulites in the Wet Mountains, Colorado: Geological Society of America Abstracts with Programs, v. 20, no. 2, p. 121-122.

Laporte, D., Rapaille, C. and Provost, A., 1997, Wetting angles, equilibrium melt geometry, and the permeability threshold of partially-molten crustal protoliths: In: Bouchez, J.L., Hutton, D.H.W. and Stephens, W.E. (eds.), *Granite: From segregation of Melt to Emplacement Fabrics*: Dordrecht, Kluwer Academic Publishers, p. 31-54.

Le Breton, N. and Thompson, A.B., 1988, Fluid-undersaturated (Dehydration) melting of biotite in metapelites in the early stages of crustal anatexis: Contributions to Mineralogy and Petrology, v. 99, p. 226-237.

Levine, J.S.F., and Mosher, S., 2010, Contrasting Grenville-aged tectonic histories across the Llano Uplift, Texas: New evidence for deep-seated high-temperature deformation in the western uplift: Lithosphere, v. 2, p. 399-410.

Liu, M., Yund, R.A., Tullis, J., Topor, L. and Navrotsky, A., 1995, Energy associated with dislocations: A calorimetric study using synthetic quartz: Physics and Chemistry of Minerals: v. 22, p. 67-73.

Luth, W.C., Jahns, R.H., and Tuttle, O.F., 1964, The granite system at pressures of 4 to 10 kilobars: Journal of Geophysical Research, v. 69, p. 759-773.

Luther, L.C., 1965, Diffusion along dislocations: The Journal of Chemical Physics, v. 43, p. 2213-2218.

Lutsko, J.F., Wolf, D., Phillpot, S.R. and Yip, S., 1989, Molecular-dynamics study of lattice-defect-nucleated melting in metals using an embedded-atom-method potential: Physical Review B, v. 40, p. 2841-2855.

McGehee, R.V., 1979, Precambrian rocks of the southeastern Llano region, Texas: University of Texas Bureau of Economic Geology Circular 79-3, 36 p.

McKenzie, D.P., 1984, The generation and compaction of partially molten rock: Journal of Petrology, v. 25, p. 713-765.

McLaren, A.C., Cook, R.F., Hyde, S.T. and Tobin, R.C., 1983, The mechanisms of the formation and growth of water bubbles and associated dislocation loops in synthetic quartz: Physics and Chemistry of Minerals, v. 9, p. 79-94.

Mancktelow, N.S., 2002, Finite-element modeling of shear zone development in viscoelastic materials and its implications for localization of partial melting: Journal of Structural Geology, v. 24, p. 1045-1053.

Marchildon, N. and Brown, M., 2001, Melt segregation in late syn-tectonic anatectic migmatites: an example from the Onawa Contact Aureole, Maine, USA: Physics and Chemistry of the Earth (A), v. 26, p. 225-229.

Marchildon, N. and Brown, M., 2002, Grain-scale melt distribution in two contact aureole rocks: implications for controls on melt localization and deformation: Journal of Metamorphic Geology, v. 20, p. 381-396.

Marchildon, N. and Brown, M., 2003, Spatial distribution of melt-bearing structures in anatectic rocks from Southern Brittany, France: Implications for melt transfer at grain- to orogen-scale: Tectonophysics, v. 364, p. 215-235.

Mehnert, K.R., 1968, Migmatites and the origin of granitic rock: Amsterdam, Elsevier Publishing Company, 405 p.

Mehnert, K.R., Büsch, W. and Scheider, G., 1973, Initial melting at grain boundaries of quartz and feldspar in gneisses and granulites: Neues Jahrbuch Fur Mineralogie, Monatschefte, v. 4, p. 165-183.

Mei, Q.S. and Lu, K., 2007, Melting and superheating of crystalline solids: From bulk to nanocrystals: Progress in Materials Science, v. 52, p. 1175-1262.

Milord, I., Sawyer, E.W. and Brown, M., 2001, Formation of diatexites migmatites and granite magma during anatexis of semi-pelitic metasedimentary rocks: An example from St. Malo, France: Journal of Petrology, v. 42, p. 487-505.

Misra, S., Burlini, L. and Burg, J.-P., 2009, Strain localization and melt segregation in deforming metapelites: Physics of the Earth and Planetary Interiors, v. 177, p.173-179.

Mizushima, S., 1960, Dislocation model of liquid structure: Journal of the Physical Society of Japan, v. 15, p. 70-77.

Mogk, D.W., 1992, Ductile shearing and migmatization at mid-crustal level in an Archean high-grade gneiss belt, northern Gallatin Range, Montana, USA: Journal of Metamorphic Geology, v. 10, p. 427-438.

Montel, J.-M., and Vielzeuf, D., 1997, Partial melting of metagraywackes. II. Compositions of minerals and melts: Contributions to Mineralogy and Petrology, v. 128, p. 176-196.

Mosher, S., 1993, Western extensions of Grenville age rocks, Texas, *in* Reed, J.C., Jr., Bickford, M.E., Houston, R.S., Link, P.K., Rankin, D.W., Sims, P.K. and Van Schmus, W.R., eds., Precambrian: Coterminous U. S.: Boulder, Colorado, Geological Society of America, Geology of North America, v. C-2, p. 366-378.

Mosher, S., 1998, Tectonic evolution of the southern Laurentian Grenville orogenic belt: Geological Society of America Bulletin, v. 110, p. 1357-1375.

Mosher, S., Hoh, A.M., Zumbro, J.A., and Reese, J.F., 2004, Tectonic evolution of the eastern Llano Uplift, central Texas: A record of Grenville orogenesis along the southern Laurentian margin: Geological society of America Memoir 197, p. 783-798.

Mosher, S., Levine, J.S.F., and Carlson, W.D., 2008, Mesoproterozoic plate tectonics: A collisional model for the Grenville-aged orogenic belt in the Llano Uplift, central Texas: Geology, v. 36, p. 55-58.

Mott, N.F., 1952, Introductory Remarks: Proceedings of the Royal Society of London. Series A, Mathematical and Physical Sciences, v. 215, p. 1-4.

Myers, J.S., 1990, Albany-Fraser Orogen, *in:* Geology and Mineral Resources of Western Australia. Memoir 3, Geological Survey of Western Australia, Perth, WA, p. 255-264.

Myers, J.S., Shaw, R.D., and Tyler, I.M., 1996, Tectonic evolution of Proterozoic Australia: Tectonics, v. 15, p. 1431-1446.

Nakamura, N., 1974, Determination of REE, Ba, Fe, Mg, Na and K in carbonaceous and ordinary chondrites: Geochemica et Cosmochimica Acta, v. 38, p. 757-775.

Nash, W.P., and Crecraft, H.R., 1985, Partition coefficients for trace elements in silicic magmas: Geochimica et Cosmochimica Acta, v. 49, p. 2309-2322.

Nelson, D.R., Myers, S.J., and Nutman, A.P., 1995, Chronology and evolution of the middle Proterozoic Albany-Fraser orogen, Western Australia: Australian Journal of Earth Sciences, v. 42, p. 481-495.

Nyström, A.I. and Kriegsman, L.M., 2003, Prograde and retrograde reactions, garnet zoning patterns, and accessory phase behaviour in SW Finland migmatites, with implications for geochronology. In: Vance, D., Müller, W., Villa, I. (Eds.), Geochronology: Linking the Isotopic Record with Petrology and Textures: Geological Society of London Special Publications, vol. 220, p. 213-230.

Ookawa, A., 1960, A model theory of liquid: Journal of the Physical Society of Japan, v. 15, p. 2191-2197.

Passchier, C.W., and Trouw, R.A.J., 1996, Microtectonics: New York, Springer, 289 p.

Patiño Douce, A.E and Johnston, A.D., 1991, Phase equilibria and melt productivity in the pelitic system: Implications for the origin of peraluminous granitoids and aluminous granites: Contributions to Mineralogy and Petrology, v. 107, p. 202-218.

Patiño Douce, A.E and Beard, J.S., 1995, Dehydration-melting of biotite gneiss and quartz amphibolite from 3-15 kbar: Journal of Petrology, v. 36, p. 707-738.

Patiño Douce, A.E and Beard, J.S., 1996, Effects of P, f(O_2) and Mg/Fe ratio on dehydration melting of model metagraywackes: Journal of Petrology, v. 37, p. 999-1024.

Patiño Douce, A.E and Harris, N., 1998, Experimental constraints on Himalayan anatexis: Journal of Petrology, v. 39, p. 689-710.

Pearce, J.A., and Norry, M.J., 1979, Petrogenetic implications of Ti, Zr, Y and Nb variations in volcanic rocks: Contributions to Mineralogy and Petrology, v. 69, p. 33-47.

Peng, C. C. J., 1970, Intergranular albite in some granites and syenites of Hong Kong: American Mineralogist, v. 55, p. 270-282.

Phillips, E.R., 1974, Myrmekite – one hundred years later: Lithos, v. 7, p. 181-194.

Phillips, E.R., 1980, On polygenetic myrmekite: Geological Magazine, v. 117, p. 29-36.

Pickering, J. M. and Johnston, A.D., 1998, Fluid-absent melting behavior of a two-mica metapelites: experimental constraints on the origin of Black Hills granite: Journal of Petrology, v. 39, p. 1787-1804.

Pluis, B., Denier van der Gon, A.W., Frenken, J.W.M. and van der Veen, J.F., 1987, Crystal-face dependence of surface melting: Physical Review Letters, v. 59, p. 2678-2681.

Poirier, J.P., 1985, Creep of Crystals: Cambridge University Press, Cambridge.

Prouteau, G., Scaillet, B., Pichavant, M., and Maury, R.C., 1999, Fluid-present melting of ocean crust in subduction zones: Geology, v. 27, p. 1111-1114.

Ramberg, H., 1962, Intergranular precipitation of albite formed by unmixing of alkali feldspar: Neues Jahrbuch für Mineralogie. Abhandlungen, v. 98, p. 14-34.

Rapp, R.P., Watson, E.B., and Miller, C.F., 1991, Partial melting of amphibolite/eclogite and the origin of Archean trondhjemites and tonalites: Precambrian Research, v. 51, p. 1-25.

Reed, J.C., Jr., Bickford, M.E., Premo, W.R., Alenikoff, J.N., and Pallister, J.S., 1987, Evolution of the Early Proterozoic Colorado province: Constraints from U-Pb geochronology: Geology, v. 15, p. 861-865.

Reed, R.M., 1999, Emplacement and deformation of late syn-orogenic Grenville-age granites in the Llano Uplift, central Texas [Ph.D. dissertation]: Austin, University of Texas at Austin, 272 p.

Reese, J.F., Mosher, S., Connelly, J., and Roback, R., 2000, Mesoproterozoic chronostratigraphy of the southeastern Llano Uplift, central Texas: Geological Society of America Bulletin, v. 112, p. 278-291.

Roback, 1996, Characterization and tectonic evolution of a Mesoproterozoic island arc in the southern Grenville Orogen, Llano uplift, central Texas: Tectonophysics, v. 265, p. 29-52.

Robin, P.-Y.F., 1979, Theory of metamorphic segregation and related processes: Geochimica et Cosmochimica Acta, v. 43, p. 1587-1600.

Rogers, J.J.W., 1961, Origin of albite in granitic rocks: American Journal of Science, v. 259, p. 186-193.

Rosenberg, C.L. and Riller, U., 2000, Partial-melt topology in statistically and dynamically recrystallized granite: Geology, v. 28, p. 7-10.
Rubie, D.C, 1983, Reaction-enhanced ductility: The role of solid-solid univariant reaction in deformation of the crust and mantle: Tectonophysics, v. 96, p. 331-352.
Rubie, D.C. and Brearley, A.J., 1990, A model for rates of disequilibrium melting during metamorphism. *In:* High Temperature Metamorphism and Crustal Anatexis (eds. Ashworth, J.R. and Brown, M.). Unwin Hyman, London, p. 57-86.
Rushmer, T., 1991, Partial melting of two amphibolites: contrasting experimental results under fluid-absent conditions: Contributions to Mineralogy and Petrology, v. 107, p. 41-59.
Rushmer, T., 1993, Experimental high-pressure granulites: Some applications to natural mafic xenoliths suites and Archean granulite terranes: Geology, v. 21, p. 411-414.
Sawyer, E.W., 1994, Melt segregation in the continental crust: Geology, v. 22, p. 1019-1022.
Sawyer, E.W., 1998, Formation and evolution of granite magmas during crustal reworking: the significance of diatexites: Journal of Petrology, v. 39, p. 1147-1167.
Sawyer, E.W., 1999, Criteria for the recognition of partial melting: Physics and Chemistry of the Earth, v. A24, p. 269-279.
Sawyer, E.W., 2000, Grain-scale and outcrop-scale distribution and movement of melt in a crystallizing granite: Royal Society of Edinburgh Transactions, Earth Sciences, v. 91, p. 73-85.
Sawyer, E.W., 2001, Melt segregation in the continental crust: distribution and movement of melt in anatectic rocks: Journal of Metamorphic Geology, v. 19, p. 291-309.
Sawyer, E.W., 2008, Atlas of migmatites: Quebec, Canadian Mineralogist Special Publication 9, Mineralogical Association of Canada, 373 p.
Sawyer, E.W., 2010, Migmatites formed by water-fluxed partial melting of a leucogranodiorite protolith: microstructures in the residual rocks and source of the fluid: Lithos, v. 116 p. 273-286.
Sawyer, E.W., Dombrowski, C. and Collins, W.J., 1999, Movement of melt during synchronous regional deformation and granulite-facies anatexis, an example from the Waluma Hills, central Australia. In: *Understanding Granites: Integrating New and Classical Techniques, Special Publication 168*, (eds Castro, A., Fernandez, C. and Vigneresse, J.L.), p. 221-237. Geological Society, London.
Schwantke, A., 1909, Die Beimischung von Ca im Kalifeldspat und die Myrmekitibildung: Zentralblatt für Geologie und Paläontologie, v.1, p. 311-316.
Selbekk, R.S., and Skjerlie, K.P., 2002, Petrogenesis of the anorthosite dyke swarm of Tromsø, north Norway: experimental evidence for hydrous anatexis of an alkaline mafic complex: Journal of Petrology, v. 43, p. 943-962.
Shaw, C.A., Heizler, M.T., and Karlstrom, K.E., 2005, $^{40}Ar/^{39}Ar$ thermochronologic record of 1.45-1.35 Ga intracontinenal tectonism in the southern Rocky Mountains: Interplay of conductive and advective heating with intracontinental deformation, in: Karlstrom, K.E. and Keller, G.R., eds., The Rocky Mountain

Region: An Evolving Lithosphere: Washington D.C., American Geophysical Union Geophysical Monograph 154, p. 163-184.
Siddoway, C.S., Givot, R.M., Bodle, C.D. and Heizler, M.T., 2000, Dynamic versus anorogeic setting for Mesoproterozoic plutonism in the Wet Mountains, Colorado: Does the interpretation depend on level of exposure?: Rocky Mountain Geology, v. 35, p. 91-111.
Simpson, C. and Wintsch, R.P., 1989, Evidence for deformation-induced K-Feldspar replacement by myrmekite: Journal of Metamorphic Geology, v. 7, p. 261-275.
Singh, J., and Johannes, W., 1996, Dehydration melting in tonalites. II. Composition of melts and solids: Contributions to Mineralogy and Petrology, v. 125, p. 26-44.
Sirong, Y., Dongcheng, L. and Kim, N., 2006, Microstructure evolution of SIMA processed Al2024: Materials Science and Engineering, v. A420, p. 165-170.
Skjerlie, K.P., and Johnston, A.D., 1992, Vapour-absent melting at 10 kbar of a biotite- and amphibole-bearing tonalitic gneiss: implications for the generation of A-type granites: Geology, v. 20, p. 263-266.
Skjerlie, K.P., and Johnston, A.D., 1996, Vapour-absent melting from 10 to 20 kbar of crustal rocks that contain multiple hydrous phases: implications for anatexis in the deep to very deep crust and active continental margins: Journal of Petrology, v. 37, p. 661-691.
Skjerlie, K.P., and Patiño Douce, A.E., 2002, The fluid-absent partial melting of a zoisite-bearing quartz eclogite from 1.0-3.2 GPa; implications for melting in thickened continental crust and for subduction-zone processes: Journal of Petrology, v. 43, p. 291-314.
Skjerlie, K.P., and Patiño Douce, A.E, and Johnston, A.D., 1993, Fluid absent melting of a crustal protolith: implications for the generation of anatectic granites: Contributions to Mineralogy and Petrology, v. 114, p. 365-378.
Slagstad, T., Jamieson, R.A., and Culshaw, N.G., 2005, Formation, crystallization and migration of melt in the mid-orogenic crust: Muskoka domain migmatites, Grenville Province, Ontario: Journal of Petrology, v. 46, p. 893-919.
Smith, D.R., Barnes, C., Shannon, W., Roback, R., and James, E., 1997, Petrogenesis of Mid-Proterozoic granitic magmas: examples from central and west Texas: Precambrian Research, v. 85, p.53-79.
Smith, R.K., Gray, W., Gibbs, T., and Gallegos, M.A., 2010, Petrogenesis of Mesoproterozoic granitic plutons, eastern Llano Uplift, central Texas, USA: Lithos, v. 118, p. 238-254.
Smoluchowski, R., 1952, Theory of grain boundary diffusion: Physical Review, v. 87, p. 482-487.
Solar, G.S. and Brown, M., 2001, Petrogenesis of migmatites in Maine, USA: Possible source of peraluminous leucogranite in plutons?: Journal of Petrology, v. 42, p. 789-823.
Solar, G.S., Pressley, R.A., Brown, M. and Tucker, R.D., 1998, Granite ascent in convergent orogenic belts: Testing a model: Geology, v. 26, p. 711-714.

Spaggiari, C.V., Bodorkos, S., Tyler, I.M., and Barquero-Molina, M, 2008, The c. 1680 Ma Dalyup Gneiss of the Albany-Fraser Orogen, Western Australia: What is it, and where did it come from?: Geological Society of Australia, Abstracts, 89, v. 232-233.

Spaggiari, C.V., Bodorkos, S., Barquero-Molina, M., and Tyler, I.M., 2009, Interpreted Bedrock Geology of the South Yilgarn and central Albany-Fraser Orogen, Western Australia. Western Australia Geological Survey, Record 2009, 77p.

Spear, F.S., 1991, On the interpretation of peak metamorphic temperatures in light of garnet diffusion during cooling: Journal of Metamorphic Geology, v. 9, p. 379-388.

Spear, F.S., 1995, Metamorphic Phase Equilibria and Pressure-Temperature-Time Paths: Mineralogical Society of America Monograph, Chelsea, Michigan, BookCrafters Inc., 799 p.

Spear, F., Kohn, M., and Cheney, J., 1999, Pressure-temperature paths from anatectic pelites: Contributions to Mineralogy and Petrology, v. 134, p.17-32.

Springer, W., and Seck, H.A., 1997, Partial fusion of basic granulites at 5 to 15 kbar: implications for the origin of TTG magmas: Contributions to Mineralogy and Petrology, v. 127, p. 30-45.

Stevenson, D.J., 1989, Spontaneous small-scale melt segregation in partial melts undergoing deformation: Geophysical Research Letters, v. 16, p. 1067-1070.

Stipp, M., Tullis, J., and Behrens, H., 2006, Effect of water on the dislocation creep microstructure and flow stress of quartz and implications for the recrystallized grain size piezometer: Journal of Geophysical Research, v. 111, B04201. doi: 10.1029/2005JB003852.

Tartaglino, U. and Tosatti, E., 2003, Strain effects at solid surfaces near the melting point: Surface Science, v. 532-535, p. 623-627.

Tropper, P., Konzett, J., and Finger, F., 2005, Experimental constraints on the formation of high-P/high-T granulites in the Southern Bohemian Massif: European Journal of Mineralogy, v. 17, p. 343-356.

Trumbull, R.B., 1988, Petrology of flecked gneisses in the northern Wet Mountains, Fremont County, Colorado: GSA Bulletin, v. 100, p. 247-256.

Tuttle, O.F., 1952, Origin of the contrasting mineralogy of extrusive and plutonic salic rocks: Journal of Geology, v. 60, p. 107-124.

Tuttle, O.F., and Bowen, N.L., 1958, Origin of granite in the light of experimental studies in the system $NaAlSi_3O_8$-$KAlSi_3O_8$-SiO_2-H_2O: Geological Society of America Memoir 74, 153 p.

Vanderhaeghe, O., 2001, Melt segregation, pervasive melt migration and magma mobility in the continental crust: The structural record from pores to orogens: Physics and Chemistry of the Earth (A), v. 26, p. 213-223.

Vernon, R.H., 2004, *A Practical Guide to Rock Microstructure*: Cambridge: Cambridge University Press, 594 p.

Vernon, R.H., and Paterson, S.R., 2001, Axial-surface leucosomes in anatectic migmatites: Tectonophysics, v. 335, is. 1-2, p. 183-192.

Vernon, R.H., Williams, V.A., and D'Arcy, W.F., 1983, Grain-size reduction and foliation development in a deformed granitic batholiths: Tectonophysics, v. 92, p. 123-145.

Vielzeuf, D. and Holloway, J.R., 1988, Experimental determination of the fluid-absent melting relations in the pelitic system: Contributions to Mineralogy and Petrology, v. 98, p. 257-276.

Walker, N., 1992, Middle Proterozoic geologic evolution of the Llano Uplift, Texas: Evidence from U-Pb zircon geochronometry: Geological Society of America Bulletin, v. 104, p. 494-504.

Waters, D. J., 1988, Partial melting and formation of granulite facies assemblages in Namaqualand, South Africa: Journal of Metamorphic Geology, v. 6, p. 387-404.

Waters, D.J., 2001, The significance of prograde and retrograde quartz-bearing intergrowth microstructures in partially melted granulite-facies rocks: Lithos, v. 56, p. 97-110.

Watt, G.R. and Harley, S.L., 1993, Accessory phase controls on the geochemistry of crustal melts and restites produced during water-undersaturated partial melting: Contributions to Mineralogy and Petrology, v. 114, p. 550-566.

Whitaker, A.J., 1992, Albany Magnetic and Gravity Interpretation (1:1,000,000 scale map). Bureau of Mineral Resources, Geology and geophysics, Canberra.

Whitaker, A.J., 1993, Esperance Magnetic and Gravity Interpretation (1:1,000,000 scale map). Australian Geological Survey Organisation, Canberra.

White, S., 1975, Tectonic deformation and recrystallization of oligoclase: Contributions to Mineralogy and Petrology, v. 50, p. 287-304.

White, S.H. and Knipe, R.J., 1978, Transformation- and reaction-enhanced ductility in rocks: Journal of the Geological Society of London, v. 135, p. 513-516.

Wickham, S.M., 1987, The segregation and emplacement of granitic magmas: Journal of the Geological Society of London, v. 144, p. 281-297.

Wintsch, R.P., 1975, Feldspathization as a result of deformation: Geological Society of America Bulletin, v. 86, p. 35-38.

Wintsch, R.P. and Dunning, J., 1985, The effect of dislocation density on the aqueous solubility of quartz and some geologic implications: a theoretical approach: Journal of Geophysical Research, v. 90, no. B5, p. 3649-3657.

Wolf, M.B. and Wyllie, P.J., 1991, Dehydration-melting of solid amphibolite at 10 kbar. Textural development, liquid interconnectivity and applications to the segregation of magma: Mineralogy and Petrology, v. 44, p. 151-179.

Wolf, M.B., and Wyllie, P.J., 1994, Dehydration-melting of amphibolite at 10 kbar: The effects of temperature and time: Contributions to Mineralogy and Petrology, v. 115, p. 369-383.

Yund, R.A. and Tullis, J., 1991, Compositional changes of minerals associated with dynamic recrystalization: Contributions to Mineralogy and Petrology, v. 108, p. 346-355.

Yurimoto, H. and Nagasawa, H., 1989, The analysis of dislocation pipe radius for diffusion: Mineralogical Journal, v. 14, p. 171-178.

Vita

Jamie Sloan Levine grew up outside of Boston, Massachusetts and in New York City. She attended the Brearley School for high school graduating in 1997. She then moved to Northfield, Minnesota where she attended Carleton College, graduating in 2001 with a BA in geology and a concentration in environmental studies. After taking a year off and working at Oregon Caves National Monument and the paleomagnetic lab at Lamont-Doherty Earth Observatory, she started a master's degree in geology at the University of Texas at Austin. Jamie received her MS in the spring of 2005 and moved to Seattle. She missed being in the world of geology and as a result she returned to the University of Texas at Austin in the fall of 2006 to begin her PhD in structural geology.

Permanent e-mail address: levinejs@gmail.com

This dissertation was typed by the author.